TAMPEREEN TEKNILLINEN YLIOPISTO
TAMPERE UNIVERSITY OF TECHNOLOGY

Ali Muhammad

Impedance Control of Redundant Manipulators

Julkaisu 986 • Publication 986

Tampere 2011

Tampereen teknillinen yliopisto. Julkaisu 986
Tampere University of Technology. Publication 986

Ali Muhammad

Impedance Control of Redundant Manipulators

Thesis for the degree of Doctor of Science in Technology to be presented with due permission for public examination and criticism in Konetalo Building, Auditorium K1702, at Tampere University of Technology, on the 4th of November 2011, at 12 noon.

Tampereen teknillinen yliopisto - Tampere University of Technology
Tampere 2011

ISBN 978-952-15-2652-7 (printed)
ISBN 978-952-15-2657-2 (PDF)
ISSN 1459-2045

ABSTRACT

This thesis presents research work related to the impedance control of redundant manipulators. The main goal is to study the effects of redundancy on the dynamic behaviour of manipulators. Firstly, theoretical developments related to redundancy, dynamics and impedance control are presented in general form without restriction to any particular manipulator. The purpose is to keep the findings useful for other developments and continue the research on a wider scale. Later, the Water Hydraulic MANipulator (WHMAN), which consists of redundant degrees of freedom, is used for simulations and experiments. WHMAN is developed at the Department of Intelligent Hydraulics and Automation at Tampere University of Technology (IHA/TUT). The purpose of this manipulator is to provide assistance during the ITER divertor maintenance and it requires position and force control during these operations.

The analytical model of WHMAN in the form of state space equations is used for mathematical analysis and numerical verification. The verified simulation model is used for the development and verification of controllers. The position controllers of the joints are developed using a linearized model and then fine-tuned using a nonlinear model and the actual manipulator. The results show that models of WHMAN can be utilized for control design and further study.

Both position-based and equivalent force-based implementations of impedance controller were tested with the simulation model of WHMAN. The simulation results showed unstable behaviour of the manipulator for equivalent force-based implementation. Therefore only the position-based implementation was used in the experiments. The results show that, in the absence of linear mapping between joint-space and operational-space, the development of equivalent force-based impedance controller is not straightforward and requires separate design for the inner-loop force controller.

The theoretical, simulation and experimental results show that the existence of redundant degrees of freedom can result in improving the dynamic performance of a manipulator and thus the impedance regulation capabilities.

PREFACE

This study was carried out from 2004 to 2010 in the Department of Intelligent Hydraulics and Automation (IHA), Tampere University of Technology (TUT).

This work, supported by the European Communities under the contract of Association between Euratom/TEKES, was carried out within the framework of the European Fusion Development Agreement. The views and opinions expressed herein do not necessarily reflect those of the European Commission.

I wish to express my deepest gratitude to Professor Tapio Virvalo for his invaluable guidance, without which it would have been impossible to complete this work. I also would like to thank Professor Matti Vilenius for providing me with the opportunity to be the part of this wonderful research facility and his support during the years.

My special thanks to Prof. Jouni Mattila and Prof. Mikko Siuko for organizing the ITER project. This offers wonderful and exciting possibilities for research work. I had invaluable discussions in the fields of hydraulics, control, robotics and mechanics with them and MSc. Hannu Saarinen. Many thanks to other colleagues at IHA for a great time and their company during the research work. Particular thanks to Janne Tuominen for providing the measurements for the thesis.

I would also like to acknowledge my family from whom I have stolen time for myself for the things that fascinate me. Their support has been a great motivation during my entire career. I am also grateful to my friends for their relaxing company, which always gives me energy to continue.

Finally, I would like to thank my love Minna for being part of my busy life, for her understanding and for providing support in the most difficult times.

TABLE OF CONTENTS

NOMENCLATURE

a	Constants in an equation	
$\boldsymbol{a_x}$	Operational-space actuator transfer-function vector	
$\boldsymbol{a_\theta}$	Joint-space actuator transfer-function vector	
$\boldsymbol{B_d}$	Desired impedance viscous matrix	[Ns/m], [Nms/rad]
$\boldsymbol{B_e}$	Environment impedance viscous matrix	[Ns/m], [Nms/rad]
$\boldsymbol{B_x}$	Operational-space Coriolis and Centrifugal matrix	[Ns/m], [Nms/rad]
$\boldsymbol{B_\theta}$	Joint-space Coriolis and Centrifugal matrix	[Ns/m], [Nms/rad]
b	Viscous friction coefficient	[Ns/m], [Nms/rad]
b_d	Desired impedance viscosity	[Ns/m], [Nms/rad]
b_e	Environment viscosity	[Ns/m], [Nms/rad]
b_{eff}	Effective bulk-modulus	[Pa]
d	Specific volume	[m^3/rad]
$\boldsymbol{F_t}$	Force transformation matrix	
$\boldsymbol{f}$	Operational-space force vector	[N], [Nm]
$\boldsymbol{f_c}$	Operational-space command force vector	[N], [Nm]
$\boldsymbol{f_e}$	Operational-space contact force vector	[N], [Nm]
$\boldsymbol{g}$	Gravity vector	[m/s^2]
$\boldsymbol{g_x}$	Operational-space gravity force vector	[N], [Nm]
$\boldsymbol{g_\theta}$	Joint-space gravity force vector	[N], [Nm]
h	General function	
$\boldsymbol{h_{fk}}$	Forward kinematic function vector	
$\boldsymbol{h_{ik}}$	Inverse kinematic function vector	
i	Link/joint/matrix row index	
$\boldsymbol{J}$	Manipulator Jacobian matrix	
j	Operational-space/matrix column index	
$\boldsymbol{K_d}$	Desired impedance stiffness matrix	[N/m], [Nm/rad]
$\boldsymbol{K_e}$	Environment stiffness matrix	[N/m], [Nm/rad]
$\boldsymbol{K_{fx}}$	Operational-space force controller matrix	[V/N], [V/Nm]
$\boldsymbol{K_{f\theta}}$	Joint-space force controller matrix	[V/N], [V/Nm]
$\boldsymbol{K_{px}}$	Operational-space position controller matrix	[V/m], [V/rad]
$\boldsymbol{K_{p\theta}}$	Joint-space position controller matrix	[V/m], [V/rad]
k	Gain	

k_a	Acceleration feedback gain	$[\mathrm{Vs^2/m}]$, $[\mathrm{Vs^2/rad}]$
k_c	Commanded stiffness	$[\mathrm{N/m}]$, $[\mathrm{Nm/rad}]$
k_{cr}	Critical gain	
k_d	Desired impedance stiffness	$[\mathrm{N/m}]$, $[\mathrm{Nm/rad}]$
k_e	Environment stiffness	$[\mathrm{N/m}]$, $[\mathrm{Nm/rad}]$
k_f	Force controller	$[\mathrm{V/m}]$, $[\mathrm{V/rad}]$
k_h	Feedback gain	
k_p	Position controller	$[\mathrm{V/m}]$, $[\mathrm{V/rad}]$
k_q	Flow coefficient	$[\mathrm{m^3/V}]$
k_{qa}	Velocity gain	$[\mathrm{mV/s}]$, $[\mathrm{radV/s}]$
k_r	Robot passive stiffness	$[\mathrm{N/m}]$, $[\mathrm{Nm/rad}]$
k_s	Hydraulic spring constant	$[\mathrm{N/m}]$, $[\mathrm{Nm/rad}]$
k_v	Velocity feedback gain	$[\mathrm{Vs/m}]$, $[\mathrm{Vs/rad}]$
l_{ce}	Leakage coefficient	$[\mathrm{m^3/Pa}]$
$\boldsymbol{M}$	Inertia matrix	[kg], $[\mathrm{kgm^2}]$
$\boldsymbol{M_d}$	Desired impedance inertia matrix	[kg], $[\mathrm{kgm^2}]$
$\boldsymbol{M_x}$	Operational-space inertia matrix	[kg], $[\mathrm{kgm^2}]$
$\boldsymbol{M_\theta}$	Joint-space inertia matrix	[kg], $[\mathrm{kgm^2}]$
m	Operational-space DOF	
m_d	Desired impedance inertia	[kg], $[\mathrm{kgm^2}]$
m_i	Inertia of the link i	[kg], $[\mathrm{kgm^2}]$
n	Joint-space degrees of freedom	
p_d	Pressure difference	[Pa]
p_A	Pressure in chamber A	[Pa]
p_B	Pressure in chamber B	[Pa]
p_N	Nominal pressure	[Pa]
p_S	Supply pressure	[Pa]
p_T	Tank pressure	[Pa]
q	Flow	$[\mathrm{m^3/s}]$
q_A	Flow in chamber A	$[\mathrm{m^3/s}]$
q_B	Flow in chamber B	$[\mathrm{m^3/s}]$
q_N	Nominal flow	$[\mathrm{m^3/s}]$
q_S	Supply flow	$[\mathrm{m^3/s}]$
q_T	Tank flow	$[\mathrm{m^3/s}]$

$\boldsymbol{R}$	Rotation matrix	
r	Roots of the equation	
$\boldsymbol{S}$	Singular value matrix	
s	Laplace operator	
t	Time	[s]
t_{set}	Settling time	[s]
t_s	Sampling time	[s]
$\boldsymbol{U}$	Orthonormal output basis matrix	
$\boldsymbol{u}$	Orthonormal output basis vector	
u	Control signal	[V]
$\boldsymbol{u_{fx}}$	Operational-space force control signal vector	[V]
$\boldsymbol{u_{f\theta}}$	Joint-space control force signal vector	[V]
$\boldsymbol{u_{px}}$	Operational-space position control signal vector	[V]
$\boldsymbol{u_{p\theta}}$	Joint-space control position signal vector	[V]
u_f	Force control signal	[V]
u_p	Position control signal	[V]
$\boldsymbol{V}$	Orthonormal input basis matrix	
$\boldsymbol{v}$	Orthonormal input basis vector	
v_o	Average contained volume in the chambers	[m^3]
w	Dynamic manipulability function	
w_1	Dynamic manipulability index	
$\boldsymbol{x}$	Operational-space position vector	[m], [rad]
$\boldsymbol{x_c}$	Operational-space commanded position vector	[m], [rad]
$\boldsymbol{x_d}$	Desired position change vector	[m], [rad]
$\boldsymbol{x_e}$	Environment position vector after contact	[m], [rad]
$\boldsymbol{x_o}$	Environment position vector before contact	[m], [rad]
$\boldsymbol{Z_d}$	Desired impedance matrix	
$\boldsymbol{Z_e}$	Environment impedance matrix	
z	Z-transform operator	
z_d	Desired impedance	
z_0	Open-loop position overshoot	[m], [rad]
$\boldsymbol{\theta}$	Joint-space position vector	[m], [rad]
θ	Joint position	[m], [rad]
$\boldsymbol{\theta_c}$	Joint-space commanded position vector	[m], [rad]

$\boldsymbol{\theta_d}$	Desired joint position change vector	[m], [rad]
$\boldsymbol{\theta_e}$	Environment joint position vector after contact	[m], [rad]
θ_e	Position after contact	[m], [rad]
$\dot{\boldsymbol{\theta}}_{\mathbf{0}}$	Null-space joints' velocity vector	[m/s], [rad/s]
$\boldsymbol{\Delta_n}$	Natural damping matrix	
δ	Desired damping	
δ_n	Natural damping	
σ	Singular value	
$\boldsymbol{\tau}$	Joint-space force vector	[N], [Nm]
τ_b	Viscous friction force	[N], [Nm]
$\boldsymbol{\tau_c}$	Joint-space command force vector	[N], [Nm]
$\boldsymbol{\tau_e}$	Joint-space force vector due to contact	[N], [Nm]
τ_e	Force due to contact	[N], [Nm]
$\boldsymbol{\Omega_n}$	Natural frequency matrix	[rad/s]
ω	Desired frequency	[rad/s]
ω_n	Natural frequency	[rad/s]
$\mathcal{L}$	Lagrangian	[J]
$\mathcal{T}$	Kinetic energy	[J]
$\mathcal{U}$	Potential energy	[J]
Ч	Dynamic manipulability matrix	
Ж	Quadratic dynamic manipulability matrix	
ж	Element of matrix Ж	

ACRONYMS

ADC	Analogue to Digital Converter
CMM	Cassette Multifunctional Mover
DAC	Digital to Analogue Converter
DME	Dynamic Manipulability Ellipsoid
DOF	Degrees Of Freedom
DTP2	Divertor Test Platform
HPU	Hydraulic Power Unit
IHA	Department of Intelligent Hydraulics and Automation
ITER	'The Way' in Latin (fusion experimental reactor)
LVDT	Linear Variable Differential Transformer
MAE	Mean Absolute Error
PCI	Peripheral Component Interconnect
RAMS	Reliability, Availability, Maintainability and Safety
TUT	Tampere University of Technology
VTT	Technical Research Centre of Finland
WHMAN	Water Hydraulic MANipulator

1 INTRODUCTION

The idea of manipulating the surrounding environment is so fundamental in nature that it guided evolution itself (Gibson, 1986) and eventually resulted in the evolution of the ultimate manipulator: human. Our appetite for manipulation has taken itself beyond the boundaries of our own environment to the deepest oceans, outer space and even further to extra-terrestrial worlds.

In the above perspective, many tools and machines around us can be considered as manipulators. According to the Robot Institute of America:

"A robot is a reprogrammable multifunctional manipulator designed to move materials, parts, tools or specialized devices through variable programmed motions for the performance of a variety of tasks."

The definition was put forwarded in 1979 and is still widely accepted (Sciavicco, et al., 2001). This definition more or less manages to shortlist the machines which are generally considered as robots or manipulators in today's industry.

The first commercial prototype of an industrial manipulator was developed by Unimation Inc. with the name of *'Unimate'* in 1959 (Encyclopædia Britannica, 2009a).The Unimate was installed at a General Motors™ die-casting plant in Trenton, New Jersey. Later, several of these manipulators were developed by Condec Corp. and installed on the assembly line to work with die-casting machines and to perform spot welding on the bodies of automobiles. In Figure 1.1 the Unimate manipulator is shown in operation at a General Electric™ assembly line.

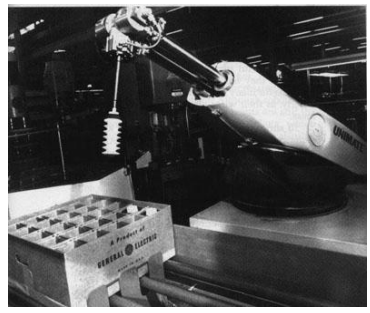

Figure 1.1: Unimate robot performing pick and place operation at General Electric™ (School of Computer Science at Carnegie Mellon University, 2006)

With ever-increasing requirements in production quantity and quality, manipulators are more in demand in industry than ever before. Over the course of five decades manipulators have

become an essential and often a major part of several industrial automation systems. Their abilities to perform tasks with high speed and repeatability with low operational cost have been significant factors for their choice in many production processes in today's industry. A short list of their industrial applications includes welding, painting, assembling, machining, inspection, packaging, sorting, etc., which shows that manipulators are an important part of every stage of modern production processes (Craig, 2004).

From the application point of view manipulators can be categorized as general purpose or special purpose manipulators. General purpose or industrial manipulators are robotic arms with six or less degrees of freedom usually driven by a similar number of joints and equipped with a programmable control system. The task of the manipulator can be varied and configured considerably as per changing requirements of the product and production process. The robotic arm and its control system are selected to be dexterous and flexible according to the range of foreseeable tasks. The joints of these manipulators are driven by electrical, hydraulic or pneumatic actuators depending on the size, payload capacity, maintainability and other performance requirements. Today many industrial manipulators are available off the shelf from the market. These manipulators are highly standardized with few possible alterations provided by the manufacturers. Some of the famous configurations of these manipulators are Cartesian, gantry, cylindrical, spherical, SCARA and anthropomorphic (Sciavicco, et al., 2001).

However, in several cases these general purpose industrial manipulators are not capable of fulfilling the performance requirements of the task. The limitation could either be imposed by the task itself or from the environment in which the task needs to be executed. In many cases the possible variations and demands of the tasks cannot be completely defined and the manipulator is designed to cope with a variety of unforeseeable situations. Not only do these manipulators provide extra degrees of freedom, but they may also be equipped with specialized actuators and sensors to execute the task and withstand environmental effects. Underground rock drilling (Poole, et al., 1998), highly radioactive nuclear power plants (Eickelpasch, et al., 1996), unliveable conditions of space (Brooks, et al., 1992), (Lane, et al., 2001) and high pressure areas of ocean depths (Yuh, 2000) are but few of such environments. Human presence in such environments is undesirable and it can become too expensive to protect them from possible dangers. This ability to perform in such harsh, hazardous and hostile environments makes the use of manipulators most advantageous.

As an example, the Canadarm installed in the NASA space shuttle has been able to reduce the number of man-missions outside the shuttle by successfully carrying out several assembly operations on the International Space Station (ISS) and other satellites remotely (Aikenhead, et

al., 1983), (Mamen, 2003). For the same reasons, ISS is also equipped with several specially designed manipulators such as Canadarm2 and Japanese Experiment Module Remote Manipulator System (JEMRMS) (Matsueda, et al., 1991). By 2011 the European Robotic Arm (ERA) is also planned to be added to the ISS (European Space Agency, 2006). A comparison between these manipulation systems is given in (Patten, et al., 2002). Photographs of Canadarm and Canadarm2 during space missions are shown in Figure 1.2.

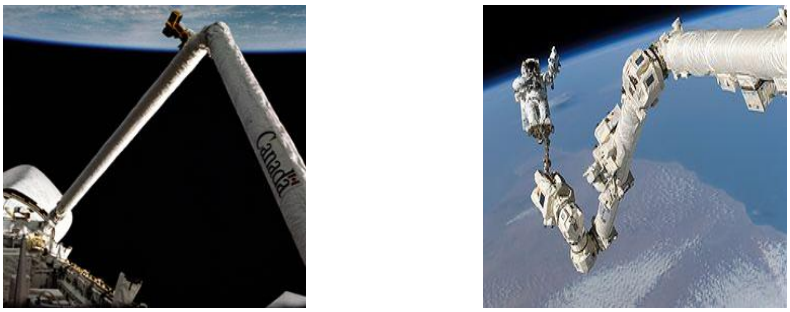

Figure 1.2: Canadarm in NASA space shuttle (left); Canadarm2 anchoring an astronaut (right). Source: Canadian Space Agency (Mamen, 2003)

Operations within these environments bring up not only the need for robots but also the concept of controlling, manipulating and operating them from the remote site. Teleoperation is a term associated with manipulators which are remotely controlled by the operator. The operator sits in a room, distant and safe from the dangers of the site, while he can fully perform the operations and control the robot at the site. The link between operator and manipulator can be mechanical, electrical or wireless.

The remote handling maintenance operations in the ITER ("journey" or "way" translated in Latin) fusion reactor are another example of highly specialized application which requires the development and testing of several new technologies related to manipulation. ITER is a part of a series of fusion experimental reactors which are meant to investigate and demonstrate the feasibility of using fusion as a practical source of energy (Smith, 2005), (Shimomura, 2004). The presence of beta and gamma activated components within the vessel, together with hazardous dust, preclude the possibility of any human access and require the use of special remotely operated equipment for the maintenance of the ITER reactor (Honda, et al., 2002).

The nuclear industry is not unfamiliar to teleoperation or the remote handling of manipulators. In fact, the first recognizable master-slave teleoperation system was invented by Goertz in 1949 for radioactive hot lab work (Goertz, 1952a), (Goertz, 1954a). These were two identical arms, with a slave arm in direct vision of the operator behind a one meter thick quartz window.

Corresponding joints of two manipulators were connected by flexible stainless steel ribbons running over pulleys. In the 1950's Goertz further improved the system with the use of electric-servo drive and close circuit video (Goertz, et al., 1952), (Goertz, et al., 1954). The limitation of fixed distance between the operator and slave manipulator disappeared and it was capable of performing in a more challenging environment such as along the whole length of a particle accelerator. In modern times such teleoperation systems driven by electrical actuators have become very sophisticated and are used with a high degree of reliability and efficiency (Rolfe, 2007), (Armada, et al., 2000), (Winfield, 2000).

Compared to previous fusion experimental reactors, the weight of the remotely handled reactor components and tooling in ITER is much larger, resulting in lower operational velocities and higher forces. The compactness of space and high load capacity limit the possibility of using electrically driven manipulators. As high forces are required with compact size actuators, hydraulics is a choice of interest in this application. Simple construction and high reliability are added advantages of hydraulics. It has been proving its worth in applications like automobiles, excavators and airplanes with a high degree of reliability and low maintenance (Measson, et al., 2003).

Much research has been done in the past regarding the teleoperation of hydraulic manipulators for industrial applications (Sepehri, et al., 1994), (Kosuge, et al., 1997), (Parker, et al., 1993), (Gravez, et al., 2003). Teleoperated hydraulic manipulators (Figure 1.3) are available off the shelf to perform demanding tasks under hostile conditions (ALSTOM, 1999), (Cybernetix, 2001), (Kraft TeleRobotics, Inc., 2009). However, these teleoperated hydraulic manipulators use oil as the pressure medium. While oil is a sufficiently good medium for the power transmission in most applications, it has several drawbacks, such as contamination of the environment with external leakages and activation from radioactivity. Both of these characteristics are highly undesirable in the ITER environment.

With developments in water hydraulics (Siuko, et al., 2003) (water is used as a pressure medium rather than oil), there is a possibility of using hydraulic manipulators for the maintenance of the ITER reactor. The advantages of hydraulics together with the characteristics of water as the pressure medium (fire and environmentally safe, chemically neutral, not activated and not affected by radiation) are highlighted in the remote handling operations of ITER (Vilenius, et al., 2002a), (Maisonnier, et al., 2001).

Figure 1.3: Maestro manipulator from Cybernetix (left) (Cybernetix, 2001); Titan manipulator from Schilling Robotics (right) (ALSTOM, 1999); Raptor manipulator from Kraft TeleRobtics Inc. (Kraft TeleRobotics, Inc., 2009)

The Department of Intelligent Hydraulics and Automation at Tampere University of Technology (IHA/TUT) has participated in the European FUSION program since 1994 for the development of ITER remote handling technologies (Siuko, 1998). IHA in collaboration with the Technical Research Centre of Finland (VTT) has been involved in the development of a remote handling system for divertor maintenance activities. The remote handling system and maintenance concepts will be tested and verified at Divertor Test Platform (DTP2), which is a full scale mock-up facility located at VTT (Palmer, et al., 2005). The participation of IHA in ITER divertor maintenance is related to the design, development and testing of remote handling equipment (Palmer, et al., 2007), (Takalo, et al., 2009) and to its expertise in the field of water hydraulics (Koskinen, et al., 1999), (Linjama, et al., 2002), (Riipinen, et al., 2003), (Virvalo, et al., 1999b).

1.1 Background

The divertor region of the ITER fusion reactor contains 54 modules namely cassettes, each weighing 9 to 10 tons. These cassettes are protected with plasma facing components which may

be damaged during the plasma operations. These cassettes need to be removed, refurbished and reinstalled into the reactor through the three service ducts available across the perimeter of the divertor (Vilenius, et al., 2002). The divertor remote handling operations are very demanding due to the sheer size and the weight of the components and due to the constricted space around the components. In addition, reliability, availability, maintainability and safety (RAMS) are prime requirements of the teleoperation system. A detailed description of remote handling requirements for ITER can be found in (Burgess, et al., 1998).

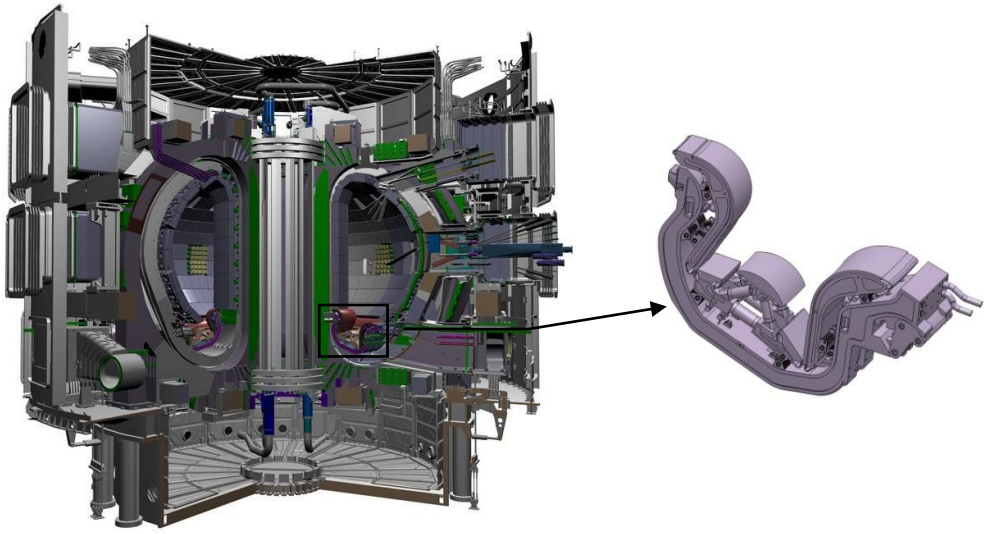

Figure 1.4: 3D model of ITER fusion reactor with a cross section of vacuum vessel (left); Magnified view of divertor modules (right)

A dexterous manipulator capable of assisting during the remote handling operation of removal and installation of these cassettes is required. For this purpose a manipulator named WHMAN (Water Hydraulic MANipulator) and its control system has been developed at IHA/TUT (Muhammad, et al., 2007). The specifications of this manipulator are given in (EADS Astrium, 2008). WHMAN is composed of eight joints: six rotational and two translational. Since a manipulator requires only six joints to acquire the desired position and orientation in operational-space, the two additional joints of WHMAN provide redundant degrees of mobility. This redundancy and dexterity is useful to cope with the demands of remote handling tasks inside the ITER divertor maintenance tunnel (Muhammad, et al., 2010a).

The environment inside the ITER reactor is noncompliant and the remote handling tasks can only be defined approximately. A strictly position-controlled manipulator (Muhammad, et al., 2009b) can result in damaging the reactor and the manipulator itself and thus cannot be

employed in such a situation. Some sort of force control along with the position control needs to be implemented for the WHMAN to be used in the remote handling system.

A possible approach to meet this requirement is to employ impedance control (Hogan, 1985). In impedance control, the idea is not to regulate either the position or the force but to regulate the dynamic and static relationship between the two. This technique has been reported as successful for various industrial manipulators driven by electric (Ferretti, et al., 2000), (Surdilovic, 2007), pneumatic (Richardson, et al., 2005) and hydraulic (Heinrichs, et al., 1997) actuators. The implementation and investigation of impedance control for redundant WHMAN can provide some useful results and insight.

Previously the effects of redundancy on the kinematic manipulability of the manipulators have been studied. Kinematic constraints such as mechanical limits, kinematic singularities and obstacles in the workspace can be avoided by the use of redundant degrees of freedom (Klein, et al., 1987), (Maciejewski, et al., 1985), (Yoshikawa, 1985a). The dynamic manipulability of manipulators has been studied by (Yoshikawa, 1985). The concept was further refined by the inclusion of gravitational forces by (Chiacchio, et al., 1991), who later proposed the more accurate characterization of dynamic manipulability for redundant manipulators (Chiacchio, et al., 1998). However, the effect of redundancy on the dynamic manipulability of a manipulator has not been considered.

1.2 Motivation

The motivation for this thesis is to study the effects of kinematic redundancy on the dynamic manipulability of manipulators such as WHMAN. The goal is to develop suitable control strategy for this manipulator to be employed in the remote handling operations of ITER divertor maintenance. In addition, since the remote handling tasks of WHMAN require both position and force control, the impedance control properties of the manipulators with redundant degrees of freedom are studied. The effect of dynamic manipulability is studied using the impedance controller designed for the manipulator. As a result suitable posture and the trajectories for the manipulator can be planned for the execution of remote handling tasks by exploiting these redundant degrees of mobility.

1.3 Objectives of the thesis

The objective of the thesis is to investigate the effects of kinematic redundancy on the dynamic manipulability of the manipulators, and to implement and study the impedance control for kinematically redundant manipulators. The goal is to find and suggest a suitable posture and trajectories for the manipulator for a given task, so that the better control of position and force can be applied, and hence to achieve the improved performance of impedance controller.

The position and force control properties of a water hydraulic vane actuator have been previously studied by (Raneda, 2004). The position-based implementation of impedance control was suggested to be more suitable due to practical limitations. The position-based approach for impedance control of hydraulic manipulators has also been suggested by other sources (Ha, et al., 2000), (Heintze, et al., 1995). In fact, the preference is so profound that the force-based implementation of impedance control has not been reported for hydraulic manipulators. An attempt has been made to further investigate the two approaches towards impedance control. In (Muhammad, et al., 2006) and (Muhammad, et al., 2009) the equivalence between position-based and force-based implementations was studied using a single degree of freedom. Here, the equivalence between these two implementations is further investigated for a general manipulator with multiple degrees of freedom. An attempt has been made to find theoretical and experimental equivalence between the two. The two implementations are also considered from the practical implementation point of view.

A further objective is to implement and verify these findings for the water hydraulic manipulator, so it can be used in a remote handling system developed for the ITER divertor environment. Since the manipulator is composed of water hydraulic components which normally exhibit higher and often inexact values of friction and leakages as compared with oil hydraulic components, therefore the idea is to find suitable control strategies to compensate for these shortcomings.

The main objectives of the thesis can be summarized as:

- To study the effects of kinematic redundancy on the dynamics and impedance control properties of the manipulators.
- To study the different implementations of impedance control for manipulators and study the equivalence between them.
- To practically implement and verify these findings for the WHMAN which is designed to carry out the remote handling maintenance operations in ITER divertor.

- To compare the dynamic manipulability via impedance control performance of the WHMAN in redundant and non-redundant configurations.
- To keep the results applicable for other applications and motivate studies from other researchers.

1.4 Limitations

The research work is concerned with the study of the effects of kinematic redundancy on the dynamic manipulability and the impedance control of manipulators. The controller has been designed and the theoretical findings verified using the WHMAN, which is a kinematically redundant manipulator.

Mechanical design and material properties of manipulator are not discussed in this thesis. The selection of sensors, water hydraulic components and other limitations imposed by the radioactive environment of ITER are beyond the scope of this work. Also the main requirements pertaining to mission critical operations such as reliability, availability, maintainability and safety (RAMS) have been taken into account in the design of WHMAN and its control system (Nieminen, et al., 2009), but these are not discussed here.

The theoretical developments are kept general without restriction to any particular manipulator, so they are applicable for other manipulators driven by oil hydraulics, pneumatics or electrical actuators. However, verification with any other type of manipulator has not been performed. The implementation of the controllers and the experiments are only performed with the WHMAN.

Rigid body dynamics are considered for manipulators, bearing in mind the fact that a wider variety of industrial manipulators can be modelled as nonflexible manipulators. Studies of manipulators with flexible links are not reported in this work.

An objective of the thesis is to study and develop control techniques for the WHMAN, which is designed to carry out remote handling operations in ITER divertor. However, the design of the teleoperation system and the performance of the manipulator during teleoperation is not evaluated and presented in this work.

Each actuator of WHMAN is equipped with two pressure sensors, which is standard practice for hydraulic manipulators. The measurements from these pressure sensors have been used at

several stages, for example, for the verification of the simulation models. However, pressure sensors are not used to determine the actuator forces for control purposes. Though it provides a cheaper solution, the idea was not found very appealing as it leaves out the significantly high friction forces in water hydraulic actuators and the gravity forces out of the control loop. Instead, a six-axis force/torque sensor attached to the wrist of the manipulator has been used to directly measure the environmental contact forces and use them to compute the control signal.

1.5 Research methods

The theoretical discussions and results in the thesis regarding impedance control and the effects of redundancy on the dynamic performance of a manipulator have been kept general without references to any particular manipulator. The purpose is to keep the findings useful for other developments and continue the research and discussion process on a wider scale. In the latter part of the thesis, WHMAN has been used for the numerical analysis, simulations and experimental verification of the theoretical results.

Both analytical and simulation models of WHMAN are utilized in this study. Initially, the analytical model of WHMAN in the form of so-called state space equation has been presented. This model has been utilised for the mathematical analysis and numerical verification of the theoretical results.

The simulation model of a single vane actuator of WHMAN is used as the starting point towards the simulation modelling of the entire manipulator. For the nonlinear model of the vane, some parameters such as friction, leakage, etc. have been obtained experimentally and several other parameters such as valve flow coefficient, valve hysteresis, etc. are obtained from the manufacturer's datasheet. Due to the availability of rich set of tools in linear control theory a linear model of the system is often desirable. The linear model can be used for theoretical analysis and for the preliminary controller design. Both linear and nonlinear models of this vane actuator are presented and verified against the measurements obtained from the actual vane actuator.

These developments are then carried on to be used in the designing of the simulation model of complete manipulator. The simulation model is developed using the Matlab/Simulink® and the Matlab/SimMechanics® toolboxes. This model of WHMAN is then verified against the pressure differences, velocity and tracking error measurements of the joints' actuators of the actual

manipulator. Developments from the linear model of a single vane actuator have been used to develop the linear model for each joint of WHMAN. These linearized models are utilized for the preliminary development of the position controllers. These controllers are then fine tuned using the nonlinear model of the manipulator.

The position controllers, kinematic solution and the desired impedance are then programmed into the Matlab/Simulink® along with the nonlinear model of the manipulator. The theoretical developments of the thesis: the effects of kinematic redundancy on dynamic manipulability and the equivalence between position and force based implementations of impedance controller are then studied through numerical simulations. The performance of the impedance controller is compared for both redundant and non-redundant configurations.

For the experiments the position controllers, kinematic solution and the desired impedance are programmed using the National Instruments/LabVIEW® which is used for the development of the control system of WHMAN. At this point the position controllers are further fine-tuned to compensate for the modelling inaccuracies. The theoretical and simulation results are compared against the experimental measurements of the real manipulator.

1.6 Contributions of this research

The main contributions of this research work are:

- Study of the effect of redundancy on dynamic manipulability and impedance control of a manipulator.
- Study of the equivalence of position-based and force-based implementations of impedance control for general n degrees of freedom case.
- Verified linear and nonlinear models of a single water hydraulic vane actuator.
- A verified model of the complete WHMAN which can be used for further study of control system, condition monitoring, task planning, etc.
- Experimental study of a redundant water hydraulic manipulator with impedance control.
- Performance estimation of impedance control in redundant and non-redundant configuration of a manipulator.

1.7 Structure of the thesis

The thesis is divided into 7 chapters covering the state of the art, presentation of hypotheses, development of tools desired for the research work, numerical simulations and experimental results. A brief description of each chapter is provided in the following paragraphs.

Chapter 2 provides the state of the art technologies relevant to the research work. The areas covered are: performance indices, impedance control, redundancy resolution of manipulators and water hydraulics. An effort has been made to comprehensively cover the impedance control of hydraulic manipulators.

In Chapter 3 the theoretical background is established for the thesis. The chapter starts with a description of the basic principles and leads to the formulation and mathematical presentation of hypotheses to be tested and verified in later chapters.

The modelling of the WHMAN is the subject of Chapter 4. Both analytical model and simulation models of WHMAN are presented in this chapter. For the simulation model, at first the linear and nonlinear models of a single actuator are derived and verified. Later, the model of the complete manipulator is presented and verified against the measured response.

Chapter 5 is dedicated to study of the theoretical developments via numerical analysis and simulations. The numerical analysis is done using the analytical model of WHMAN. The design of the impedance controller is presented and the results are verified using the nonlinear simulation model of the manipulator.

The experimental verification of the theoretical findings is presented in Chapter 6. The controllers developed and verified using the numerical simulations are implemented for the real manipulator. The obtained measurements are verified against the simulation results obtained in Chapter 5.

A summary and the conclusions of the research work are presented in Chapter 7. The chapter also contains a brief discussion about topics which may require further study and investigation.

Three appendices are added at the end of this thesis. Appendices A and B cover the description of the kinematics and the dynamic parameters of the WHMAN respectively. Appendix C provides a description of hydraulic system of the manipulator. Several tables have been used to list the essential parameters and their numerical values used in the simulation model and for the controller design.

2 STATE OF THE ART

This chapter is an attempt to cover the background and current status of the various technologies addressed in this thesis. A survey of the research work to specify certain performance indices for design and control of manipulators is presented in Section 2.1. Section 2.2 describes the state of the art in the impedance control of manipulators. The techniques for the resolution of redundant degrees of freedom in a manipulator are discussed in Section 2.3. Since a considerable amount of development and experimental work in thesis has been done with WHMAN (Water Hydraulic MANipulator), an overview of the relevant water hydraulic technologies is presented in Section 2.4

2.1 Performance indices of manipulators

Today, a majority of manipulation tasks in industry can be achieved by utilizing one of the many off the shelf standard industrial manipulators. These manipulators are available in various configurations, workspace envelops and load capacities. They are equipped with programmable control systems and can be programmed to execute a variety of tasks. However, a large number of applications require the employment of specialized manipulators. The design of such manipulators is based on performance indices such as workspace, load capacity, dynamic response, etc. It requires a great deal of experience and intuition to design a manipulator with optimized performance (Gupta, et al., 1982).

The selection of the manipulator structure and design can benefit if these performance indices can be quantified numerically. The design engineer can use these numerical values to make a meaningful comparison and choice among the competing designs. This can be useful to correctly select the link lengths and materials, and avoid actuator over-sizing (Kircanski, 1994). These indices are also useful in determining the optimum posture of the manipulator and to control it during the task planning and execution phases. These can be used, for example, to avoid singularities, avoid joint limits, minimize actuators' torques, etc. (Angeles, et al., 1992).

In principle, a manipulator is a highly nonlinear and complex mechanical structure and it is hard to quantify its performance with a single numerical value; nevertheless, such indices have been found useful for the design, evaluation and control of manipulators (Hollerbach, 1985), (Ranjbaran, et al., 1996), (Singh, et al., 1995), (Yoshikawa, 1985b).

The first such notable index was manipulability measure, which can be used to evaluate the manipulation capability of a mechanical structure (manipulator) in a given posture (Yoshikawa, 1984). For a given posture, the manipulability measure determines the capability of the manipulator to change its position/orientation in space or impart forces on the environment. The manipulability measure reduces to zero when the manipulator is in a singular position. Hence this measure can be effectively used to avoid the kinematic singularities in the manipulator's workspace.

Both the velocity and force manipulability of a manipulator can be presented as velocity manipulability ellipsoids and force manipulability ellipsoids respectively. The length of the ellipsoids' axes determines the velocity and force manipulation capability in a particular direction. The volume of the ellipsoid is proportional to the product of singular values of the manipulator's Jacobian and can be utilized to determine the optimum posture during task execution (Yoshikawa, 1985a). Several standard industrial manipulator structures have been analysed using this measure in (Yoshikawa, 1985b).

The majority of industrial manipulators are designed as an arm which is fitted with a spherical wrist at the end. The arm is primarily used to achieve the desired position and the wrist is used to achieve the desired orientation. In this way the problem of solving the kinematics can be decomposed and greatly simplified (Paul, et al., 1986), (Pieper, 1968). The manipulability measure can also be split into translational manipulability measure and rotational manipulability measure and can be used to determine and avoid arm and wrist singularities respectively. In fact, the total manipulability measure of the manipulator is the product of translational and rotational manipulability measures (Yoshikawa, 1991).

Several variations of this index have been used to study and optimize the design of kinematic structure of the manipulators. The conditioning index is defined as the percentage of the reciprocal of the minimum value of the condition number of the Jacobian of the manipulator's structure (Angeles, et al., 1992), which in fact determines the invertibility of the Jacobian matrix. The ratio of the largest and the smallest singular values of the Jacobian matrix have been termed the dexterity measure (Kircanski, 1994). The measure has been used to determine the isotropy of the manipulators, which is defined as the capability to achieve similar manipulability in all directions. Another way to obtain dexterity measure is to use the ratio of the norm of the Jacobian matrix and the smallest singular value. This determines the lowest bound on the joint velocity, which is a sufficient condition to preserve the rank of the Jacobian matrix (Mayorga, et al., 1990).

The above indices describe the static and kinematic characteristics of the manipulator. A similar index is the dynamic manipulability measure to determine the dynamic performance of the manipulator in a given posture (Yoshikawa, 1985). The measure provides dynamic manipulability ellipsoids whose axes' lengths are given by the singular values of the matrix, which is the product of manipulator's Jacobian and inverse of its inertia matrix. The lengths of these axes determine the manipulator acceleration capability in a particular direction. The effect of gravitational forces can be included in the dynamic manipulability measure, which results in the translation of the centre of dynamic manipulability ellipsoid without affecting its volume (Chiacchio, et al., 1991). (Chiacchio, et al., 1998) later proposed a more accurate characterization of dynamic manipulability for redundant manipulators. A combination of dynamic manipulability measure and force manipulability ellipsoid can be utilized to determine the robot compliant motion capabilities (Koeppe, et al., 1997).

The acceleration radius is another index used for the evaluation of dynamic performance (Graettinger, et al., 1988). Acceleration radius is the formulation of the end-effector's acceleration in terms of upper and lower bounds on the actuators' torques. The criterion determines the isotropic acceleration capability of the manipulator in the operational-space. The isotropic acceleration and inertial characteristics were also considered in the measure termed motion isotropy hyper-surface (Bowling, et al., 1998). This measure optimizes the dynamic manipulability ellipsoid so that its surface is tangent to the cube defined by the upper and lower bounds on the torques. On the basis of this technique a cost function comprising the norms and condition numbers of the manipulator's mass, inertia and normalized Jacobian matrices (Khatib, et al., 1996) can be formulated. The manipulator's Jacobian and inertia matrices can be decomposed to separately investigate the dynamic capability of the arm and wrist. This approach is also helpful to avoid discrepancies among the translational and rotational units of inertia, position, velocity, acceleration and force.

2.2 Impedance control

The primary purpose of a robot is to perform certain manipulation tasks in its environment. These manipulation tasks can be categorized into two major classes: non-contact tasks and contact tasks. In the case of non-contact tasks, a manipulator performs motions in an unconstrained environment and follows defined position trajectories in free space. Spray painting, welding and simple pick-and-place operations (when the geometry of the object and

the environment is known accurately) are examples of non-contact tasks where position control of manipulators can provide satisfactory performance.

However, a wide variety of robot applications require the end-effector of the manipulator to come into contact with unknown environment and perform complex manipulation tasks. This category of manipulation tasks is classified as contact tasks. Assembling, drilling and machining are a few examples of contact tasks where motions through unstructured and insufficiently known environments are required. In such cases, operational-space force control of manipulators becomes essential. Force control manipulators, though not a new topic, nevertheless remain an interesting one. An overview of force control of manipulators can be found in (Whitney, 1985), (De Schutter, et al., 1998).

In exclusive force control a desired force is commanded to the manipulator in operational-space rather than the position or the velocity as the input (Volpe, et al., 1993). It is possible to avoid the use of force sensor and instead force can be obtained as a product of position error and defined stiffness (Uebel, et al., 1992). However, an explicitly force controlled manipulator is of very little use in most applications. In practice, some sort of position control is always desired along with the force control. Two major approaches have been widely adopted for simultaneous control of force and position of manipulators: hybrid force/position control (Raibert, et al., 1981), (Khatib, 1987), (Chiaverini, et al., 1993) and impedance control (Hogan, 1985), (Field, et al., 1993).

In hybrid force/position control, the operational-space is divided into degrees of freedom in which either position or force is controlled. The force controlled is applied in the directions normal to the contact surface, while position is controlled along the other directions. Direct force control involves the use of measured or calculated contact force error to compute the desired forces of the joints of the manipulator (Raibert, et al., 1981). Several other variations of hybrid force/position control exist. The joints' positions, velocities and the dynamic model of the manipulator can be used to compute the desired joints' torques to follow the desired force trajectory in the operational-space. The technique can also be employed by utilizing only the position feedback and avoiding the noisy velocity feedback (Gourdeau, et al., 1999).

In the case of impedance control, a dynamic relationship between position and force at the end-effector of the manipulator is controlled rather than position or force. Hybrid force/position control and impedance control have also been combined into hybrid impedance control (Anderson, et al., 1988), which allows the simultaneous regulation of impedance and either force or position. In this case the operational-space is decomposed into purely motion controlled directions and purely force controlled directions. The impedance control is used in position

controlled directions to achieve the compliant motion. The desired values of inertia and damping can be introduced in the force controlled direction to improve the dynamic behaviour of the manipulator (Liu, et al., 1991).

The objective of an impedance controller is to establish a desired dynamic relationship between the end-effector position and the environment contact forces. The feedback loops at the manipulator joints are closed in a way that the manipulator appears as specified impedance to its environment, which, in turn, behaves as admittance to the manipulator. Two types of implementations of impedance control have been investigated and implemented since its introduction (Hogan, 1985): position-based implementation and force-based implementation. Position-based implementation consists of an inner position feedback loop with an outer force feedback loop. In this approach the contact force information is used to modify the desired position of the end-effector. In effect, this implementation softens a stiff position source. The force-based implementation consists of an inner force feedback loop with an outer position feedback loop. In this approach, position is measured and force commands are issued to meet the target impedance. In effect, this implementation stiffens a soft force source.

Most research on impedance control deals with electrical manipulators, where the actuator torque is proportional to the input current. In such cases force control of the manipulator can be straightforward and an internal force loop can easily be implemented. However, most research has been concentrated on the position-based implementation of impedance control (Bruni, et al., 1996), (Carignan, et al., 1997), (Matko, et al., 1999). As most of the industrial manipulators are readily provided with a position servo controller, position-based implementation can avoid redesign of the controller. The added difficulty of force-based implementation is the requirement of velocity and acceleration feedbacks in the outer loop (Lawrence, 1988). Though these measurements can be obtained by numerical differentiation of position and velocity signals from the joints' position sensors, this will result in the amplification of quantization noise and the obtained signal will not be useful for the control anymore. A possibility is to obtain the reference acceleration signal from the desired impedance model and use it to drive the required joints' forces (Goldenberg, 1988). The estimation of the desired trajectory can also be performed either by using force error or by estimating the environmental parameters (Seraji, et al., 1993).

The position-based implementation of impedance control is well-suited for application where the environment is more compliant and higher stiffness values are required. On the other hand, the force-based implementation of impedance control is better suited to provide a small degree

of stiffness when the environment is noncompliant. It is suited where manipulator gravity loads are well compensated and motions are slow (Lawrence, 1988).

Considering the manipulator as an ideal position source, the impedance controller should mask the original dynamics of the manipulator and introduce the new desired dynamics such that the manipulator behaves as the desired impedance to the environment. In practice this is difficult to achieve for complicated nonlinear systems such as manipulators. A technique referred to as computed torque control has been proposed to deal with nonlinearities of manipulator structure (Khosla, et al., 1988). The computed torque method is a nonlinear control law which results in linearized and decoupled dynamics (Fu, et al., 1987), (Craig, 2004) and hence improves the design and performance of position controller in the inner loop. However, the technique is heavily dependent on the accuracy of the manipulator's dynamic model and sensitive to robot parameters (An, et al., 2003). In practice it is difficult to know the accurate values of these parameters and they may change over time or in some cases may be completely unavailable. However, the technique has been successfully used to improve the tracking performance of robots with flexible and geared joints (Bayo, 1988). Apart from structural nonlinearities the model of a manipulator contains a fair number of uncertainties which are difficult to determine and model, such as frictions and backlashes. To overcome these nonlinearities and uncertainties researchers have proposed adaptive (Colbaugh, et al., 1991), (Lu, et al., 1991), robust (Harada, et al., 1992) and observer-based (Henriksson, et al., 2001), (Jassemi-Zargani, et al., 1995) techniques for impedance control.

The force control of manipulators driven by hydraulic actuators is not so straightforward and presents considerable challenge (Tafazoli, et al., 1998). Hydraulic actuators are essentially position/velocity sources, where actuator velocity is proportional to input valve voltages, in contrast to electrically driven manipulators where actuators are torque sources and torque is proportional to the input control signal. Also, the nonlinear behaviour of pressure dynamics inside the chambers of hydraulic actuators and other nonlinearities such as friction, non-linear flow, leakage, etc. make the control of actuator forces much more difficult (Watton, 1989).

Position-based implementation of impedance control has been widely applied and reported for hydraulic manipulators (Heinrichs, et al., 1997), (Bilodeau, et al., 1998), (Muhammad, et al., 2010). In all these implementations a same second order impedance transfer function has been used in the outer loop. A notable variation is in the inner loop providing the position control, the performance of which plays a vital role in the position-based implementation of impedance controller. If the manipulator is assumed to be equipped with an ideal position controller (reference and feedback position match all the time or at least with negligible dynamics) the

desired second order dynamics can be imposed with the outer loop (Matko, et al., 1999), (Seraji, et al., 1993a).

The assumption of an ideal position controller which can hide the original dynamics of the manipulator can be valid in the case of small manipulators with high bandwidth. Hydraulic manipulators are considerably large in size, designed to manipulate heavier loads and the hydraulic actuators depict much more nonlinear behaviour. Thus, the dynamics of hydraulic manipulators are not easy to overcome with a position controller. It is normally desirable to identify and compensate for the dynamics and nonlinearities of hydraulic manipulators (Tafazoli, et al., 1999). A possible approximation is to consider the inner position loop as a first order system and compensate the dynamics with a stabilized inverse of this first order system (Salcudean, et al., 1997).

Even with an idealized position controller the values of the desired dynamic parameters cannot be chosen arbitrarily and have to fulfil the condition of stability (Tafazoli, et al., 2002). In addition, the stiffness of the manipulator cannot be lowered infinitely and the lowest value is bounded by the stiffness of the environment (Heinrichs, et al., 1999). The dynamics of the environment need to be taken into consideration when selecting the desired dynamic parameters for the manipulator. An improper selection of parameters can lead to a completely unstable system on coming into contact with the environment (Eppinger, et al., 1992).

The force-based implementation of impedance control for hydraulic manipulators is more challenging as it requires the tuning of highly nonlinear inner force loop and requires velocity and the acceleration feedbacks in the outer loop (Lawrence, 1988). Force-based implementation for hydraulic manipulators has been studied only recently (Muhammad, et al., 2006), (Muhammad, et al., 2009). Also a relationship between position-based and force-based implementations of impedance control was obtained and it was shown that equivalent controllers can be obtained using the relationship for single degree of freedom.

It is widely understood that equivalence exists between explicit force control and impedance control. Both types of controllers can be converted to each other, and when optimized should have similar bandwidths (De Schutter, et al., 1998). Expressions to obtain equivalent position-based impedance controller and explicit force controllers have been derived, implemented and verified by several researchers, for example (Heinrichs, et al., 1999), (Volpe, et al., 1995).

2.3 Redundancy resolution

A manipulator is required to have a minimum of six degrees of freedom if it needs to be able to acquire any random position and orientation in operational-space. Assuming one joint is required for each degree of freedom, such a manipulator needs to be composed of a minimum of six joints. A standard practice is to implement three degrees of freedom in the robotic arm so it can acquire the desired position in the operational-space. The arm is then fitted with a wrist composed of three joints to acquire the desired orientation. Such a manipulator structure is referred to as non-redundant. Though non-redundant manipulators are kinematically simple to design and solve, the non-redundancy leads to two fundamental problems: singularities and inability to avoid obstacles.

The singularities which are embedded into the inverse kinematic solution of these mechanical structures are present both in the arm and the wrist and can occur anywhere inside the workspace of the manipulator. While passing through these singularities, the manipulator can effectively lose certain degrees of freedom, resulting in uncontrollability along those directions (Featherstone, 1983), (Paul, et al., 1983). Obstacle avoidance is another desirable characteristic to effectively plan the motion trajectories, especially for manipulators designed to perform demanding tasks in constricted environments (Nieminen, et al., 2009).

The above two problems can be solved by adding additional degrees of freedom to the manipulator (Hollerbach, 1985). These additional degrees of freedom can be added to the joints, which effectively become singular in certain postures (shoulder, elbow and wrist) and can be utilised to overcome the singularities or avoid obstacles. In principle, redundancy is related to the task assigned to the manipulator. A six degrees of freedom manipulator even though not intrinsically redundant becomes functionally redundant if the task specifies only five or less constraints on the motion (Sciavicco, et al., 2001).

Most redundancy resolution schemes are implemented by using Moore-Penrose pseudo-inverse of the Jacobian (Whitney, 1969). A projector matrix is utilized, which can effectively project the joint motions and torques into the null space of the end-effector's motion and force respectively. An objective function which is a gradient in the manipulator's joint-space can be utilized to generate these internal motions and forces (Liegeois, 1977). Hence, the objective function defines the scheme for redundancy resolution. Popular ways to define objective functions are to avoid the manipulator's joint limits (Klein, et al., 1987), (Zghal, et al., 1990), avoid obstacles (Maciejewski, et al., 1985) and avoid singularities (Yoshikawa, 1985a).

An additional benefit of having redundant degrees of freedom is to be able to select the optimized posture of the manipulator for dynamic performance (Hirakawa, et al., 1997), (Hollerbach, et al., 1987). Many of the static and dynamic performance indices described in Section 2.1 can be utilized to resolve the redundancy to enhance the performance of the controller of the manipulator.

The improved performance of the manipulator largely depends on the strategy used for the resolution of redundancy and the way they are implemented in the controller. Unfortunately, in the majority of cases these schemes are computationally heavy and are difficult to implement in real-time. Additionally, they carry numerical instability, which makes their implementation more difficult (Martin, et al., 1989).

2.4 Water hydraulics

The earliest existing records about the development of hydraulic systems point towards the use of water as the pressure medium by the Greek physicist and inventor Ctesibius of Alexandria (Encyclopædia Britannica, 2009). Ctesibius invented a two-piston pump to run a water organ so that the air was forced through the organ pipes by pressurized water instead of falling lead weights. In 1795 Joseph Bramah invented his unique hydraulic press using Pascal's principle and water as the transmission medium (Pearce, 2005).

In recent years water hydraulic technology has shown signs of fast development and the trend seems to be for it to continue in future. The environmental hazards caused by the use of mineral oils encourage the use of water as pressure medium in several applications (Siuko, et al., 2003). However, with the emergence of bio-degradable oils in the field of hydraulics the use of water as the power transmission medium has lost some of its significance (Conrad, 1997). The potential areas of applications are food, chemical, mining, pharmaceuticals, steel and the nuclear industry (Conrad, et al., 1997).

Current developments in the field of water hydraulics can be categorized into the domains of studying the properties of water as a hydraulic transmission medium, namely the development of materials and components suitable for water hydraulics and the development of control technology related to water hydraulic servo systems.

In principle, water hydraulic components such as valves, cylinders, pumps, motors, etc. are essentially identical to their respective oil hydraulic components (Trostmann, 1996). Hence,

many existing manufacturing technologies and most design solutions can be used or adapted from oil hydraulics to water hydraulics. In 1994 Danfoss™ introduced the first generation of water hydraulic components known as Nessie® suitable for use with tap water (Conrad, 2005).

The physical and chemical properties of water dictate the choices of materials and impose design and manufacturing constraints. The low viscosity of water requires very tight tolerances among the moving parts to limit internal and external leakages. At the same time water without additives is a poor lubricant, which may result in higher friction losses. In addition, the chemically aggressive nature of water may result in the corrosion and erosion of components. These corrosive particles can result in degraded performance of the components or even result in a complete failure. It is highly recommended to keep the water hydraulic systems clean and free of these corrosive particles (Trostmann, et al., 2001).

Water is also a suitable medium for the growth of micro-organisms such as bacteria and fungi. These micro-organisms accumulate as a layer on the inner walls of hydraulic components and result in a shortened lifetime of filters. Special care is required to avoid high pressure differences across the filters due to microbial growth on the filter fibres (Riipinen, et al., 2002).

The servo-valve is an essential component for high performance hydraulic servo systems (Urata, et al., 1998). The development of a water hydraulic servo-valve poses its own challenges. One of the major issues is the low viscosity of water, which results in higher internal leakages. The problem can be solved by using tighter tolerances at the expense of higher machining costs. However, these tight tolerances may reduce the reliability of the valve as small particles may hinder the movement of the spool. Low cost on-off digital valves can be used to overcome these limitations. These valves not only improve the reliability of the system but excellent dynamic and static performance can be obtained by the use of proper control techniques (Linjama, et al., 2002a), (Linjama, et al., 2008).

Water as the pressure medium in a hydraulic position servo system does not influence the controller design process significantly. The main differences arise from characteristics such as friction and leakages of the components, resulting in higher nonlinear behaviour of the system (Mäkinen, 2001). Several other studies have also shown that a similar performance can be obtained using oil or water as the pressure mediums in close-loop position control servo systems for cylinder drives (Mäkinen, et al., 1999), (Yamashina, et al., 1996), (Virvalo, et al., 2000) or axial piston motor drive (Mochizuki, et al., 1997). The use of water, because of its high bulk modulus, can result in higher pressure peaks in the system and have a higher risk of cavitations. Coulomb friction is responsible for most of the damping of the system (Virvalo, et al., 1999a).

Studies on the force control properties of water hydraulic servo systems shows that water hydraulic directional control servo-valves are also suitable force control applications. Even though reasonable accuracy can be obtained by using the pressure feedback signal, nevertheless internal friction has a significant effect on the accuracy (Virvalo, et al., 1999), (Virvalo, et al., 2000). Better performance can be obtained by using a feedback signal from a force sensor (Mattila, et al., 2005).

Among hydraulic actuators, the vane is considered to be a simple one from the design point of view. However, tight tolerances between the axel and the chamber make the construction of this actuator a demanding task. The challenge is to find an optimum balance between the internal friction and leakage. Despite these difficulties, such actuators are ideal for the construction of the joints of a hydraulic manipulator. The high force to size ratio of actuators results in direct driven manipulator joints with reduced components and mechanical backlashes. Several industrial manipulators have been designed using vane actuators with oil as the pressure medium (ALSTOM, 1999), (Bilodeau, et al., 1998), (Cybernetix, 2001), (Lischinsky, et al., 1999).

However, little research has been performed with manipulators driven by water hydraulic vane actuators. Researchers have presented experiments and analysis with a single water hydraulic vane actuator. Assessment shows that such actuators can be used for the design of water hydraulic manipulators (Raneda, 2004). The design and modelling of such actuators has been shown to follow the same principles as for oil hydraulic vane actuators (Dubus, et al., 2008), (Muhammad, et al., 2009a). Recently the development of Water Hydraulic MANipulator (WHMAN) has been reported (Muhammad, et al., 2007a). The joints of this manipulator are driven by water hydraulic vane actuators (Nieminen, et al., 2009). The position and force control properties of such manipulators require a significant amount of further research.

3 DYNAMIC MANIPULABILITY AND IMPEDANCE CONTROL

The theoretical foundation for the research work is developed in this chapter. In Section 3.1 the dynamic model of a general n degrees of freedom manipulator is presented both in the joint-space and the operational-space. In utilizing these models, the formulation of dynamic manipulability for non-redundant and redundant manipulators is provided in Section 3.2. Section 3.3 investigates the effect of redundancy on the dynamic manipulability of the manipulator.

Section 3.4 is dedicated to the development and analysis of the desired impedance model for the implementation of impedance controller. The position-based and force-based implementations of impedance control are presented in Section 3.5. The equivalent implementations of position-based and force-based impedance controllers are investigated in Section 3.6.

In Section 3.7 redundancy resolution has been devised to exploit the redundant degrees of freedom for improved dynamic performance of the manipulator. The major developments in the chapter are summarized in Section 3.8.

The theoretical developments in this chapter are restricted to the idealized behaviour of the manipulator, so the main findings can be highlighted. The limitations to practical implementation are taken into consideration in the later sections, where non-ideal characteristics are modelled and compensated in the controller design.

In this chapter and the rest of the thesis the term position has been used to describe both the translational and angular displacement (orientation) of the manipulator. Similarly, the term force has been used to describe both translational and angular forces (torque) of the manipulator. Throughout this text, matrices are presented with bold face uppercase letters, vectors are presented with bold face lowercase letters and scalar values are presented with a regular small case letter.

3.1 Manipulator model

The modelling of manipulators has been discussed in several robotics books, such as (Craig, 2004), (Paul, 1981), (Sciavicco, et al., 2001). In general, the control of manipulators is

performed in the joint or the actuator-space. The joint and actuator variables such as position, current, pressures, torque, etc. are used as feedback to control the position and force of each joint and thus to estimate the positions and forces at the end-effector. This leads to the disadvantage of controlling operational-space variables in an open-loop manner, so that the mechanical uncertainties and controller inaccuracies are left outside the control loop.

However, the approach of joint-space control has the advantage of keeping the mechanical design of the manipulator simple. The installation of transducers to measure the joint variables is straightforward and many times inherent in the design. On the other hand, installation of transducers to measure the operational-space variables can be complex and expensive. Another disadvantage of the operational-space control of manipulators is the algorithmic complexity of the controller, as the inverse kinematics becomes part of control loop (Sciavicco, et al., 2001).

The dynamic model of the manipulator mechanism in joint-space can be derived either using Lagrange's method based on energy balancing or the Newton-Euler method based on force balancing. We consider a manipulator with n degrees of freedom in joint-space and with joint position variables represented as θ_i, where $i = 1, 2, \dots, n$. The manipulator has m degrees of freedom in the operational-space and depending on the assigned task $n \geq m$. The dynamic model of this manipulator can be given as:

$$\boldsymbol{\tau} = \boldsymbol{M_\theta}(\boldsymbol{\theta}) \cdot \ddot{\boldsymbol{\theta}} + \boldsymbol{B_\theta}\left(\boldsymbol{\theta}, \dot{\boldsymbol{\theta}}\right) \cdot \dot{\boldsymbol{\theta}} + \boldsymbol{g_\theta}(\boldsymbol{\theta}) + \boldsymbol{\tau_e} \tag{3.1}$$

Here $\boldsymbol{\theta} = [\theta_1, \theta_2, \dots, \theta_n]^T \in \mathcal{R}^n$ ($\mathcal{R}$ is the Euclidian space) is the vector of joint position variables and $\boldsymbol{\tau} = [\tau_1, \tau_2, \dots, \tau_n]^T \in \mathcal{R}^n$ is the vector of joint forces. $\boldsymbol{M_\theta}(\boldsymbol{\theta}) \in \mathcal{R}^{n \times n}$ is the inertia matrix, $\boldsymbol{B_\theta}(\boldsymbol{\theta}, \dot{\boldsymbol{\theta}}) \in \mathcal{R}^{n \times n}$ represents the centrifugal and Coriolis forces matrix and $\boldsymbol{g_\theta}(\boldsymbol{\theta}) \in \mathcal{R}^n$ is the vector of gravity forces. $\boldsymbol{\tau_e} \in \mathcal{R}^n$ is the vector of joint-space forces due to environmental contact.

Equation 3.1 is a representation of manipulator dynamics in the joint-space and it is distinguished with the subscript θ. It needs to be pointed out that non-conservative forces such as static, columbic and viscous frictions have been ignored in the model of Equation 3.1. As mentioned earlier, only the idealized behaviour of the manipulator is considered here and such nonlinear characteristics will be compensated during the numerical simulations and practical implementation of the controller.

The joint-space description of the manipulation tasks can only be used for well-defined environment and task geometries. In general, it is much more convenient to define the manipulator tasks in operational-space, especially where the manipulator needs to perform a variety of contact-tasks in an unknown and unstructured environment.

In addition, for the sake of impedance control it is initiative to define the impedance parameters in the operational-space and then to transform the control signals in the joint/actuator-space. In such cases, manipulators are regularly fitted with a wrist-force/torque sensor, which, despite the complex installation, provides an accurate measure of contact forces. For these reasons it is worth considering the dynamic model of the manipulator in the operational-space. The equivalent operational-space representation of Equation 3.1 is given as:

3.2 $$\boldsymbol{f} = \boldsymbol{M_x}(\boldsymbol{x}) \cdot \ddot{\boldsymbol{x}} + \boldsymbol{B_x}(\boldsymbol{x}, \dot{\boldsymbol{x}}) \cdot \dot{\boldsymbol{x}} + \boldsymbol{g_x}(\boldsymbol{x}) + \boldsymbol{f_e}$$

Here $\boldsymbol{x} = [x_1, x_2, \dots, x_m]^T \in \mathcal{R}^m$ is the vector of end-effector's position and $\boldsymbol{f} = [f_1, f_2, \dots, f_m]^T \in \mathcal{R}^m$ is the vector of forces acting on the end-effector of the manipulator. $\boldsymbol{M_x}(\boldsymbol{x}) \in \mathcal{R}^{m \times m}$, $\boldsymbol{B_x}(\boldsymbol{x}, \dot{\boldsymbol{x}}) \in \mathcal{R}^{m \times m}$ and $\boldsymbol{g_x}(\boldsymbol{x}) \in \mathcal{R}^m$ are the representations of the same inertia, Coriolis and gravity matrices and vectors in the operational-space respectively. $\boldsymbol{f_e} \in \mathcal{R}^m$ is the vector of environmental contact forces. Equation 3.2 is the representation of manipulator dynamics in the operational-space and the subscript x has been used to distinguish this fact.

The relationship between the operational-space and joint-space parameters can be given by the following set of equations:

3.3 $$\boldsymbol{M_x} = (\boldsymbol{J} \cdot \boldsymbol{M_\theta^{-1}} \cdot \boldsymbol{J}^{\mathrm{T}})^{-1}$$

3.4 $$\boldsymbol{B_x}\dot{\boldsymbol{x}} = \boldsymbol{M_x} \cdot \boldsymbol{J} \cdot \boldsymbol{M_\theta^{-1}} \cdot \boldsymbol{B_\theta}\dot{\boldsymbol{\theta}} - \boldsymbol{M_x} \cdot \dot{\boldsymbol{J}} \cdot \dot{\boldsymbol{\theta}}$$

3.5 $$\boldsymbol{g_x} = \boldsymbol{M_x} \cdot \boldsymbol{J} \cdot \boldsymbol{M_\theta^{-1}} \cdot \boldsymbol{g_\theta}$$

The general relationships between the joint-space and the operational-space position and force variables are given as:

3.6 $$\dot{\boldsymbol{x}} = \boldsymbol{J} \cdot \dot{\boldsymbol{\theta}}$$

3.7 $$\boldsymbol{\tau} = \boldsymbol{J^T} \cdot \boldsymbol{f}$$

Where $\boldsymbol{J} \in \mathcal{R}^{m \times n}$ is the Jacobian matrix of the manipulator, which in general is the function of joint position variables. A useful numerical aproximation of Equation 3.6 is given as:

3.8 $$\Delta\boldsymbol{x} = \boldsymbol{J} \cdot \Delta\boldsymbol{\theta}$$

The above aproximation is only valid for small values of **Δ,** Where Δ represents the change. The dependence on operational-space and joint-space variable has been omitted from Equations 3.3 to 3.8 for the sake of brevity. This practice will be followed in the rest of the text where such dependencies are obvious.

3.2 Dynamic manipulability

The dynamic characteristic of a manipulator can be studied by using the Dynamic Manipulability Ellipsoid (DME). The work in this section has been originally presented by (Yoshikawa, 1985), (Chiacchio, et al., 1991) and (Chiacchio, et al., 1998). Here it has been reproduced for the sake of discussion and to form the basis of further developments in Section 3.3.

Dynamic manipulability can be characterised in terms of the manipulator's capability to accelerate in the operational-space for a given set of joint-space forces. It is assumed that the manipulator is at rest and its end-effector is not constrained by the environment, i.e. $\dot{\boldsymbol{\theta}} = \mathbf{0}$ and $\boldsymbol{\tau_e} = \mathbf{0}$. Substituting these values in Equation 3.1 will result in:

$$\boldsymbol{\tau} = \boldsymbol{M_\theta} \cdot \ddot{\boldsymbol{\theta}} + \boldsymbol{g_\theta} \tag{3.9}$$

For the true characterization of the manipulator's acceleration capability the gravitational forces need to be included, as in Equation 3.9. However, the inclusion of gravitational forces results only in the translation of the centre of DME without affecting its volume (Chiacchio, et al., 1991). Since a manipulator should be capable of holding its own weight and as the purpose here is to compare the effects of redundancy on dynamic manipulability of the manipulators, i.e. the volume of the ellipsoid, the gravitational forces can be omitted from Equation 3.9 through a change of variables.

$$\tilde{\boldsymbol{\tau}} = \boldsymbol{M_\theta} \cdot \ddot{\boldsymbol{\theta}} \tag{3.10}$$

Where,

$$\tilde{\boldsymbol{\tau}} = \boldsymbol{\tau} - \boldsymbol{g_\theta} \tag{3.11}$$

Now $\tilde{\boldsymbol{\tau}} \in \mathcal{R}^n$ is the vector of joint-space forces available to move the manipulator. Realistically, if a manipulator is required to execute any task, the joint actuators should be capable of accelerating the manipulator besides holding its own weight. This constraint on the joint forces can be given as:

$$|\tilde{\tau}_i| \leq \tilde{\tau}_{i\,max} \tag{3.12}$$

Where, $\tilde{\tau}_{i\,max}$ is the maximum available force from the actuator to drive the *ith* joint and $\tilde{\tau}_i$ is the desired force to accelerate. Generally, the bond of Equation 3.12 is not the same for all the joints of the manipulator. To obtain a meaningful index on the acceleration capabilities of a manipulator the joint-space forces should be normalized as:

3.13 $$\hat{\boldsymbol{\tau}} = \boldsymbol{T}_{\boldsymbol{max}}^{-\mathbf{1}} \cdot \tilde{\boldsymbol{\tau}}$$

Where $\hat{\boldsymbol{\tau}} \in \mathcal{R}^n$ is the vector of normalized joint-space forces, and

3.14 $$\boldsymbol{T}_{\boldsymbol{max}} = diag(\tilde{\tau}_{1\,max}, \tilde{\tau}_{2\,max}, \dots, \tilde{\tau}_{n\,max})$$

The $diag(\cdot)$ denotes the diagonal matrix. Now substituting the value of $\tilde{\boldsymbol{\tau}}$ from Equation 3.10 into Equation 3.13,

3.15 $$\hat{\boldsymbol{\tau}} = \widehat{\boldsymbol{M}}_{\boldsymbol{\theta}} \cdot \ddot{\boldsymbol{\theta}}$$

Where,

3.16 $$\widehat{\boldsymbol{M}}_{\boldsymbol{\theta}} = \boldsymbol{T}_{\boldsymbol{max}}^{-\mathbf{1}} \cdot \boldsymbol{M}_{\boldsymbol{\theta}}$$

Equation 3.15 now can be used to derive the DME for manipulators in general. Below the cases of non-redundant and redundant configurations are discussed separately.

3.2.1 Non-redundant manipulators

If the manipulator requires m degrees of freedom in the operational-space for the execution of a task, it must require a minimum of m degrees of freedom in the joint-space. If the manipulator is composed of exactly $n = m$ degrees of freedom in joint-space, the manipulator is said to be kinematically non-redundant. In this case the Jacobian of the manipulator is a square matrix. Differentiating Equation 3.6 with respect to time will provide a relationship between operational-space and joint-space accelerations.

3.17 $$\ddot{\boldsymbol{x}} = \boldsymbol{J} \cdot \ddot{\boldsymbol{\theta}} + \dot{\boldsymbol{J}} \cdot \dot{\boldsymbol{\theta}}$$

Since the manipulator is stationary, the second term in the above relationship can be omitted. Solved for $\ddot{\boldsymbol{\theta}}$ the Equation 3.17 is:

3.18 $$\ddot{\boldsymbol{\theta}} = \boldsymbol{J}^{-\mathbf{1}} \cdot \ddot{\boldsymbol{x}}$$

Substituting the value of $\ddot{\boldsymbol{\theta}}$ into Equation 3.15, the relationship between the joint-space forces and operational-space accelerations can be devised as:

3.19 $$\hat{\boldsymbol{\tau}} = \widehat{\boldsymbol{M}}_{\boldsymbol{\theta}} \cdot \boldsymbol{J}^{-\mathbf{1}} \cdot \ddot{\boldsymbol{x}}$$

The norm of the normalized joint-forces is given as a unit sphere in the joint-space.

3.20 $$\hat{\boldsymbol{\tau}}^{\boldsymbol{T}} \cdot \hat{\boldsymbol{\tau}} \leq 1$$

This unit sphere can be used to characterize the operational-space acceleration capability of a manipulator by substituting the value of $\hat{\boldsymbol{\tau}}$ from Equation 3.19:

3.21 $$(\ddot{\boldsymbol{x}}^{\boldsymbol{T}}) \cdot \boldsymbol{J}^{-\boldsymbol{T}} \cdot \widehat{\boldsymbol{M}}_{\boldsymbol{\theta}}{}^{\boldsymbol{T}} \cdot \widehat{\boldsymbol{M}}_{\boldsymbol{\theta}} \cdot \boldsymbol{J}^{-\mathbf{1}} \cdot (\ddot{\boldsymbol{x}}) \leq 1$$

Equation 3.21 is an ellipsoid in the operational-space referred to as DME, which can be used to characterize the dynamic performance of a non-redundant manipulator.

3.2.2 Redundant manipulators

If the manipulator is composed of n degrees of freedom for execution of the same task, such that $n > m$, then the manipulator possesses free degrees of mobility in the joint-space and is said to be kinematically redundant. In this case the Jacobian of the manipulator is a rectangular matrix with m rows and n columns. The solution of the Equation 3.18 is of the form:

3.22 $$\ddot{\boldsymbol{\theta}} = \boldsymbol{J}^{\dagger} \cdot \ddot{\boldsymbol{x}} + (\boldsymbol{I} - \boldsymbol{J}^{\dagger} \cdot \boldsymbol{J}) \cdot \ddot{\boldsymbol{\theta}}_{\mathbf{0}}$$

Here $\boldsymbol{I} \in \mathcal{R}^{n \times n}$ is the identity matrix and $\boldsymbol{J}^{\dagger}$ is the right pseudo-inverse of the Jacobian matrix (Whitney, 1969) and it is given as:

3.23 $$\boldsymbol{J}^{\dagger} = \boldsymbol{J}^{\boldsymbol{T}} \cdot (\boldsymbol{J} \cdot \boldsymbol{J}^{\boldsymbol{T}})^{-1}$$

The matrix $(\boldsymbol{I} - \boldsymbol{J}^{\dagger} \cdot \boldsymbol{J})$ projects the joint-space accelerations $\ddot{\boldsymbol{\theta}}_{\mathbf{0}}$ into the nonempty null space of the Jacobian, i.e. $Ker(\boldsymbol{J})$. In other words, it can be said that there exist a set of joint-space accelerations or torques, which do not produce any accelerations in the operational-space of the manipulator. Now substituting the value of $\ddot{\boldsymbol{\theta}}$ into Equation 3.15, the relationship between the joint-space forces and operational-space accelerations can be devised as:

3.24 $$\hat{\boldsymbol{\tau}} = \widehat{\boldsymbol{M}}_{\boldsymbol{\theta}} \cdot \boldsymbol{J}^{\dagger} \cdot \ddot{\boldsymbol{x}} + \widehat{\boldsymbol{M}}_{\boldsymbol{\theta}} \cdot (\boldsymbol{I} - \boldsymbol{J}^{\dagger} \cdot \boldsymbol{J}) \cdot \ddot{\boldsymbol{\theta}}_{\mathbf{0}}$$

Since the matrix $(\boldsymbol{I} - \boldsymbol{J}^{\dagger} \cdot \boldsymbol{J})$ will project any values of vector $\ddot{\boldsymbol{\theta}}_{\mathbf{0}}$ into the null space of Jacobian, the choice of $\ddot{\boldsymbol{\theta}}_{\mathbf{0}}$ is free. For the maximum dynamic capability (all joint-space forces are utilized for operational-space accelerations) $\ddot{\boldsymbol{\theta}}_{\mathbf{0}} = \mathbf{0}$. Hence, Equation 3.24 reduces to.

3.25 $$\hat{\boldsymbol{\tau}} = \widehat{\boldsymbol{M}}_{\boldsymbol{\theta}} \cdot \boldsymbol{J}^{\dagger} \cdot \ddot{\boldsymbol{x}}$$

Now, proceeding in the same way as before, the DME for redundant manipulators can be obtained by substituting the value of $\hat{\boldsymbol{\tau}}$ from Equation 3.25 into Equation 3.20.

3.26 $$(\ddot{\boldsymbol{x}}^{\boldsymbol{T}}) \cdot \boldsymbol{J}^{\dagger^{\boldsymbol{T}}} \cdot \widehat{\boldsymbol{M}}_{\boldsymbol{\theta}}{}^{\boldsymbol{T}} \cdot \widehat{\boldsymbol{M}}_{\boldsymbol{\theta}} \cdot \boldsymbol{J}^{\dagger} \cdot (\ddot{\boldsymbol{x}}) \leq 1$$

Equation 3.26 is an ellipsoid in the operational-space referred to as DME, which can be used to characterize the dynamic performance of a redundant manipulator.

3.3 Effect of redundancy

There is a considerable amount of delay between the peripheral sensory feedback and the actuation of muscles in primates (Miall, et al., 1996). Despite this fact, primates can regulate the impedance of their limbs without trouble when interacting with the environment. Evidence shows that kinematic redundancy in the limbs is one of the fundamental factors effecting impedance regulation (Hogan, 1985). Considering manipulators as the machine equivalent of limbs, redundancy may play a similar role in the dynamic performance of manipulators. Here, we try to investigate this matter using the DME presented in the last section.

The DME for non-redundant and redundant manipulators has been formulated in Equations 3.21 and 3.26 respectively. The volume of this ellipsoid characterising the dynamic manipulability can be completely specified by the quadratic core of these equations. Now, we define these matrices as:

3.27 $$Ч_{\boldsymbol{n=m}} = \boldsymbol{J} \cdot \widehat{\boldsymbol{M}}_{\boldsymbol{\theta}}{}^{\boldsymbol{-1}}$$

3.28 $$Ч_{\boldsymbol{n>m}} = \boldsymbol{J} \cdot \widehat{\boldsymbol{M}}_{\boldsymbol{\theta}}{}^{\boldsymbol{-1}}$$

Here, $Ч_{\boldsymbol{n=m}} \in \mathcal{R}^{m \times m}$ and $Ч_{\boldsymbol{n>m}} \in \mathcal{R}^{m \times n}$ and the cases of non-redundant and redundant manipulator have been distinguished by the subscripts $n = m$ and $n > m$ respectively. The singular value decomposition of these matrices is given as:

3.29 $$Ч_{\boldsymbol{n=m}} = \boldsymbol{U}_{\boldsymbol{n=m}} \cdot \boldsymbol{S}_{\boldsymbol{n=m}} \cdot \boldsymbol{V}^{\boldsymbol{T}}_{\boldsymbol{n=m}}$$

3.30 $$Ч_{\boldsymbol{n>m}} = \boldsymbol{U}_{\boldsymbol{n>m}} \cdot \boldsymbol{S}_{\boldsymbol{n>m}} \cdot \boldsymbol{V}^{\boldsymbol{T}}_{\boldsymbol{n>m}}$$

Where $\boldsymbol{U}_{\boldsymbol{n=m}} \in \mathcal{R}^{m \times m}$ and $\boldsymbol{U}_{\boldsymbol{n>m}} \in \mathcal{R}^{m \times m}$, and their columns form the set of orthonormal output basis vector directions for $Ч_{\boldsymbol{n=m}}$ and $Ч_{\boldsymbol{n>m}}$ respectively. $\boldsymbol{V}_{\boldsymbol{n=m}} \in \mathcal{R}^{m \times m}$, $\boldsymbol{V}_{\boldsymbol{n>m}} \in \mathcal{R}^{n \times n}$,

and their columns form the set of orthonormal input basis vector directions for $Ч_{\boldsymbol{n=m}}$ and $Ч_{\boldsymbol{n>m}}$ respectively. $\boldsymbol{S_{n=m}} \in \mathcal{R}^{m\times m}$ and $\boldsymbol{S_{n>m}} \in \mathcal{R}^{m\times n}$ are the diagonal matrices containing the singular values, such that:

3.31 $$\boldsymbol{S_{n=m}} = \begin{bmatrix} \sigma_1 & 0 & 0 & 0 \\ 0 & \sigma_2 & 0 & 0 \\ 0 & 0 & \cdot & 0 \\ 0 & 0 & 0 & \sigma_m \end{bmatrix}$$

3.32 $$\boldsymbol{S_{n>m}} = \begin{bmatrix} \sigma_1 & 0 & 0 & 0 & \vdots & \\ 0 & \sigma_2 & 0 & 0 & \vdots & \boldsymbol{0} \\ 0 & 0 & \cdot & 0 & \vdots & \\ 0 & 0 & 0 & \sigma_m & \vdots & \end{bmatrix}$$

Where,

3.33 $$\sigma_1 \geq \sigma_2 \geq \cdots \geq \sigma_m \geq 0$$

According to Equations 3.29 and 3.30 the principal axes of DME are given as:

3.34 $$\sigma_1 \cdot \boldsymbol{u_1}, \sigma_2 \cdot \boldsymbol{u_2}, \dots, \sigma_m \cdot \boldsymbol{u_m}$$

Here, the omission of subscript indicates the fact that the statement is valid in either case. $\boldsymbol{u_i} \in \mathcal{R}^m$ is the *ith* column vector of matrix $\boldsymbol{U}$ which are the directions of the ellipsoid axes. The singular values represent the length of the axes of ellipsoid. Equation 3.34 highlights the fact that the DME can be completely characterized by the singular values and the orthogonal matrix $\boldsymbol{U}$. Hence, based on DME the local dynamic performance of the manipulator can be given by a general function:

3.35 $$w(\theta) = f(\sigma_1, \sigma_2, \dots, \sigma_m, \boldsymbol{u_1}, \boldsymbol{u_2}, \dots, \boldsymbol{u_m})$$

Based on DME presentation the axes of ellipsoid are given by Equation 3.35 such that the directions of these axes are given by the orthogonal column vectors of matrix $\boldsymbol{U}$ and the lengths of these axes are given by the respective singular values. A local performance index referred to as dynamic manipulability measure is given as (Yoshikawa, 1985):

3.36 $$w_1 = \sigma_1 \cdot \sigma_2 \cdot \dots \cdot \sigma_m$$

Where w_1 is proportional to the volume of ellipsoid. When the manipulator is in a singular posture, i.e. the $rank(\boldsymbol{J}) < m$, a singular value of Ч is zero and thus the volume of this elliposid is zero. Hence, in principle higher singular values will result in a larger ellipsoid, indicating greater dynamic manipulability.

The inertia matrix in Equations 3.27 and 3.28 is symmetric and positive definite with positive entries on the diagonal. For a reasonable design of a manipulator this matrix is diagonal dominant, i.e.

3.37 $$\widehat{m}_{ii} \gg \left|\widehat{m}_{ij}\right|$$

Where, $\widehat{m}_{ii}$ are the elements of matrix $\widehat{\boldsymbol{M}}_{\boldsymbol{\theta}}$. For the sake of simplicity it is assumed here that the inertia matrix is diagonal, i.e. $\widehat{m}_{ij} = 0$, Hence, the diagonal enteries of its inverse are simply the reciprocals of the diagonal entries of the original matrix. Now we first consider the case of redundant manipulators and define $Ж_{\boldsymbol{n>m}} \in \mathcal{R}^{m\times m}$ as:

3.38 $$Ж_{\boldsymbol{n>m}} = Ч_{\boldsymbol{n>m}} \cdot Ч^{\mathrm{T}}_{\boldsymbol{n>m}}$$

The trace of this matrix is given as:

3.39 $$trace(Ж_{\boldsymbol{n>m}}) = \sum_{i=1}^{m} ж_{ii} = \sum_{j=1}^{m}\sum_{i=1}^{n}\left(j_{ji}\cdot\frac{1}{\widehat{m}_{ii}}\right)^2$$

For the non-redundant configuration of the manipulator the Jacobian and inertia matrices can be obtained by removing the rows and columns corresponding to the joint-space degree of freedom. Now we define $Ж_{\boldsymbol{n=m}} \in \mathcal{R}^{m\times m}$ as

3.40 $$Ж_{\boldsymbol{n=m}} = Ч_{\boldsymbol{n=m}} \cdot Ч^{\mathrm{T}}_{\boldsymbol{n=m}}$$

The trace of this matrix is given as:

3.41 $$trace(Ж_{\boldsymbol{n=m}}) = \sum_{i=1}^{m} ж_{ii} = \sum_{j=1}^{m}\sum_{i=1}^{m}\left(j_{ji}\cdot\frac{1}{\widehat{m}_{ii}}\right)^2$$

The relationship between Equations 3.39 and 3.41 is given as:

3.42 $$\sum_{j=1}^{m}\sum_{i=1}^{n}\left(j_{ji}\cdot\frac{1}{\widehat{m}_{ii}}\right)^2 = \sum_{j=1}^{m}\sum_{i=1}^{m}\left(j_{ji}\cdot\frac{1}{\widehat{m}_{ii}}\right)^2 + \sum_{j=1}^{m}\sum_{i=\mathrm{m}+1}^{n}\left(j_{ji}\cdot\frac{1}{\widehat{m}_{ii}}\right)^2$$

Unless all the entries in a column of Jacobian matrix are zero ($rank(\boldsymbol{J}) < m$), from the relationship of Equation 3.42 it is clear that the following inequality holds:

3.43 $$trace(Ж_{\boldsymbol{n>m}}) > trace(Ж_{\boldsymbol{n=m}})$$

A relationship between the trace and singular values can be obtained by using the Frobenius matrix norm, which is:

3.44 $$\|Ч\|_{\text{Frobenius}} = \sqrt{trace(Ч \cdot Ч^{T})} = \sqrt{trace(Ж)} = \sqrt{\sum_{i=1}^{m} {\sigma_i}^2}$$

Or,

3.45 $$trace(Ж) = \sum_{i=1}^{m} {\sigma_i}^2$$

Now a comparison of Equations 3.43 and 3.45 leads to the following conclusion:

3.46 $$\sum_{i=1}^{m} {\sigma_i}^2 \Big|_{n>m} > \sum_{i=1}^{m} {\sigma_i}^2 \Big|_{n=m} \Longrightarrow \sum_{i=1}^{m} \sigma_i \Big|_{n>m} > \sum_{i=1}^{m} \sigma_i \Big|_{n=m}$$

Since the m is fixed, it means that some of the singular values must be larger for the case of redundant manipulator ($n > m$) as compared to the case of non-redundant manipulator ($n = m$). Since these singular values specify the lengths of DME axes, according to Equation 3.36 the volume of manipulability ellipsoid must be larger if the manipulator has redundant degrees of mobility. The above discussion shows that redundant degrees of freedom can help in improving the dynamic performance of the manipulator.

The above proof relies on the assumptions that extra degrees of freedom can be added to the manipulator without significantly affecting the inertia matrix and the inertia matrix is diagonal dominant. However, in practice additional degrees of freedom require additional actuators and the resizing of existing actuators, which can result in a significant alteration of the inertia matrix. Hence, the above approach is only useful to determine the effect of existing redundant degrees of freedom or in cases where such degrees of freedom can be added with small actuators with large force capacity such as in hydraulics.

If the non-diagonal entries of inertia matrix are significantly large and cannot be ignored it will not be straightforward to determine the effect of redundancy on the dynamic manipulability of the manipulator. However, for a reasonable design the non-diagonal entries of the inertia matrix should be much lower than the diagonal entries. In Chapter 5 these results will be further explored without making the assumption of Equation 3.37.

3.4 Impedance model

Fundamentally, when the manipulator comes into contact with the environment it requires the changing of either the position or the force set point of the manipulator to regulate the impedance. The capability of the manipulator to make the adjustment to this new set point can be characterized by its dynamic manipulability. The faster the dynamics, or in other words the higher the bandwidth of the manipulator, the faster and smoother it can make this adjustment in the set point (Matko, et al., 1999), (Seraji, et al., 1993a). This will not only result in improved impedance control but will also improve the stability characteristics of the impedance controller. Therefore, impedance control capabilities can provide insight into the dynamic manipulability of a manipulator.

In this section the desired impedance model of the manipulator has been discussed. This desired impedance model is then used in Section 3.5 for the development of impedance controller.

3.4.1 Operational-space impedance model

With the assumption that the impedance controller is capable of completely masking the original dynamics of the manipulator and the manipulator behaves as the desired impedance to the environment, the interaction between manipulator and environment can be modelled as shown in Figure 3.1. The manipulator is modelled as a mass-damper-spring system, which is a standard practice in the design of impedance controller (Eppinger, et al., 1992), (Heinrichs, et al., 1997) and (Lawrence, 1988). The environment has been modelled as a damper-spring system.

In this model, $\boldsymbol{M_d} \in \mathcal{R}^{m\times m}$, $\boldsymbol{B_d} \in \mathcal{R}^{m\times m}$ and $\boldsymbol{K_d} \in \mathcal{R}^{m\times m}$ represent the matrices containing the inertial, viscous and stiffness parameters of the desired impedance ($\boldsymbol{Z_d}$) respectively. $\boldsymbol{B_e} \in \mathcal{R}^{m\times m}$ and $\boldsymbol{K_e} \in \mathcal{R}^{m\times m}$ represent the matrices containing the viscous and stiffness parameters of environmental impedance ($\boldsymbol{Z_e}$) respectively. $\boldsymbol{x} \in \mathcal{R}^{m}$ and $\boldsymbol{x_e} \in \mathcal{R}^{m}$ are the nominal desired and actual measured positions of the manipulator respectively. It is assumed that both manipulator and the contacted environment are firmly connected to the ground at the other ends.

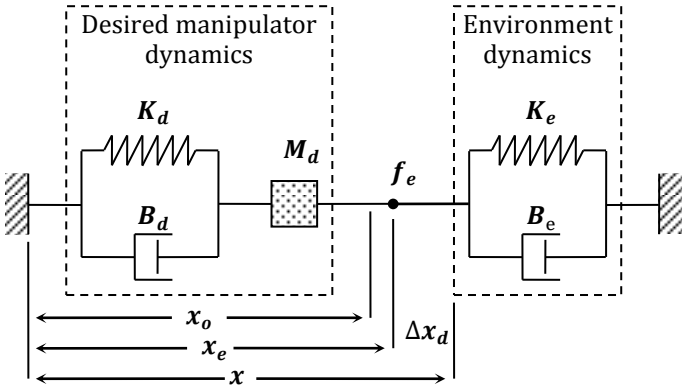

Figure 3.1: Impedance model of the manipulator and the environment

In free space the manipulator is driven along the nominal trajectory $\boldsymbol{x}$. On coming into contact with the environment, the manipulator will impart force $\boldsymbol{f_e} \in \mathcal{R}^m$ on the environment. Depending on the impedance of the environment it will be displaced from its initial position $\boldsymbol{x_o} \in \mathcal{R}^m$. The same environmental force will also act on the manipulator in the opposite direction, and if the manipulator behaves as the defined desired impedance, the end-effector of the manipulator will be displaced by $\Delta\boldsymbol{x_d} \in \mathcal{R}^m$ in order to balance out this force. This change in the position of the manipulator is given as:

3.47 $$\Delta\boldsymbol{x_d} = \boldsymbol{x} - \boldsymbol{x_e}$$

Considering the standard dynamic relationship between the environmental force $\boldsymbol{f_e}$ and the displacement $\Delta\boldsymbol{x_d}$ with $\boldsymbol{Z_d}$ being the desired impedance:

3.48 $$\boldsymbol{f_e} = \boldsymbol{Z_d} \cdot \Delta\boldsymbol{x_d}$$

The relationship of Equation 3.48 highlights the fact that during free space motion $\boldsymbol{f_e} = \boldsymbol{0}$, and the manipulator follows the nominal position trajectory, i.e. $\Delta\boldsymbol{x_d} = \boldsymbol{0}$ and $\boldsymbol{x} = \boldsymbol{x_e}$. As a result no switching of the control law is required when the manipulator moves from free space motion to the contact regime and vice versa. Substituting the value of $\Delta\boldsymbol{x_d}$ from Equation 3.47 into Equation 3.48:

3.49 $$\boldsymbol{f_e} = \boldsymbol{Z_d} \cdot (\boldsymbol{x} - \boldsymbol{x_e})$$

Substitution of the impedance parameters from the model of Figure 3.1 in Equation 3.49 will result in the following dynamic relationship:

3.50 $$\boldsymbol{f_e} = \boldsymbol{M_d} \cdot (\ddot{\boldsymbol{x}} - \ddot{\boldsymbol{x}}_{\boldsymbol{e}}) + \boldsymbol{B_d} \cdot (\dot{\boldsymbol{x}} - \dot{\boldsymbol{x}}_{\boldsymbol{e}}) + \boldsymbol{K_d} \cdot (\boldsymbol{x} - \boldsymbol{x_e})$$

Equation 3.50 provides the desired dynamics between the manipulator position and the contact forces from the environment. Taking the Laplace transform, Equation 3.50 can be written in the form of the following transfer function, which can be used for the implementation of impedance controller in operational-space.

3.51 $$\boldsymbol{x}(s) - \boldsymbol{x_e}(s) = \frac{\mathbf{1}}{\boldsymbol{Z_d}(\mathrm{s})} \cdot \boldsymbol{f_e}(\boldsymbol{s})$$

Where, $\mathbf{1}/\boldsymbol{Z_d}(\mathrm{s})$ is the transfer function matrix of the form:

3.52 $$\begin{bmatrix} \left(\frac{1}{m_d s^2 + b_d s + k_d}\right)_{1,1} & \left(\frac{1}{m_d s^2 + b_d s + k_d}\right)_{1,2} & \cdots & \cdots \\ \left(\frac{1}{m_d s^2 + b_d s + k_d}\right)_{2,1} & \left(\frac{1}{m_d s^2 + b_d s + k_d}\right)_{2,2} & \cdots & \cdots \\ \cdots & \cdots & \ddots & \cdots \\ \cdots & \cdots & \cdots & \left(\frac{1}{m_d s^2 + b_d s + k_d}\right)_{m,m} \end{bmatrix}$$

Where m_d, b_d and k_d are the scalar values of the desired inertia, damping and stiffness respectively along a certain axis of motion. The transfer functions in the above matrix define the desired dynamic relationship between operational-space positions and forces. This model can be used for the implementation of impedance controller in operational-space.

3.4.2 Joint-space impedance model

As discussed earlier, for most of the manipulators the controller is implemented in joint-space. Hence, it is worth discussing the representation of impedance model in the joint-space. The relationship between the environmental force $\boldsymbol{f_e}$ and displacement $\Delta\boldsymbol{x_d}$ given by Equation 3.48 can be restated as:

3.53 $$\boldsymbol{f_e} = \boldsymbol{M_d} \cdot \Delta\ddot{\boldsymbol{x}}_{\boldsymbol{d}} + \boldsymbol{B_d} \cdot \Delta\dot{\boldsymbol{x}}_{\boldsymbol{d}} + \boldsymbol{K_d} \cdot \Delta\boldsymbol{x_d}$$

The relationship between the operational-space and joint-space accelerations can be obtained by differentiating Equation 3.6 with respect to time.

3.54 $$\ddot{\boldsymbol{x}} = \boldsymbol{J} \cdot \ddot{\boldsymbol{\theta}} + \dot{\boldsymbol{J}} \cdot \dot{\boldsymbol{\theta}}$$

With the assumption that manipulator velocities are small and thus the rate of change of Jacobian is also very small, the second term in Equation 3.54 can be ignored. Now Equations 3.6, 3.7, 3.8 and 3.54 can be substituted in Equation 3.53 to obtain the representation of desired impedance in joint-space.

3.55 $$\boldsymbol{\tau_e} = (\boldsymbol{J^T} \cdot \boldsymbol{M_d} \cdot \boldsymbol{J}) \cdot \Delta\ddot{\boldsymbol{\theta}}_{\boldsymbol{d}} + (\boldsymbol{J^T} \cdot \boldsymbol{B_d} \cdot \boldsymbol{J}) \cdot \Delta\dot{\boldsymbol{\theta}}_{\boldsymbol{d}} + (\boldsymbol{J^T} \cdot \boldsymbol{K_d} \cdot \boldsymbol{J}) \cdot \Delta\boldsymbol{\theta_d}$$

Taking the Laplace transform, Equation 3.55 can be written in the form of the transfer function matrix similar to Equation 3.52, which can be used for the implementation of impedance controller in joint-space. This transfer function matrix will be an approximation which describe the mapping of desired operational-space impedance into the joint-space of the manipulator and will only work for small values of Δ.

However, the impedance controller can be implemented entirely by using the operational-space representation of desired impedance either by measuring the operational-space contact forces directly with a wrist force/torque sensor or estimating them from joint forces.

3.4.3 Stability of the impedance model

In Figure 3.1 the dynamic relationship between the displacement $\boldsymbol{x_e} - \boldsymbol{x_o}$ of the environment and the contact force $\boldsymbol{f_e}$ can be given as:

3.56 $$\boldsymbol{f_e} = \boldsymbol{Z_e} \cdot (\boldsymbol{x_e} - \boldsymbol{x_o})$$

Now equating Equations 3.49 and 3.56 and taking the Laplace transform will provide the transfer function matrix of the close-loop position controller, which can be compactly written as:

3.57 $$\boldsymbol{x_e}(s) = \frac{\boldsymbol{Z_d}(s)}{\boldsymbol{Z_e}(s) + \boldsymbol{Z_d}(s)} \cdot \boldsymbol{x}(s) + \frac{\boldsymbol{Z_e}(s)}{\boldsymbol{Z_e}(s) + \boldsymbol{Z_d}(s)} \cdot \boldsymbol{x_o}(s)$$

Equation 3.57 indicates the involvement of environmental impedance parameters in the close-loop dynamics of the impedance controller. Hence, the dynamics of the environment need to be taken into consideration while selecting the desired dynamic parameters of the manipulator (Salcudean, et al., 1997). An improper selection of parameters can lead to a completely unstable system on coming into contact with the environment (Eppinger, et al., 1992). The elements of

the matrix in Equation 3.57 are transfer functions and characteristic equation of each transfer function is of the form:

3.58 $$z_e(s) + z_d(s) = m_d \cdot s^2 + (b_d + b_e) \cdot s + (k_d + k_e) = 0$$

Where b_e and k_e are the scalar values of environmental damping and stiffness respectively along a certain axis of motion. For the close-loop dynamics of the impedance controller to be stable the roots of each characteristic equation must lie on the left hand side of the complex plane. Since the same desired dynamics relationship needs to be established, Equation 3.58 provides sufficient condition for the stability of either position-based or force-based implementations of the impedance controller (Lawrence, 1988).

3.5 Impedance controller

As mentioned earlier, the objective of the impedance controller is to establish a desired dynamic relationship between the position of the manipulator's end-effector and the environmental contact forces (Hogan, 1987). The two implementations of impedance controller are referred as the position-based and the force-based schemes (Lawrence, 1988). In this section both implementations of impedance controller are presented.

3.5.1 Position-based implementation

The position-based implementation of impedance controller has been widely discussed, for example by (Bilodeau, et al., 1998), (Heinrichs, et al., 1997) and (Salcudean, et al., 1997). In position-based implementation when the manipulator comes into contact with the environment a deflection $\Delta \boldsymbol{x_d}$ is calculated using the environmental contact force $\boldsymbol{f_e}$ information and desired dynamic relationship $\boldsymbol{Z_d}$. This deflection is then subtracted from the nominal trajectory of the manipulator to generate the modified position command signal $\boldsymbol{x_c} \in \mathcal{R}^m$. Hence, by making this adjustment in position the contact force is regulated.

3.59 $$\boldsymbol{x_c} = \boldsymbol{x} - \Delta \boldsymbol{x_d}$$

The position command signal calculated in Equation 3.59 is used as the input to the position controller. Thus, position-based implementation consists of an inner position control loop with an outer force feedback loop and the contact force information is used to modify the position of the end-effector. In effect, this approach softens a stiff position source.

In the case of no contact, Equation 3.59 reduces to $\boldsymbol{x} = \boldsymbol{x_c}$ and if the manipulator acts as a perfect position source then $\boldsymbol{x_c} = \boldsymbol{x_e}$, which recovers the original relationship of Equation 3.47. Hence, the efficacy of the position-based impedance controller heavily depends upon the performance of inner position control loop.

Using the operational-space model of the manipulator from Equation 3.2, and the impedance model from Equation 3.51 and Equation 3.59, the position-based implementation of impedance control can be presented in operational-space as in Figure 3.2.

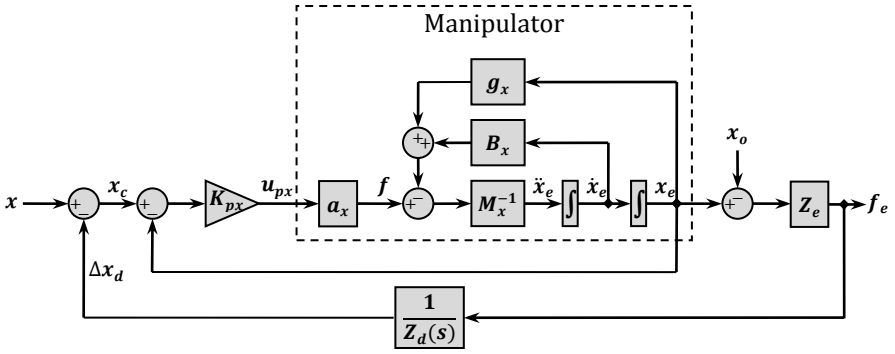

Figure 3.2: Position-based implementation in operational-space

In the block diagram of Figure 3.2 the $\boldsymbol{K_{px}} \in \mathcal{R}^{m \times m}$ is the matrix of position controller gains, which is usually diagonal and $\boldsymbol{a_x} \in \mathcal{R}^m$ is the vector of the actuators' dynamics in operational-space. For a given manipulator the complete behaviour can be characterized by the control signal trajectories used as the input command to the actuators. The control signal $\boldsymbol{u_{px}} \in \mathcal{R}^m$ to the manipulator can be obtained from the above block diagram as:

3.60 $$\boldsymbol{u_{px}} = \boldsymbol{K_{px}} \cdot (\boldsymbol{x_c} - \boldsymbol{x_e})$$

Substituting the value of $\boldsymbol{x_c}$ from Equation 3.59 to Equation 3.60 will result in:

3.61 $$\boldsymbol{u_{px}} = \boldsymbol{K_{px}} \cdot (\boldsymbol{x} - \boldsymbol{x_e}) - \boldsymbol{K_{px}} \cdot \Delta \boldsymbol{x_d}$$

Now substituting the value of $\Delta \boldsymbol{x_d}$ from Equation 3.48, the control law for the position-based impedance controller is given as:

3.62 $$\boldsymbol{u_{px} = K_{px} \cdot (x - x_e) - K_{px} \cdot \frac{1}{Z_d(s)} \cdot f_e}$$

The presentation of Figure 3.2 and Equation 3.62 is important for the design of impedance control, but is not useful for the implementation purpose. As discussed in Section 3.1, the measurement of position in operational-space is not practical. In practice, for most of the manipulators the controller is implemented in joint-space.

In joint-space implementation of the impedance controller the operational-space command is transformed into joint-space command $\boldsymbol{\theta_c} \in \mathcal{R}^n$. This joint-space command is then used as the input for the joint position controllers. The measured joint variables $\boldsymbol{\theta_e} \in \mathcal{R}^n$ are used as the feedback signal for the control loop. Equation 3.64 can equivalently be written in the joint-space as:

3.63 $$\boldsymbol{\theta_c = \theta - \Delta\theta_d}$$

Using the joint-space model from Equation 3.1 and Equation 3.63, the position-based implementation of impedance control in the joint-space is shown in Figure 3.3.

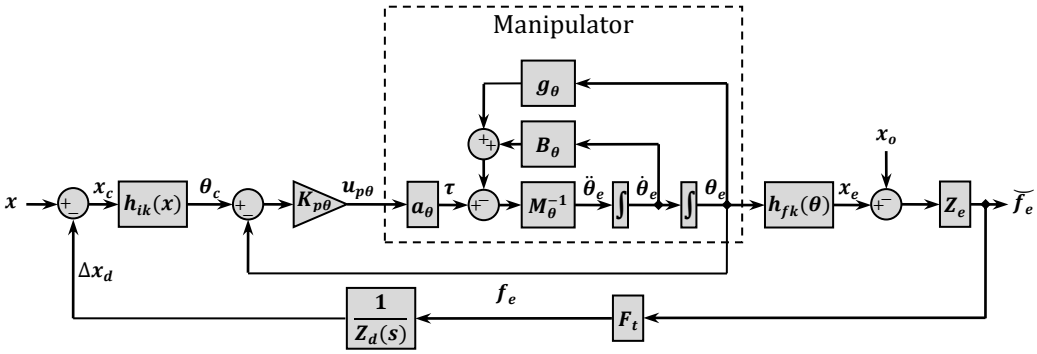

Figure 3.3: Position-based implementation in joint-space

In the above block diagram the $\boldsymbol{K_{p\theta}} \in \mathcal{R}^{n \times n}$ is the matrix of the joint position controller gains, which is usually diagonal. The above implementation is presented with the assumption that contact forces are measured directly with a force/torque sensor attached to the end-effector of the manipulator.

As can be seen, the above implementation requires several transformations between coordinates and also between joint and operational-space variables. Generally referred to as forward kinematics, $\boldsymbol{h_{fk}}(\theta) \in \mathcal{R}^m$ is the vector of functions to estimate the end-effector position from the joint variables. The force measured by the force sensor $\widetilde{\boldsymbol{f_e}} \in \mathcal{R}^m$ is in a moving frame of

reference and needs to be transformed via coordinate transformation matrix $\boldsymbol{F_t} \in \mathcal{R}^{m\times m}$ into a fixed reference frame, which normally is the base of the manipulator. These transformations are numerically costly (Lawrence, 1988); however, with the computation power of modern computers the significance of this factor has been minimized.

The operational-space position trajectory is transformed into joint-space position trajectories using the vector of functions $\boldsymbol{h_{ik}(\theta)} \in \mathcal{R}^n$, which is generally referred to as the closed form inverse kinematics solution (Craig, 2004). Several other methods can be utilized for this purpose, such as transpose of Jacobian matrix (Wolovich, et al., 1984), unit quaternion (Aydin, et al., 2006), etc. Regardless of the method used, the calculation of inverse kinematics is a fundamental problem in robotics (Paul, 1981). At singularities the manipulator can lose certain degrees of freedom and fail to regulate the contact forces along those axes.

Additionally, in the operational-space the orientation is normally represented by Euler angles, which have the fundamental drawbacks of non-uniqueness and singularity. In fact, two different sets of wrist joint angles can result in the same set of Euler angles. The problem, however, can be handled with quaternion or direction cosines, but requires careful handling (Sciavicco, et al., 2001).

Since the measurement of position in operational-space is usually not feasible, the end-effector position is estimated with forward kinematic equation using joint positions. The accuracy of this estimated position depends on accurate knowledge of manipulator geometry. On the other hand, contact force is directly measured in the operational-space. This can lead to inconsistency between operational-space position and force feedback and may result in unstable behaviour of the manipulator during impedance regulation.

The control signal $\boldsymbol{u_{p\theta}} \in \mathcal{R}^n$ to the actuators of the manipulator's joints can be obtained from the block diagram of Figure 3.3 as:

$$\boldsymbol{u_{p\theta}} = \boldsymbol{K_{p\theta}} \cdot (\boldsymbol{\theta_c} - \boldsymbol{\theta_e}) \tag{3.64}$$

Expanding Equation 3.64 will result in:

$$\boldsymbol{u_{p\theta}} = \boldsymbol{K_{p\theta}} \cdot \boldsymbol{h_{ik}}(\boldsymbol{x} - \Delta\boldsymbol{x_d}) - \boldsymbol{K_{p\theta}} \cdot \boldsymbol{\theta_e} \tag{3.65}$$

Now substituting the value of $\Delta\boldsymbol{x_d}$ from Equation 3.48, the control law for the position-based impedance controller is given as:

$$\boldsymbol{u_{p\theta}} = \boldsymbol{K_{p\theta}} \cdot \boldsymbol{h_{ik}}\left(\boldsymbol{x} - \frac{\mathbf{1}}{\boldsymbol{Z_d}(s)} \cdot \boldsymbol{f}_{\mathrm{e}}\right) - \boldsymbol{K_{p\theta}} \cdot \boldsymbol{\theta_e} \tag{3.66}$$

The control laws of Equations 3.62 and 3.66 are reduced to same scalar form for the case of single degree of freedom as below.

3.67 $$u_p = k_p \cdot (\theta - \theta_e) - k_p \cdot \frac{1}{z_d} \cdot \tau_{\mathrm{e}}$$

where all the variables are represented as equivalent scalar quantities.

The control signals presented in Equations 3.62, 3.66 and 3.67 are composed of two components comprising the position and forces of the manipulator. The position control of the manipulator is the primary objective of the controller and the force control act as the secondary objective. During free space motion the force control term disappears and the primary objective is fulfilled. On coming into contact with the environment the controller output is compensated according to the secondary objective of force control. As a result, neither the position nor the force is controlled, but a defined relationship between the two.

3.5.2 Force-based implementation

The force-based implementation (Goldenberg, 1988), (Muhammad, et al., 2006) of impedance controller is much less investigated compared to the position-based counterpart because of practical limitations (Tafazoli, et al., 2002). A detailed discussion on the implementation can be found in (Lawrence, 1988). In the force-based implementation of impedance controller the commanded position trajectory and the desired dynamic relationship $\boldsymbol{Z_d}$ are used to generate the force command signal $\boldsymbol{f_c} \in \mathcal{R}^m$. Hence, the position trajectories are tracked via inner force controller.

During free space motion the manipulator follows the nominal position trajectory $\boldsymbol{x}$. When the manipulator comes into contact with the environment, the environmental force causes the manipulator to deviate from its nominal position trajectory by $\Delta \boldsymbol{x_d}$. This deviation is then tracked by the modification in the command signal $\boldsymbol{f_c}$. The force command signal in the case of force-based impedance controller can be given as:

3.68 $$\boldsymbol{f_c} = \boldsymbol{Z_d} \cdot \Delta \boldsymbol{x_d}$$

Thus, force-based implementation consists of an inner force control loop with an outer position feedback loop and the deviation in the position trajectory is used to modify the commanded force to the end-effector. Hence, the efficacy of the force-based impedance controller heavily

depends upon the performance of the inner force control loop. Indeed, this can be regarded as a scheme which stiffens a soft force source.

Using the operational-space model of manipulator from Equation 3.2 and the impedance model from Equation 3.68, the force-based implementation of impedance control can be presented in operational-space as in Figure 3.4.

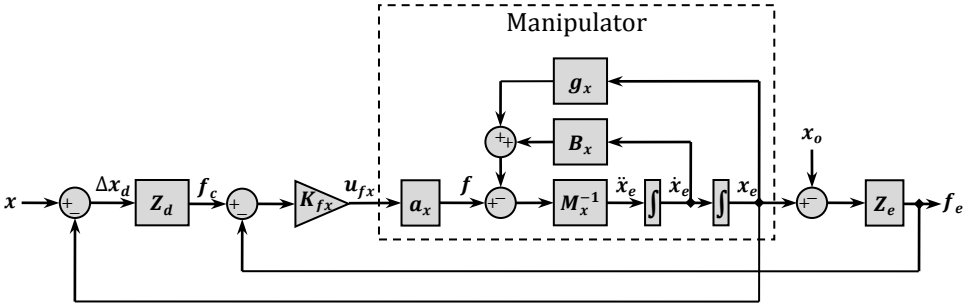

Figure 3.4: Force-based implementation in operational-space

In the block diagram of Figure 3.4 the $\boldsymbol{K_{fx}} \in \mathcal{R}^{m \times m}$ is the matrix of force controller gains, which is usually diagonal. The control signal $\boldsymbol{u_{fx}} \in \mathcal{R}^{m}$ to the manipulator can be obtained from the above block diagram as:

3.69 $$\boldsymbol{u_{fx}} = \boldsymbol{K_{fx}} \cdot (\boldsymbol{f_c} - \boldsymbol{f_e})$$

Substitution of the value of $\boldsymbol{f_c}$ from Equation 3.68 to the above equation will result in:

3.70 $$\boldsymbol{u_{fx}} = \boldsymbol{K_{fx}} \cdot (\boldsymbol{Z_d} \cdot \Delta \boldsymbol{x_d}) - \boldsymbol{K_{fx}} \cdot \boldsymbol{f_e}$$

Now substituting the value of $\Delta \boldsymbol{x_d}$ from Equation 3.47, the control law for the force-based impedance controller is given as:

3.71 $$\boldsymbol{u_{fx}} = \boldsymbol{K_{fx}} \cdot \boldsymbol{Z_d} \cdot (\boldsymbol{x} - \boldsymbol{x_e}) - \boldsymbol{K_{fx}} \cdot \boldsymbol{f_e}$$

As discussed in Section 3.1, the measurement of the position in operational-space is not practical. In practice, the measurement and control of position of the manipulators is performed in joint-space. Hence, the presentation of Figure 3.4 and Equation 3.71 is not useful for the implementation purpose.

In joint-space implementation the operational-space command is transformed into joint-space command $\boldsymbol{\tau_c} \in \mathcal{R}^{n}$. This joint-space command is then used as an input for the joint force

controllers. Using the joint-space model from Equation 3.1, the force-based implementation of impedance control in the joint-space is shown in Figure 3.5.

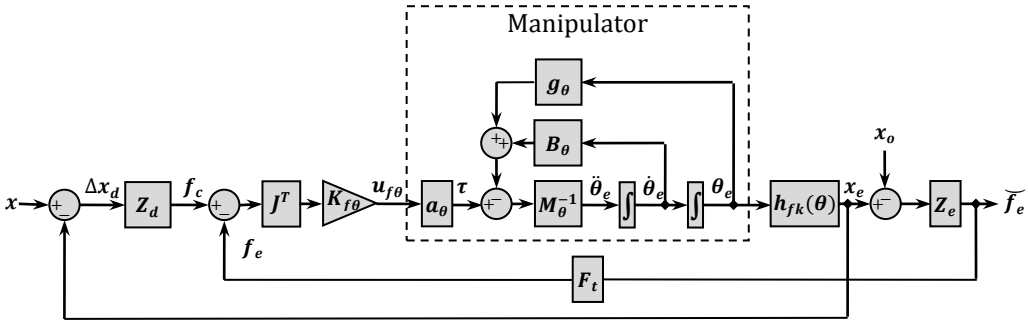

Figure 3.5: Force-based implementation in joint-space

In the block diagram of Figure 3.5 the $\boldsymbol{K_{f\theta}} \in \mathcal{R}^n$ is the matrix of the joint force controller gains, which is usually diagonal. The above scheme is presented with the assumption that contact forces are measured directly with a force/torque sensor attached to the end-effector. As in the case of position-based implementation, the above scheme also requires similar transformations between coordinates and also between joint and operational-space variables.

The control signal $\boldsymbol{u_{f\theta}} \in \mathcal{R}^n$ to the actuators of the manipulator's joints can be obtained from the block diagram of Figure 3.5 as:

3.72 $$\boldsymbol{u_{f\theta} = K_{f\theta} \cdot J^T \cdot (f_c - f_e)}$$

Now expanding Equation 3.72 and substituting the value of $\boldsymbol{f_c}$ from Equation 3.68 will result in:

3.73 $$\boldsymbol{u_{f\theta} = K_{f\theta} \cdot J^T \cdot Z_d \cdot \Delta x_d - K_{f\theta} \cdot J^T \cdot f_e}$$

Substituting Equation 3.47:

3.74 $$\boldsymbol{u_{f\theta} = K_{f\theta} \cdot J^T \cdot Z_d \cdot (x - x_e) - K_{f\theta} \cdot J^T \cdot f_e}$$

Which gives the control law for the force-based impedance controller in joint-space. The control laws of Equations 3.71 and 3.74 are reduced to the same scaler form for the case of single degree of freedom as below.

3.75 $$u_f = k_f \cdot z_d \cdot (\theta - \theta_e) - k_f \cdot \tau_e$$

where all the variables are represented as equivalent scalar quantities.

The control signals presented in Equations 3.71, 3.74 and 3.75 are composed of two components controlling the position and the forces. In contrast to the case of position-based implementation, force control of the manipulator is the primary objective of the controller and position control is the secondary objective. In free space motion the position control term disappears and the primary objective is fulfilled, while on coming into contact with the environment the controller output is compensated according to the secondary objective of position control. As a result, neither the position nor the force is controlled, but the impedance is defined as the ratio of the two.

3.6 Equivalence of position and force based implementations

It is understood that equivalence exists between explicit force control and impedance control. Both types of controllers can be converted to each other, and when optimized should have similar bandwidths (De Schutter, et al., 1998). Expressions to obtain equivalent position-based impedance controller and explicit force controllers have been derived, implemented and verified by several researchers, for example (Heinrichs, et al., 1999), (Volpe, et al., 1995). In the following an attempt is made to establish a relationship between position and force based implementations of impedance controller.

In the last section the equations for the controller output are derived for position and force-based implementations of impedance controller. A comparison of Equations 3.62 and 3.71 shows that in both cases the control signals are the function of the same variables, which are the manipulator's position and force. In principle, for a given set of variables if the same control signal trajectories are applied, the behaviour of the system should remain invariable. Therefore, if the same control signal is calculated, then equivalent implementations of position and force-based impedance controllers can be obtained. Therefore, comparing the coefficients of Equations 3.62 and 3.71 the relationship between the two controllers can be found as below.

3.76 $$\boldsymbol{K_{fx} = K_{px} \cdot \frac{1}{Z_d(s)}}$$

Equation 3.76 shows that equivalent control signal can be applied to the manipulator, which should result in equivalent position and force trajectories. In other words, it can be stated that for any position controller designed for position-based impedance controller, there is an equivalent force controller for force-based implementation, and vice versa.

Similarly, the comparison between the coefficients of Equations 3.67 and 3.75 can provide the same result in the scalar form for a single degree of freedom.

3.77 $$k_f = k_p \cdot \frac{1}{z_d}$$

However, the comparison of Equations 3.66 and 3.74, which represent position-based and force-based implementations of impedance controller in joint-space respectively does not reveal such a straightforward relationship. The ambiguity arises from the fact that the joint-space and operational-space position of manipulator are related via nonlinear function, i.e. $\boldsymbol{h_{ik}(\theta)}$. In cases where a linear relationship can be established between joint-space and operational-space, the impedance control law of Equation 3.66 can be restated as:

3.78 $$\boldsymbol{u_{p\theta} = K_{p\theta} \cdot J^{-1} \cdot x - K_{p\theta} \cdot J^{-1} \cdot \frac{1}{Z_d(s)} \cdot f_e - K_{p\theta} \cdot \theta_e}$$

Where the manipulator's Jacobian $\boldsymbol{J}$ has been utilized for the linear mapping, which, according to Equation 3.8, is true for small manipulator motions. Now, expanding the above equation and using the relationship of Equation 3.7 it can be written as:

3.79 $$\boldsymbol{u_{p\theta} = K_{p\theta} \cdot (\theta - \theta_e) - K_{p\theta} \cdot J^{-1} \cdot \frac{1}{Z_d(s)} \cdot J^T \cdot \tau_e}$$

Proceeding similarly with Equation 3.74 will result in:

3.80 $$\boldsymbol{u_{f\theta} = K_{f\theta} \cdot J^T \cdot Z_d \cdot J \cdot (\theta - \theta_e) - K_{f\theta} \cdot \tau_e}$$

Now the comparison of Equations 3.79 and 3.80 reveals an equivalent relationship in the joint-space.

3.81 $$\boldsymbol{K_{f\theta} = K_{p\theta} \cdot J^{-1} \cdot \frac{1}{Z_d(s)} \cdot J^{-T}}$$

However, the above relationship is only an approximation and is not valid for a general case, and can only be applied for a certain types of manipulators where the joint-space and operational-space position have a linear relationship. Such cases are Caresian and Gantry type manipulators, where each axis of motion in operational-space is a function of a single joint variable and motions are completely decoupled. In fact, in such cases the Jacobian of the manipulator is an identity matrix and the relationship of Equation 3.81 simply reduces to Equation 3.76. Additionally, in such cases the impedance model will have the same representation in operational-space and joint-space of the manipulator.

Hence, from the practical implementation point of view, though equivalent performance can be obtained from either implementation of impedance control, in general it will require the separate tuning of internal position and force controllers.

3.7 Redundancy resolution

In the last section impedance control and its implementation for the manipulators has been discussed. Fundamentally, the impedance controller modifies either the position or the force set point of the manipulator to regulate the impedance. The capability of the manipulator to make the adjustment to this new set point can be characterized by its dynamic characteristics. The faster the dynamics, or in other words the higher the bandwidth of the manipulator, the faster and smoother it can make this adjustment in the set point (Matko, et al., 1999), (Seraji, et al., 1993a). This will not only result in improved impedance control but will also improve the stability characteristics of the impedance controller.

It is widely understood that in using the redundant degrees of freedom, a manipulator is capable of generating internal joint-space velocities without producing any operational-space velocities (Sciavicco, et al., 2001). Using these internal motions, the manipulator's joints can be reconfigured to attain a posture which can suitably fulfil an additional higher level objective function (Liegeois, 1977).

This objective function can be defined in a variety of ways to improve the kinematic (Klein, et al., 1987), (Zghal, et al., 1990), (Maciejewski, et al., 1985), (Yoshikawa, 1985a) or the dynamic (Hirakawa, et al., 1997), (Hollerbach, et al., 1987) performance of the manipulator. In the following an objective function based on DME has been devised to optimize the dynamic behaviour of the manipulator and thus to enhance the performance of the impedance controller.

According to Equation 3.6, at any instant for the given Jacobian of the manipulator the joint-space velocities can be expressed as a function of operational-space velocities. Considering the manipulator is redundant and Jacobian has more columns than rows, Equation 3.6 has an infinite number of solutions. A practical approach is to implement the solution in a way that satisfies Equation 3.6 and minimises the quadratic cost function of the joint velocities. In this case the solution is of the form:

$$\dot{\boldsymbol{\theta}} = \boldsymbol{J}^{\dagger} \cdot \dot{\boldsymbol{x}} + (\boldsymbol{I} - \boldsymbol{J}^{\dagger} \cdot \boldsymbol{J}) \cdot \dot{\boldsymbol{\theta}}_{\boldsymbol{0}} \tag{3.82}$$

Here $\boldsymbol{I} \in \mathcal{R}^{n \times n}$ is the identity matrix and $\boldsymbol{J}^{\dagger}$ is the right pseudo-inverse of the Jacobian matrix (Whitney, 1969) and it is given as:

$$\boldsymbol{J}^{\dagger} = \boldsymbol{J}^{\boldsymbol{T}} \cdot (\boldsymbol{J} \cdot \boldsymbol{J}^{\boldsymbol{T}})^{-1} \tag{3.83}$$

The first term of Equation 3.82 is related to the primary objective of a minimum norm of joint velocities. The second term tries to achieve the secondary objective defined by the constraint $\dot{\boldsymbol{\theta}}_{\mathbf{0}}$. In fact, the matrix $(\boldsymbol{I} - \boldsymbol{J}^{\dagger} \cdot \boldsymbol{J})$ projects the joint-space velocities $\dot{\boldsymbol{\theta}}_{\mathbf{0}}$ into the null space of $\boldsymbol{J}$ so as not to cause any motions at the end-effector. Therefore, for $\dot{\boldsymbol{x}} = \mathbf{0}$, internal joint-space motions can be generated to reconfigure the posture of the manipulator, which suits better for the task execution.

For the case when optimized dynamic performance of the manipulator is desireable, the posture can be configured using the DME discussed in Section 3.2. As a result, the desired joint-space forces can be minimized to improve the acceleration capability of the manipulator. One such index is referred to as dynamic manipulability index (Yoshikawa, 1985) and is given as:

$$w_1(\boldsymbol{\theta}) = \prod_{i=1}^{m} \sigma_i \Longrightarrow \sqrt{\det\left(\boldsymbol{J} \cdot \left(\boldsymbol{M_{\theta}}^{\boldsymbol{T}} \cdot \boldsymbol{M_{\theta}}\right)^{-\mathbf{1}} \cdot \boldsymbol{J}^{\boldsymbol{T}}\right)} \tag{3.84}$$

Using the index of Equation 3.84, the secondary constraint $\dot{\boldsymbol{\theta}}_{\mathbf{0}}$ can be obtained as:

$$\dot{\boldsymbol{\theta}}_{\mathbf{0}} = k \cdot \left(\frac{\partial w_1(\boldsymbol{\theta})}{\partial \boldsymbol{\theta}}\right)^{T} \tag{3.85}$$

Here $k > 0$ is the weighing factor and can be modifed to tighten or soften the secondary constraint. Now substituting the value of $\dot{\boldsymbol{\theta}}_{\mathbf{0}}$ from Equation 3.85 into Equation 3.82, the solution to exploit the redundant degrees of mobility for the optimized dynamic performance can be presented as:

$$\dot{\boldsymbol{\theta}} = \boldsymbol{J}^{\dagger} \cdot \dot{\boldsymbol{x}} + k \cdot (\boldsymbol{I} - \boldsymbol{J}^{\dagger} \cdot \boldsymbol{J}) \cdot \left(\frac{\sqrt{\det\left(\boldsymbol{J} \cdot \left(\boldsymbol{M_{\theta}}^{\boldsymbol{T}} \cdot \boldsymbol{M_{\theta}}\right)^{-\mathbf{1}} \cdot \boldsymbol{J}^{\boldsymbol{T}}\right)}}{\partial \boldsymbol{\theta}}\right) \tag{3.86}$$

The above index for the optimized dynamic performance has been presented by (Yoshikawa, 1985) and is well-known for redundancy resolution and relies on maximizing the product of the singular values of matrix $\boldsymbol{J} \cdot \boldsymbol{M_{\theta}}^{-\mathbf{1}}$ where the inertia matrix has been used in its original form rather then the normalized form as in Section 3.2. It is intuitive since the requirement is not to compare the design of different manipulators, but control of the existing manipulator.

Unfortunately, the index $w_1(\boldsymbol{\theta})$ has the serious disadvantage of computational complexity. In fact, it is practically impossible to compute it in symbolic form as the function of joint variables, except for the simplest of cases (Sciavicco, et al., 2001). It is much more reasonable to numerically evaluate the index $w_1(\boldsymbol{\theta})$, for various manipulator configurations. Then the selected joints of manipulator can be forced into configuration such that the index is maximized.

One such objctive funtion to keep the joints within a certain range of motion is given as in (Sciavicco, et al., 2001):

3.87 $$h(\boldsymbol{\theta}) = -\frac{1}{2n}\sum_{i=1}^{n}\left(\frac{\theta_i - \bar{\theta}_i}{\theta_{i_{max}} - \theta_{i_{min}}}\right)^2$$

Where, $\theta_{i_{max}}$ and $\theta_{i_{min}}$ are the maximum and minium range of motion of joint i respectively, and $\bar{\theta}_i$ is the middle value of joint range. Thus, by maximizing the index of Equation 3.87 the the redundant degrees of freedom can be exploited by forcing certain manipulator's joints into the desired range of motion. Now, using the index of Equation 3.87, the secondary constraint $\dot{\boldsymbol{\theta}}_{\boldsymbol{o}}$ can be obtained as:

3.88 $$\dot{\boldsymbol{\theta}}_{\mathbf{0}} = k \cdot \left(\frac{\partial h(\boldsymbol{\theta})}{\partial \boldsymbol{\theta}}\right)^T$$

Hence, a redundancy resolution scheme can be formed by introducing an artificial joint range of motion, as below:

3.89 $$\dot{\boldsymbol{\theta}} = \boldsymbol{J}^{\dagger} \cdot \dot{\boldsymbol{x}} + k \cdot (\boldsymbol{I} - \boldsymbol{J}^{\dagger} \cdot \boldsymbol{J}) \cdot \left(\frac{-\frac{1}{2n}\sum_{i=1}^{n}\left(\frac{\theta_i - \bar{\theta}_i}{\theta_{i_{max}} - \theta_{i_{min}}}\right)^2}{\partial \boldsymbol{\theta}} \right)$$

Like Equation 3.86, the redundancy resolution scheme of Equation 3.89 does not guarantee to keep the manipulator in the exact optimized posture, but very close to it, and it is far simpler to compute. Since manipulator posture selection is within the close vicinity of maximum singular values, the scheme also ensures the avoidance of singularities. In Chapter 5 this scheme will be elaborated further using numerical analysis.

3.8 Summary

The dynamic manipulability of the manipulator is discussed in the context of DME (Dynamic Manipulability Ellipsoid). As one of the contributions of this thesis work, DME formulation has been used to show that the presence of redundant degrees of mobility can result in improved dynamic performance of the manipulator. The results show that due to redundant degrees of freedom the singular values of the matrix $\boldsymbol{J} \cdot \widehat{\boldsymbol{M}}_{\boldsymbol{\theta}}{}^{-1}$ will be larger. Since these singular values represent the lengths of the axes of DME, this will result in a larger volume of DME.

The model of the manipulator and its interaction with the environment has been presented. This model is then used for the development of impedance controller. Both operational-space and joint-space presentations of position-based and force-based implementations of impedance controller are discussed. As another contribution of this thesis, the equivalence between position-based and force-based implementations of impedance controller is discussed for a general case of multi-degrees of freedoms. It was shown that equivalent implementation can be obtained in cases where a linear relationship exists between the joint-space and operational-space variables. In such cases the relationship between the inner loop position and force controllers can be given by Equations 3.76, 3.77 and 3.81.

In the end, a cost function has been devised to exploit the redundant degrees of freedom for improved dynamic performance and thus improved impedance control of the manipulator. The results of the above contributions can be combined to develop suitable impedance control strategies for the manipulators.

The discussion and results in this chapter regarding impedance control and the effects of redundancy on the dynamic performance of a manipulator have been kept general, without references to any particular manipulator. The purpose is to keep the findings useful for other developments and continue the research and discussion process on a wider scale. In later chapters the findings will be verified by numerical simulation and experiments with WHMAN (Water Hydraulic MANipulator), which consists of redundant degrees of freedom in joint-space.

4 MODELLING OF THE MANIPULATOR

Further study of the results obtained in Chapter 3 has been done using the WHMAN (Water Hydraulic MANipulator) as a case study, which contains redundant degrees of freedom. For the preliminary verification of the theoretical results and the designing of the controller a reasonably accurate model of this manipulator is essential. Therefore, this chapter is dedicated to the development of analytical and simulation models of WHMAN.

The structure and the instrumentation of WHMAN are provided in Section 4.1. In Section 4.2 an analytical model of WHMAN in the form of Equation 3.1 is developed using Lagrange's energy balance principle. As a first step towards the development of the simulation model, the model of a single vane actuator is developed and verified in Section 4.3. In Section 4.4 the model of a single vane actuator is used to develop the model for the entire WHMAN. This model is then verified against the measurements from the actual manipulator. These developments are summarized in Section 4.5.

4.1 Description of WHMAN

As shown in the 3D model of Figure 4.1, the WHMAN is composed of eight joints. The arm of the manipulator is composed of three rotational and one linear joint. The rotational joints provide a spherical workspace, while the linear joint provides the telescopic motion of the arm. Hence, it is an anthropomorphic arm with linear extension joint between shoulder and elbow joints. A spherical wrist composed of three rotational joints is attached at the end of the arm to achieve the desired orientation. Together the arm and the wrist provide six degrees of freedom in operational-space of the manipulator. The rotational joints are driven by the water hydraulic vane actuators, while the telescopic arm extension is driven by a water hydraulic cylinder. The complete manipulator is mounted on top of the Cassette Multifunctional Mover (CMM) via a linear slide, which is directly driven by an electric motor via a screw shaft and forms the eighth joint of the WHMAN. However, during the experiments the manipulator is installed on top of a test stand, where the linear slide is driven by a water hydraulic cylinder. A complete detail of the kinematic and hydraulic parameters can be found in Appendices A and C respectively.

The water hydraulic vanes and cylinder are driven by flow control servo valves with a flow rate of $6.8 \times 10^{-5}\,\mathrm{m}^3/\mathrm{s}$ at a nominal pressure of $3.5\,\mathrm{MPa}$ per control notch. Each valve is

controlled by a signal of ± 10 mA. A supply pressure of 21 MPa has been used to drive the actuators. The linear slide is driven by an electric motor with a torque constant of $0.45\ \mathrm{Nm/A}$. The motor can provide a peak torque of 6.6 Nm and a continuous torque of 2.1 Nm. The motor is controlled via a drive for which the control signal is ± 10 V.

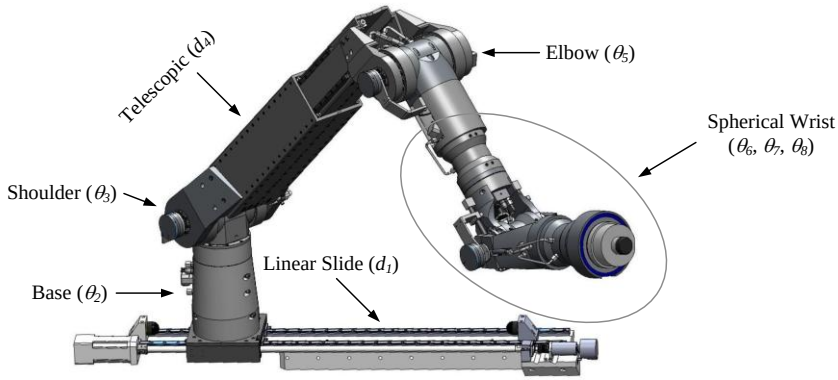

Figure 4.1: 3D CAD model of WHMAN

Each vane and cylinder is equipped with two pressure sensors with a measuring range up to 35 MPa. The torque of the motor can be read from analogue output of the drive through which the axial force on the manipulator via screw shaft can be estimated.

The angular position of the vane actuators is measured via dual speed resolvers with an absolute accuracy of $\pm 9.3° \times 10^{-4}$. The linear position of the cylinder is measured with a LVDT (Linear Variable Differential Transformer), which provides an accuracy of $\pm 6.1 \times 10^{-6}$ m. The linear slide is equipped with two resolvers which act together as a dual speed resolver. From these resolvers the position of the manipulator on the linear slide can be measured with an accuracy of $\pm 4.63 \times 10^{-6}$ m.

Figure 4.2: WHMAN during operation

For the measurement of environmental contact forces a six axes force/torque sensor is attached at the end of the WHMAN wrist. The minimum resolution of the sensor is $1\,\mathrm{N}/1\,\mathrm{Nm}$. The WHMAN is shown in the photograph in Figure 4.2.

4.2 Analytical model of WHMAN

The dynamic model of a mechanical system such as a manipulator can be derived using for example the Lagrange's formulation based on energy balancing or the Newton-Euler formulation based on force balancing. Here, Lagrange's formulation has been utilized, as with this approach the equations of motion for a mechanical system can be derived in a systematic and recursive way. The Lagrangian of a mechanical system is given as:

4.1 $$\mathcal{L} = \mathcal{T} - \mathcal{U}$$

Here $\mathcal{T}$ and $\mathcal{U}$ are the kinetic and potential energies of the system respectively. Using the Lagrangian $\mathcal{L}$ the equation of motion of the system is given as:

4.2 $$f_i = \frac{d}{dt}\frac{\partial \mathcal{L}}{\partial \dot{\theta}_i} - \frac{\partial \mathcal{L}}{\partial \theta_i} = \frac{d}{dt}\frac{\partial \mathcal{T}}{\partial \dot{\theta}_i} - \frac{\partial \mathcal{T}}{\partial \theta_i} + \frac{\partial \mathcal{U}}{\partial \theta_i}$$

Here f_i is the force associated with the coordinate θ_i and t is the time. For a mechanical structure such as a manipulator the natural choice of coordinates are the joint variables. With a manipulator composed of n joints the total kinetic energy and potential energy can be given as the sum of kinetic and potential energies of each link respectively, as given by Equations 4.3 and 4.4 respectively.

4.3 $$\mathcal{T} = \frac{1}{2}\left(\sum_{i=1}^{n} m_i \dot{\boldsymbol{\theta}}^{\boldsymbol{T}} \boldsymbol{J}_{\boldsymbol{i}}^{(\boldsymbol{x})^{\boldsymbol{T}}} \boldsymbol{J}_{\boldsymbol{i}}^{(\boldsymbol{x})} \dot{\boldsymbol{\theta}} + \sum_{i=1}^{n} \dot{\boldsymbol{\theta}}^{\boldsymbol{T}} \boldsymbol{J}_{\boldsymbol{i}}^{(\boldsymbol{r})^{\boldsymbol{T}}} \boldsymbol{R}_{\boldsymbol{i}} \boldsymbol{M}_{\boldsymbol{i}}^{\boldsymbol{i}} \boldsymbol{R}_{\boldsymbol{i}}^{\boldsymbol{T}} \boldsymbol{J}_{\boldsymbol{i}}^{(\boldsymbol{r})} \dot{\boldsymbol{\theta}}\right)$$

4.4 $$\mathcal{U} = \sum_{i=1}^{n} m_i \boldsymbol{g}^{\boldsymbol{T}} \boldsymbol{x}_{\boldsymbol{i}}$$

Here i is the link index actuated by the respective joint. m and $\boldsymbol{M}$ are the scalar mass and the inertia tensor matrix of the link respectively. $\boldsymbol{J}^{(\boldsymbol{x})}$ and $\boldsymbol{J}^{(\boldsymbol{r})}$ are the translational and rotational Jacobian matrices respectively. $\boldsymbol{R}$ is the rotation matrix, $\boldsymbol{x}$ is the position vector and $\boldsymbol{g}$ is the vector of acceleration due to gravity.

Using Equations 4.1 to 4.4, the analytical model of the WHMAN with eight degrees of freedom in joint-space ($n = 8$) can be developed in the form of Equation 4.5 below.

4.5 $$\boldsymbol{\tau} = \boldsymbol{M_\theta}(\boldsymbol{\theta})\ddot{\boldsymbol{\theta}} + \boldsymbol{B_\theta}(\boldsymbol{\theta}, \dot{\boldsymbol{\theta}})\dot{\boldsymbol{\theta}} + \boldsymbol{g_\theta}(\boldsymbol{\theta})$$

where $\boldsymbol{\theta} = [\theta_1, \theta_2, \dots, \theta_n]^T \in \mathcal{R}^n$ is the vector of joint variables and $\boldsymbol{\tau} = [\tau_1, \tau_2, \dots, \tau_n]^T \in \mathcal{R}^n$ is the vector of joint forces. $\boldsymbol{M_\theta}(\boldsymbol{\theta}) \in \mathcal{R}^{n \times n}$ is the inertia matrix of the manipulator, which is symmetric, positive definite and can be computed as:

4.6 $$\boldsymbol{M_\theta}(\boldsymbol{\theta}) = \sum_{i=1}^{n} \left(m_i \boldsymbol{J_i^{(x)^T}} \boldsymbol{J_i^{(x)}} + \boldsymbol{J_i^{(r)^T}} \boldsymbol{R_i} \boldsymbol{M_i^i} \boldsymbol{R_i}^T \boldsymbol{J_i^{(r)}} \right)$$

Matrix $\boldsymbol{B_\theta}(\boldsymbol{\theta}, \dot{\boldsymbol{\theta}}) \in \mathcal{R}^{n \times n}$ represents the centrifugal and Coriolis forces. Its elements referred to as the Christofell symbols can be computed using Equation 4.7.

4.7 $$\boldsymbol{b_{ij}}(\boldsymbol{\theta}, \dot{\boldsymbol{\theta}}) = \sum_{k=1}^{n} \frac{1}{2} \left(\frac{\partial m_{ij}}{\partial \theta_k} + \frac{\partial m_{ik}}{\partial \theta_j} - \frac{\partial m_{jk}}{\partial \theta_i} \right)$$

$\boldsymbol{g_\theta}(\boldsymbol{\theta}) \in \mathcal{R}^n$ is the vector of gravity forces and can be computed using Equation 4.8.

4.8 $$\boldsymbol{g_\theta}(\boldsymbol{\theta}) = -\sum_{i=1}^{n} m_i \boldsymbol{g^T} \boldsymbol{J_i^{(x)}}$$

For the development of the analytical model the links of the WHMAN are assumed to be in the form of slender rods, with the centre of gravity located at the middle of the link and the mass distributed evenly across the link length. Due to these assumptions the inertia tensor matrices of the manipulator's links become diagonal. This results in a simplified and so-called stick-figure model of the manipulator. Without these simplifications the model of the manipulator becomes too cumbersome, computationally heavy and does not provide much additional information.

The values of the above matrices and vectors in Equation 4.5 along with the other parameters of the manipulator are provided in Appendix B.

4.3 Simulation model of single actuator

The study of force and position control properties of the vane actuator with water as the pressure medium has been previously conducted by (Raneda, 2004). The vane was originally

designed to be used with oil as the pressure medium. Apart from this, little research has been done with vanes designed to be used with water as the pressure medium (Muhammad, et al., 2009a).

In this section the characteristics and the modelling of a water hydraulic vane actuator are presented. The vane has been designed to actuate the joints of WHMAN which is required to carry out several remote handling operations in the divertor region of ITER (Siuko, et al., 2003). The modelling of this vane actuator is the essential starting step towards modelling of the water hydraulic manipulator.

Both the linear and nonlinear models of the vane actuator are developed here. The linear model is used to take advantage of rich linear control theory and to develop the controller for the system. The nonlinear model, many times referred to as the "true model", is useful to validate the performance of the controller and to analyse the behaviour of several system parameters.

4.3.1 Description of vane actuator

The structure of the vane actuator's control and measurement system is shown in the schematic of Figure 4.3. The total range of motion is $4.7\ \text{rad}\ (270°)$ which is divided around 0° such that the actual movement is $\pm 135°$. The specific volume of the vane is $2.8 \times 10^{-5}\ \text{m}^3/\text{rad}$. The actuator is designed to operate at a pressure of $21\ \text{MPa}$ resulting in the maximum torque of $600\ \text{Nm}$. During the experiments and measurements a supply pressure of $20\ \text{MPa}$ has been used. A load mass of $37\ \text{kg}$ is attached at the end of the arm length of $1\ \text{m}$. The estimated inertial load is around $28.5\ \text{kgm}^2$ and the estimated maximum torque is around $370\ \text{Nm}$ at the vane actuator. This gives the system the realistic behaviour of a manipulator link.

The vane is driven by a flow control servo valve with a flow rate of $6.8 \times 10^{-5}\ \text{m}^3/\text{s}$ at a nominal pressure of 3.5 MPa per control notch. The valve is controlled by a signal of $\pm 10\ \text{mA}$ (or $\pm 10\ \text{V}$ to the amplifier). The vane is equipped with two pressure sensors with a range up to $35\ \text{MPa}$. The position of the arm is measured by using a pulse encoder with a resolution of $5000 \times 50 \times 4\ \text{pulses/revolution}\ (3.6° \times 10^{-4})$.

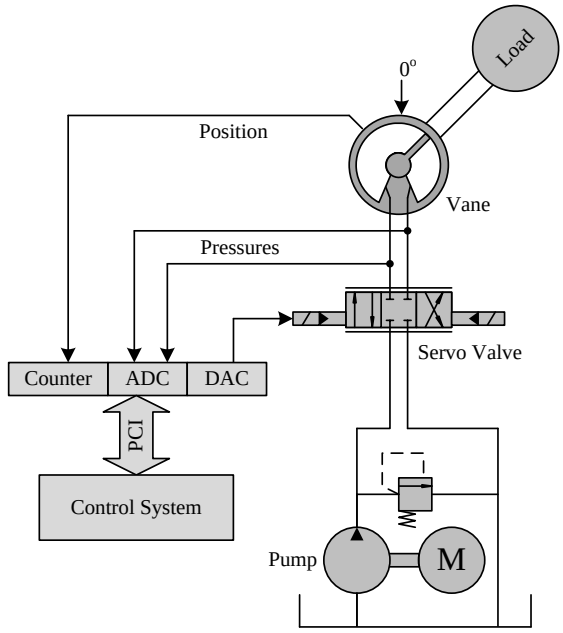

Figure 4.3: Single vane actuator setup

4.3.2 Linear model

Due to the availability of a rich set of tools in linear control theory a linear model of the system is often desirable. The linear model can be used for theoretical analysis and for preliminary controller design. Many of the following equations can be found in hydraulic texts, such as (Merritt, 1967), (Jelali, et al., 2002). Here they have been reproduced for the sake of reference and discussion.

The linear model of the hydraulic position servo system can be described by the block diagram of Figure 4.4. Here, b_{eff} is the effective bulk-modulus of the system, v_0 is the average contained volume in the chambers and l_{ce} is the combined leakage coefficient of the valve and vane. u, k_q and q are the input signal, flow coefficient and the output flow of the valve respectively. p_d, d, τ, and θ are the pressured difference, specific volume, torque and the angular position of the vane actuator. b and τ_b are the viscous friction coefficient and the viscous friction torque respectively. m_i is the inertia load of the arm.

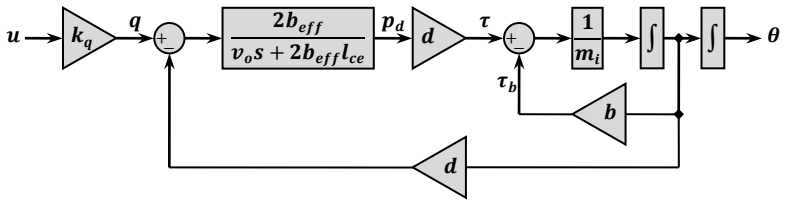

Figure 4.4: Block diagram of the linear model

Correspondingly, the above model can be written as the transfer function of Equation 4.9.

4.9 $$\frac{\theta(s)}{u(s)} = \frac{\frac{k_q}{d}}{s\left(\left(\frac{m_i v_0}{2b_{eff} d^2}\right)s^2 + \left(\frac{2m_i b_{eff} l_{ce} + b v_0}{2b_{eff} d^2}\right)s + 1\right)}$$

where s is the Laplace operator. Equation 4.9 can be expressed in terms of standard second order transfer function of Equation 4.10 along with an integrator.

4.10 $$\frac{\theta(s)}{u(s)} = \frac{k_{qa}\omega_n^2}{s(s^2 + 2\delta_n\omega_n s + \omega_n^2)}$$

Comparing with Equation 4.9, the parameters of the linear model: velocity gain k_{qa}, natural frequency ω_n and the natural damping ratio δ_n of the system are given below by Equations 4.11, 4.12 and 4.13 respectively.

4.11 $$k_{qa} = \frac{q_N\sqrt{\frac{\Delta p}{\Delta p_N}}}{d u_{max}}$$

4.12 $$\omega_n = \sqrt{\frac{2b_{eff} d^2}{m_i v_0}}$$

4.13 $$\delta_n = \frac{l_{ce}}{d}\sqrt{\frac{m_i b_{eff}}{2v_0}} + \frac{b}{4d}\sqrt{\frac{2v_0}{m_i b_{eff}}}$$

Here, q_N and Δp_N are the nominal flow and pressure difference respectively. From Equation 4.11 the value of velocity gain is calculated to be $0.405\ (\mathrm{rad/s})/\mathrm{V}$, which is same as the measured value.

The parameters in Equation 4.12 are well-defined. With the value of $b_{eff} = 2100 \times 10^6$ Pa, which is the bulk modulus of the water, the natural frequency is calculated as $42.2\ (\mathrm{rad/s})$,

which is a little higher than the experimental value. It is common practice to use much lower values of bulk modulus to determine the natural frequency of the hydraulic system. Since no flexible hoses are present and the valve is directly mounted on the actuator the reason for lower bulk modulus can be the entrapped air in the water in this case. With the value of $b_{eff} = 1700 \times 10^6$ Pa the natural frequency is $37.62\ \mathrm{rad/s}$, which is very close to the measured value of $38\ \mathrm{rad/s}$.

When Equation 4.13 is used for the estimation of damping ratio, much larger and non-realistic values of the parameters need to be used. According to (Virvalo, et al., 1999a), internal leakage and viscous friction plays a minor role to provide any damping to the system. Almost half of the damping comes from the coulomb friction. Equation 4.14 below includes the damping component due to coulomb friction.

$$\delta_n = \frac{l_{ce}}{d}\sqrt{\frac{m_i b_{eff}}{2v_0}} + \frac{b}{4d}\sqrt{\frac{2v_0}{m_i b_{eff}}} + \frac{2\tau_c}{\pi k_s z_0} \tag{4.14}$$

Here, τ_c is the Columbic friction torque, k_s is the stiffness of the hydraulic spring and z_0 is the overshoot in the open-loop response of the system. Using Equation 4.14, the value of natural damping is 0.37, which is very close to the experimentally determined value of 0.38.

Substituting the above values of velocity gain, natural frequency and damping into Equation 4.10, the linear model of the system can be obtained. The simulated open-loop response of this model is compared against the measured velocity and the position of the vane actuator. The comparison is shown in the plots of Figure 4.5. Both velocity and position outputs of the model match reasonably well with the measured outputs of the system.

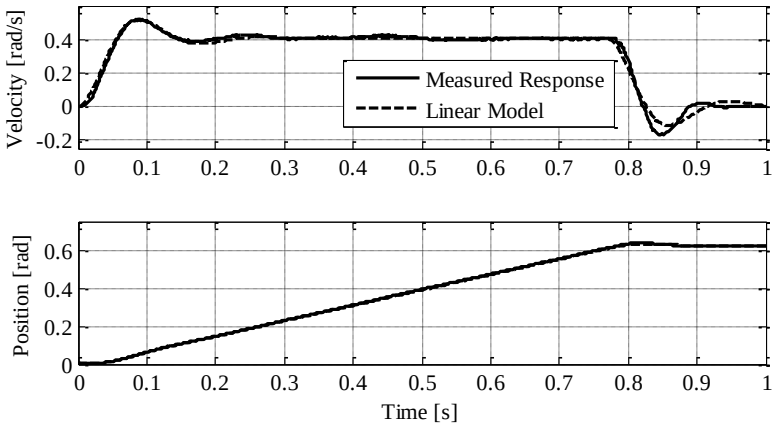

Figure 4.5: Measured and simulated response of linear model

4.3.3 Nonlinear model

The performance of the hydraulic servo systems is a function of several nonlinearities which exist in the valve and the actuator. The most dominant of these nonlinearities are the valve offset and hysteresis, the friction in the load and the actuator and leakages both in the valve and the actuator. Considering these nonlinearities of hydraulic components, the situation actually gets worse with water hydraulic servo systems. The choice of water hydraulic components in the market is much more limited and the quality of water hydraulic servo valves is not as high as that of oil hydraulic servo valves. The leakage is normally higher due to low viscosity, and so is the friction in the actuator. Hence, an understanding of these nonlinearities is of prime importance in the design of water hydraulic servo systems.

To investigate these nonlinearities, a component-based approach is adopted for the modelling of the overall system of Figure 4.3. The model is divided into three major sub-models/components, namely servo valve, vane actuator and arm mechanism. The parameters of each component are obtained either from the manufacturer's datasheets or experimentally. These components are then connected to obtain the entire model of the system. The schematic of the model as Simulink® block diagram is shown in Figure 4.6.

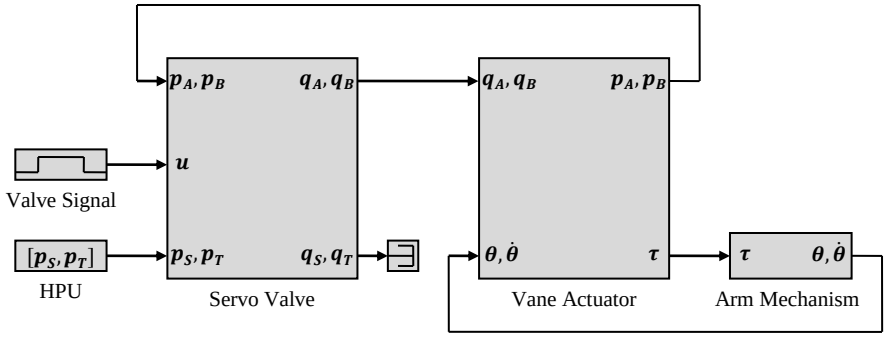

Figure 4.6: Simulink® block diagram of nonlinear model

The nonlinear model of the servo valve developed by (Linjama, 1998) is used. The values of the nonlinearities such as internal leakage and hysteresis are obtained from the manufacturer's data sheet. The valve offset is determined experimentally. A list of nonlinear characteristics of the valve and their values are given in Table 4.1.

The vane actuator is modelled using the continuity equation. The leakage coefficient and friction parameters are determined experimentally. The internal leakage is modelled as laminar flow, which is directly proportional to the pressure difference between the chambers. Friction is

modelled using the LuGre friction model (Canudas-de-Wit, et al., 1995), which includes static, Coulomb and viscous friction regimes, as well as Stribeck effect. A list of nonlinear characteristics of the valve and their values are given in Table 4.2.

Table 4.1: Nonlinear characteristics of the valve

Parameter	Value	Units
Internal leakage	3.3×10^{-13}	m^3/s (0.2 l/min)
Hysteresis	3	%
Offset	-0.3	V

Table 4.2: Nonlinear characteristics of the vane

Parameter	Value	Units
Internal leakage	3.84×10^{-13}	$(m^3/s)/Pa$
Static friction	60	Nm
Coulomb friction	44	Nm
Viscous friction coefficient	0.1	Nm/(rad/s)

The mechanics of the arm and the load mass is modelled using the fundamental equations of motion. The mass, inertia and other geometrical parameters are obtained from the CAD (Computer Aided Design) software SolidWorks® and the modelling is done using Matlab/Simulink® and Matlab/SimMechanics®.

The simulated open-loop response of the model of Figure 4.6 is compared against the measured velocity, position and pressure difference of the vane actuator. The comparison is shown in the plots of Figure 4.7. Velocity and position outputs of the model match quite well with the measured outputs of the system. Despite the matched shape there is a significant difference between the peak value of pressure difference. The reason is expected to be the un-modelled flexibility of the seals in the actuator.

From Figure 4.7 it can be noted that instead of comparing individual pressures in the chambers, only the pressure difference is compared for the validation of the model. The matching of individual chamber pressures demands much more modelling effort, as it requires the accurate modelling of four individual notches of the servo valve. Since the main goal is to obtain the model of WHMAN, which is composed of seven water hydraulic actuators, this will lead to the modelling of twenty eight notches of seven servo valves. In addition, the behaviour of the selected water hydraulic servo valves has been found to be quite non-steady (varying hysteresis,

spool-offset, etc.) on a day-to-day basis. This adds to the complexity of the accurate modelling of control notches of servo valves. Additionally, the generality of the model is compromised as with a change in servo valve the notches need to be remodelled. As this modelling effort is non-significant for this study, it has not been conducted.

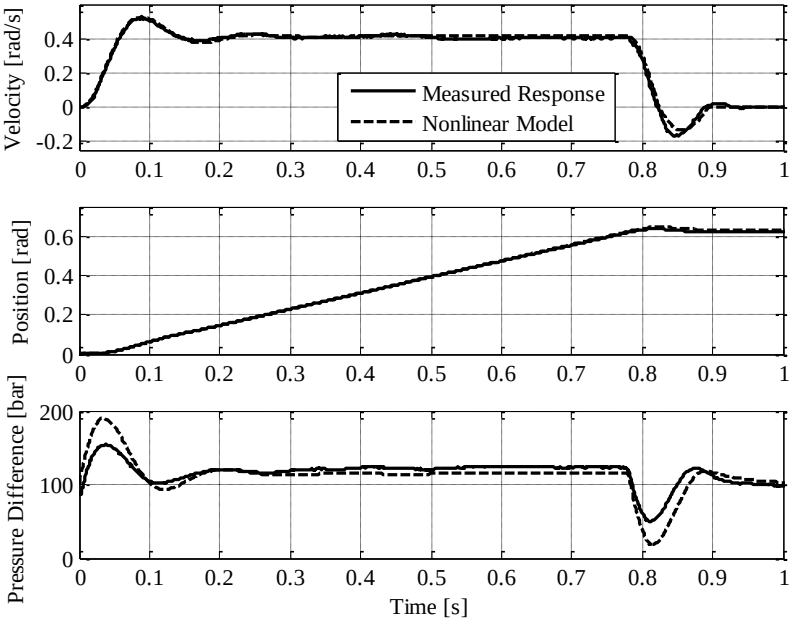

Figure 4.7: Measured and simulated response of nonlinear model

4.4 Simulation model of WHMAN

The rotational joints of WHMAN are driven by similar vane actuators to those described in the last section. These vane actuators employ the same mechanical design and sealing solution and only differ in size and output torque capacity. Hence, ignoring the manufacturing tolerances and inaccuracies, use of the same model with modified torque parameters can be a good starting step towards the modelling of WHMAN.

For the verification of the model of hydraulic servo system it is customary to compare the measured and simulated open-loop velocity responses and the pressures in the chambers for a given step input signal to the valve as presented in the last section. However, a step is not a realistic input signal for the manipulator joints in open-loop. Most of the time manipulators are

required to follow smooth position profiles in space. These profiles are designed according to the structural and dynamic limitations of the manipulator and the task at hand. In most hydraulic manipulators, the driving velocity is limited because of large manipulator size and limited supply flow.

Manipulators like WHMAN are designed to handle heavy loads and move at slow velocities. The step input signal to the valves or to the motor drive will move the manipulator's joints with quite large velocities and this may result in undesired stress on the manipulator's structure. The manipulator is not designed for such motions and these can cause permanent damage to it.

Hence, the manipulator's joints can only be run in close-loop following smooth position trajectories. In this case a possible approach for the validation of the simulation model is to compare the joints' velocities, position tracking errors and pressure differences across chambers, provided that the same controllers and gains are used for the simulation model and the real manipulator.

To run the manipulator joints in close-loop, a proportional controller is designed using Equation 4.15.

4.15 $$\boldsymbol{K_{p\theta}} = \frac{1}{2}\boldsymbol{K_{qa}}^{-1}\boldsymbol{\delta_n}\boldsymbol{\omega_n}^{T}$$

Here, $\boldsymbol{k_{p\theta}} \in \mathcal{R}^8$ is the vector of the joint position controller for WHMAN, and

4.16 $$\boldsymbol{K_{qa}} = diag\left(k_{qa1}, k_{qa2}, \dots, k_{qa8}\right)$$

4.17 $$\boldsymbol{\omega_n} = [\omega_{n1}, \omega_{n2}, \dots, \omega_{n8}]^T$$

4.18 $$\boldsymbol{\delta_n} = [\delta_{n1}, \delta_{n2}, \dots, \delta_{n8}]^T$$

The elements of the matrix and vectors in Equations 4.16, 4.17 and 4.18 are calculated using Equations 4.11, 4.12 and 4.14 respectively for each joint of the manipulator.

The proportional controller designed using Equation 4.15 normally gives a very sluggish response; however, for the model validation the choice is made for its simplicity and robustness against the model uncertainties. Also the proportional controller has a very limited influence on the system dynamics.

The sampling frequency of the control system is 1 kHz. The measurements are obtained at a sampling rate of 100 Hz. The control and data acquisition are performed using National Instruments® hardware and LabVIEW® software. The modelling and simulation of the manipulator is performed using Matlab/Simulink® and Matlab/SimMechanics®.

The manipulator joints are run simultaneously, covering a 90% range of motion in both directions and such that the manipulator does not collide with the environment or itself. The comparison of simulated and measured position error, velocity and pressure difference are shown in the plots of Figure 4.8 to Figure 4.15 in descending order from joint 8 to joint 1 respectively. Mean Absolute Error (MEA) between the measured and simulated values is also indicated as reference along with each plot. The simulated position tracking error and pressure differences in the actuators' chambers match well. Slight variations arise due to manufacturing tolerances and the nonlinear behaviour of the seals. Experience shows that these slight variations in dimensions can result in a significant change of internal frictions and leakages, thus altering the behaviour of the actuators. Additionally, the compression of the seals is a nonlinear function of pressure difference in the chambers and depends on the direction of motion.

The modelling of nonlinearities caused due to manufacturing tolerances and such seal behaviour requires considerable effort and can result in a complicated and inefficient model. For the design of position and impedance controller the accuracy of the model is reasonable. Hence, the modelling of these characteristics is considered beyond the scope of this research work.

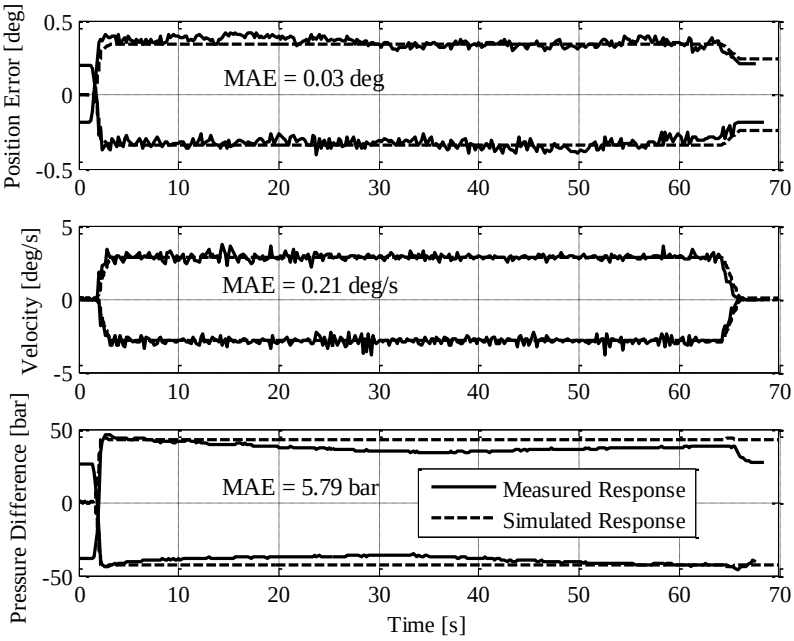

Figure 4.8: Measured and simulated response of θ_8 (Tool Rotation)

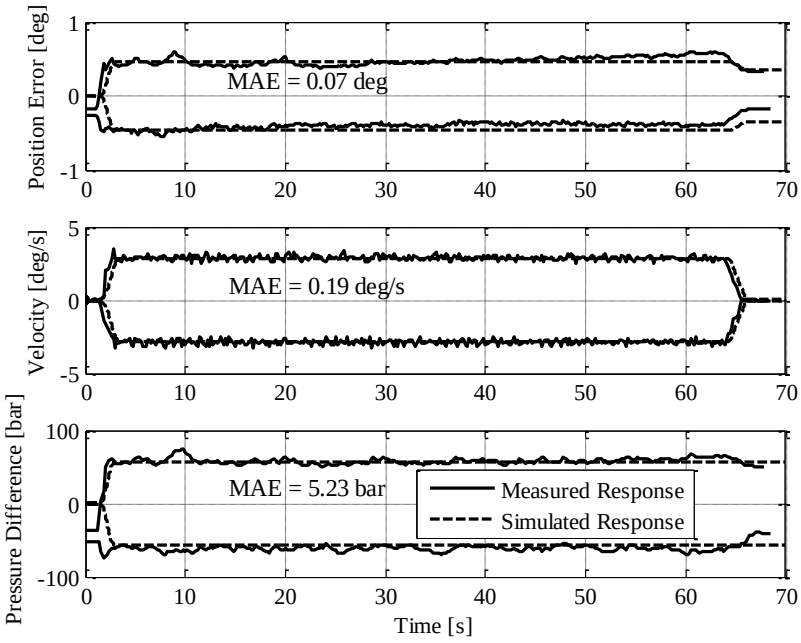

Figure 4.9: Measured and simulated response of θ_7 (Wrist)

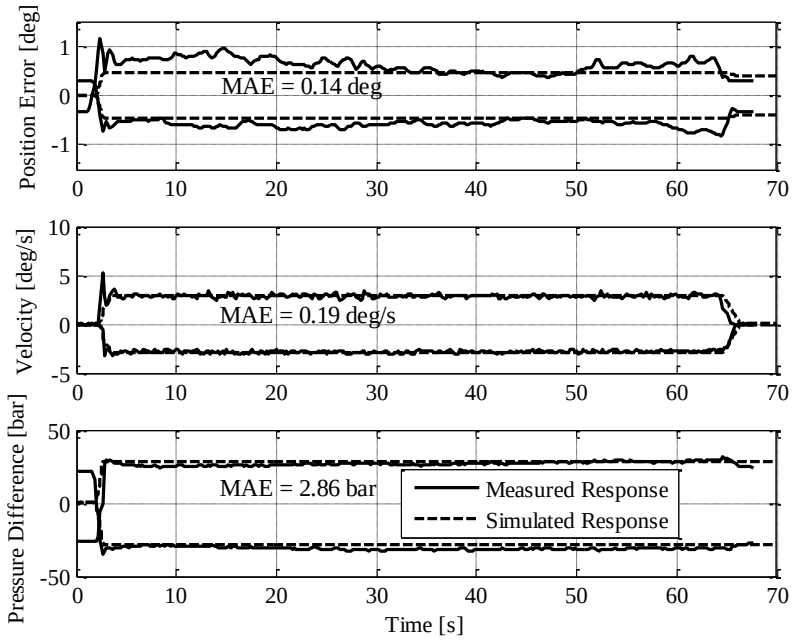

Figure 4.10: Measured and simulated response of θ_6 (Azimuth)

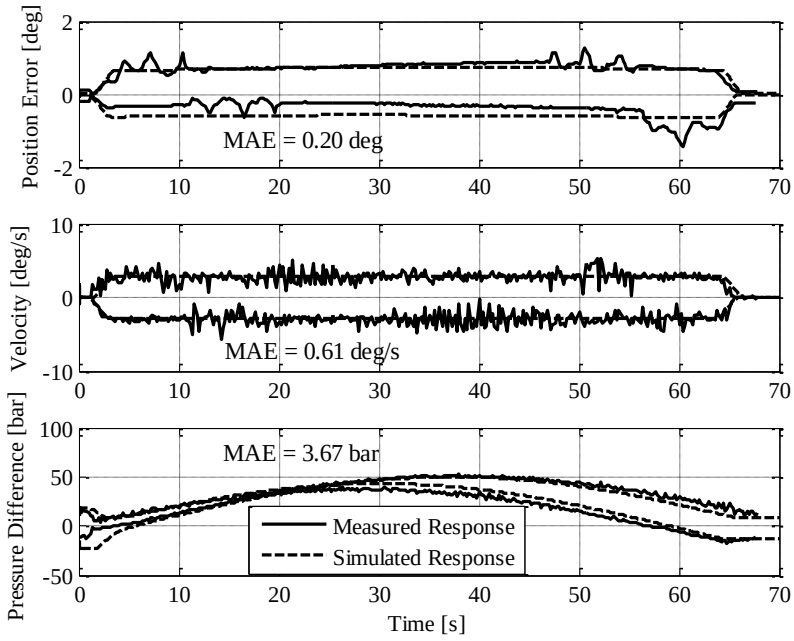

Figure 4.11: Measured and simulated response of θ_5 (Elbow)

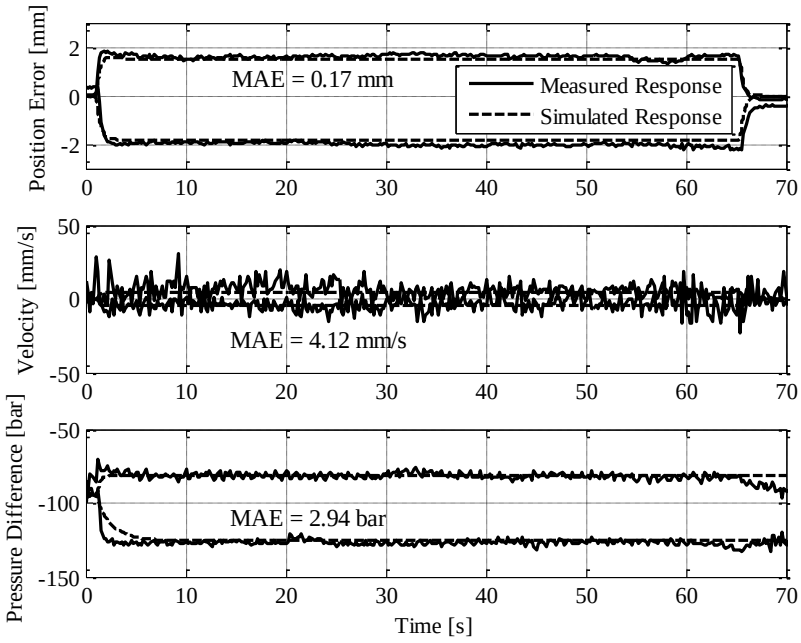

Figure 4.12: Measured and simulated response of d_4 (Telescopic)

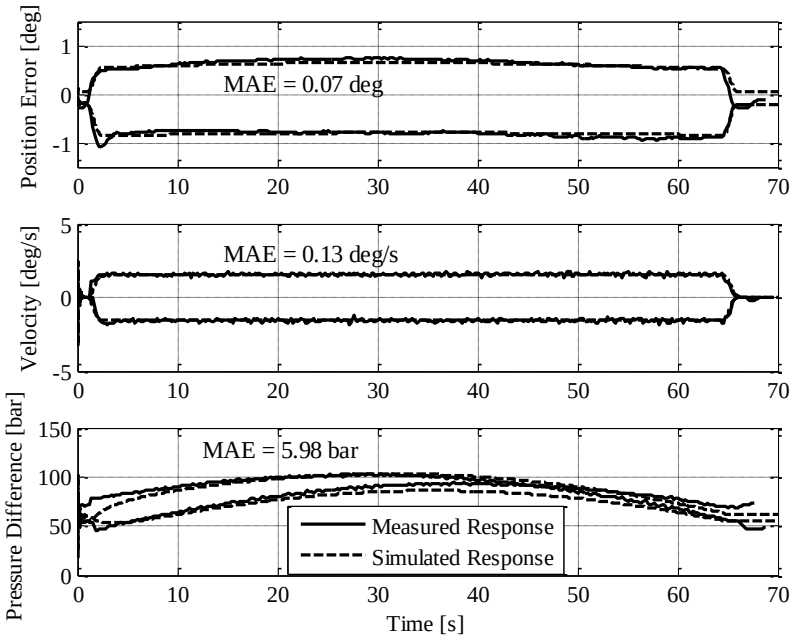

Figure 4.13: Measured and simulated response of θ_3 (Shoulder)

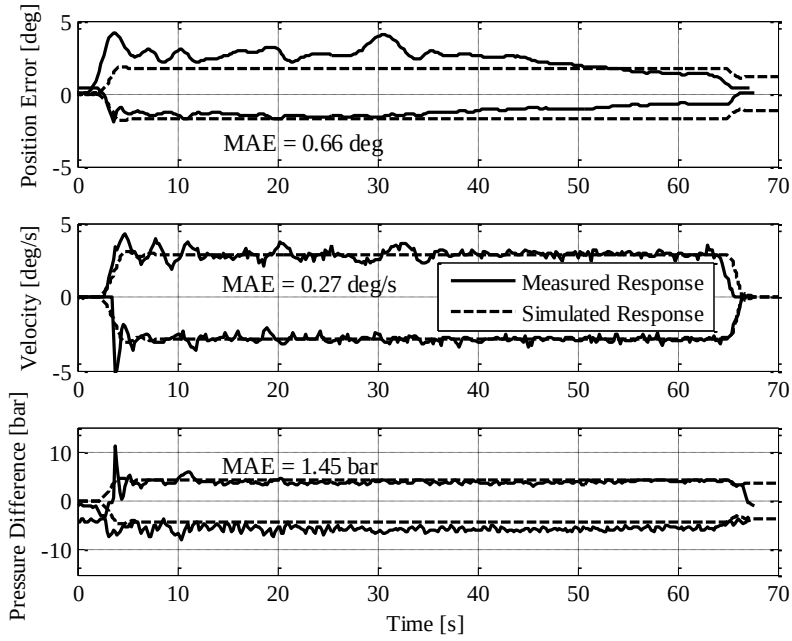

Figure 4.14: Measured and simulated response of θ_2 (Base)

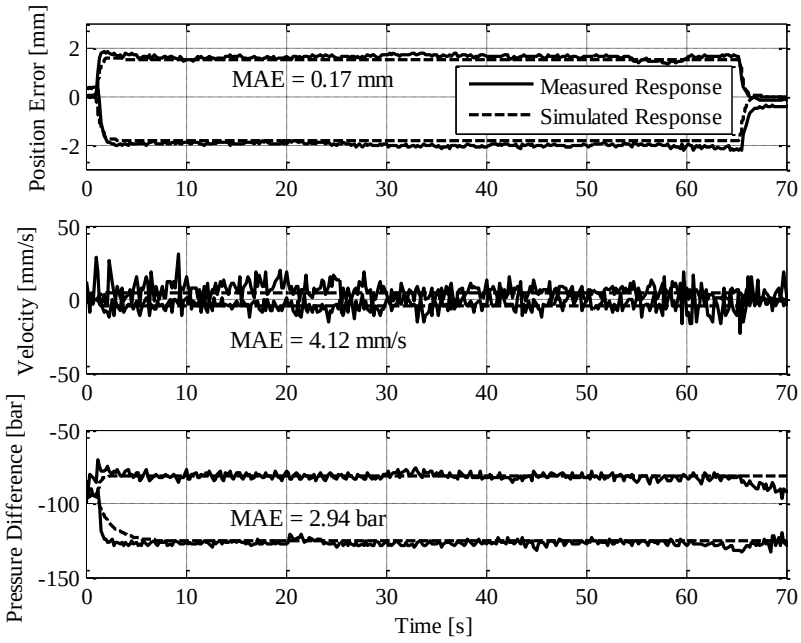

Figure 4.15: Measured and simulated response of d_1 (Linear Slide)

4.5 Summary

The modelling of WHMAN has been discussed in this chapter. Both analytical and simulation models of the manipulator are presented. For the analytical model the geometrical and inertial parameters obtained from the CAD model of the manipulator have been utilized. For the simulation model the majority of the modelling parameters are obtained from the components' datasheets and few are obtained experimentally.

The modelling of a single actuator of WHMAN has been used as the starting point for the development of a simulation model of the entire WHMAN. Both linear and nonlinear verified models of the actuator are presented. These developments are then carried on for the development of the simulation model of WHMAN. The measurements show that a reasonably accurate model useful for this study can be obtained for the WHMAN.

These analytical and simulation models will be utilized in the next chapter for the development of controllers and verification of the findings presented in Chapter 3.

5 NUMERICAL ANALYSIS AND SIMULATIONS

This chapter is dedicated to the study of the results obtained in Chapter 3 via numerical analysis and simulations. The analytical and simulation models of WHMAN (Water Hydraulic MANipulator) presented in Chapter 4 have been utilized here. The design of the position controllers for the manipulator's joints and the impedance controller are also described in this chapter. The controllers are implemented along with the simulation model of WHMAN in Matlab/Simulink®.

The redundancy resolution scheme devised for the joints of WHMAN is presented in Section 5.1. Section 5.2 is focused on the position controllers for the joints designed using the verified simulation model of WHMAN presented in Section 4.4. The design of the impedance controller is then discussed in Section 5.3. The desired impedance parameters are selected according to the performance of the position controller. The performance of the position-based impedance controller is shown via position, force and impedance plots. The designing of force-based impedance controller utilizing the gains of position controller and impedance parameters is discussed in Section 5.4. The equivalent implementation of force-based impedance controller is then studied according to Equation 3.81.

The effect of redundancy on the dynamic performance of the manipulator is studied in Section 5.5. The numerical analysis of the dynamic manipulability of WHMAN is presented in Section 5.5.1. The dynamic manipulability of WHMAN has been analyzed using the Dynamic Manipulability Ellipsoid (DME) (Yoshikawa, 1985). To study the effects of kinematic redundancy, the dynamic manipulability of WHMAN is compared in redundant and non-redundant configurations. In Section 5.5.2 the dynamic performance of the manipulator is analyzed with impedance controller using the simulation model. The performance of the impedance controllers is compared for redundant and non-redundant configurations of WHMAN. The results of the numerical simulations are presented as position, force and impedance response plots. These developments are summarized in Section 5.6.

5.1 Redundancy resolution

As mentioned earlier, a manipulator requires a minimum of six degrees of freedom in operational-space if it needs to be able to acquire any random position and orientation during

task execution. Assuming one joint is required for each degree of freedom, such a manipulator needs to be composed of a minimum of six joints. As described in Chapter 4, the WHMAN is composed of eight joints: six rotational and two translational. Hence, the two additional joints of WHMAN provide the redundant degrees of mobility in the joint-space. These redundant degrees of freedom can be exploited to optimize the kinematic or dynamic behaviour of the WHMAN, such as providing the desired dexterity to cope with the constricted space inside the ITER divertor maintenance tunnel or being able to select a suitable posture for better dynamic performance during the task execution.

As discussed in Section 3.7, for the case when optimized dynamic performance of the manipulator is desireable, the posture can be configured using the DME. The solution to exploit the redundant degrees of mobility for the optimized dynamic performance was presented using the dynamic manipulability index (Yoshikawa, 1985) which is given as:

$$w_1(\boldsymbol{\theta}) = \prod_{i=1}^{6} \sigma_i \Longrightarrow \sqrt{\det\left(\boldsymbol{J} \cdot \left(\boldsymbol{M_\theta}^{\boldsymbol{T}} \cdot \boldsymbol{M_\theta}\right)^{-\mathbf{1}} \cdot \boldsymbol{J}^{\boldsymbol{T}}\right)} \tag{5.1}$$

Since it is nearly impossible to obtain the above index in symbolic form for a manipulator like WHMAN, a possible approach is to compute this index numerically as a function of joint variables to determine the effect of joint configuration. Considering the kinematic structure of WHMAN (Figure 4.1 and Appendix A), the redundant degrees of mobility exist only in the arm of the manipulator. Further, it can be noticed that the base joint (θ_2) provides motion perpendicular to the plane of the WHMAN arm and does not contribute to the redundancy. Therefore, the effect of θ_2 deos not need to be analyzed.

Hence, the posture of the shoulder and elbow joints (θ_3 and θ_5 respectively) can be reconfigured using the redundant degrees of freedom provided by linear-slide and telescopic joints (d_1 and d_4 respectively). The plots of dynamic manipulabilty index as the function d_1, θ_3 and d_4 against the sum of θ_3 and θ_5 are shown in Figure 5.1, Figure 5.2 and Figure 5.3 respectively. Since the configurations of θ_3 and θ_5 are not independent, the effect of θ_5 is not considered seperately.

It is evident from the plots that the change in d_1 does not have any impact on the dynamic manipulability index, while the minimization of joint d_4 results in a minor improvement in the index. The joint θ_3 has the largest effect on the dynamic performance of the manipulator and the index steadly increases as the joint is moved from 0° to 90°. The other noticeable fact from all the plots is that the index is maximized when the sum of θ_3 and θ_5 is kept around $-60°$ for elbow up configuration and 60° or 115° for elbow down configuration.

Due to constricted space inside the ITER divertor maintenance tunnel, the position of the shoulder joint (θ_3) cannot be maximized. In this case the approach towards redundancy resolution to maximize the dynamic manipulability index is to adjust the position of d_4 such that the sum of θ_3 and θ_5 is kept around $-60°$ for elbow up configuration, and $60°$ or $115°$ for elbow down configuration. This can be achived by applying the artificial joint range limits on the elbow joint by using the function of Equation 5.2 (Sciavicco, et al., 2001).

$$h(\boldsymbol{\theta}) = -\frac{1}{2n}\sum_{i=1}^{n}\left(\frac{\theta_i - \bar{\theta}_i}{\theta_{i_{max}} - \theta_{i_{min}}}\right)^2 \tag{5.2}$$

where, $\theta_{i_{max}}$ and $\theta_{i_{min}}$ are the maximum and minium range of motion of joint i respectively, and $\bar{\theta}_i$ is the middle value of joint range. Therefore, the redundancy resolution scheme can be formed by introducing artificial joint range of motion, as below:

$$\dot{\boldsymbol{\theta}} = \boldsymbol{J}^{\dagger} \cdot \dot{\boldsymbol{x}} + k \cdot (\boldsymbol{I} - \boldsymbol{J}^{\dagger} \cdot \boldsymbol{J}) \cdot \left(\frac{-\frac{1}{2n}\sum_{i=1}^{n}\left(\frac{\theta_i - \bar{\theta}_i}{\theta_{i_{max}} - \theta_{i_{min}}}\right)^2}{\partial \boldsymbol{\theta}} \right) \tag{5.3}$$

Here, $k > 0$ is the weighing factor and can be modifed to tighten or soften the secondary constraint, which is useful to ensure the possibility to derive the WHMAN as per required task without enforcing the artificial joint ranges.

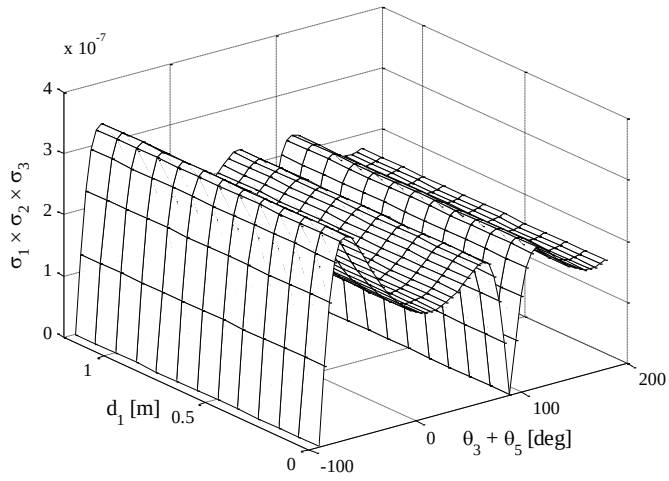

Figure 5.1: Dynamic manipulability index as a function of d_1 and $\theta_3 + \theta_5$

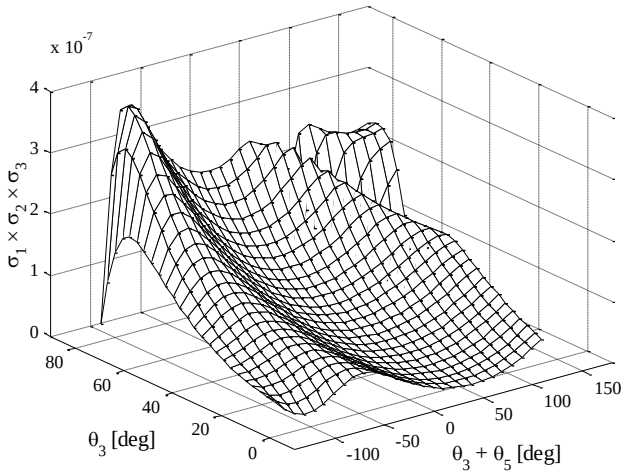

Figure 5.2: Dynamic manipulability index as a function of θ_3 and $\theta_3 + \theta_5$

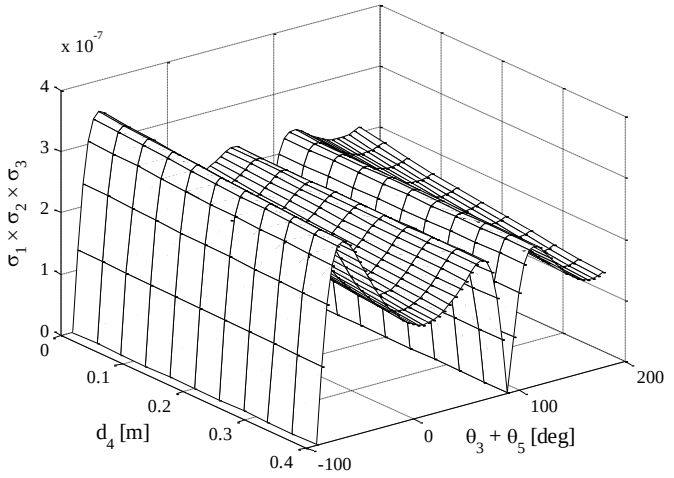

Figure 5.3: Dynamic manipulability index as a function of d_4 and $\theta_3 + \theta_5$

5.2 Position Controller

From the discussion in Section 3.5, it is clear that the position controller in the inner loop plays a vital role in the performance of the position-based implementation of impedance controller. A

position controller with fast dynamics, minimum overshoot and good steady state accuracy is desirable in this case. In the following paragraphs the development of position controller for WHMAN is discussed in detail.

The most popular controller used in hydraulic position servo systems is the proportional controller. Though robust, it gives a very sluggish response when tuned using robustness criteria (Linjama, et al., 2001). Another drawback of the P-controller is that it provides a very limited possibility to influence the system dynamics. As a result, a lot of research has been done to investigate and to develop better solutions.

In (Sepehri, et al., 1997) the traditional PI-controller has been modified to implement a nonlinear PI-controller. However, the testing of the controller was limited only to a single joint of a hydraulic manipulator. On the other hand, (Virvalo, 2001) has suggested avoiding the integral term in controllers for hydraulic position servo systems. It has been shown that because of the nonlinearities in the valve, the use of the integrator can lead to a hunting type behaviour. Moreover, in (Virvalo, et al., 2001) the performances of the proportional controller, the filtered proportional controller (proportional controller with the first order lag) and the state-feedback controller with varying loads have been compared. The results show that the performance of the state-feedback controller depends on the load variation. (Linjama, et al., 2001) analysed the robustness of the same controllers with focus on the parameter variations and sampling time.

Linjama concluded that one has to be careful when state-feedback control is realized in practice. In (Andersen, et al., 2005) a set of linear controllers on a two joint manipulator driven by linear hydraulic drives have been compared. (Bonchis, et al., 2002) documented the performance of a very wide range of controllers for hydraulic drives.

Since hydraulic drives exhibit nonlinear and variable characteristics, many researchers have investigated solutions using nonlinear and adaptive controllers. The use of linearized pressure dynamics as a feedback has been studied in (Andersen, et al., 2005a). The system was found to be robust against the load and parameter variations, but the position tracking results were not remarkable. In the same study adaptive controllers on a two joint manipulator driven by linear hydraulic drives were tested. In this case, despite attaining better accuracy, the position tracking exhibited chattering due to the noise in the velocity feedback signal. (Tochizawa, et al., 1999) conducted experiments with a two joint manipulator driven by rotary hydraulic actuators. The controllers were compared under the condition of varying load on the manipulator. The adaptive controller was found to be much more complicated to implement, but it did not guarantee any more accuracy than the classical controller.

Since hydraulic components (both water and oil) exhibit low damping, the performance can be improved by using control techniques that can improve the dynamics of the system. It is well-known that the use of states such as velocity and acceleration as feedback can considerably improve the dynamics of fluid power (hydraulic or pneumatic) servo systems. As a result, higher close-loop gains can be used for improved dynamic response and reduced steady state error. Controllers employing such a technique are widely termed state-feedback controllers. The characteristics of the state-feedback controller can be useful in hydraulic manipulators, where the dynamic response of each drive propagates further, to strongly diminish the end-effector positioning response. The choice of the state feedback controller is made for its reasonable complexity and its capability to affect the system performance (Muhammad, et al., 2009b).

The design of the state-feedback controller is based on the principal of selecting new pole locations. Figure 5.4 shows the implementation of state-feedback controller.

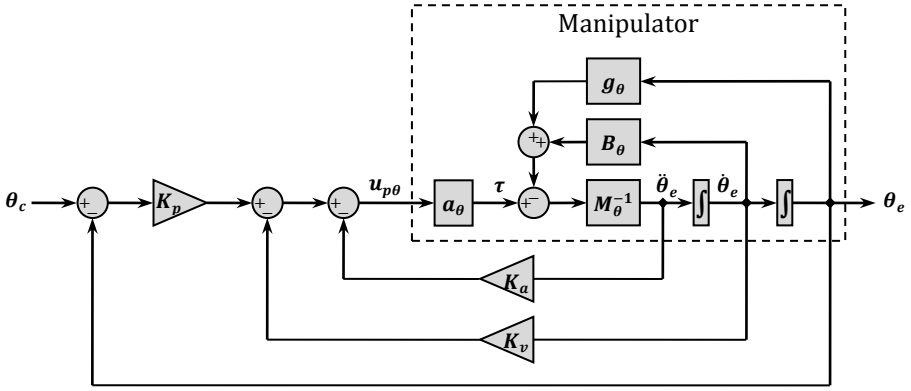

Figure 5.4: Block diagram representation of state-feedback controller

In the above block diagram $\boldsymbol{K}_v \in \mathcal{R}^8$ and $\boldsymbol{K}_{\boldsymbol{a}} \in \mathcal{R}^8$ are the diagonal matrices of velocity and acceleration feedback gains respectively. Considering the linearized model of hydraulic servo system given by Equation 4.10, the close-loop transfer function for a single joint actuator of the manipulator can be written as in Equation 5.4.

$$\frac{\theta_c(s)}{\theta_e(s)} = \frac{k_p k_{qa} \omega_n^2}{s^3 + \left(2\delta_n \omega_n + k_a k_{qa} \omega_n^2\right) s^2 + \omega_n^2 \left(1 + k_v k_{qa}\right) s + k_p k_{qa} \omega_n^2} \tag{5.4}$$

From Equation 5.4 it is clear that the joint actuators of the manipulator will have improved dynamics (higher effective values of damping and natural frequency). Thus, higher close-loop gain can be chosen for improved dynamic response and reduced steady state error.

The initial tuning parameters of state-feedback controller for each joint of the manipulator can be found following the procedure below:

5.5 $$k_p = \frac{(1 \dots 2)k_{cr}}{k_{qa}k_h}$$

5.6 $$k_v = \frac{(\omega/\omega_n)^2 - 1}{k_{qa}}$$

5.7 $$k_a = \frac{2\delta_n\big((\omega/\omega_n)(\delta/\delta_n) - 1\big)}{k_{qa}\omega_n}$$

where ω and δ are the new desired frequency and damping ratio. Typically, $\omega = 1.1 \times \omega_n$ and $\delta = 0.7$. Considering small accelerations and velocities, only the gravitational forces are compensated to decouple and linearize the dynamics. The natural frequency and damping for each vane actuator is determined from the open-loop response of the model of WHMAN developed in Section 4.4. The state-feedback controller is designed at the highest natural frequency for each actuator to ensure the stability of WHMAN in the entire workspace and it is tuned to obtain the fastest dynamic response without any overshoot. The tracking accuracy is further improved by using the velocity feed forward signal.

The manipulator is subjected to a third order operational-space position profile with maximum velocity of 0.05 m/s or 0.05 rad/s and maximum acceleration of 0.001 m/s^2 or 0.001 rad/s^2 along each axis of motion. The profile is designed to move the manipulator in the region where majority of the tasks are perceived to be executed inside the divertor maintenance tunnel, and additionally, in a manner such that the manipulator needs to reverse the directions of motion during the execution of profile. The tracking response of the manipulator along different axes is shown in Figure 5.5 to Figure 5.10. The desired and feedback profiles appear to be overlapped due to small tracking error. For the sake of clarity the tracking error has been shown below each profile.

The manipulator shows a reasonably good position tracking performance. The tracking error remains around or less than 2 mm in case of position tracking and less than 0.1 deg in the case of orientation tracking. The steady state error remains less than 0.4 mm in the case of position and less than 0.005 deg in the case of orientation.

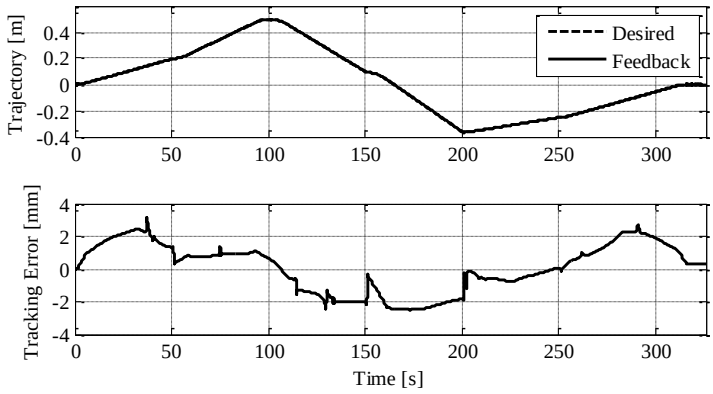

Figure 5.5: Position tracking response (top) and error (bottom) of WHMAN along x-axis

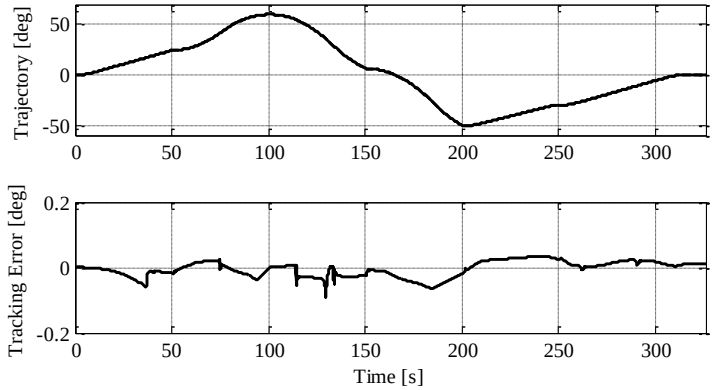

Figure 5.6: Rotation tracking response (top) and error (bottom) of WHMAN about x-axis

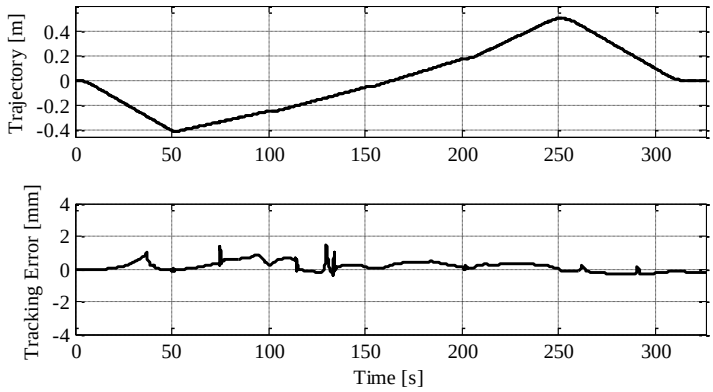

Figure 5.7: Position tracking response (top) and error (bottom) of WHMAN along y-axis

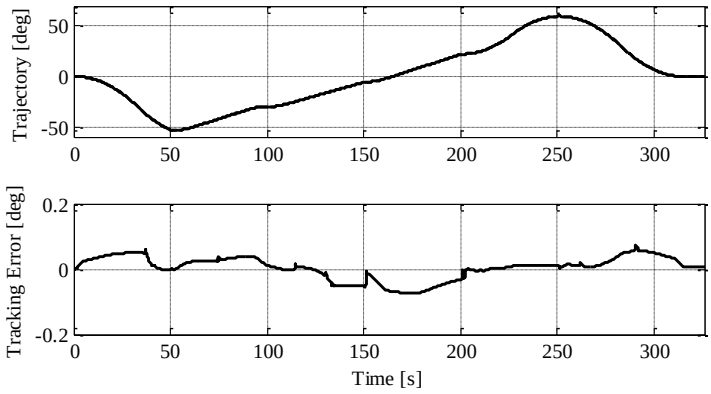

Figure 5.8: Rotation tracking response (top) and error (bottom) of WHMAN about y-axis

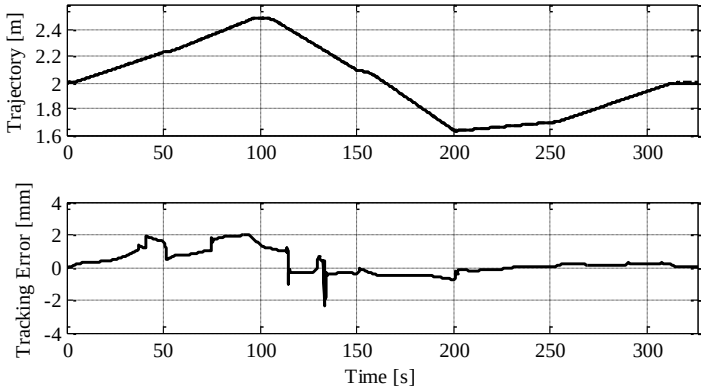

Figure 5.9: Position tracking response (top) and error (bottom) of WHMAN along z-axis

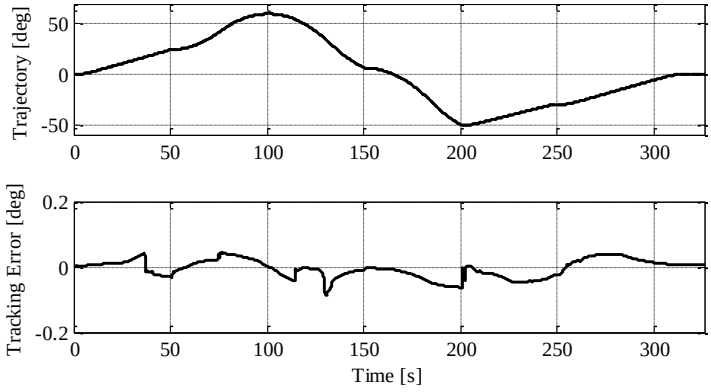

Figure 5.10: Rotation tracking response (top) and error (bottom) of WHMAN about z-axis

To further demonstrate the dynamic behaviour of the manipulator, the responses to a small step input in both directions along different axes are shown in Figure 5.11, Figure 5.12 and Figure 5.13. The step input is selected such that the input to the valve is not saturated during the entire motion. Undershoots and overshoots in the step responses are due to the difference in settling times for different joints of WHMAN. The longest settling time is around 0.5 s, which is along the x-axis. The performance of WHMAN will be practically evaluated at the Divertor Test Platform (DTP2) facility. These tests will reveal if the achieved position accuracy is adequate to carry out divertor maintenance operations. At this stage, this performance of the position controller is considered sufficient for the position-based implementation of impedance controller.

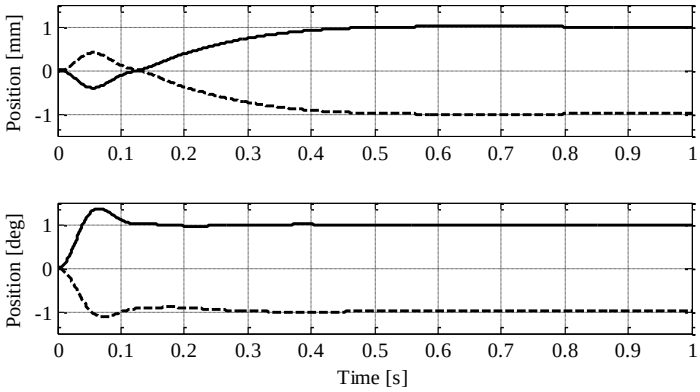

Figure 5.11: Step response of WHMAN along and about x-axis in both directions

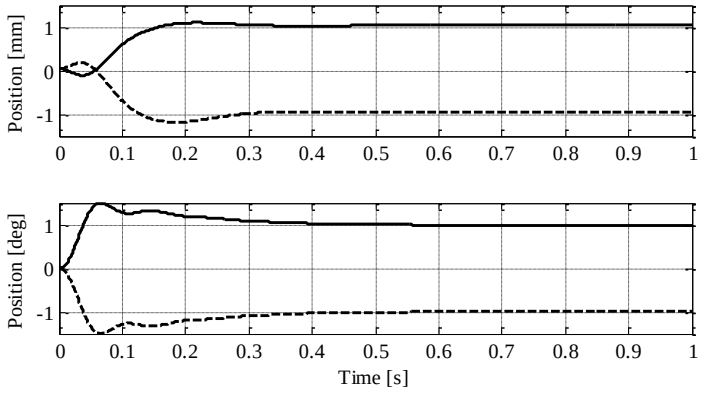

Figure 5.12: Step response of WHMAN along and about y-axis in both directions

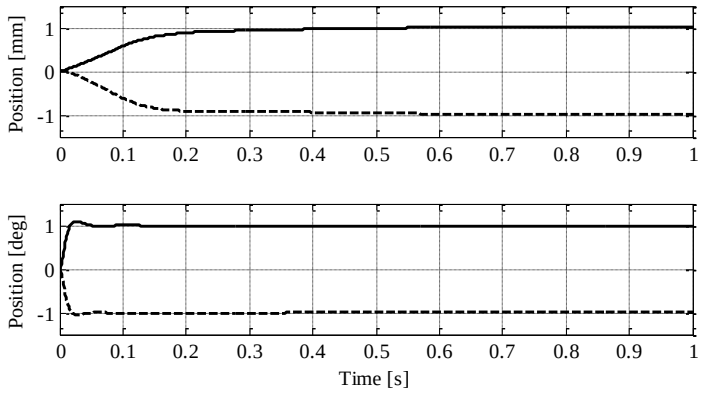

Figure 5.13: Step response of WHMAN along and about z-axis in both directions

5.3 Position-based impedance controller

The tracking and step responses of the position controller of WHMAN are presented in the last section. The design of impedance filter is discussed in this section. The position controller, along with the impedance filter, is then used to implement the position-based impedance controller for the simulation model of WHMAN. The results are shown using the position and force response of the manipulator along each axis.

5.3.1 Design of impedance filter

The operational-space impedance model was derived in Section 3.4.1 in the form of a transfer function matrix of Equation 3.52. The equation can be written in the following compact form:

$$\boldsymbol{x}(s) - \boldsymbol{x_e}(s) = [\boldsymbol{M_d} \cdot s^2 + \boldsymbol{B_d} \cdot s + \boldsymbol{K_d}]^{-1} \cdot \boldsymbol{f_e}(\boldsymbol{s}) \quad (5.8)$$

For WHMAN, $\boldsymbol{M_d} \in \mathcal{R}^{6\times6}$, $\boldsymbol{B_d} \in \mathcal{R}^{6\times6}$ and $\boldsymbol{K_d} \in \mathcal{R}^{6\times6}$ represent the matrices containing the inertial, viscous and stiffness parameters of the desired impedance ($\boldsymbol{Z_d}$) respectively. $\boldsymbol{x} \in \mathcal{R}^6$ and $\boldsymbol{x_e} \in \mathcal{R}^6$ are the nominal desired and actual measured positions of the manipulator respectively and $\boldsymbol{f_e} \in \mathcal{R}^6$ represents the environmental contact forces.

The matrices $\boldsymbol{M_d}$, $\boldsymbol{B_d}$ and $\boldsymbol{K_d}$ do not need to be diagonal or constants. By using non-diagonal entries the impedance can be coupled between the motion axes (Lawrence, 1988). This feature can be useful in certain tasks where the environment has coupled dynamics. By properly selecting the non-diagonal entries in the desired impedance matrices, decoupling can be achieved. Additionally, the entries of these matrices can be the function of manipulator and environmental variables if desired. However, in this study only non-coupled and constant matrices for the desired impedance are considered.

The discussion in Section 3.4.3 indicates the involvement of environmental parameters in the selection of desired impedance parameters. The characteristic equation from each of the transfer function of the matrix in Equation 5.8 describing the dynamics of close-loop system were determined to be of the form:

$$z_e(s) + z_d(s) = m_d \cdot s^2 + (b_d + b_e) \cdot s + (k_d + k_\mathrm{e}) = 0 \tag{5.9}$$

where m_d, b_d and k_d are the scalar values desired inertia, damping and stiffness respectively, and b_e and k_e are the scalar values of environmental damping and stiffness respectively along a certain axis of motion. Equation 5.9 reveals the fact that even with the idealized position controller the values of the desired dynamic parameters cannot be chosen arbitrarily and need to fulfil the condition of stability (Tafazoli, et al., 2002). The dynamics of the environment need to be taken into consideration while selecting the desired dynamic parameters for the manipulator. An improper selection of parameters can lead to a completely unstable system when comes in contact with the environment (Eppinger, et al., 1992). For the close-loop dynamics of the impedance controller to be stable the roots of each characteristic equation of the transfer function matrix must lie on the left hand side of the complex plane.

Unfortunately, the estimation of environmental impedance is not a straightforward task; besides, this approach will limit the application of impedance controller particularly to the environment. The impedance filter will require reconfiguration according to the contact impedance.

A better approach is to reduce the dependence of impedance filter design on the environmental parameters. The dependence on environmental damping can be omitted from Equation 5.9 by considering the fact that, normally, $b_d \gg b_e$. It is a desirable practice to ensure that contact energy is dissipated by the manipulator and not to rely on the environment for the purpose. Then the roots of the second order polynomial can be given by quadratic formula as:

5.10 $$r_{1,2} = -\frac{b_d \pm \sqrt{{b_d}^2 - 4m_d(k_d + k_e)}}{2m_d}$$

Now, if $k_d \gg {b_d}^2$ such that the roots are complex conjugates Equation 5.10 can be written as:

5.11 $$r_{1,2} = -\frac{b_d}{2m_d} \pm i\frac{\sqrt{4m_d(k_d + k_e) - {b_d}^2}}{2m_d}$$

Equation 5.11 shows that as long as k_d is considerably larger than b_d, the roots are complex conjugates and the real parts of the complex conjugate roots do not depend on k_d or k_e and remain negative, thus ensuring the stability of the close-loop dynamics. Hence, the dependence on environmental stiffness can be omitted by keeping the value of desired stiffness sufficiently large. This is in accordance with the previous finding that the stiffness of the manipulator cannot be lowered arbitrarily (Heinrichs, et al., 1999).

Considering the fact that the impedance controller relies on changing the position set point, the parameters of the impedance filter can be chosen considering the dynamic response of the inner position loop. The step responses shown in Figure 5.11, Figure 5.12 and Figure 5.13 describe the dynamics of the inner position control loop of WHMAN. The impedance filter should be fast enough, such that the manipulator is capable of responding to the environmental contact forces and resumes the position set point on returning to free space.

The desired dynamics between the force and position are given by the second order transfer function of the form:

5.12 $$x(s) - x_e(s) = \frac{1}{m_d \cdot s^2 + b_d \cdot s + k_d} \cdot f_e(s)$$

To ensure stability, the impedance filter can also be implemented by using the standard second order transfer function to define the desired dynamics between the position and the force, i.e.

5.13 $$x(s) - x_e(s) = \frac{1}{k_d} \cdot \frac{{\omega_n}^2}{s^2 + 2 \cdot \delta_n \cdot \omega_n \cdot s + {\omega_n}^2} \cdot f_e(s)$$

where ω_n and δ_n are known as natural frequency and natural damping respectively. Following this approach, the design of the desired impedance filter along a single axis is presented here. The same approach can be followed to find out the transfer function elements of the entire matrix in Equation 5.8.

Considering that the WHMAN is required to carry out remote handling operations in the master-slave mode, a settling time t_{set} of 0.1 s is chosen for the desired impedance filter. This settling time should be suitable for providing reliable force-feedback to the operator during the execution of contact tasks. Then, for a desired natural damping of 0.7 the natural frequency can be calculated as:

5.14 $$\omega_n = \frac{4.6}{\delta_n \cdot t_{set}} = 65.7 \text{ rad/s}$$

Substituting these values along with the desired stiffness k_d in Equation 5.13 will result in the impedance filter defining the desired dynamic relationship between environmental contact forces and position command signal. The equivalent values of parameters m_d and b_d in Equation 5.12 can be obtained by comparing it with Equation 5.13, as below:

5.15 $$m_d = \frac{k_d}{{\omega_n}^2}$$

5.16 $$b_d = 2 \cdot \delta_n \cdot \omega_n \cdot m_d$$

In fact, in either of Equations 5.12 or 5.13, the same desired dynamic relationship will result. The advantage of Equation 5.13 is its direct calculation and normalized form. Therefore, the stiffness of the manipulator can be varied without affecting the dynamic response of the impedance filter. The calculation of parameters in Equation 5.12 is indirect and no single parameter can be varied independently. Following a similar procedure, the impedance filter can be designed along other axes.

5.3.2 Simulation results

Using the designed impedance filter and the position controlled simulation model, the position-based impedance controller is implemented for WHMAN. The simulation responses of the implementation for several desired stiffness values of 50×10^3 N/m, 100×10^3 N/m and 150×10^3 N/m are shown as the plots of position tracking (left), contact force (right) and the tracked stiffness (bottom) along each axis in Figure 5.14 to Figure 5.19. The plots of the measured stiffness values are shifted artificially in time for the sake of clarity.

The trajectory is chosen in the most probable workspace of WHMAN. The contact forces are introduced along all axes of motion simultaneously. The contact is simulated as a spring-

damper system with stiffness ($k_e = 4 \times 10^8$ N/m, Nm/rad) and damping ($b_e = 1 \times 10^3$ N s/m, Nm s/rad) respectively. It can be seen from the plots that on coming into contact with the environment the position and force response of the manipulator remains stable. The contact with the environment is obvious at the point when the manipulator starts to deviate significantly from desired position trajectory and force appears at the end-effector.

To further verify the implemented impedance controller, the stiffness can be calculated from the position and force responses using the equation below.

5.17 $$k_d = \frac{f_e}{x - x_e} \text{ N/m, Nm/rad}$$

It is evident from the plots that the measured values of stiffness match very well with the desired values. In the case of Figure 5.15 the observed spikes in the stiffness plots for the rotation about x-axis are due to the fact that during initial contact a small vibration in the manipulator position causes $x - x_e \to 0$, and hence does not point to any real instability. The stable behaviour of the manipulator can be observed from the position tracking and contact force plots.

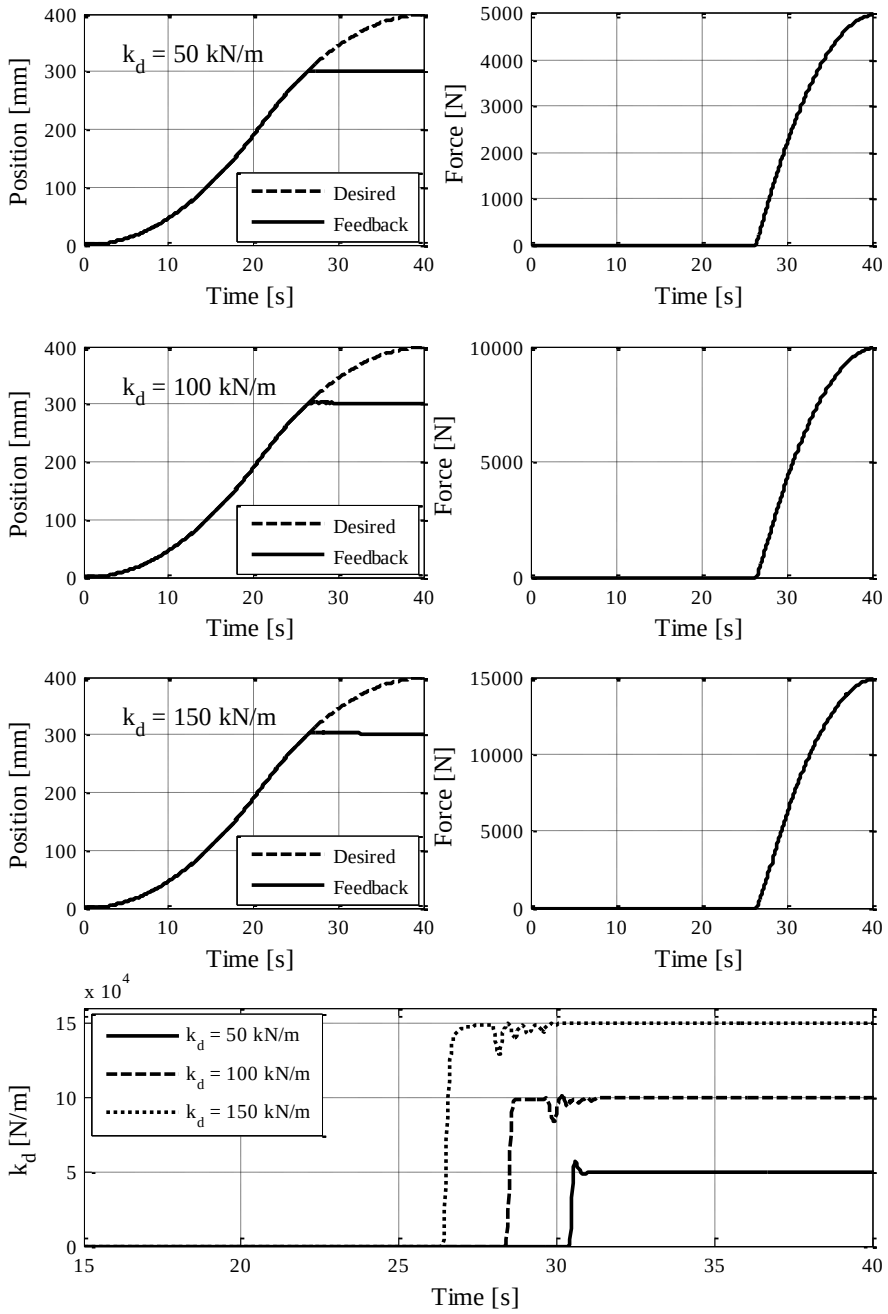

Figure 5.14: Position tracking (left), contact force (right) and impedance response (bottom) along x-axis for three different values of desired stiffness

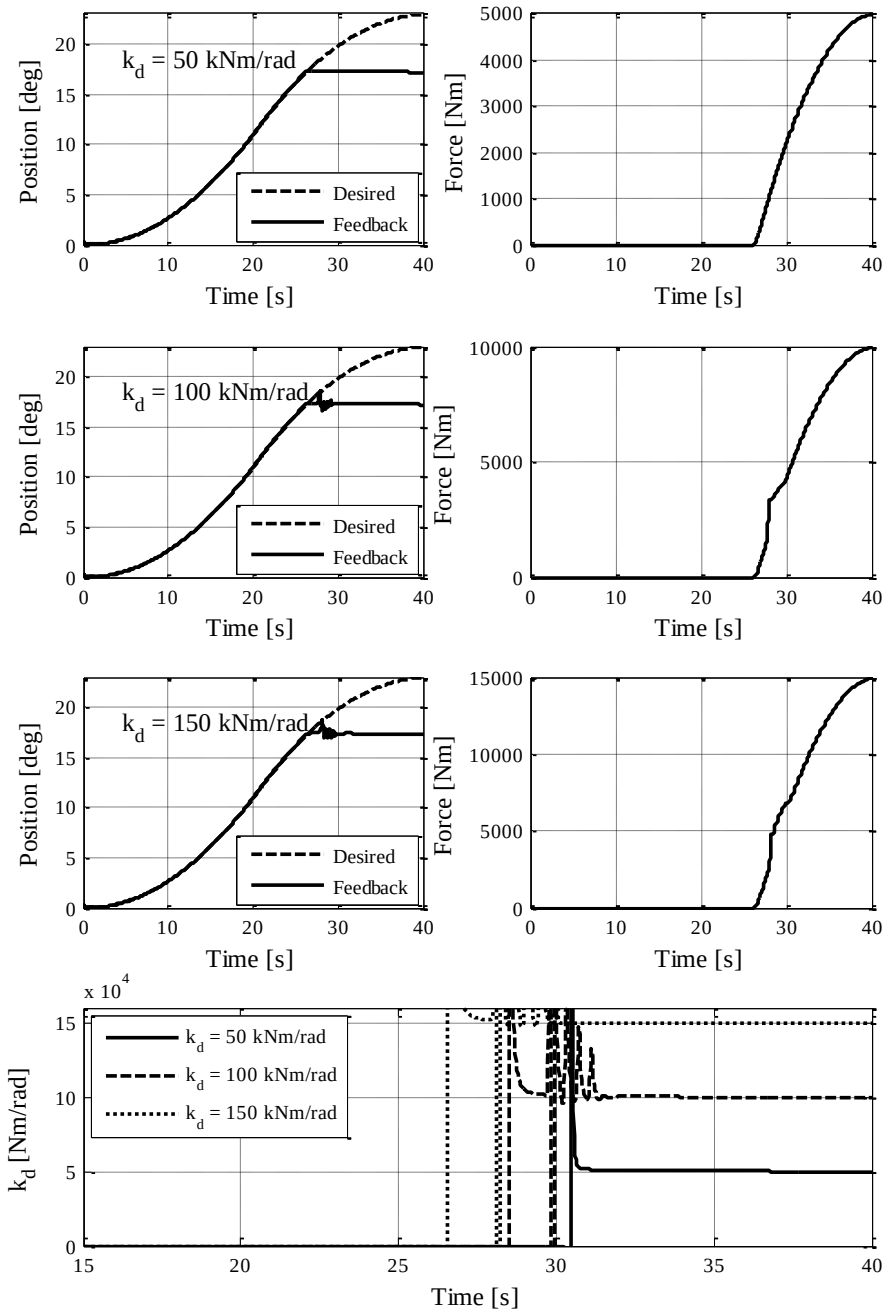

Figure 5.15: Position tracking (left), contact force (right) and impedance response (bottom) about x-axis for three different values of desired stiffness

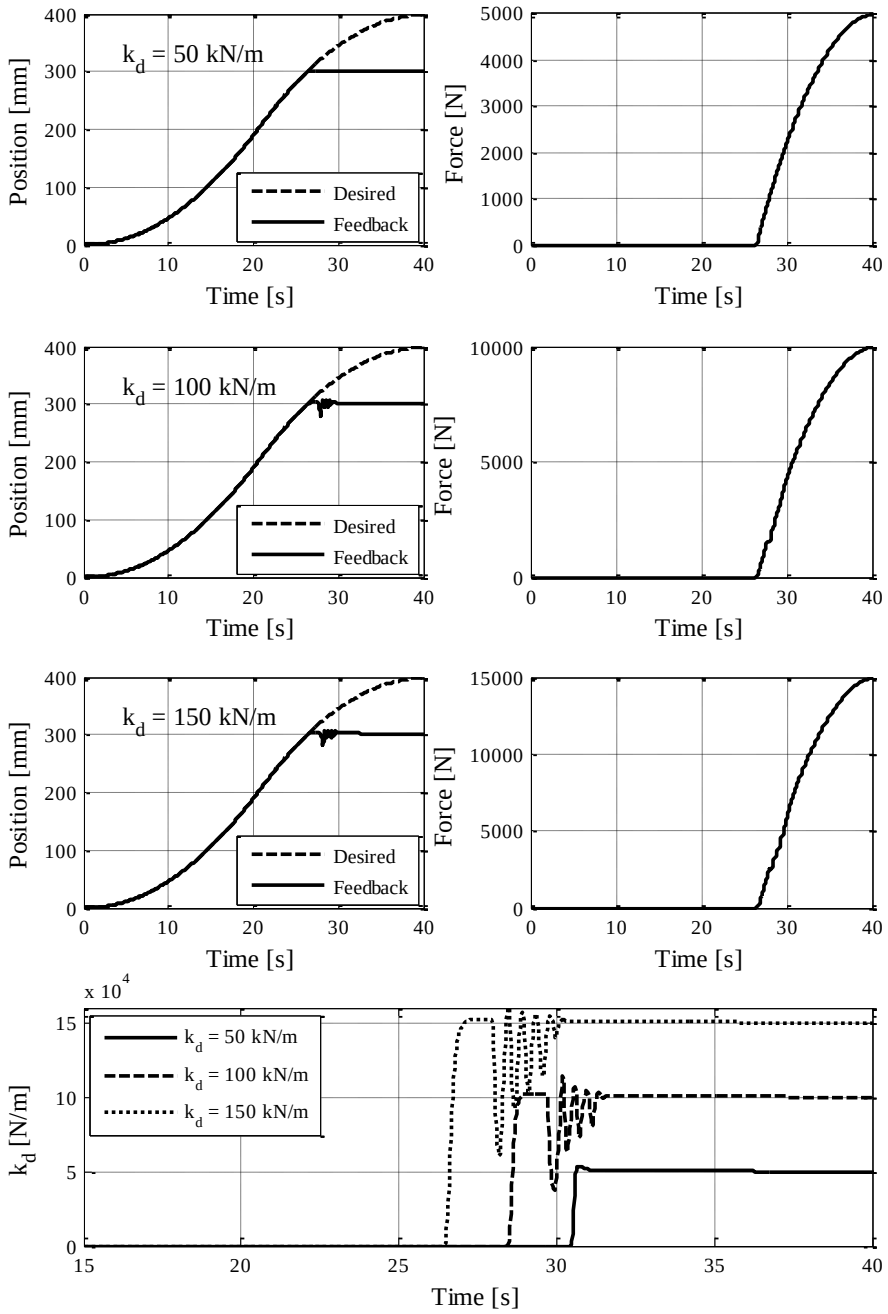

Figure 5.16: Position tracking (left), contact force (right) and impedance response (bottom) along y-axis for three different values of desired stiffness

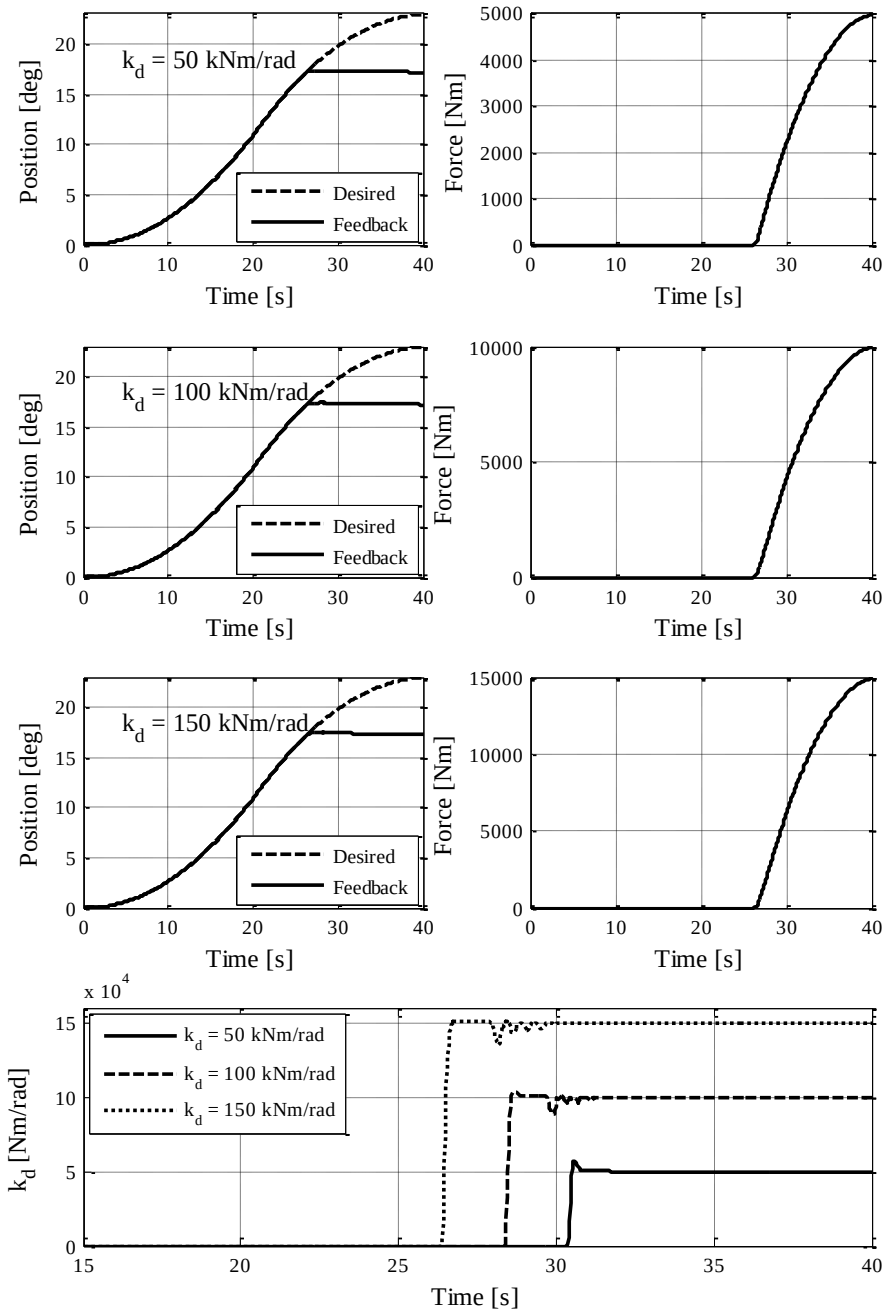

Figure 5.17: Position tracking (left), contact force (right) and impedance response (bottom) about y-axis for three different values of desired stiffness

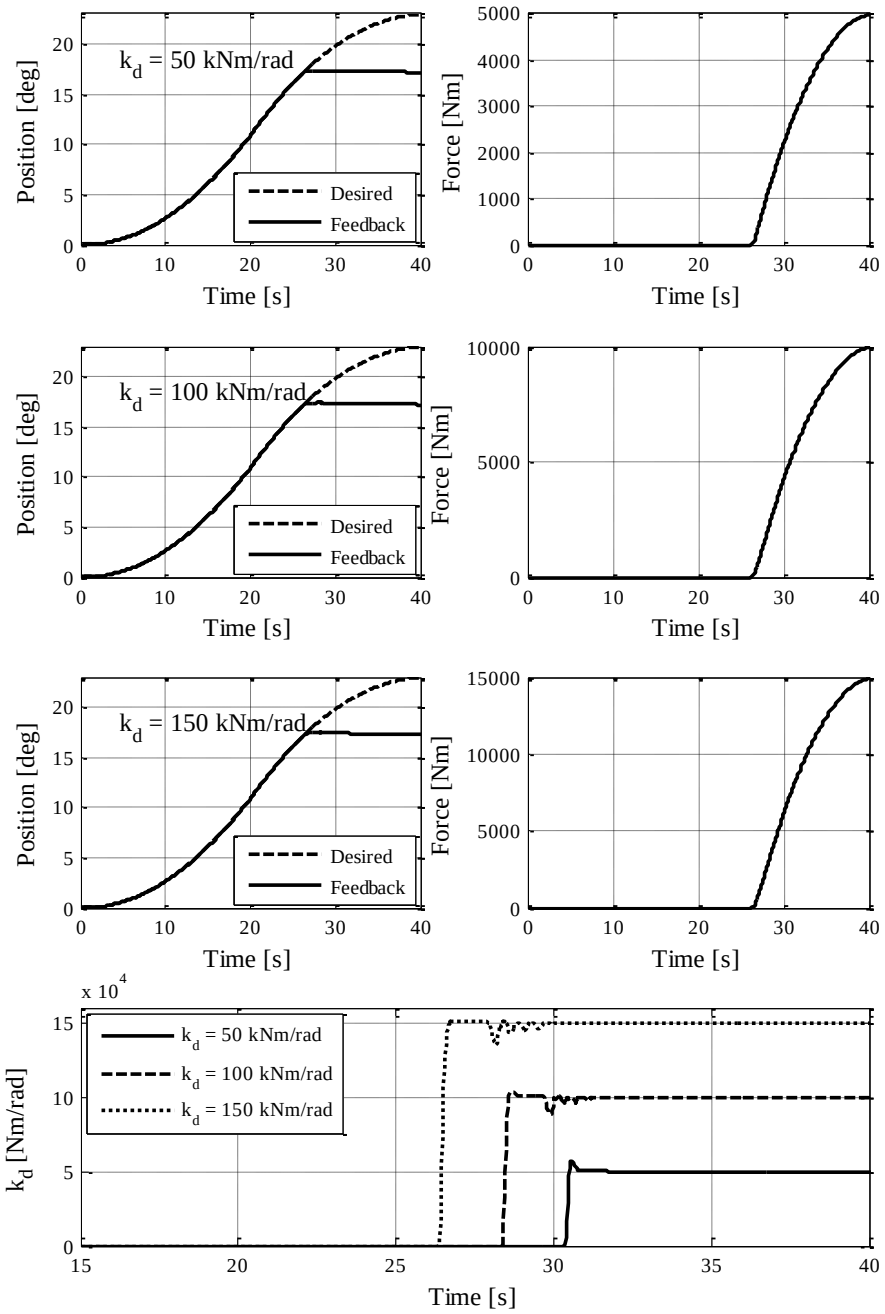

Figure 5.18: Position tracking (left), contact force (right) and impedance response (bottom) along z-axis for three different values of desired stiffness

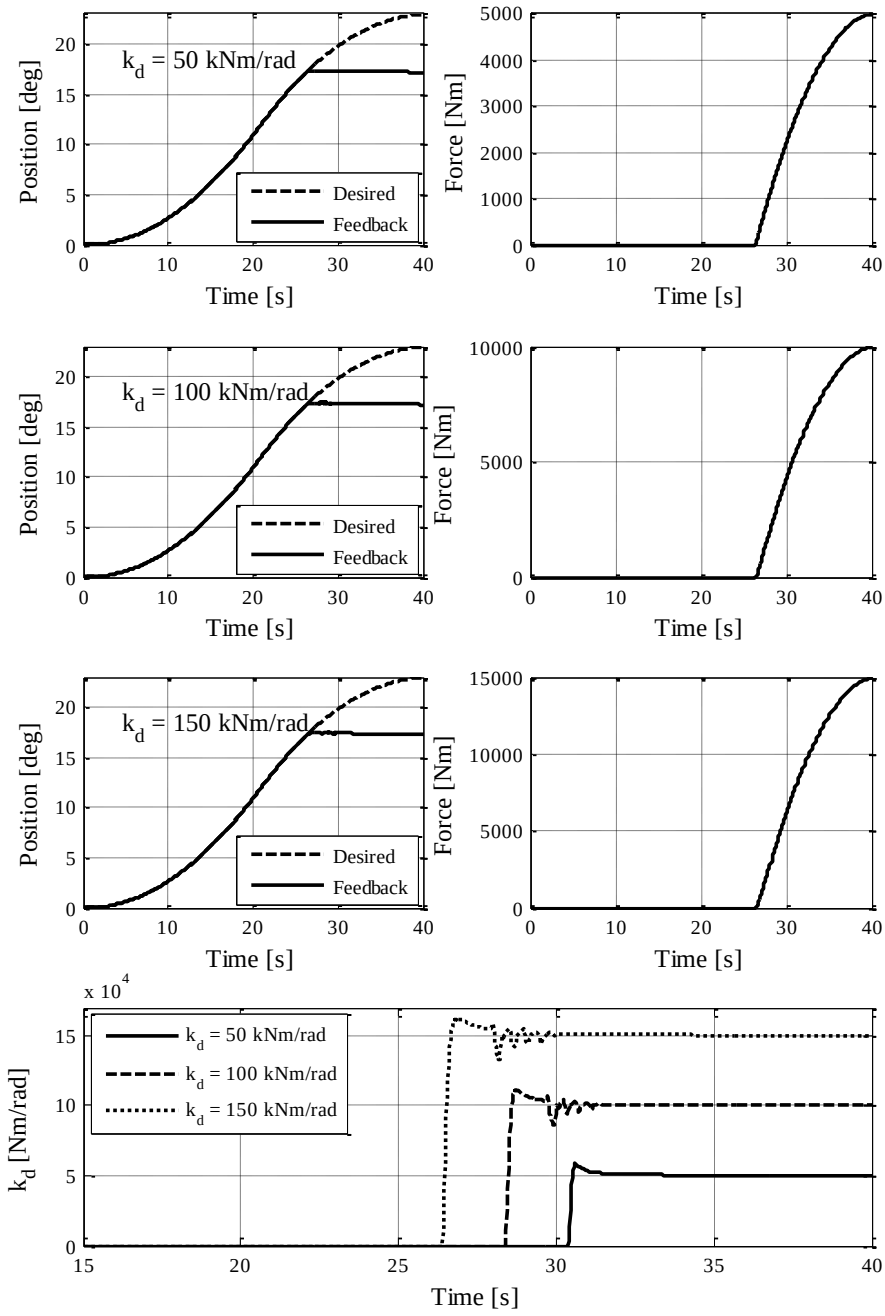

Figure 5.19: Position tracking (left), contact force (right) and impedance response (bottom) about z-axis for three different values of desired stiffness

5.4 Equivalent force-based impedance controller

The position and force control properties of a single water hydraulic vane actuator have been previously studied by (Raneda, 2004). The position-based implementation of impedance control was suggested to be more suitable due to practical limitations. The position-based approach for impedance control of hydraulic manipulators has also been suggested by other sources (Ha, et al., 2000), (Heintze, et al., 1995). In fact, the preference is so profound that the force-based implementation of impedance control has not been reported for hydraulic manipulators.

Force-based impedance control requires the force controller to be in the inner loop of the impedance controller (Lawrence, 1988). The tuning of the force controller for the manipulators presents considerable challenges, as it requires the compensation of the manipulator's dynamic forces. In practice, it is difficult to know the accurate values of the manipulator's dynamic parameters and they may change over time or in some cases may be completely unavailable. Additionally, as discussed in Section 3.5.2 (Figure 3.4 and Figure 3.5), the force-based impedance controller requires velocity and acceleration feedbacks in the outer loop. Since the measurement of velocity and acceleration is impractical in operation-space, these signals are therefore obtained by numerical differentiation of joint-space position feedback and using the relationships of Equations 3.6 and 3.54 respectively. This results in the amplification of measurement noise, and the obtained signal is not useful for control anymore.

On the other hand, the majority of industrial manipulators are already provided with position controllers, providing high positioning accuracy and repeatability. In such cases the implementation of impedance controller requires only the implementation of impedance filter in the outer loop. Additionally, as seen in the last section, for the position-based impedance controller the desired impedance is modelled as a second order filter, which also serves the purpose of attenuating the noise from the force sensor. These features make position-based implementation a much more attractive approach.

Coming to the subject of hydraulic manipulators, the force control of hydraulic actuators presents further challenges (Tafazoli, et al., 1998). Hydraulic actuators are essentially position/velocity sources, where actuator velocity is proportional to input valve voltages, in contrast to electrically driven manipulators where the actuators are torque sources and torque is proportional to the input control signal. Also, the nonlinear behaviour of pressure dynamics inside the chambers of hydraulic actuators, and other nonlinearities such as friction, non-linear flow, leakage, etc. make the control of actuator forces much more difficult.

In Section 3.6 it was shown that it could be possible to obtain the inner loop force controller for force-based impedance controller by comparing the controller outputs of the two implementations. The established relationship in the operational-space is given as:

5.18 $$\boldsymbol{k_{fx}} = \frac{\mathbf{1}}{\boldsymbol{Z_d(s)}} \cdot \boldsymbol{k_{px}}$$

where $\boldsymbol{k_{fx}} \in \mathcal{R}^8$ and $\boldsymbol{k_{px}} \in \mathcal{R}^8$ are the vectors of inner loop force and position controllers respectively, for the respective implementations of impedance controller. The equivalent relationship in its scalar form can be used for the case of single degree of freedom.

5.19 $$k_f = \frac{1}{z_d} \cdot k_p$$

The relationship of Equation 5.19 has been verified for the force-based implementation of impedance controller in (Muhammad, et al., 2006) and (Muhammad, et al., 2009). However, for a general manipulator with multiple degrees of freedom Equation 5.18 cannot be utilized, as it represents controllers in operational-space and for the majority of the manipulators the controller is implemented in the joint-space.

Unfortunately, a relationship similar to Equations 5.18 and 5.19 does not exist in the joint-space. The reason is the nonexistence of linear mapping between the joint-space and operational-space position and acceleration. With the assumption that the manipulator's Jacobian can be utilized for such linear mapping, the following approximate relationship was developed:

5.20 $$\boldsymbol{k_{f\theta}} = \boldsymbol{k_{p\theta}} \cdot \boldsymbol{J^{-1}} \cdot \frac{\mathbf{1}}{\boldsymbol{Z_d(s)}} \cdot \boldsymbol{J^{-T}}$$

For further investigation, an approximation of Equation 5.20 is utilized to implement the force-based impedance controller for WHMAN. The manipulator is subjected to the same position trajectories as in the case of position-based implementation.

The results are shown in the plots of position tracking, contact force and the tracked stiffness along each axis in Figure 5.20 to Figure 5.25 for the desired stiffness value of $50 \times 10^3\ N/m$. It can be observed that the manipulator is unstable and it is not possible to track either position or force, and hence the desired impedance. Therefore, the approximation of Equation 5.20 is not valid in general. From the implementation point of view, though equivalent performance can be obtained from either implementation of impedance control, in general it will require the separate tuning of internal position and force controllers.

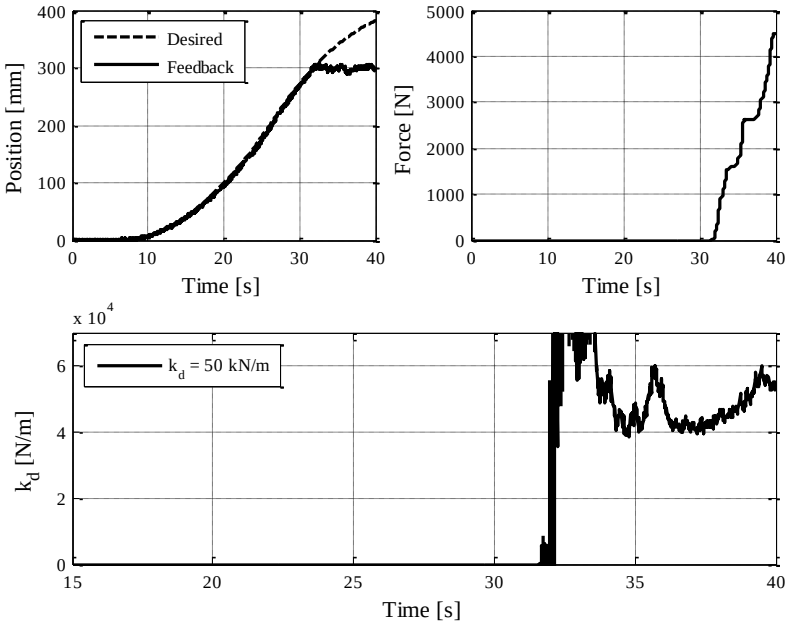

Figure 5.20: Position tracking, contact force and impedance response along z-axis

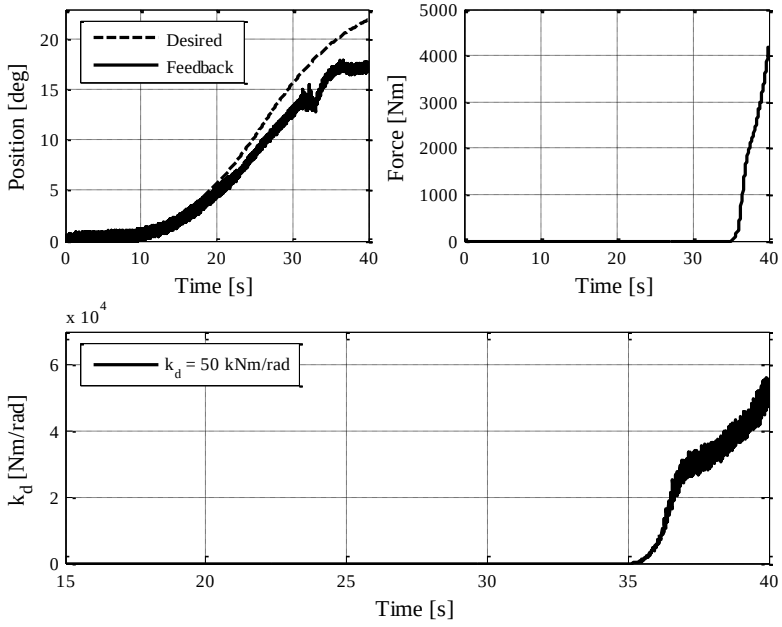

Figure 5.21: Position tracking, contact force and impedance response about x-axis

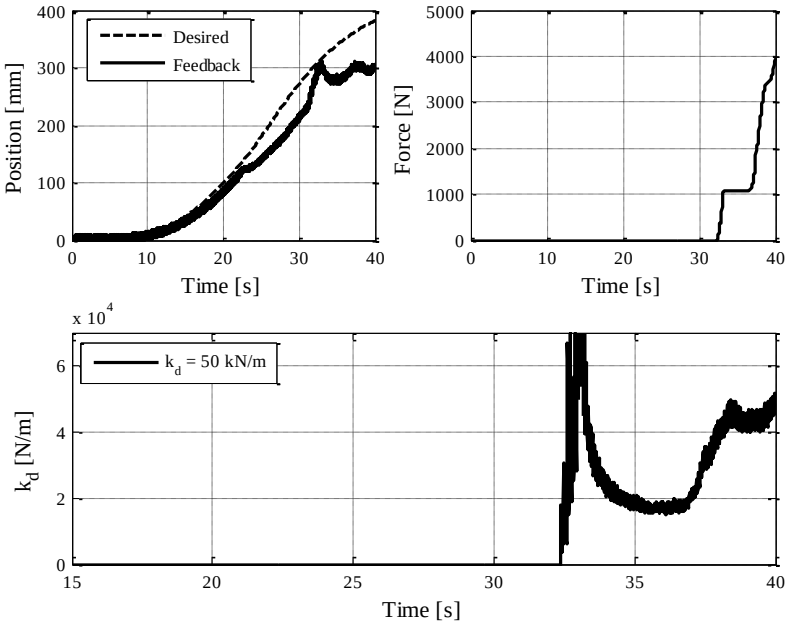

Figure 5.22: Position tracking, contact force and impedance response along y-axis

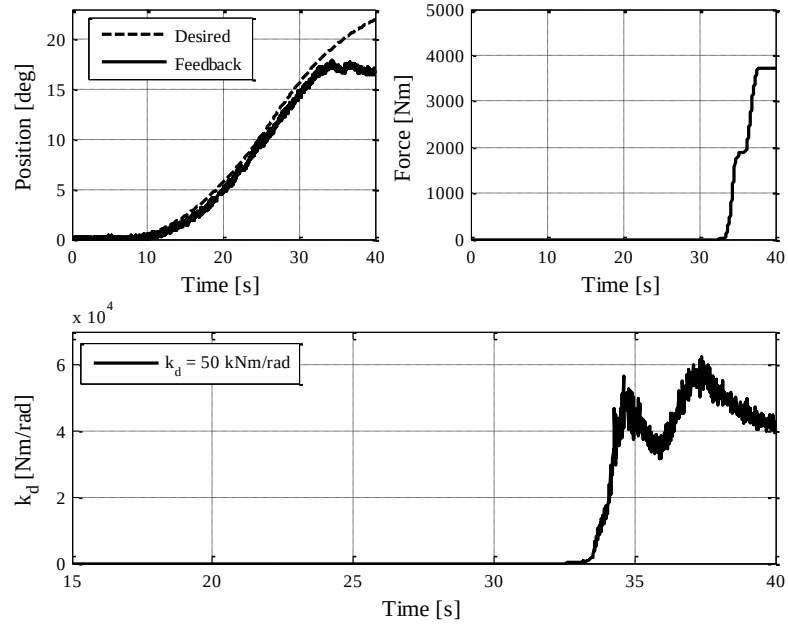

Figure 5.23: Position tracking, contact force and impedance response about y-axis

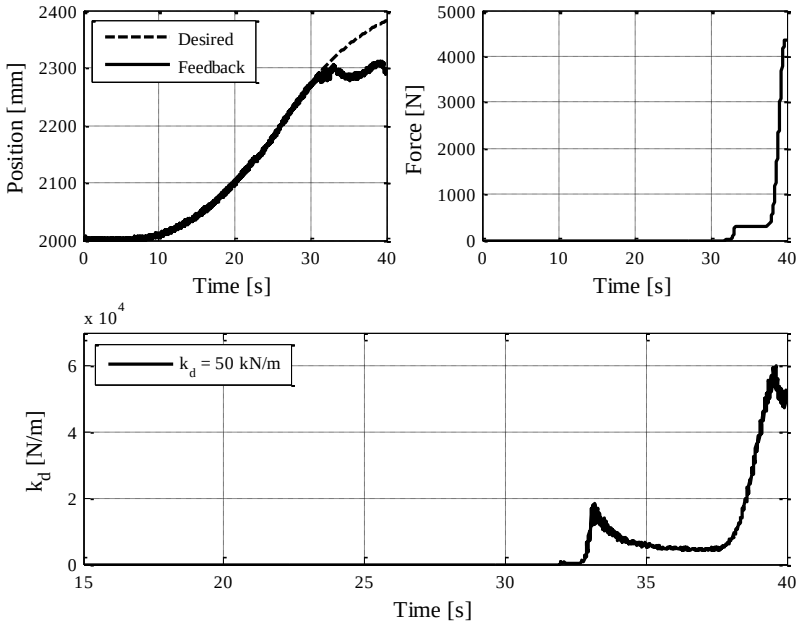

Figure 5.24: Position tracking, contact force and impedance response along z-axis

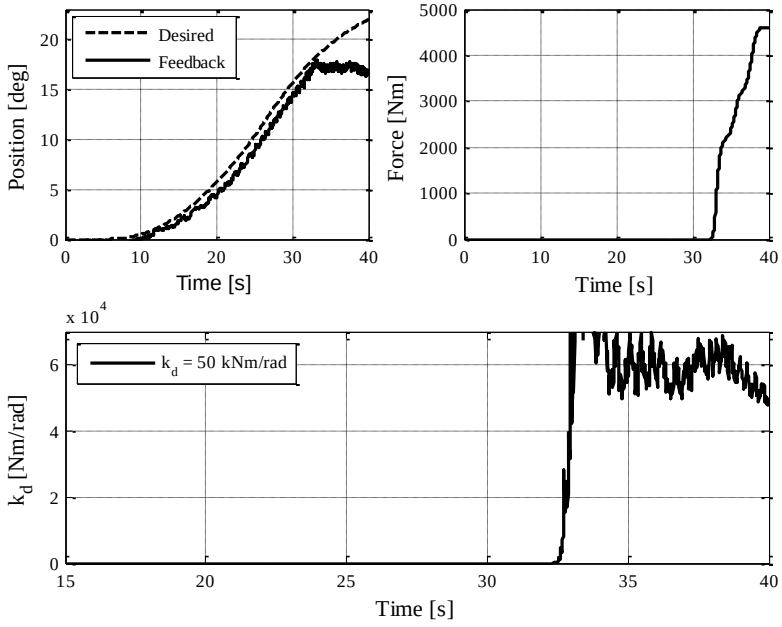

Figure 5.25: Position tracking, contact force and impedance response about z-axis

However, as discussed earlier the force control of manipulators driven by hydraulic actuators is not so straightforward and presents considerable challenges (Tafazoli, et al., 1998). The nonlinear behaviour of pressure dynamics inside the chambers of hydraulic actuators and other nonlinearities such as friction, non-linear flow, leakage, etc. make the control of actuator forces much more difficult (Watton, 1989). A reasonably good design of the force controller for hydraulic actuators requires separate pressure control of individual chambers via 3/2 servo-valves (Jansson, et al., 1990). Direction control servo-valves produce high pressure gain with small control signal ($\pm 3\%$), which decreases to zero with further signal. On the other hand, the flow gain remains linear for almost the entire range of control signal. This characteristic makes it very challenging to combine the force control along with the motion of the hydraulic actuator (Virvalo, et al., 2000). Actuators of WHMAN are equipped with 4/3 servo-valves which omit such a possibility, thus making the velocity or position control the best option.

As shown in Section 4.4, in the case of WHMAN the leakage and friction across the vane actuators can significantly vary as a result of manufacturing tolerances, expansion of seals and direction of motion. Thus, these nonlinearities are the functions of the actuators' position, pressure differences and direction of motion. Such behaviour is very difficult to model and thus compensate and can significantly degrade the performance of the force controller.

Additionally, since WHMAN possesses redundant degrees of freedom, during force control it will not be possible to exploit them for the kinematic or dynamic improved performance of the manipulator. The force controlled redundant joints will move freely and reach their mechanical limits, making it difficult to control the behaviour of the manipulator. Hence, the design of force controller for WHMAN is a considerable challenge and is beyond the scope of this study.

5.5 Effect of redundancy

In this section the effect of redundancy on the dynamic manipulability of the manipulators is studied using the example of WHMAN. First, the acceleration capability of the manipulator is compared in redundant and non-redundant configurations using the Dynamic Manipulability Ellipsoid (DME). Then the performance of the manipulator is analysed in non-redundant configuration using the position-based impedance controller and compared against the performance of redundant configuration in Section 5.3.

5.5.1 Numerical analysis

In Section 3.2 the dynamic manipulability of the manipulators was described using the DME (Yoshikawa, 1985). With DME the dynamic manipulability of a manipulator can be characterized by the singular values of the matrix $Ч = \boldsymbol{J} \cdot \widehat{\boldsymbol{M}}_{\boldsymbol{\theta}}^{-1}$. Where $\boldsymbol{J} \in \mathcal{R}^{m \times n}$ and $\widehat{\boldsymbol{M}}_{\boldsymbol{\theta}} \in \mathcal{R}^{n \times n}$ are the Jacobian and the normalized inertia matrices of the manipulator respectively. It was shown that when the manipulator has redundant degrees of freedom in joint-space, i.e. $n > m$ the matrix Ч has larger singular values, compared to the case where $n = m$. Since the singular values are the lengths of the axes of DME, larger singular values represent the larger DME.

A description of WHMAN is provided in Chapter 4. The WHMAN is an intrinsically redundant manipulator having eight degrees of freedom in joint-space and six degrees of freedom in operational-space ($m = 6$ and $n = 8$). For a given posture the Jacobian and the normalized inertia matrices of WHMAN are given as $\boldsymbol{J} \in \mathcal{R}^{6 \times 8}$ and $\widehat{\boldsymbol{M}}_{\boldsymbol{\theta}} \in \mathcal{R}^{8 \times 8}$ respectively. The kinematic and dynamic parameters of WHMAN are given in Appendices A and B respectively.

To analyse the effects of redundancy on dynamic manipulability, it is useful to consider only the dynamic manipulability of the arm of WHMAN, since the arm possesses redundant degrees of freedom and not the wrist. In fact, for most manipulators the redundant degrees of freedom are present in the arm. Apart from a few cases (Wampler, 1989), (Yoshikawa, et al., 1989) redundant degrees of freedom in the wrist are avoided due to structural complexities.

In addition, considering the DME separately for arm and wrist gives the singular values of matrix Ч more physical significance. Since the arm of the manipulator is used mainly to achieve the position and wrist to achieve orientation in space, the singular values and associated orthogonal vectors will represent the axes of DME in the Cartesian coordinate system. Also with this approach ambiguity between the translational and rotational units of position and force can be avoided.

The Jacobian and inertia matrices of the manipulator's arm and wrist can be decoupled by locating the tool frame at the point of intersection of the orthogonal spherical wrist. The mass of the wrist can be added to the tip of the arm. This simplification provides the manipulability measure of the manipulator's arm for analytical purposes. These simplified calculations are also useful for redundancy resolution of the arm during controller design.

For a given posture the Jacobian and the normalized inertia matrices of the redundant WHMAN arm are given as $\boldsymbol{J} \in \mathcal{R}^{3 \times 5}$ and $\widehat{\boldsymbol{M}}_{\boldsymbol{\theta}} \in \mathcal{R}^{5 \times 5}$ respectively. The redundant degrees of freedom in

the joint-space of WHMAN can be removed by considering the first and the fourth joints of the arm as of fixed lengths. In this way, the manipulator does not loses any degrees of freedom in the operational space. For the non-redundant case the Jacobian and normalized inertia matrices are given as $\boldsymbol{J} \in \mathcal{R}^{3\times3}$ and $\widehat{\boldsymbol{M}}_{\boldsymbol{\theta}} \in \mathcal{R}^{3\times3}$ respectively. These Jacobian and inertia matrices can directly be obtained by removing the corresponding rows and columns of the respective matrices of the redundant manipulator arm.

The planar projections of DME for redundant and non-redundant configurations in several different postures are shown in Figure 5.26, Figure 5.27 and Figure 5.28, where the ellipsoids have been scaled down for the sake of clarity.

The sums of the lengths of the ellipsoid axes (singular values) for each posture of the manipulator are also shown in these figures. This confirms the findings of Section 3.3 that the volume of manipulability ellipsoid is larger if the manipulator has redundant degrees of mobility. Hence, the redundant degrees of freedom can help in improving the dynamic performance of the manipulator. In Section 3.3 the manipulator's inertia matrix was assumed to be diagonal or at least diagonal dominant; however, no such assumptions are made here.

In Section 3.3 it was also assumed that redundant degrees of freedom can be added to the manipulator without significantly affecting the inertia matrix. However, in practice additional degrees of freedom require additional actuators and the resizing of existing actuators, which can result in a significant alteration of the inertia matrix. To elaborate this case, DME for the redundant and non-redundant configurations of WHMAN are drawn again in Figure 5.29 in the same plane as in Figure 5.26. This time it is assumed that the redundant degrees of freedom provide only one tenth of the rated forces while keeping the same inertial parameters. However, in this case the condition of Equation 3.12 ($|\tilde{\tau}_i| \leq \tilde{\tau}_{i\,max}$) used for developing the DME representation in Chapter 3 is not valid anymore and manipulator is not capable of supporting its own gravity load.

It is evident that in such cases the addition of redundant degrees of freedom can actually result in a poorer dynamic performance. Hence, the added degrees of freedom can result in the improved dynamic performance of the manipulator with actuators having high force to size ratio. It is true in the case of hydraulic manipulators, in which the actuators are normally compact, lightweight and capable of delivering high forces to directly drive the manipulator joints. In the case of electrical manipulators, such behaviour can be achieved by delocalizing the actuators and using wire or chain transmission; however, this will result in a complicated structure and increased mechanical nonlinearities.

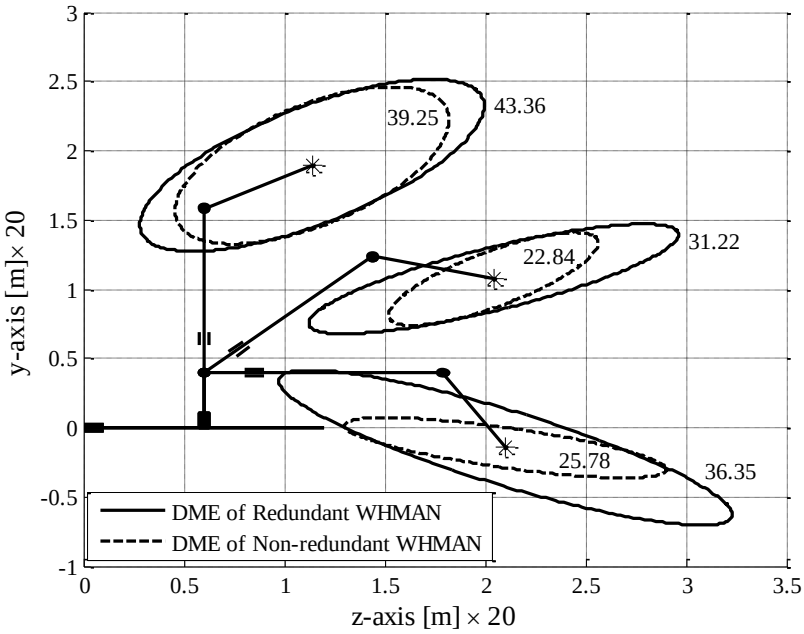

Figure 5.26: DME of WHMAN in yz-plane

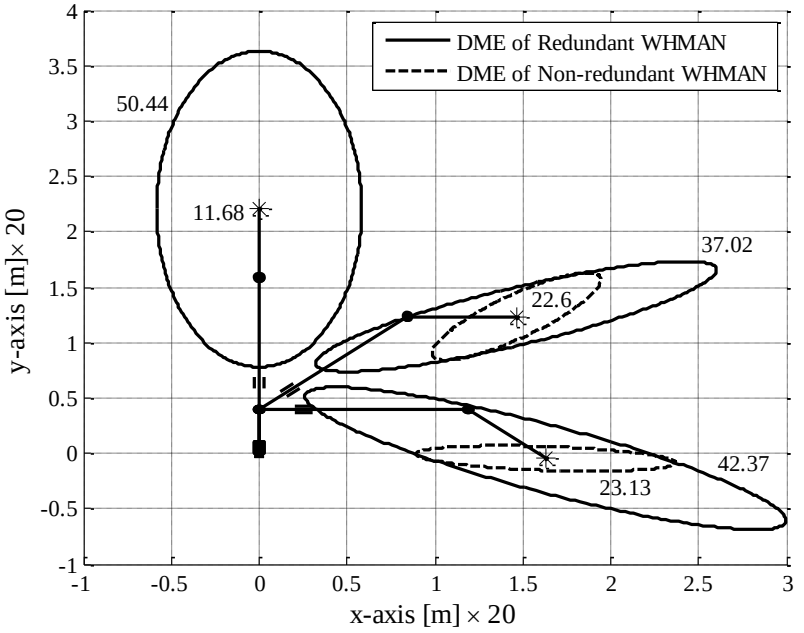

Figure 5.27: DME of WHMAN in xy-plane

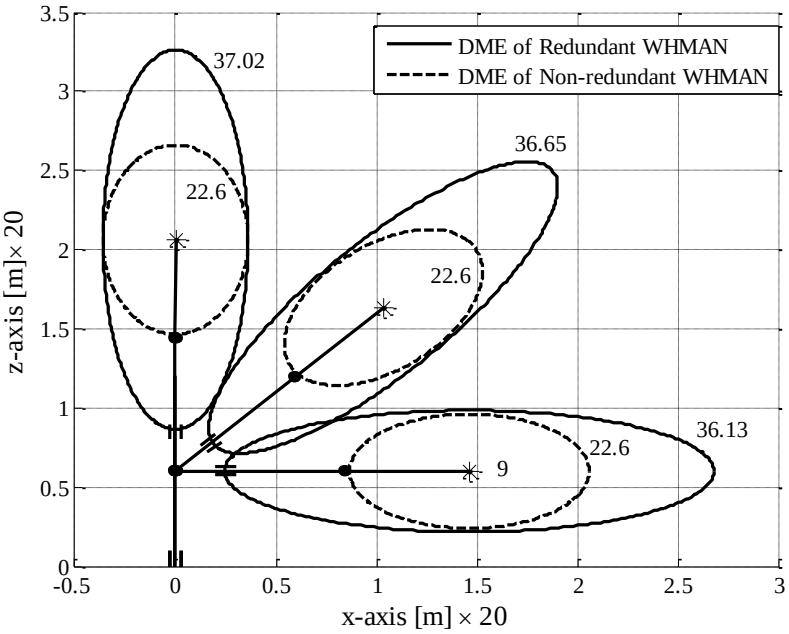

Figure 5.28: DME of WHMAN in xz-plane

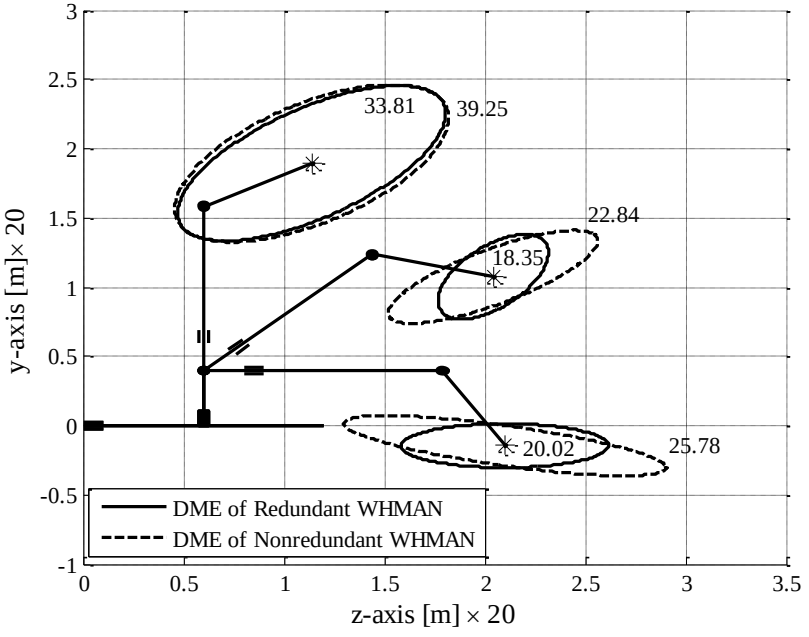

Figure 5.29: DME of WHMAN in yz-plane with reduced actuator forces

5.5.2 Simulation analysis

To further analyze the effect of redundancy on the dynamic performance of the manipulators, the response of the WHMAN is tested with the impedance controller of Section 5.3 in non-redundant configuration. The redundant joints d_1 and d_4 (linear slide and telescopic extension) are position controlled to fixed values. In this way these joints do not contribute to the impedance regulation and the manipulator does not lose any degrees of freedom in operational-space. The manipulator is subjected to the same position profiles for the desired stiffness values of 50×10^3 N/m, 100×10^3 N/m and 150×10^3 N/m.

The zoomed position tracking response of the manipulator on coming into contact with the environment is shown for redundant (left) and non-redundant (right) configurations next to each other in Figure 5.30, Figure 5.31 and Figure 5.32. The value of tracked stiffness along each axis is also shown at the bottom for each case. The plots of the measured stiffness values are shifted artificially in time for the sake of clarity.

From the comparison of plots it is clear that the impedance regulation capability of the manipulator deteriorates with the loss of redundant degrees of freedom. The major difference can be observed along the directions (y-axis and z-axis) in which the motion of redundant joints contributes to the maximum motion of end-effector in the given posture.

5.6 Summary

In this chapter the theoretical developments of Chapter 3 were studied using the simulation model of WHMAN. At the start, a scheme for the resolution of redundancy was devised for the manipulator. The effect of the manipulator's posture on the Dynamic Manipulability Index was determined. Using redundant degrees of freedom, the manipulator's joints were kept in range such that the index was maximized. This scheme results in a computationally simple and efficient algorithm.

A position controller for the WHMAN was designed using the verified simulation model presented in Section 4.4. The manipulator dynamics were decoupled using gravity compensation and the position controller designed in a decentralized fashion, such that the controller for each joint takes into consideration only the dynamics of the respective joint. The

linearized dynamic model of each joint was obtained using the simulation model of the manipulator. The controller was tuned using the velocity and acceleration feedback as the states. The position tracking performance of the manipulator was further improved by using the velocity feed-forward signal. The choice of this control strategy was made because of its simplicity and the performance of the position controller was found satisfactory.

The design of the impedance filter was presented for the desired dynamic behaviour. Then the impedance control properties of the WHMAN were studied using the position controlled simulation model and designed impedance filter for position-based implementation. The response of the manipulator was studied for several values of desired stiffness. The results are shown as position tracking, contact force and stiffness plots. On coming into contact with the environment the manipulator remains stable and behaves according to the defined desired impedance.

The equivalent force-based implementation of impedance controller was studied, whereby the force controller for the inner loop was designed using the relationship of Equation 5.20. As expected, the manipulator became unstable, losing position and force tracking and therefore the desired dynamic behaviour. It was found that the approximation of Equation 5.20 is not valid in general. From the implementation point of view, though equivalent performance can be obtained from either implementation of impedance control, in general it will require the separate tuning of internal position and force controllers. Since the WHMAN was found to be unstable, the equivalent implementation will not be further investigated through experiments.

Finally, the effect of redundant degrees of freedom on the manipulator was studied using both the numerical and simulation models of WHMAN. The ellipsoids of the dynamic manipulability (DME) of the manipulator were plotted using the numerical model of WHMAN for both redundant and non-redundant configurations. The ellipsoids showed that redundant degrees of freedom of WHMAN do result in higher dynamic manipulability. It was found that the dynamic manipulability of the manipulator can be improved if redundant degrees of freedom can be added to the manipulator without significantly altering its inertia matrix. This fact is significant in the case of hydraulic manipulators, where actuators deliver a high force to size ratio.

The effect of redundancy on the dynamic manipulability of manipulators was further studied with the impedance control response of the manipulators using the simulation of model of WHMAN. The position tracking and the impedance regulation performance of the manipulator in redundant configuration were compared against non-redundant configuration. The results

show that the impedance regulation capability of the manipulator can be improved with the presence of redundant degrees of freedom.

In the next chapter the findings of redundancy resolution, position and impedance controllers are implemented for the actual WHMAN and the results are studied through experiments.

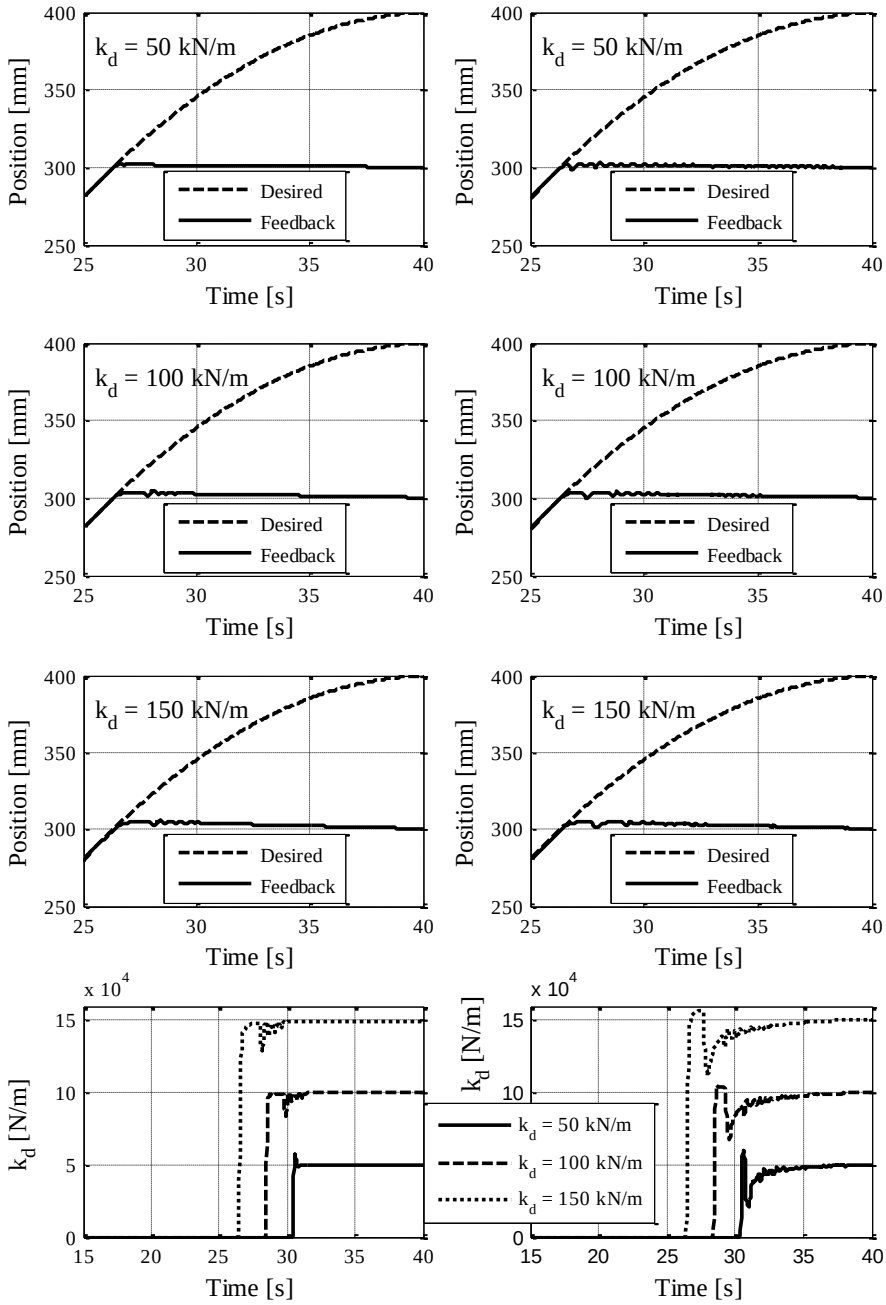

Figure 5.30: Position tracking and impedance response for redundant (left) and for non-redundant (right) configurations along x-axis for three different values of desired stiffness

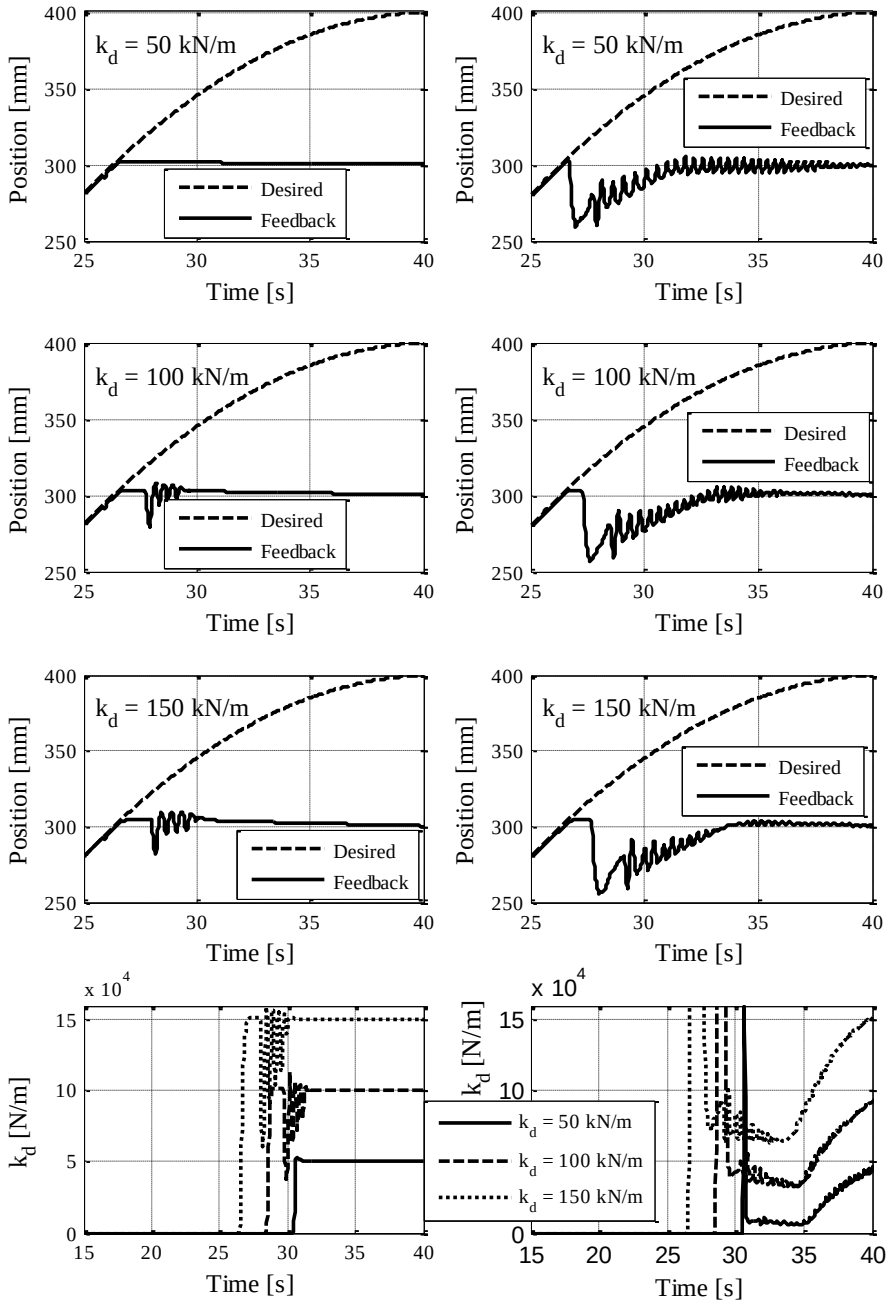

Figure 5.31: Position tracking and impedance response for redundant (left) and for non-redundant (right) configurations along y-axis for three different values of desired stiffness

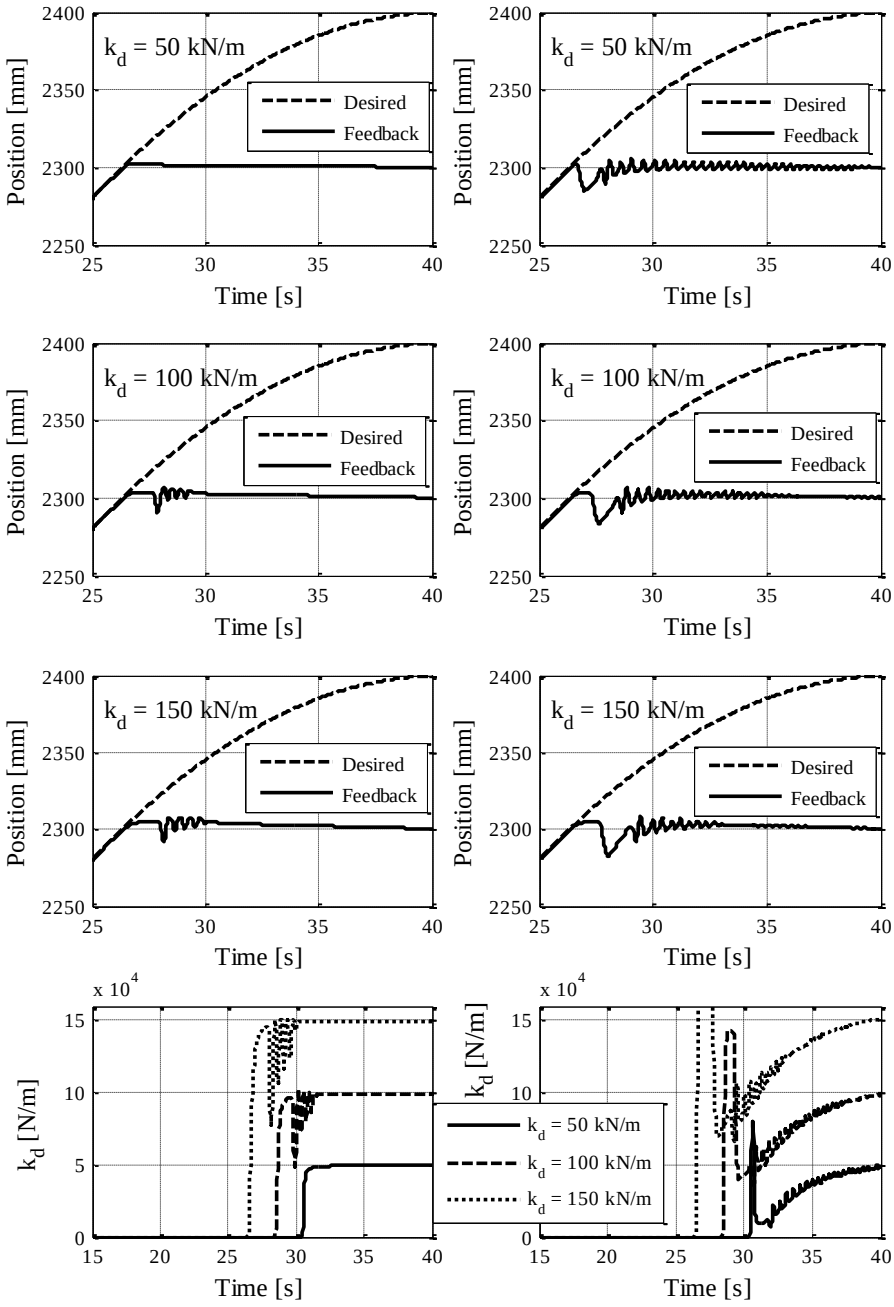

Figure 5.32: Position tracking and impedance response for redundant (left) and for non-redundant (right) configurations along z-axis for three different values of desired stiffness

6 EXPERIMENTAL ANALYSIS

In this chapter the results obtained from the numerical analysis and simulations in the last chapter are implemented for the WHMAN (Water Hydraulic MANipulator) to verify the theoretical findings of Chapter 3 via experiments.

The tuning and the performance of the position controller are discussed in Section 6.1. The practical implementation of designed position controller of Section 5.2 is tested against the modelling inaccuracies of WHMAN.

The performance of the impedance controller is evaluated next in Section 6.2. The desired impedance parameters are selected according to the performance of the position controller. The manipulator is then driven against a noncompliant environment to estimate the performance of the impedance controller. The performance of the position-based impedance controller is shown via position, force and impedance plots.

The effect of redundancy on the dynamic performance of the manipulator is studied in Section 6.3 via impedance controller. The performance of impedance controllers is compared for redundant and non-redundant configurations of WHMAN. The results of the experiments are presented as position, force and impedance response plots. These results of the experimental study are summarized in Section 6.4.

6.1 Position controller

In Section 5.2 the joints' velocity and acceleration were utilized to develop state-feedback position controllers for the joints of WHMAN. Utilization of velocity and acceleration as feedback can considerably improve the dynamics of the system, and as a result higher close-loop gains can be used for improved dynamic response and reduced steady state error. This characteristic is of particular importance for hydraulic servo systems which regularly provide low damping, limiting the performance of controller.

The design of the state-feedback controller is based on the principal of selecting new pole locations. Assuming ideal feedback of the states (velocity and acceleration) and the system as practically linear, the poles of the system can be selected as desired, by modifying the feedback gains. In practice, this means using both velocity and acceleration sensors, which will result in

additional cost and complicated instrumentation, especially in systems with several hydraulic actuators. If the velocity sensor is used alone, the quality of the acceleration signal will depend on the resolution of the velocity sensor, and if the acceleration sensor is used alone, the integration will result in an offset in the velocity signal.

In practice, velocity and acceleration signals are obtained by numerical differentiation of the position signal. This results in poor quality velocity and acceleration signals. The reason is the quantisation noise, which is inversely proportional to the resolution of position sensor and directly proportional to the sampling frequency. Increasing the resolution of the position sensor may improve the performance, but this will result in increased instrumentation cost. In addition, it does not provide the complete answer, because the quantisation noise may still appear at small velocities. In Figure 6.1 the realization of the state-feedback controller is shown where only position feedback signal is available.

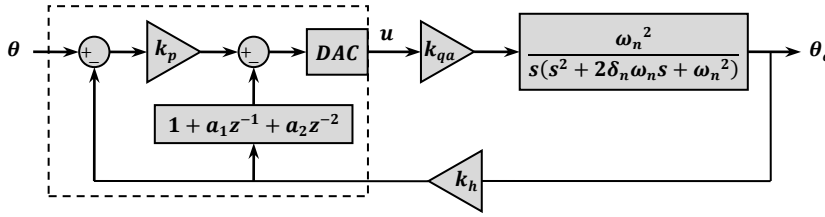

Figure 6.1: Realization of state feedback controller

To fully utilize the capabilities of the state-feedback controller, velocity and acceleration signals of relatively good quality are required. This requirement reduces its practical application in several cases (Linjama, et al., 2001). In (Mäkinen, et al., 2002) the effects of the feedback signal quality on the position servo control of a pneumatic drive were evaluated. The best results were achieved by using an observer to calculate the velocity and the acceleration feedback signals. It was also found that the use of a filter results either in too much delay or in failure to eliminate the quantisation noise completely. In (Virvalo, et al., 1997) it was concluded that reasonably high resolution of the position encoder is required to implement the state-feedback controller for hydraulic drives. The study also showed that good results can be obtained when an n-sample estimator is used to calculate the velocity and acceleration signals. Implementation of an n-sample estimator is shown in Equation 6.1.

$$\dot{\theta}(k) = \frac{\theta(k) - \theta(k-n)}{n.t_s} \tag{6.1}$$

Here, n is the number of samples and t_s is the sampling time. In (Muhammad, et al., 2008) it was shown that a state-feedback controller tuned with velocity and acceleration feedbacks obtained from the state observer is a good choice for hydraulic manipulators, otherwise gains need to be lowered significantly (Muhammad, et al., 2009b). The principle of the observer and its implementation is shown in Figure 6.2. More details on the implementation of observer can be found in (Franklin, et al., 1997).

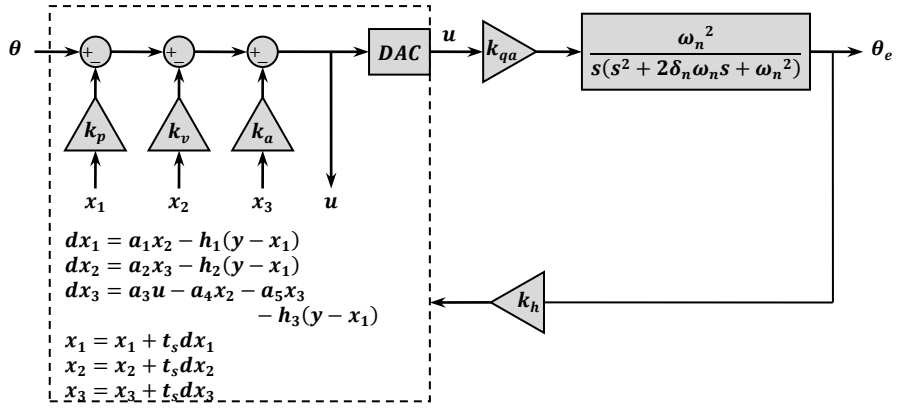

Figure 6.2: Realization of states' observer

The goal of the observer is to keep a minimum error between the actual and the calculated states of the system. Normally, the observer is designed with the same sampling time as the controller and solved once per sampling period. The observer calculates the states of the system using the difference equations shown in Figure 6.2. The calculations will produce a better result if a smaller sampling time is used for the integrators and the observer can be solved more than once during the sampling period of the controller. Since the control system of WHMAN is implemented with National Instruments/LabVIEW® it is relatively easy to achieve because of the ease of the multi-loop programming and the availability of the high computational power of multi-core processors. This approach was tested in (Muhammad, et al., 2008) and the results showed improved performance of the observer.

The same state-feedback controller developed with the simulation model in Section 5.2 along with the state-observer was implemented for WHMAN. The dynamic response and steady-state accuracy of the manipulator was observed to improve considerably as compared to the proportional controller of Section 4.4. During the test runs, though the manipulator largely remained stable, unstable behaviour was observed in certain specific postures for certain joints. The reduction in controller gains did not improve the situation and a certain limit-cycle was always observed. The possible cause can be the non-linearities resulting from the manufacturing

tolerances and the behaviour of the seals as described in Section 4.4. To guarantee the stability of the manipulator in the entire workspace the use of state-feedback controller was dropped and the manipulator joints were tuned with a proportional controller along with a nonlinear integrator. A small dead-band is added around the desired accuracy before the input of the integrator. This avoids the hunting behaviour commonly observed in the case of a linear integrator with hydraulic position control systems (Virvalo, 2001).

The manipulator is subjected to the same operational-space position profile used for testing the behaviour of the simulation model in Section 5.2, where the profile has the velocity of $0.05\ \mathrm{m/s}$ or $0.05\ \mathrm{rad/s}$ and acceleration of $0.001\ \mathrm{m/s^2}$ or $0.001\ \mathrm{rad/s^2}$ along each axis of motion. The profile is designed to move the manipulator in the region where the majority of the tasks are perceived to be executed inside the divertor maintenance tunnel, and additionally in a manner such that the manipulator needs to reverse the directions of motion during the execution of profile. The tracking response of the manipulator along different axes is shown in Figure 6.4 to Figure 6.9. The measured error (solid line) along each axis is plotted next to the simulated position error (dashed line) from Section 5.2 for the sake of comparison.

The sampling frequency of the control system is 1 kHz. The measurements are obtained at a sampling rate of 100 Hz. The control and data acquisition was performed using the National Instruments® hardware and LabVIEW® software.

The measured tracking error is slightly higher along certain axes due to non-modelled nonlinearities of the WHMAN. A particularly noted behaviour is shown in Figure 6.3, which is the tracking response and error of the base joint (θ_2 in Figure 4.1) of the manipulator. The joint has no gravity load and thus practically requires zero torque (zero pressure difference) to hold the manipulator in the horizontal plane (xz-plane) and requires very small torque (pressure difference of 5 to 10 bar as shown in Figure 4.14) for free-space movement.

According to the observations, without a certain amount of minimum pressure difference the seals allow considerable leakage between the actuator's chambers. The leakage decreases with an increase in pressure difference. The phenomenon is especially dominant when requiring the actuator to reverse the direction of motion, and can be approximated as backlash. Similar behaviour was observed from other actuators under the absence of gravity load. However, since this actuator is constantly free of gravity load and is located at the base of the manipulator, its contribution is more significant to the position error of the end-effector. A comparison of Figure 6.3 and Figure 6.4 clearly shows the reason for the significantly higher error of around 5 mm) along the x-axis. The error profiles have exactly the same shapes. The error along the z-axis is compensated due to the significantly good position control of the linear slide (d_1 in Figure 4.1).

For further details the kinematics of WHMAN can be referred to in Appendix A. Several compensation techniques were tried to mitigate this behaviour, but without success. It was found that the compression of seals is a nonlinear function of pressure difference in the chambers and depends on the direction of motion. The modelling of such seal behaviour requires considerable effort and can result in complicated and inefficient models and compensation techniques. Thus it is considered beyond the scope of this study.

An obvious difference between the simulated and measured errors is the spikes in the measured error when there is a change in the velocity of the manipulator. The reason for this is the use of a state-feedback controller for the joints during the simulations, which improved the dynamic behaviour of the manipulator, while a nonlinear PI controller is utilized for the joints of the actual manipulator. However, these position profiles were chosen to be quite aggressive to test the performance of the position controller. Realistically, WHMAN is not required to go through sudden changes of velocity during remote maintenance operations of the divertor.

The tracking and steady state error remains around or less than $2\ \mathrm{mm}$ in the case of position tracking along the y and z-axes and around or less than $5\ \mathrm{mm}$ along the x-axis. The rotation tracking error remains around 0.1 to $0.2\ \mathrm{deg}$ about all the axes. The performance of WHMAN will be practically evaluated at the Divertor Test Platform (DTP2) facility. These tests will reveal if the achieved position accuracy is adequate to carry out divertor maintenance operations.

The dynamic behaviour of the manipulator is further demonstrated by small step input along different axes. The measured and simulated responses are shown in Figure 6.10, Figure 6.11 and Figure 6.12. The step input is selected such that the input to the valve is not saturated during the entire motion. The simulated settling time is shorter due to the use of state-feedback controller which permits higher close-loop gains. The step response along the x-axis (Figure 6.10) is sluggish due the backlash in the base joint actuator (θ_2) discussed earlier. As fast motions are not expected from WHMAN inside the divertor, this performance of the position controller can be considered sufficient for the position-based implementation of impedance controller.

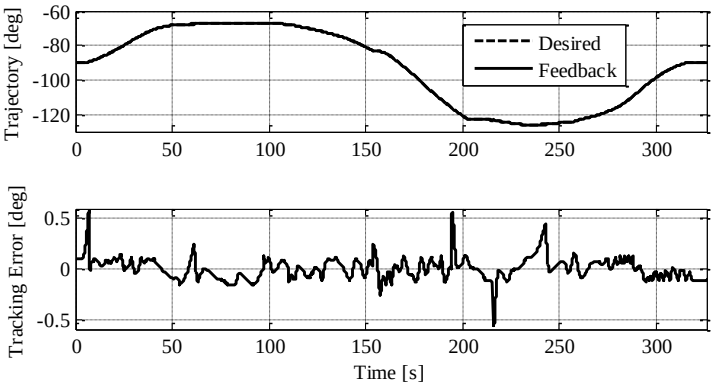

Figure 6.3: Position tracking response and error of base joint (θ_2)

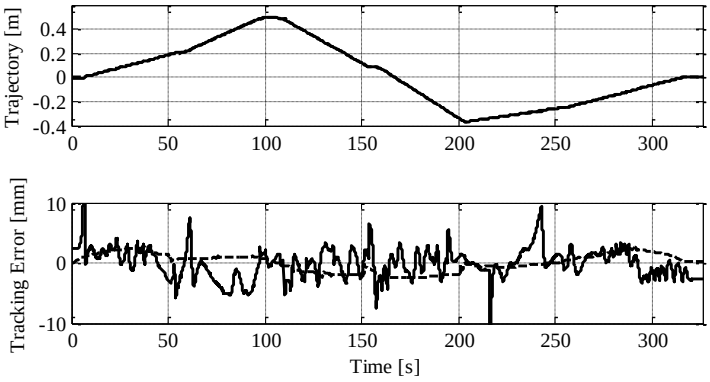

Figure 6.4: Position tracking, measured and simulated errors of WHMAN along x-axis

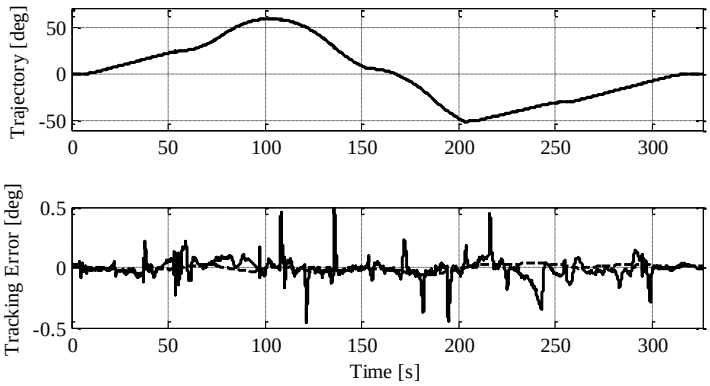

Figure 6.5: Rotation tracking, measured and simulated errors of WHMAN about x-axis

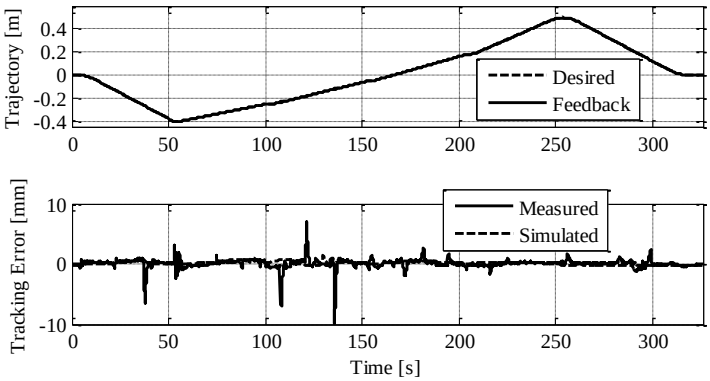

Figure 6.6: Position tracking, measured and simulated errors of WHMAN along y-axis

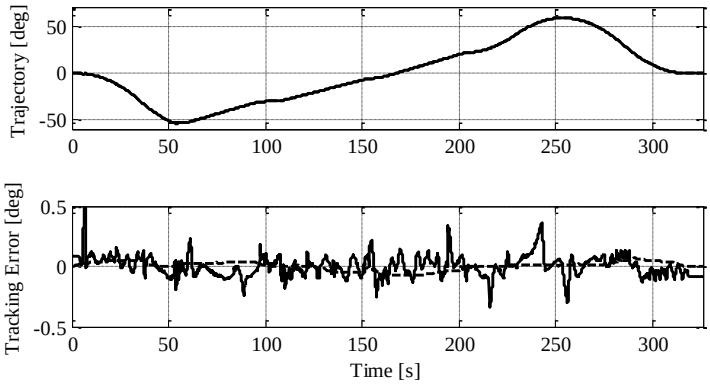

Figure 6.7: Rotation tracking, measured and simulated errors of WHMAN about y-axis

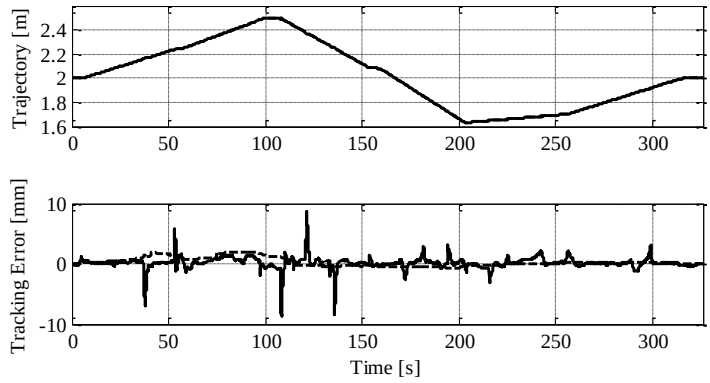

Figure 6.8: Position tracking, measured and simulated errors of WHMAN along z-axis

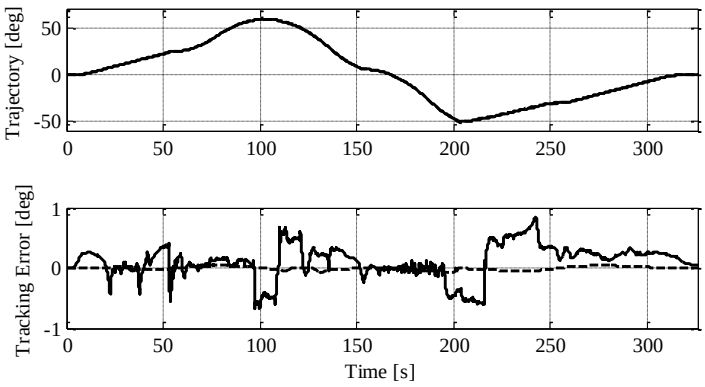

Figure 6.9: Rotation tracking, measured and simulated errors of WHMAN about z-axis

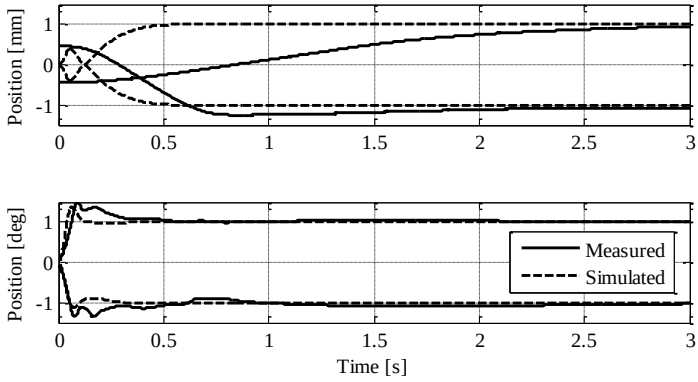

Figure 6.10: Measured and simulated step responses of WHMAN along and about x-axis

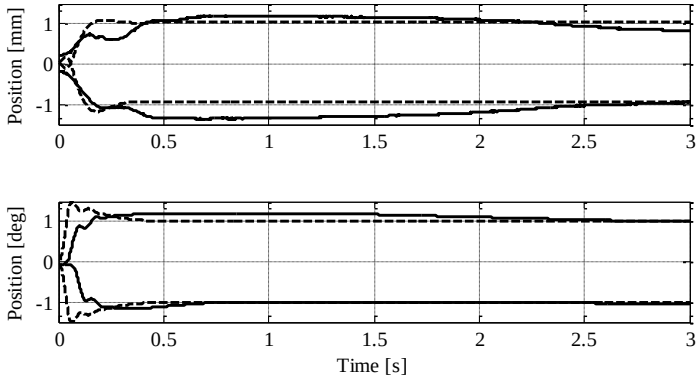

Figure 6.11: Measured and simulated step responses of WHMAN along and about y-axis

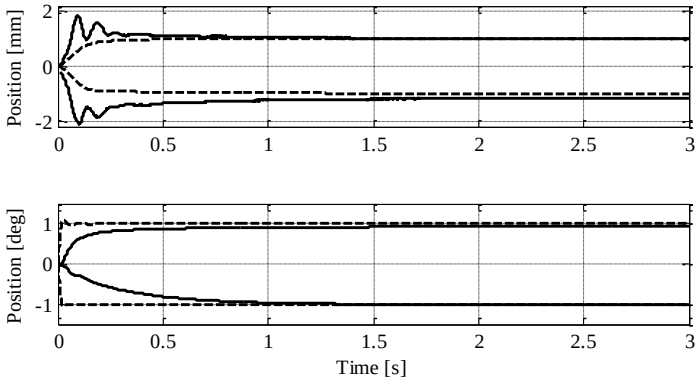

Figure 6.12: Measured and simulated step responses of WHMAN along and about z-axis

6.2 Position-based impedance controller

The tracking and step responses of the position controller of WHMAN are presented in the last section. The design of the impedance filter is discussed in this section. The position controlled WHMAN along with the impedance filter is then used to implement the position-based impedance controller for the manipulator. The results are shown using the position and force response of the manipulator along each axis.

6.2.1 Design of impedance filter

In Section 5.3.1 the standard second order transfer function was used to define the desired dynamics between the position and the force, i.e.

$$x(s) - x_e(s) = \frac{1}{k_d} \cdot \frac{{\omega_n}^2}{s^2 + 2 \cdot \delta_n \cdot \omega_n \cdot s + {\omega_n}^2} \cdot f_e(s) \qquad 6.2$$

where ω_n and δ_n are known as the natural frequency and natural damping respectively. Normally, the settling time of the impedance filter should be chosen longer than the settling time of the inner position loop to ensure impedance tracking. However, WHMAN is required to move quite slowly inside the divertor tunnel, and since it is required to carry out remote handling operations in the master-slave mode, a settling time t_s of 0.1 s is chosen for the

desired impedance filter. This settling time should be suitable for providing reliable force-feedback to the operator during the execution of contact tasks.

Then for a desired damping of 0.7 the natural frequency can be calculated by following the procedure of Section 5.3.1. The impedance filter can be designed along each axis of motion by setting the desired stiffness.

6.2.2 Experimental results

To test the performance of the impedance controller the WHMAN is brought into contact with a steel structure present in its workspace. The position and contact force of the manipulator are measured for the desired stiffness values of 150×10^3 N/m, 200×10^3 N/m and 250×10^3 N/m along the position axes. For any lower stiffness values the manipulator went into hunting behaviour on coming into contact with the environment. Similar results for low stiffness value have been reported and investigated by other researchers, such as (Eppinger, et al., 1992) and (Heinrichs, et al., 1999).

The most likely reason for this unstable behaviour is un-modelled and nonlinear contact dynamics, for example due to the attachment assembly of force sensor, tool changer, etc. Additionally, since the operational-space position of the manipulator is estimated from the joint-space variables while the force is measured directly in the operational-space via force sensor, un-calibrated geometrical errors can results in an inconsistent relationship between the operational-space position and force. This inconsistency becomes dominant as the desired stiffness of the manipulator is lowered, leading to instability.

The position, contact force and the tracked stiffness along each axis are shown in Figure 6.13, Figure 6.14 and Figure 6.15. The position plots are zoomed near the contact point. The stiffness is calculated using Equation 6.3 below. The stiffness plots are shifted artificially in time for the sake of clarity.

$$k_d = \frac{f_e}{x - x_e} \text{ N/m, Nm/rad} \tag{6.3}$$

It can be seen from the plots that on coming into contact with the environment the position and force response of the manipulator remains stable. The response of the manipulator is considerably damped. Additionally, the measured stiffness of the manipulator remains below

the desired value along the x and z axes. The reason is the passive compliance present in the manipulator's joints. This passive compliance is the result of the flexibility and the non-linear compression of the vane actuators' seals, as discussed in Section 4.4. As a result, the joints of the manipulator behave like a spring-damper system. This phenomenon is especially prominent in the horizontal plane due to the base joint (θ_2 in Figure 4.1) of the manipulator. The joint has no gravity load and thus practically requires zero torque (zero pressure difference) to hold the manipulator in the horizontal plane (xz-plane) and requires very small torque (pressure difference of 5 to 10 bar as shown in Figure 4.14) for free-space movement.

The performance of the impedance controller can be tested by using Equation 6.4 as indicated in (Salcudean, et al., 1997).

$$k_c = \frac{f_e}{x - x_c} \ \mathrm{N/m, Nm/rad} \tag{6.4}$$

Here, k_c is the commanded stiffness and the modified position value from the impedance filter has been utilized instead of a measured contact position to estimate it. The estimated value of the commanded stiffness is shown in the plots of Figure 6.16, where it reaches the desired value.

To further investigate the behaviour, the passive compliance of the manipulator is estimated along each position axis. For this purpose, the manipulator is brought into contact with the same steel structure while driven in pure position control. The position error and the contact forces are recorded to estimate the stiffness of the manipulator. These measurements along each axis are shown in Figure 6.17, Figure 6.18 and Figure 6.19.

The passive compliance of the manipulator acts together in series with the active compliance commanded by the impedance controller. Hence, the effective value of stiffness can be computed using Equation 6.5.

$$\frac{1}{k_d} = \frac{1}{k_c} + \frac{1}{k_r} \ \mathrm{m/N, rad/Nm} \tag{6.5}$$

Here, k_r is the passive stiffness of the robot. Utilizing the above equation, the effective stiffness of the manipulator in Figure 6.13, Figure 6.14 and Figure 6.15 match very well with the calculated value.

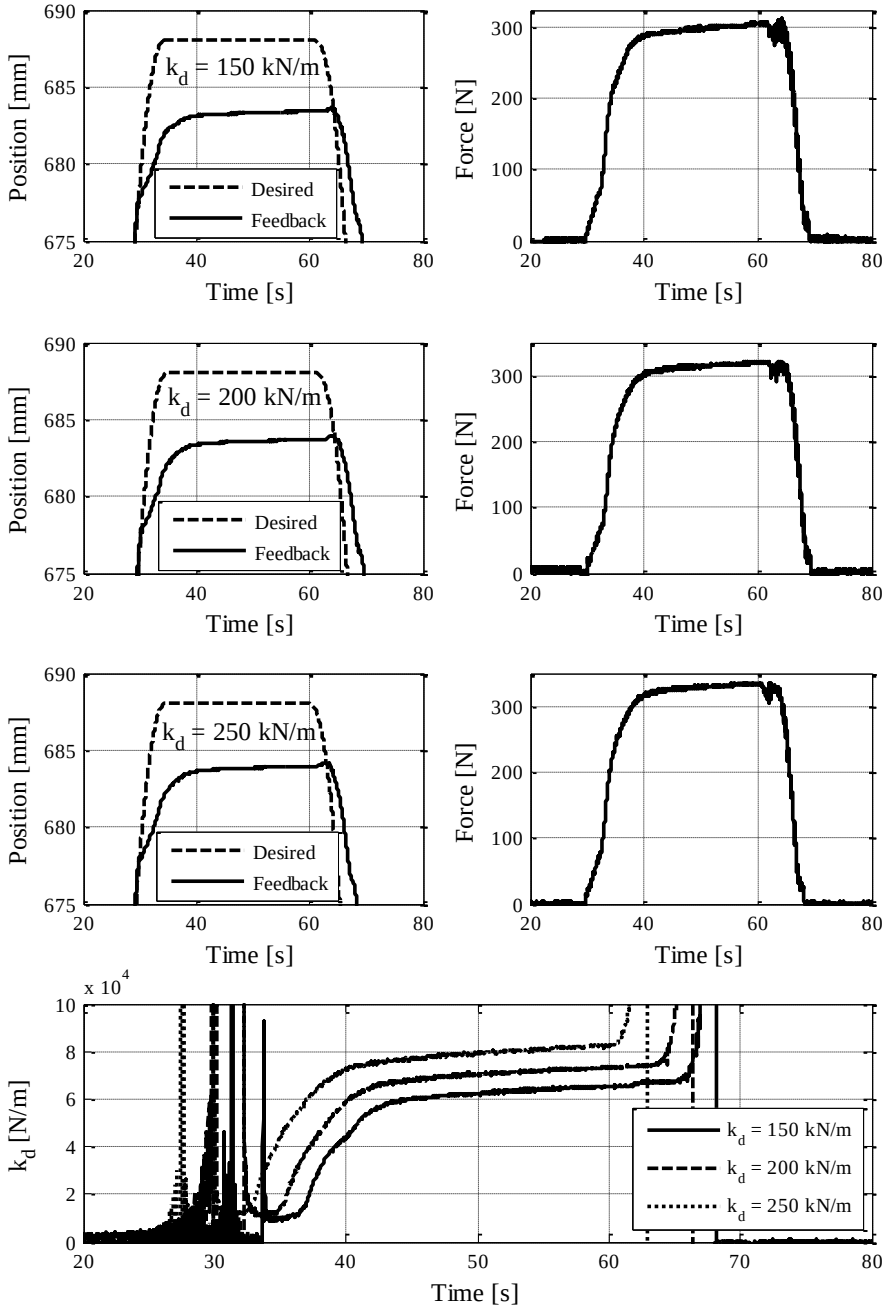

Figure 6.13: Position tracking (left), contact force (right) and impedance response (bottom) along x-axis for three different values of desired stiffness

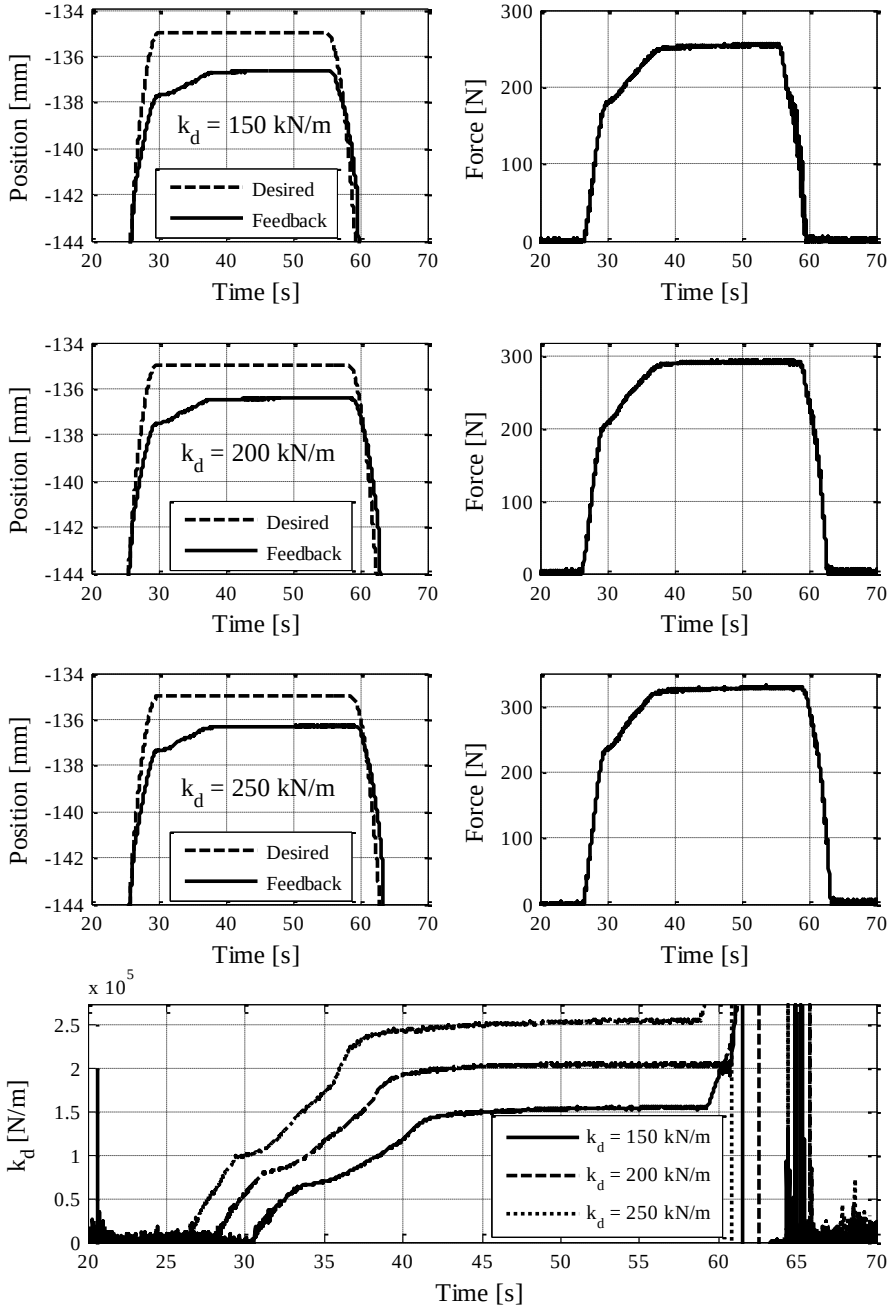

Figure 6.14: Position tracking (left), contact force (right) and impedance response (bottom) along y-axis for three different values of desired stiffness

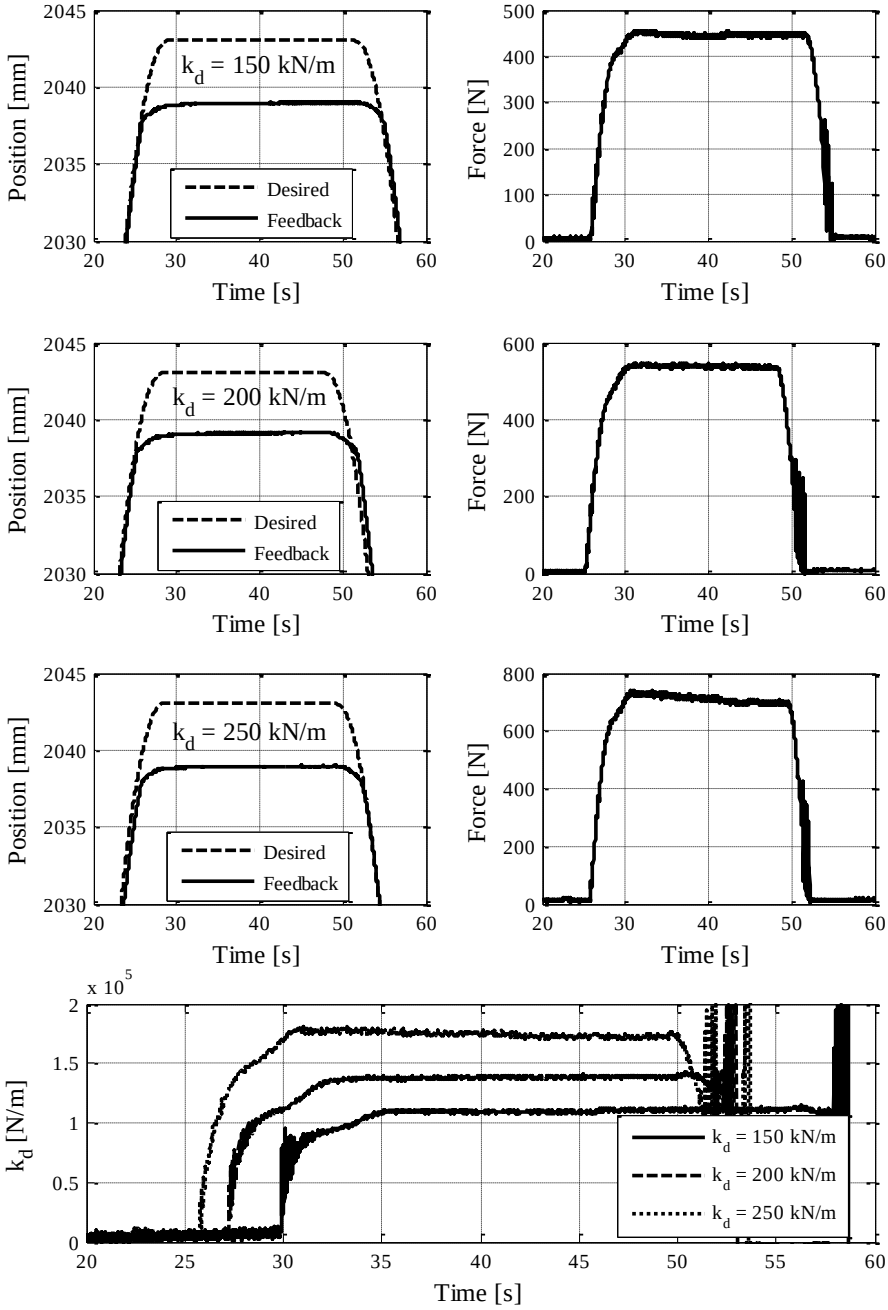

Figure 6.15: Position tracking (left), contact force (right) and impedance response (bottom) along z-axis for three different values of desired stiffness

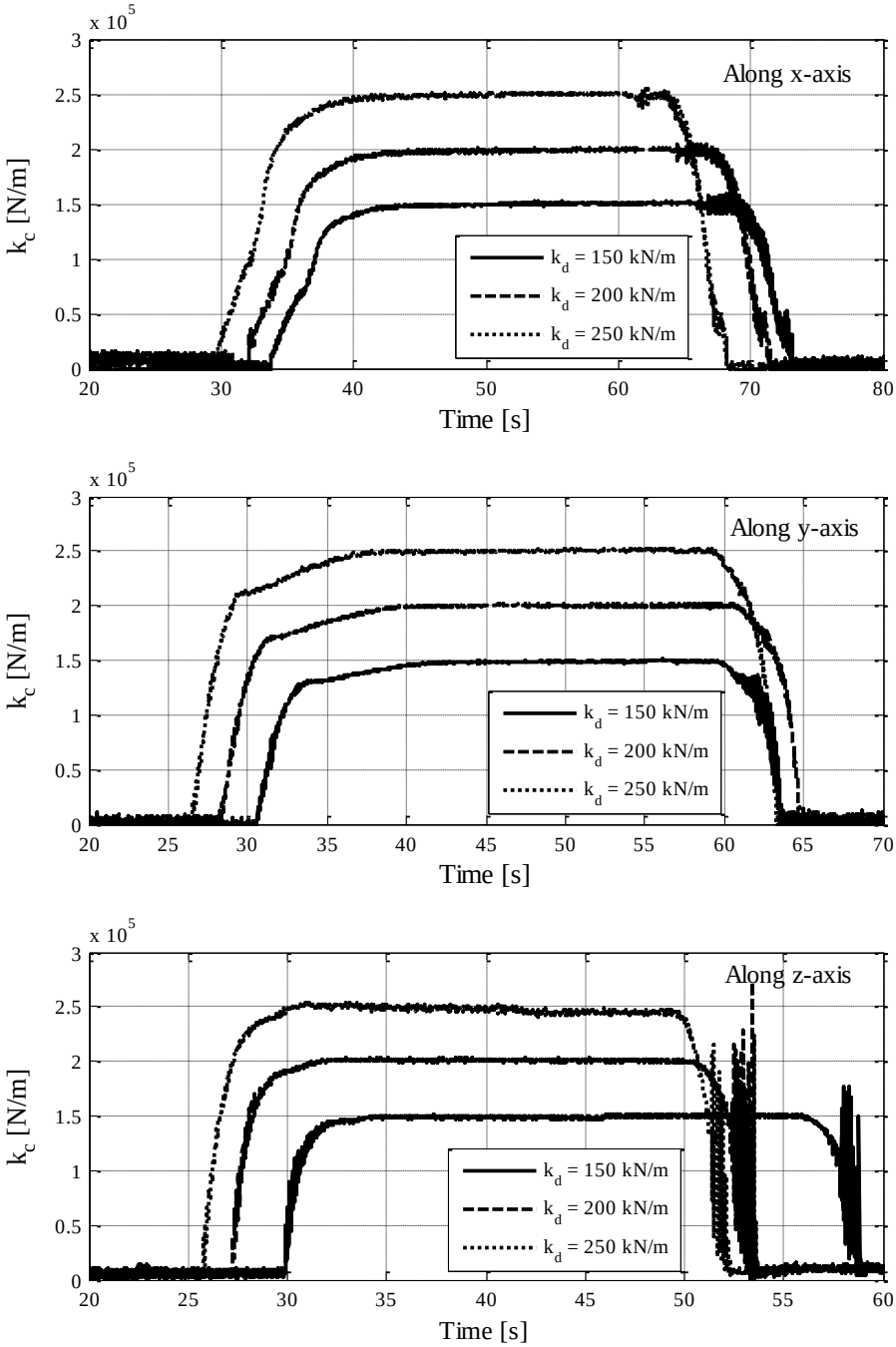

Figure 6.16: Commanded stiffness value along position axes

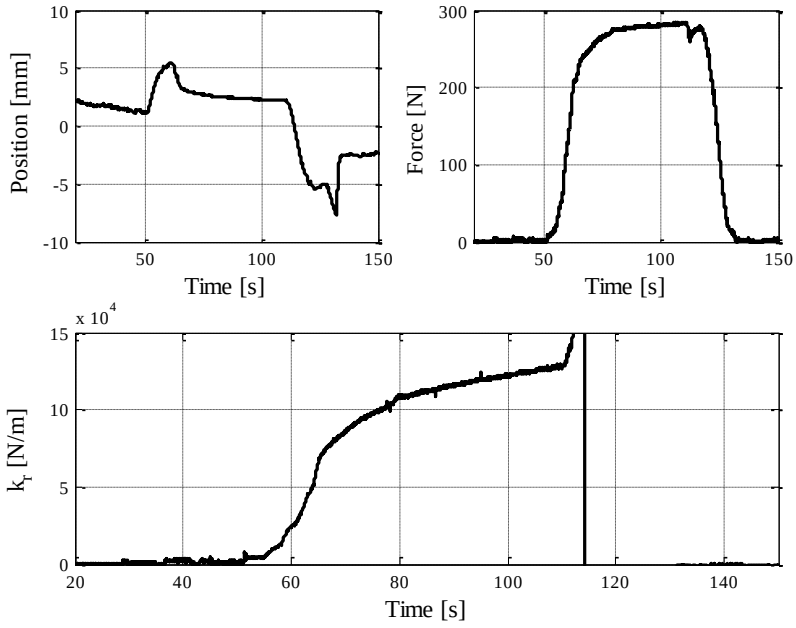

Figure 6.17: Position error (left), contact force (right) and stiffness (bottom) along x-axis

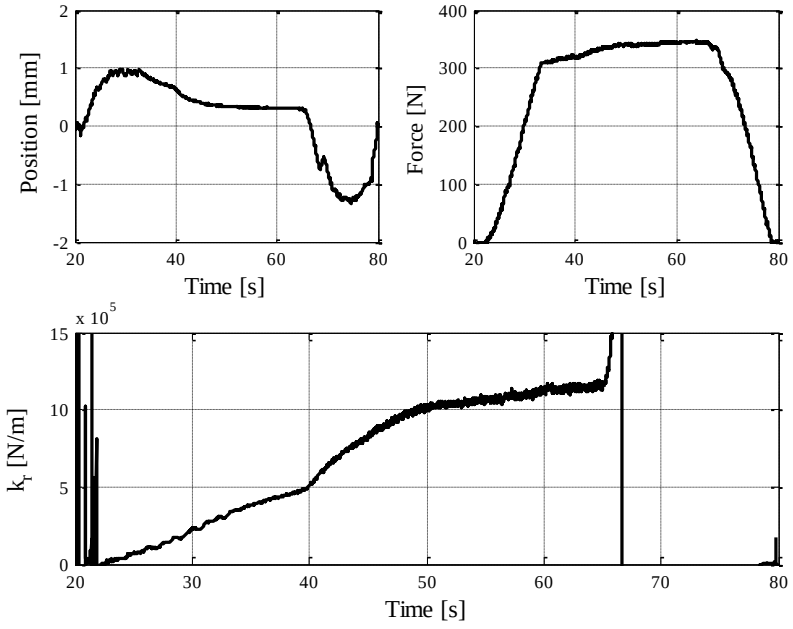

Figure 6.18: Position error (left), contact force (right) and stiffness (bottom) along y-axis

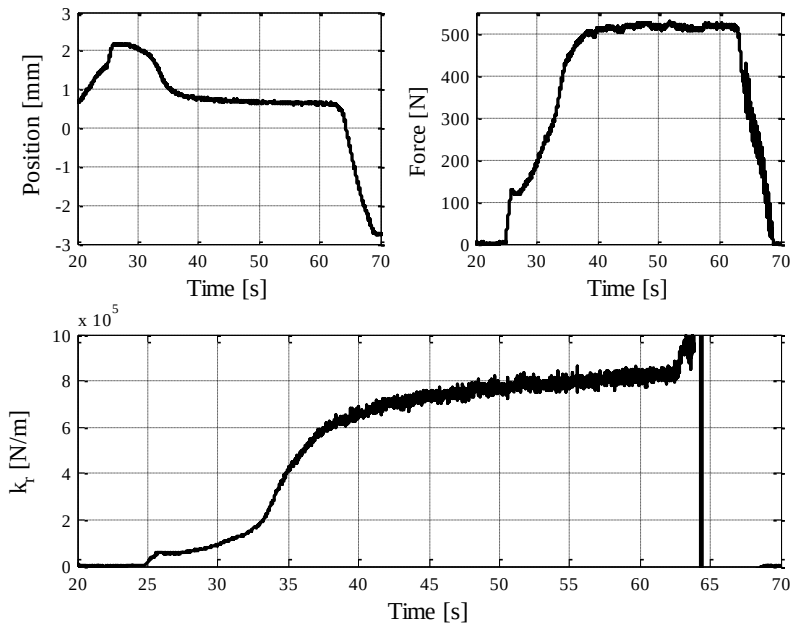

Figure 6.19: Position error (left), contact force (right) and stiffness (bottom) along z-axis

The performance of the impedance controller was also tested along the rotation axes for the desired stiffness values of 10×10^3 Nm/rad, 25×10^3 Nm/rad and 50×10^3 Nm/rad. The stiffness of the manipulator along the position axes was chosen to be 250×10^3 N/m to study the effect of rotational impedance controller. A metal pin was attached to the gripper and the manipulator was commanded to have a rotary motion for the pin to come into contact with the environment. The results are shown in Figure 6.20, Figure 6.21 and Figure 6.22. Again, the manipulator does not achieve the desired stiffness values about the y-axis, where the torque is coupled with the force along the x-axis. A slight backlash between the pin and the gripper was noticed about the z-axis, which prevented the desired stiffness to rise above a certain value, as can be seen in Figure 6.22.

The observed spikes in the stiffness plots along certain axes are due to the fact that during the initial contact, a small vibration in the manipulator position causes $x - x_e \rightarrow 0$ in Equation 6.3. Hence, it does not point to any real instability. The stable behaviour of the manipulator can be observed from position tracking and contact force plots.

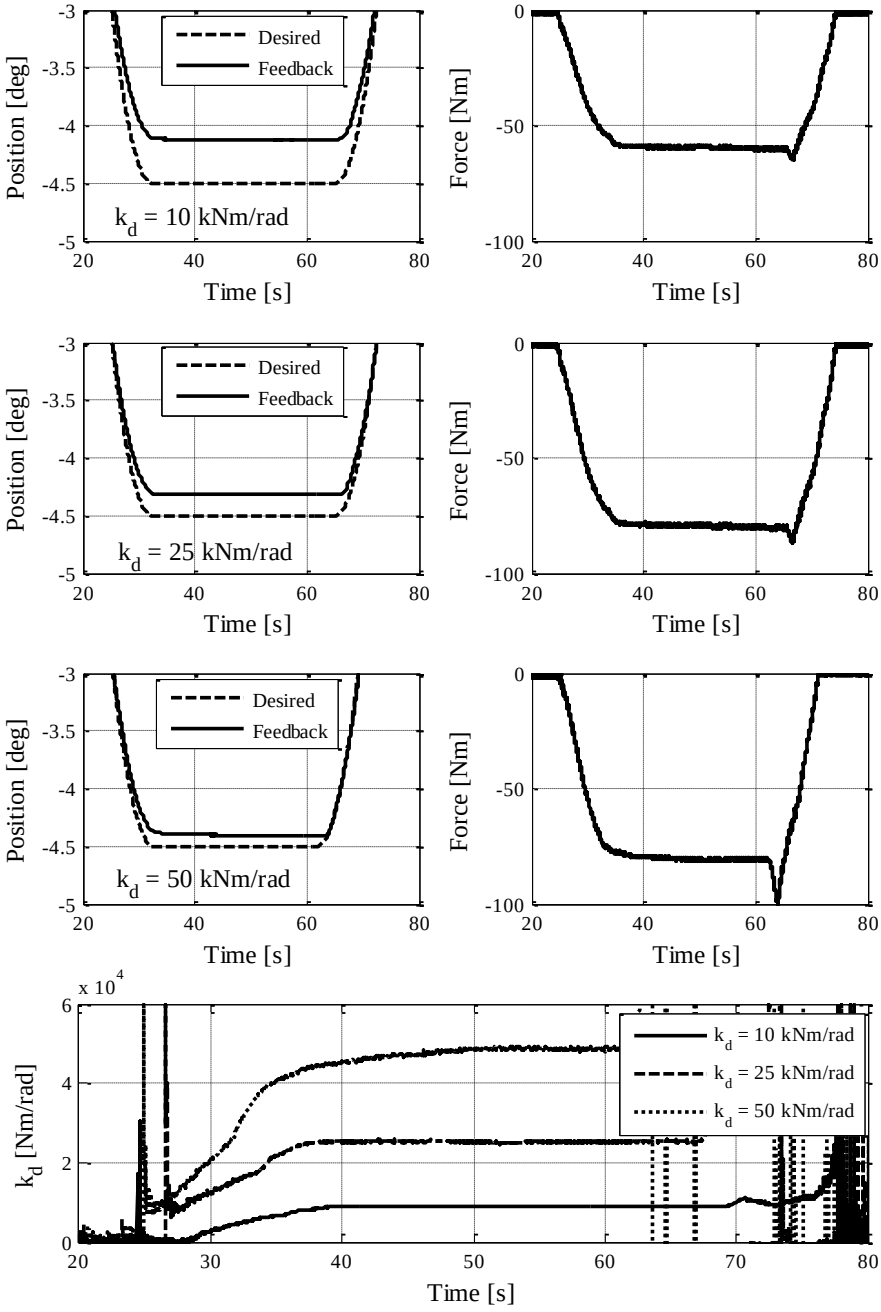

Figure 6.20: Position tracking (left), contact force (right) and impedance response (bottom) about x-axis for three different values of desired stiffness

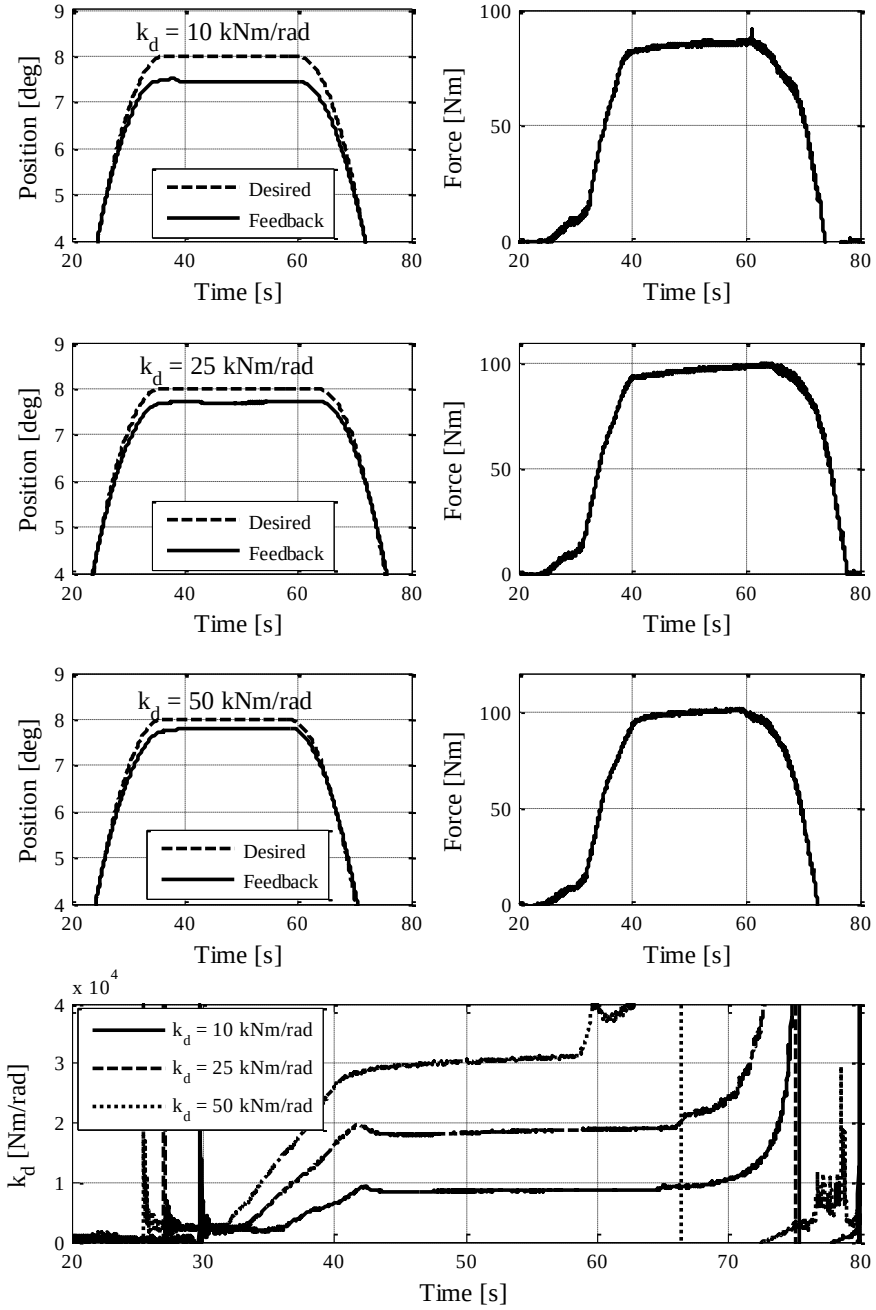

Figure 6.21: Position tracking (left), contact force (right) and impedance response (bottom) about y-axis for three different values of desired stiffness

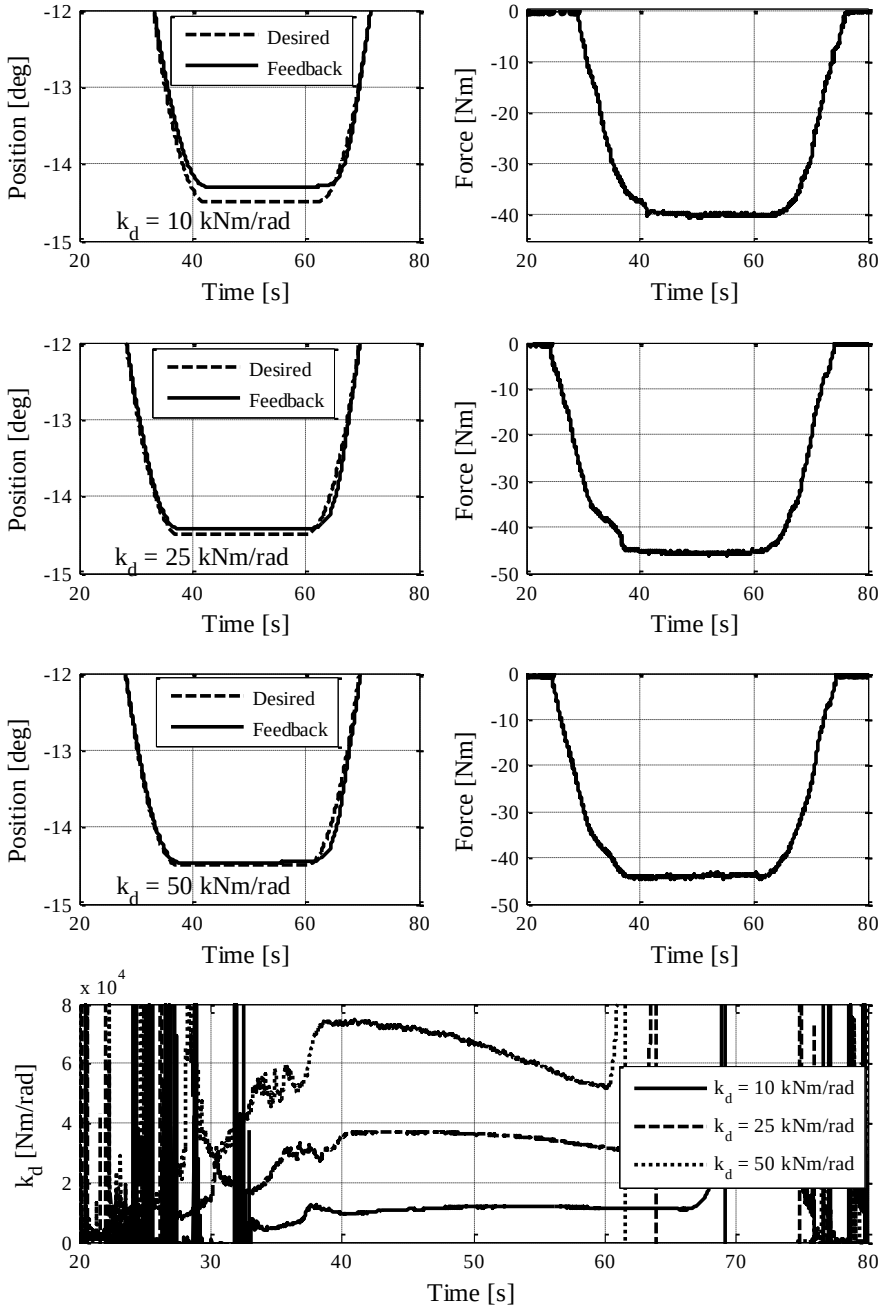

Figure 6.22: Position tracking (left), contact force (right) and impedance response (bottom) about z-axis for three different values of desired stiffness

6.3 Effect of redundancy

Here the performance of the WHMAN is analysed experimentally in non-redundant configuration using the position-based impedance controller and is compared against the performance of redundant configuration in the last section. The redundant joints d_1 and d_4 (linear slide and telescopic extension in Figure 4.1) are position controlled to fixed values. In this way these joints do not contribute to the impedance regulation and the manipulator does not lose any degrees of freedom in operational-space. The manipulator is subjected to the same position profiles for the same desired stiffness values of the last section.

The position tracking response of the manipulator on coming into contact with the environment is shown for redundant (left) and non-redundant (right) configurations next to each other along each axis in Figure 6.23, Figure 6.24 and Figure 6.25. The value of tracked stiffness along each axis is also shown at the bottom for each case.

From the comparison of plots it is clear that the impedance regulation capability of the manipulator deteriorates with the loss of redundant degrees of freedom. In fact, manipulator goes into periodic oscillation for the desired stiffness value of 150×10^3 N/m along the y-axis in non-redundant configuration (Figure 6.24). No particular difference in the response of the manipulator along the x-axis can be noted. The major difference can be observed along the directions (y-axis and z-axis) in which the motion of redundant joints contributes to the maximum motion of end-effector in the given posture.

Since the manipulator joints provide a considerable amount of passive damping the behaviour is not much highlighted in the slow motion trajectories of Figure 6.23, Figure 6.24 and Figure 6.25. The trajectories are kept slow for safety reasons.

To further elaborate the effect of redundancy the manipulator was driven with higher velocity for smaller trajectories along the z-axis to come into contact with the environment. The position and force response of the manipulator for redundant and non-redundant configurations is shown in Figure 6.26 and Figure 6.27 respectively for three selected values of stiffness.

Compared to redundant configuration, a considerable amount of vibrations can be noted when the manipulator comes into contact with the environment in non-redundant configuration. The response of the manipulator for the stiffness value of 150×10^3 N/m was, in fact, considered unacceptable for maintenance operations. Hence, the dynamic manipulability of the manipulator can be improved by the presence of redundant degrees of freedom.

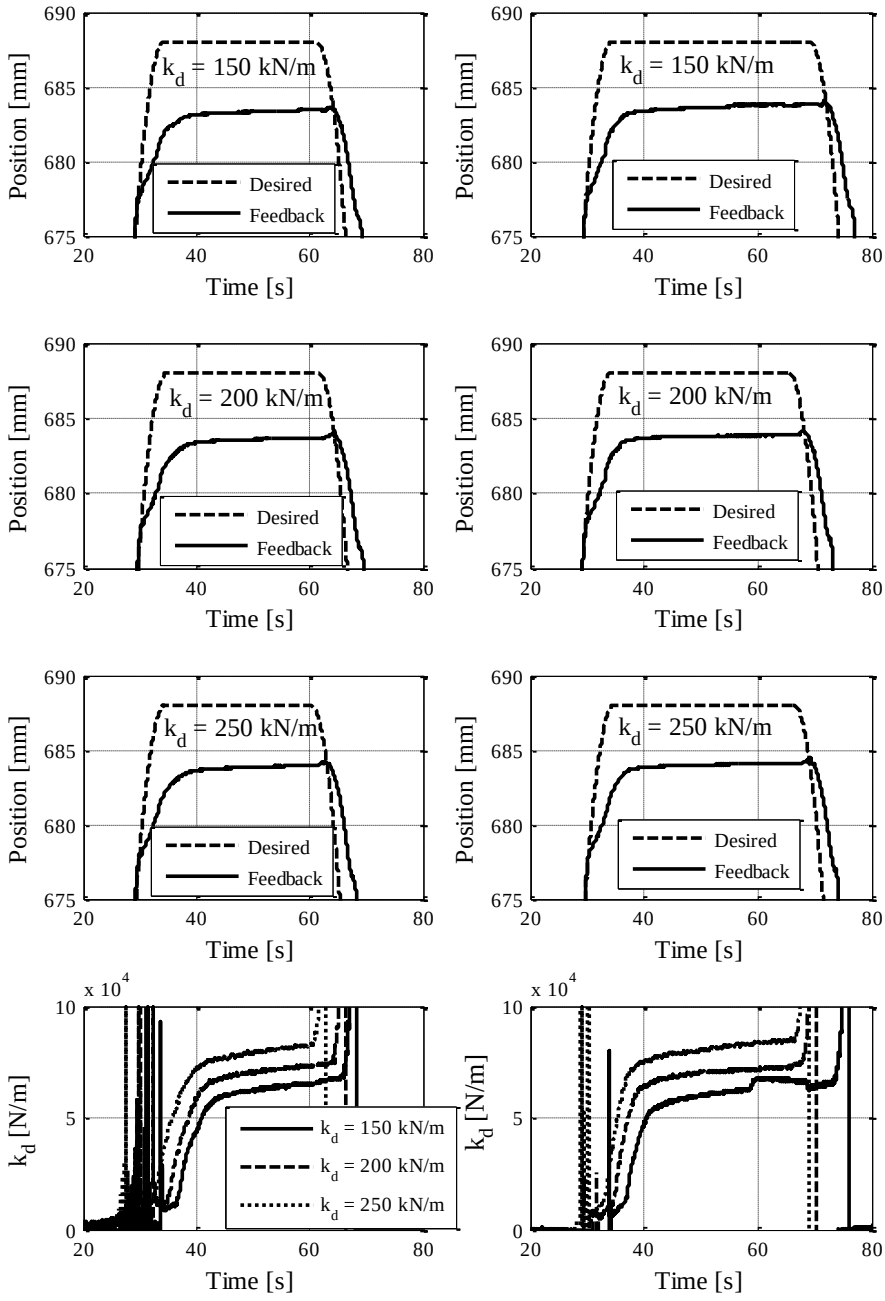

Figure 6.23: Position tracking and impedance response for redundant (left) and for non-redundant (right) configurations along x-axis for three different values of desired stiffness

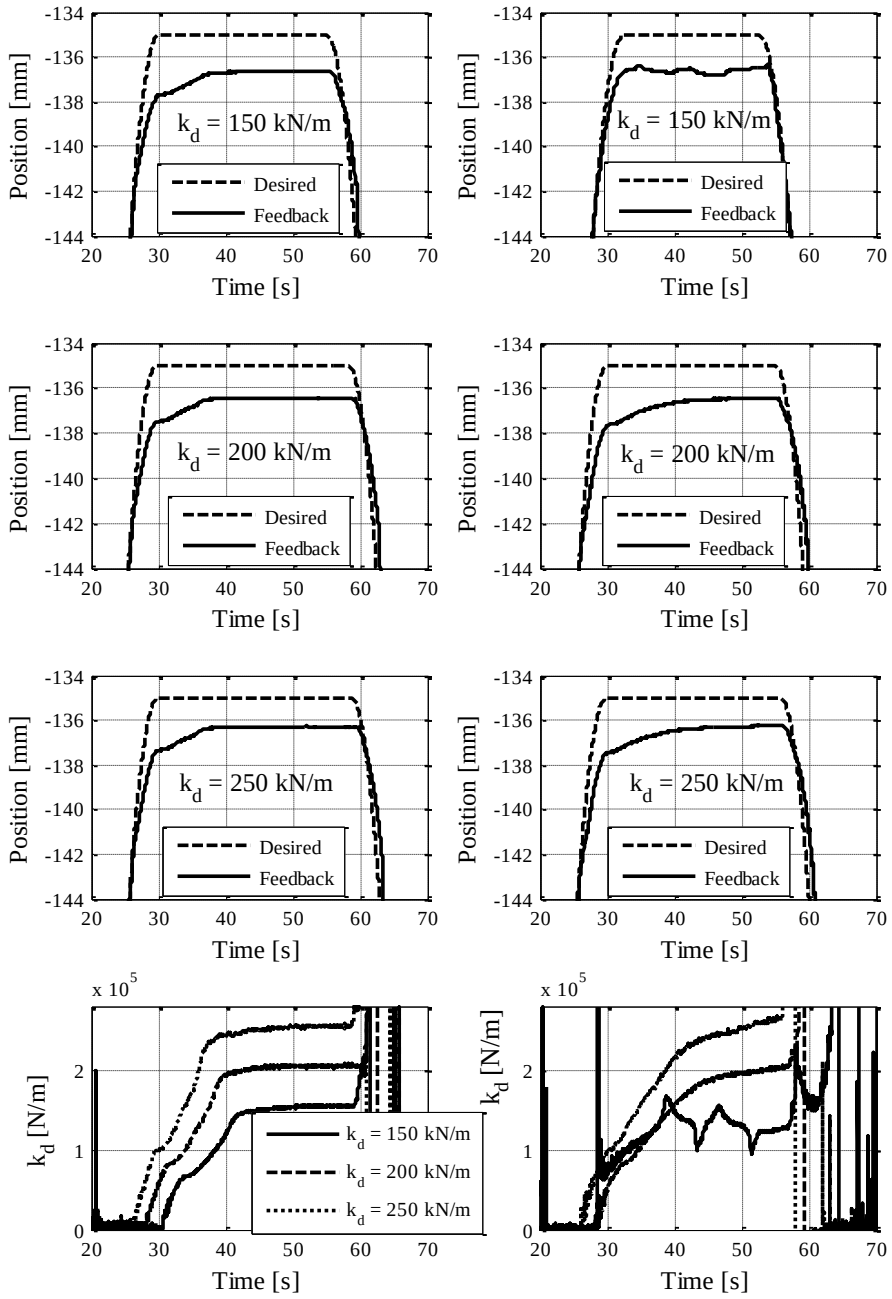

Figure 6.24: Position tracking and impedance response for redundant (left) and for non-redundant (right) configurations along y-axis for three different values of desired stiffness

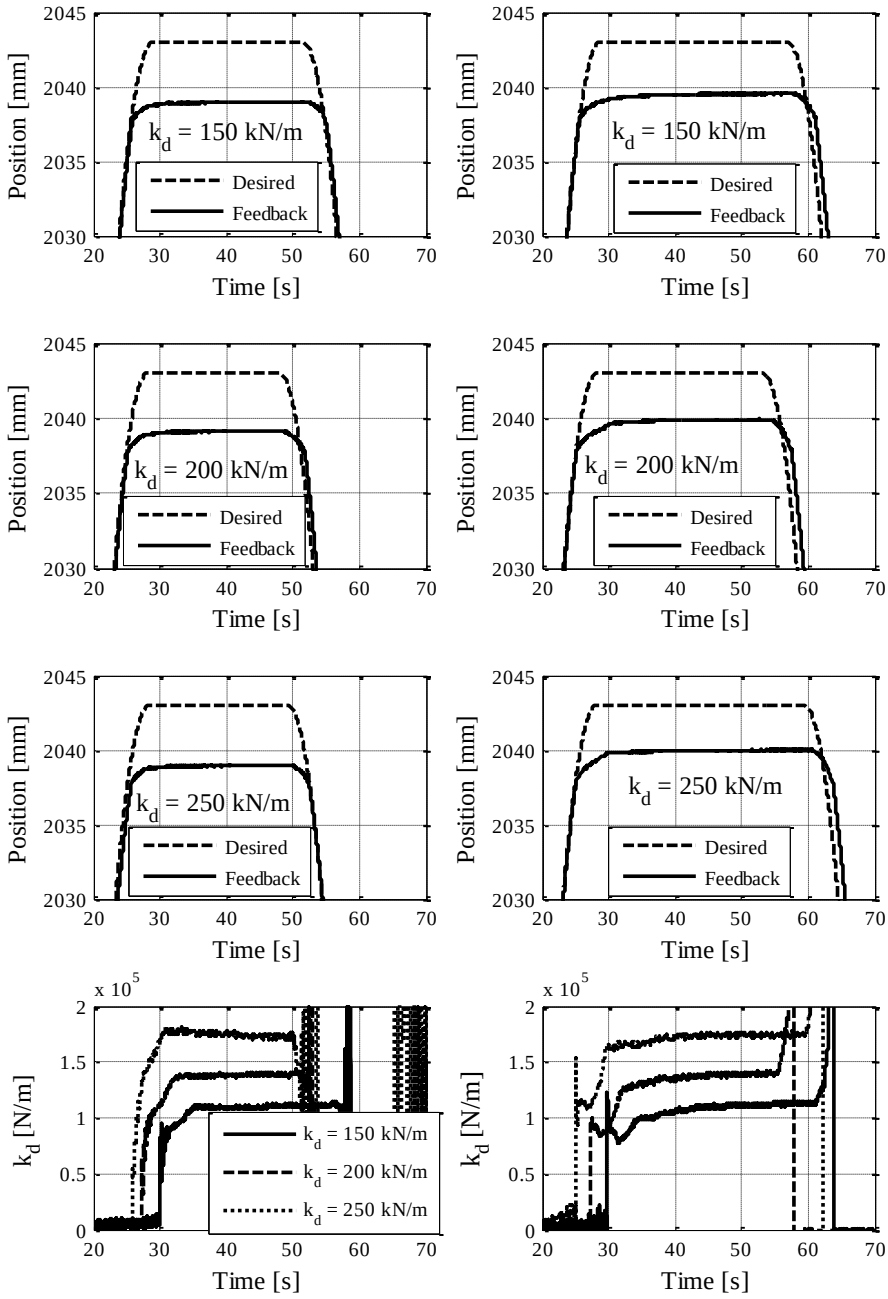

Figure 6.25: Position tracking and impedance response for redundant (left) and for non-redundant (right) configurations along z-axis for three different values of desired stiffness

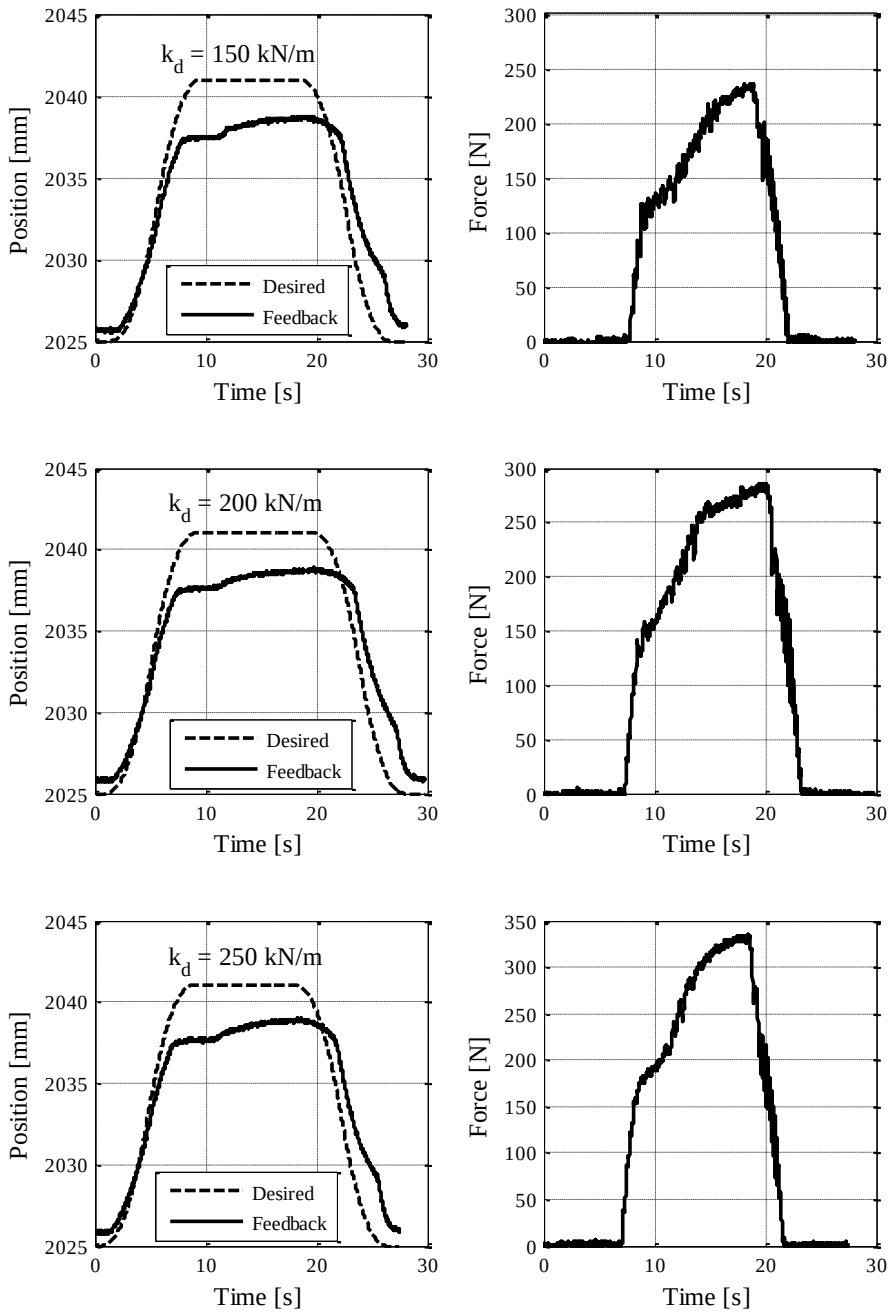

Figure 6.26: Position tracking (left) and contact force (right) in redundant configuration along z-axis

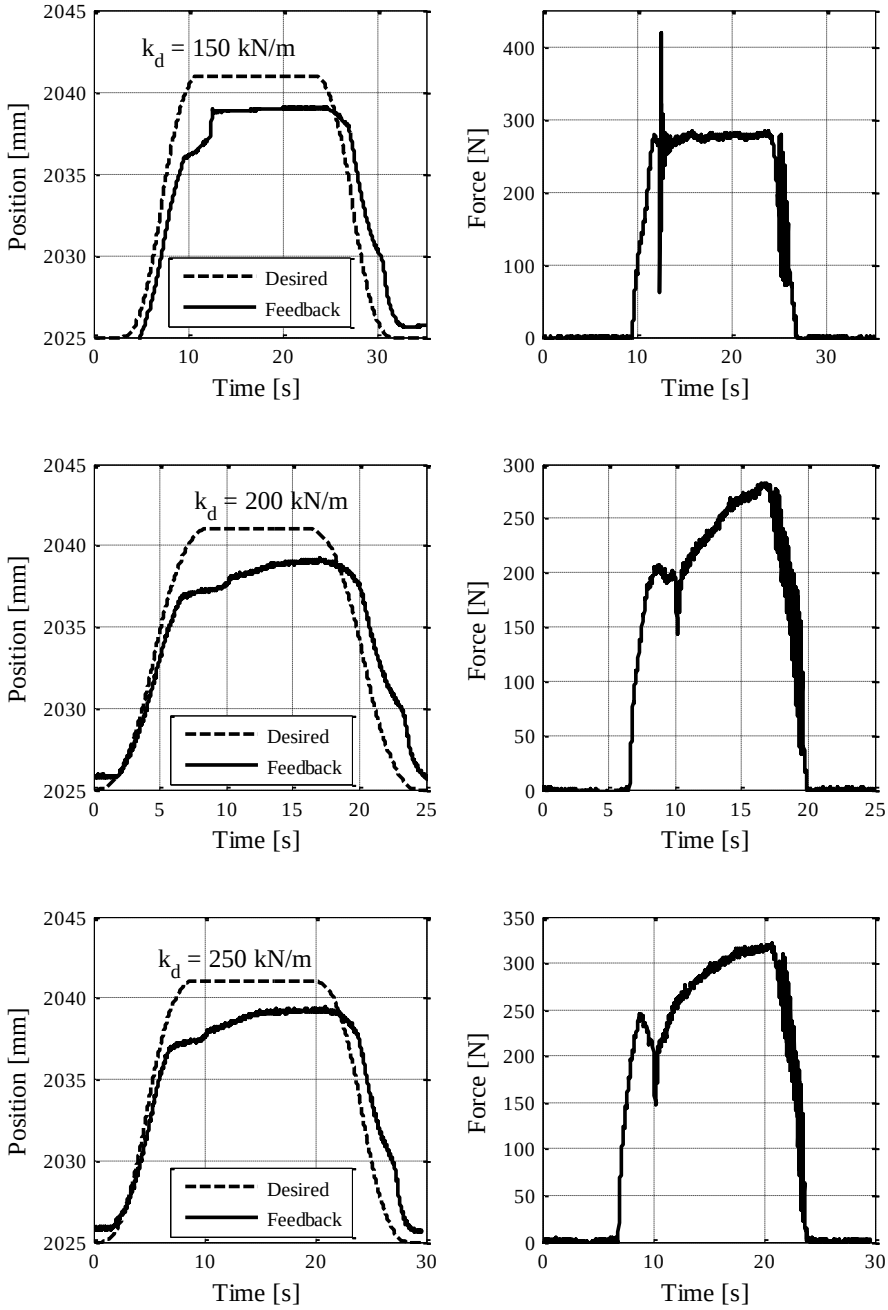

Figure 6.27: Position tracking (left) and contact force (right) in non-redundant configuration along z-axis

6.4 Summary

In this chapter the theoretical developments of Chapter 3 were studied through experiments with WHMAN. The position controller for the WHMAN designed in Section 4.4 was implemented for WHMAN, where the feedback was obtained with a state observer. Though the manipulator largely remained stable, unstable behaviour was observed in certain specific postures for certain joints. The possible cause can be the non-linearities resulting from the manufacturing tolerances and the behaviour of the seals as described in Section 4.4. To guarantee stability the joints of the manipulator are tuned with nonlinear PI controllers. The simulation results of position controller were utilized and compared against the practical measurements. The measured tracking error was found slightly higher along certain axes due to the non-modelled nonlinearities of the WHMAN. Overall, the performance of the position controller was found suitable for the implementation of impedance controller.

The design of the impedance filter was presented for the desired dynamic behaviour and stiffness value. Then the impedance control properties of the WHMAN were studied through position and force measurements on coming into contact with the environment. The results were shown as position tracking, contact force and stiffness plots. On coming into contact with the environment the manipulator remains stable. However, the achieved stiffness remained lower than the desired stiffness along several axes. The presence of passive compliance in the manipulator's joints is a major cause of this behaviour.

The effect of redundancy on dynamic manipulability of manipulators was further studied with the impedance control response of the WHMAN. The position tracking and impedance regulation performance of the manipulator in redundant configuration were compared against the non-redundant configuration. The results show that the impedance regulation capability of the manipulator can be improved with the presence of redundant degrees of freedom.

7 SYNOPSIS

The effect of redundancy on dynamic manipulability and impedance control of a manipulator have been studied. The dynamic manipulability of the manipulator is discussed in the context of DME (Dynamic Manipulability Ellipsoid). As one of the contributions of this thesis, the DME formulation has been used to show that the presence of redundant degrees of mobility can result in improved dynamic performance of the manipulator. A cost function has been devised to exploit the redundant degrees of freedom for improved dynamic performance and thus improved impedance control of the manipulator. The effect of the manipulator's posture on the Dynamic Manipulability Index is determined. Using the redundant degrees of freedom the manipulator's joints are kept in range such that the index is maximized. This scheme results in a computationally simple and efficient algorithm.

Both analytical and simulation models of WHMAN are presented. For the analytical model the geometrical and inertial parameters obtained from the CAD model of the manipulator have been utilized. Modelling of a single actuator of WHMAN has been used as the starting point for the development of a simulation model for the entire WHMAN. Both linear and nonlinear models of the actuator are presented. These developments are then carried on for the development of the simulation model of WHMAN. For the simulation model the majority of the modelling parameters are obtained from the components' datasheets and a few are obtained experimentally. The results show that a reasonably accurate model useful for this study can be obtained for the WHMAN.

The effect of redundant degrees of freedom on the manipulator is studied using the numerical model of WHMAN. The ellipsoids of the dynamic manipulability (DME) of the manipulator are plotted using the numerical model of WHMAN for both redundant and non-redundant configurations. The ellipsoids showed that redundant degrees of freedom of WHMAN do result in higher dynamic manipulability.

The position controller for the WHMAN is designed using the verified simulation model. The manipulator dynamics are decoupled using gravity compensation and the position controller is designed in a decentralized fashion, such that the controller for each joint takes into consideration only the dynamics of respective joint. The linearized dynamic model of each joint is obtained using the simulation model of the manipulator. The controller has been tuned using velocity and acceleration feedback as the states. The position tracking performance of the manipulator has been further improved by using the velocity feed-forward signal. The choice of

this control strategy was made because of its simplicity and the performance of the position controller was found satisfactory.

The model of the manipulator and its interaction with the environment has been presented. This model is then used for the development of impedance controller. Both operational-space and joint-space presentations of position-based and force-based implementations of impedance controller are discussed. The design of the impedance filter is presented for the desired dynamic behaviour.

Then the impedance control properties of the WHMAN are studied using the position controlled simulation model and the designed impedance filter for position-based implementation. The response of the manipulator is studied for several values of desired stiffness. The results are shown as position tracking, contact force and stiffness plots. On coming into contact with the environment the manipulator remains stable and behaves according to the defined desired impedance.

The equivalent force-based implementation of impedance controller is studied, whereby the force controller for the inner loop is designed using the position controller and desired impedance. As expected, the manipulator became unstable, losing the position and force tracking and therefore the desired dynamic behaviour.

The effect of redundancy on the dynamic manipulability of manipulators is further studied with the impedance control response of the manipulators using the simulation of model WHMAN and experimentally with an actual manipulator. The position tracking and the impedance regulation performance of the manipulator in redundant configuration are compared against the non-redundant configuration. The results show that impedance regulation capability of the manipulator can be improved with the presence of redundant degrees of freedom.

In the end theoretical developments are studied through experiments with WHMAN. The state-feedback controller tested the WHMAN with a simulation model. The manipulator largely remained stable; however, it became unstable in certain specific postures for certain joints. This behaviour can be caused by the non-linearities resulting from manufacturing tolerances and the nonlinear behaviour of the seals. To guarantee stability the joints of the manipulator are tuned with nonlinear PI controllers. Overall, the performance of the position controller was found suitable for the implementation of impedance controller.

The impedance filter is designed for the desired dynamic behaviour and stiffness values. The impedance control properties of the WHMAN are studied through position and force measurements. On coming into contact with the environment the manipulator remains stable.

However, the achieved stiffness remained lower than the desired stiffness along several axes. The presence of passive compliance in the manipulator's joints is a major cause of this behaviour.

The effect of redundancy on the dynamic manipulability of manipulators is further studied with the impedance control response of the WHMAN. The position tracking and the impedance regulation performance of the manipulator in redundant configuration are compared against non-redundant configuration. The results show that the impedance regulation capability of the manipulator can be improved with the presence of redundant degrees of freedom.

7.1 Conclusions

The theoretical discussions and results in the thesis regarding impedance control and the effects of redundancy on the dynamic performance of a manipulator have been kept general without references to any particular manipulator and are equally applicable for the manipulator driven by hydraulic, pneumatic or electrical actuators. The purpose is to keep the findings useful for other developments and continue the research and discussion process on a wider scale. However, due to the availability of WHMAN, which is a redundant manipulator driven by water hydraulic actuators, it has been used for the numerical analysis, simulations and experimental verification of the theoretical results in the later part of the thesis.

It has been shown that the presence of redundant degrees of mobility in a manipulator can result in improved dynamic performance. It was found that the dynamic manipulability of the manipulator can be improved if redundant degrees of freedom can be added without significantly altering its inertia matrix. This fact is significant in the case of hydraulic manipulators where actuators deliver a high force to size ratio.

The equivalence between the position-based and force-based implementations of impedance controller is discussed for a general case of multiple degrees of freedom. It was shown that equivalent implementation can be obtained in cases where a linear relationship exists between the joint-space and operational-space variables. From the implementation point of view, though equivalent performance can be obtained from either implementation of impedance control, in general it will require the separate tuning of internal position and force controllers.

The Water Hydraulic MANipulator (WHMAN) was used for the simulations and the experiments in this study. The impedance controller was designed and tested for several values

of stiffness. Though the manipulator response remained quite stable, the desired stiffness was not achieved along several of the motion axes. The presence of passive compliance in the manipulator's joints is a major cause of this behaviour.

The performance of the impedance controller was tested both in redundant and non-redundant configurations of WHMAN. The position and force measurements showed that the response of the impedance controller degraded in non-redundant configuration. On the basis of the presented theory, numerical analysis, simulations and experiments it can be concluded that redundant degrees of freedom can improve the dynamic manipulability of a manipulator.

7.2 Future research

The proportional-integral position controller designed for WHMAN provides satisfactory tracking and steady state performance; however, the dynamic behaviour of the manipulator may require further improvement. The dynamic performance of the manipulator can further be improved by utilizing a state-feedback controller. The dynamics of the manipulator can further be linearized by utilizing techniques such as computed torque control. This will require further modelling effort and adding further details into the model of the manipulator.

The purpose of the WHMAN is to provide assistance during remote maintenance operations of the ITER divertor. Since the tasks required to be carried out with the manipulator cannot be completely defined, it should be possible to teleoperate the manipulator in master-slave fashion with force-feedback to the operator. The impedance controller for the WHMAN has been implemented during this study, and the impedance of the manipulator can be transferred to the master arm to reflect the contact forces. Several factors may require investigation during the implementation of the master-slave scheme for WHMAN, such as position and force scaling factors and the slow dynamics of WHMAN.

During this study, it was observed that manufacturing tolerances and the flexible nature of the hydraulic vane actuators contribute significantly to the nonlinear behaviour of the manipulator. The compensation of these nonlinearities is not straightforward. Further study may be required to reduce the manufacturing tolerance of water hydraulic vane actuators and to find a better sealing solution to provide low and predictable values of friction and leakage.

REFERENCES

Aikenhead, Bruce A., Daniell, Robert G. and Davis, Frederick M. 1983. Canadarm and the space shuttle. *Journal of Vacuum Science & Technology A: Vacuum, Surfaces, and Films.* 1983, Vol. 1, 2, pp. 126-132.

ALSTOM. 1999. TITAN 3 : Remote manipulator system. s.l. : ALSTOM Automation Schilling Robotics, 1999.

An, C. H., Atkeson, C. G. and Hollerbach, J. M. 2003. *Model-based Control of a Robot Manipulator.* New Edition Edition. s.l. : MIT Press, 2003.

Andersen, T. O., et al. 2005. Comparison of linear controllers for a hydraulic servo system. [book auth.] Japan Fluid Power System Society. [ed.] T. Tsukiji. *Proceedings of the 6th JFPS International Symposium on Fluid Power by Japanese Fluid.* Tsukuba : Sangyo Kikaku Co. Ltd., 2005, pp. 449-454.

—. 2005a. Feedback linearisation applied on a hydraulic servo system. [book auth.] Japan Fluid Power System Society. [ed.] T. Tsukiji. *Proceedings of the 6th JFPS International Symposium on Fluid Power by Japanese Fluid.* Tsukuba : Sangyo Kikaku Co. Ltd., 2005a, pp. 167-172.

Anderson, R. J. and Spong, M. W. 1988. Hybrid impedance control of robotic manipulators. *IEEE Journal of Rbotics and Automation.* 1988, Vol. 4, 5, pp. 549-556.

Angeles, J., Ranjbaran, F. and Patel, R. V. 1992. On the design of the kinematic structure of seven-axes redundant manipulators for maximum conditioning. *Proceedings of IEEE International Conference on Robotics and Automation.* 1992, Vol. 1, pp. 494-499.

Armada, M., et al. 2000. From remotely controlled manipulators to tele-operation of advanced climbing and walking robots. [ed.] Tyler Schilling. *Telerobotic Applications.* s.l. : Professional Engineering Publishing Limited, 2000, pp. 131-146.

Aydin, Y. and Kucuk, S. 2006. Quaternion based inverse kinematics for industrial robot manipulators with Euler wrist. *Proceedings of the IEEE International Conference onMechatronics.* 2006, pp. 581-586.

Bayo, E. 1988. Computed torque for the position control of open-chain flexible robots. *Proceedings of IEEE International Conference on Robotics and Automation.* 1988, Vol. 1, pp. 316-321.

Bilodeau, G. and Papadopoulos, E. 1998. A model-based impedance control scheme for high-performance hydraulic joints. *Proceedings of the International Conference on Intelligent Robots and Systems.* Victoria : s.n., 1998.

Bonchis, A., Corke, P. I. and Rye, D. C. 2002. Experimental evaluation of position control methods for hydraulic systems. *IEEE Transactions on Control Systems Technology.* 2002, Vol. 10, 6, pp. 876-882 .

Bowling, A. and Khatib, O. 1998. The motion isotropy hypersurface: a characterization of acceleration capability. *Proceedings of the IEEE/RSJ International Conference on Intelligent Robots and Systems.* 1998, Vol. 2, pp. 965-971.

Brooks, T. L. and Ince, I. 1992. Operator vision aids for telerobotic assembly and servicing in space. *Proceedings of IEEE International Conference on Robotics and Automation.* 1992, Vol. 1, pp. 886-891.

Bruni, F., et al. 1996. Experiments of impedance control on an industrial robot manipulator with joint friction. *Proceedings of the IEEE International Conference on Control Applications.* 1996, pp. 205-210.

Burgess, T., et al. 1998. Remote maintenance of in-vessel components for ITER. *Fusion Engineering and Design.* s.l. : Elsevier, 1998, Vol. 42, 1-4, pp. 455-461.

Canudas-de-Wit, C., et al. 1995. A new model for the control of systems with friction. *IEEE Transactions on Automatic Control.* 1995, Vol. 40, 3, pp. 419-425.

Carignan, C. R. and Akin, D. L. 1997. Achieving impedance objectives in robot teleoperation. *Proceedings of IEEE International Conference on Robotics and Automation.* 1997, Vol. 4, pp. 3487-3492.

Chiacchio, P. and Concilio, M. 1998. The Dynamic Manipulability Ellipsoid for Redundant Manipulators. *Proceedings of the IEEE International Conference on Robotics and Automation.* 1998, Vol. 1, pp. 95-100.

Chiacchio, P., et al. 1991. Reformulation of dynamic manipulability ellipsoid for robotic manipulators. *Proceedings of IEEE International Conference on Robotics and Automation.* 1991, Vol. 3, pp. 2192-2197.

Chiaverini, S. and Sciavicco, L. 1993. The parallel approach to force/position control of robotic manipulators. *IEEE Transactions on Robotics and Automation.* 1993, Vol. 9, 4, pp. 361-373.

Colbaugh, R., Seraji, H. and Glass, K. 1991. Direct adaptive impedance control of manipulators. *Proceedings of the 30th IEEE Conference on Decision and Control.* 1991, Vol. 3, pp. 2410-2415.

Conrad, Finn and Adelstorp, A. 1997. Pure water hydraulic systems and applications. [ed.] C. R. Burrows and K. A. Edge. *Fluid Power Series.* s.l. : RSP, Research Studies Press LTD, John Wiley & Sons, 1997, Vol. 9, 12.

Conrad, Finn. 1997. Hydraulic Systems with Tap Water versus Bio-oils. *Procedings of Fluid Power Theme Days in IHA - Water hydraulics.* Tampere : Tampere University of Technology, 1997.

—. 2005. Trends in design of water hydraulics - Motion control and open-ended solutions. *Proceedings of the sixth JFPS International Symposium on Fluid Power.* Tsukuba : s.n., 2005.

Craig, John J. 2004. *Introduction to Robotics: Mechanics and Control.* 3rd Edition. s.l. : Prentice Hall, 2004.

Cybernetix. 2001. Maestro : Advanced hydraulic telemanipulator. s.l. : Cybernetix Group, 2001.

De Schutter, J., et al. 1998. Force control: A bird's eye view. *Control Problems in Robotics and Automation: Future Directions.* San Diego : Springer Berlin / Heidelberg, 1998, Vol. 230, pp. 1-17.

Dubus, G., et al. 2008. Making hydraulic manipulators cleaner and safer: From oil to demineralized water hydraulics. *IEEE/RSJ International Conference on Intelligent Robots and Systems.* 2008, pp. 430-437.

EADS Astrium. 2008. *Cassette Multifunctional Mover Manipulator ArM : CMM MAM.* European Aeronautic Defence and Space Company. 2008. Performance and Design Requirements Document.

Eickelpasch, N., Steiner, H. and Priesmeyer, U. 1996. Remote techniques for the underwater dismantling of reator internals at the nuclear power plant Gunderemmingen unit A. [ed.] British Nuclear Energy Society. *Proceedings of International Conference on Remote Techniques for Hazardous Environments.* London : s.n., 1996.

Encyclopædia Britannica. 2009. Ctesibius Of Alexandria. *Encyclopædia Britannica Online.* [Online] 28 June 2009. http://www.britannica.com/EBchecked/topic/145475/Ctesibius-of-Alexandria.

—. 2009a. Robot. *Encyclopædia Britannica Online.* [Online] 23 June 2009a. http://www.britannica.com/EBchecked/topic/505818/robot.

Eppinger, S. D. and Seering, W. P. 1992. Three dynamic problems in robot force control. *IEEE Transactions on Robotics and Automation.* 1992, Vol. 8, 6, pp. 751-758.

European Space Agency. 2006. ERA: European Robotic Arm Factsheet. *European Space Agnecy.* [Online] 31 March 2006. [Cited: 23 June 2009.] http://www.esa.int/esaHS/ESAQEI0VMOC_iss_0.html.

Featherstone, R. 1983. Position and velocity transformations between robot end-effector coordinates and joint angles. *International Journal of Robotics Research.* s.l. : SAGE Publications, 1983, Vol. 2, 2, pp. 35-45.

Ferretti, G., et al. 2000. Impedance control for industrial robots. *Proceedings of IEEE International Conference on Robotics and Automation.* 2000, Vol. 4, pp. 4027 - 4032.

Field, G. and Stepanenko, Y. 1993. Model reference impedance control of robotic manipulators. *IEEE Pacific Rim Conference on Communications, Computers and Signal Processing.* 1993, Vol. 2, pp. 614-617.

Franklin, Gene F., Powell, David J. and Workman, Michael L. 1997. *Digital Control of Dynamic Systems.* 3rd Edition. s.l. : Prentice Hall, 1997.

Fu, K. S., Gonzalez, R. C. and Lee, C. S. G. 1987. *Robotics: Control, Sensing, Vision, and Intelligence.* 1st Edition. s.l. : Mcgraw-Hill Book Company, 1987.

Gibson, James J. 1986. *The ecological approach to visual perception.* Illustrated Edition. s.l. : Lawrence Elrbaum Associates, 1986.

Goertz, R. C. and Bevilacqua, F. 1952. A force-reflecting positional servomechanism. *Nucleonics.* 1952, Vol. 10, 11, pp. 43-45.

Goertz, R. C. and Thompson, R. C. 1954. Electrically controlled manipulator. *Nucleonics.* 1954, Vol. 12, 11, pp. 46-47.

Goertz, R. C. 1952a. Fundamentals of general-purpose remote manipulators. *Nucleonics.* 1952a, Vol. 10, 11, pp. 36-42.

—. 1954a. Mechanical master-slave manipulator. *Nucleonics.* 1954a, Vol. 12, 11, pp. 45-46.

Goldenberg, A. A. 1988. Implementation of force and impedance control in robot manipulators. *Proceedings of IEEE International Conference on Robotics and Automation.* 1988, Vol. 3, pp. 1626-1632.

Gourdeau, R., Blouin, S. and Hurteau, R. 1999. Computed torque control of robots without joint velocity measurements. *IEEE Canadian Conference on Electrical and Computer Engineering.* 1999, Vol. 3, pp. 1413-1418.

Graettinger, T. J. and Krogh, B. H. 1988. The acceleration radius: a global performance measure for robotic manipulators. *IEEE Journal of Robotics and Automation.* 1988, Vol. 4, 1, pp. 60-69.

Gravez, Philippe, et al. 2003. Model-based remote handling with the MAESTRO hydraulic manipulator. *Fusion Engineering and Design.* s.l. : Elsevier, 2003, Vol. 69, 1-4, pp. 147-152.

Gupta, K. C. and Roth, B. 1982. Design considerations for manipulator workspace. *Transactions of ASME Journal of Mechanical Design.* New York : ASME, 1982, Vol. 104, 4, pp. 704-711.

Ha, Q. P., et al. 2000. Impedance control of a hydraulically actuated robotic excavator. *Automation in Construction.* s.l. : Elsevier Science B.V., 2000, Vol. 9, 5-6, pp. 421-435.

Harada, T., et al. 1992. Robust Implementations Of Impedance Control Using Impedance Error Feedback. *Proceedings of the lEEE/RSJ International Conference on Intelligent Robots and Systems.* 1992, Vol. 3, pp. 1998-2004.

Heinrichs, B. and Sepehri, N. 1999. A limitation of position-based impedance control in static force regulation: theory and experiments. *Proceedings of IEEE International Conference on Robotics and Automation.* 1999, Vol. 3, pp. 2165-2170.

—. 1999. Relationship of position-based impdeance control to explicit force control: theory and experiments. *Proceedings of the American Control Conference.* San Diego : s.n., 1999, pp. 2072-2076.

Heinrichs, B., Sepehri, N. and Thornton-Trump, A.B. 1997. Position-based impedance control of an industrial hydraulic manipulator. *IEEE Control Systems Magazine.* 1997, Vol. 17, 1, pp. 46-52.

Heintze, J. and van der Weiden, J. J. 1995. Inner-loop design and analysis for hydraulic actuators, with an application to impedance control. *Control Engineering Practice.* s.l. : Elsevier Science Ltd., 1995, Vol. 3, 9, pp. 1323-1330.

Henriksson, D., Johansson, R. and Robertsson, A. 2001. Observer-based impedance control in robotics. *Proceedings of 5th IFAC Symposium on Nonlinear Control Systems.* St. Petersburg : s.n., 2001, pp. 360-365.

Hirakawa, A. R. and Kawamura, A. 1997. Trajectory planning of redundant manipulators for minimum energy consumption without matrix inversion. *Proceedings of the IEEE International Conference on Robotics and Automation.* 1997, Vol. 3, pp. 2415-2420.

Hogan, N. 1985. Impedance control: An approach to mainpulation: Parts I, II and III. *Journal of Dynamic Systems, Measurement and Control.* s.l. : ASME, 1985, Vol. 107, pp. 1-24.

—. 1987. Stable execution of contact tasks using impedance control. *Proceedings of IEEE International Conference on Robotics and Automation.* 1987, Vol. 4, pp. 1047-1054.

Hollerbach, J. and Suh, K. 1987. Redundancy resolution of manipulators through torque optimization. *IEEE Journal of Robotics and Automation.* 1987, Vol. 3, 4, pp. 308-316.

Hollerbach, J. M. 1985. Optimum kinematic design for a seven degree of freedom manipulator. [ed.] H. Hanafusa and H. Inoue. *Second International Symposium on Rbotics Research.* Cambridge : MIT Press, 1985, pp. 215-222.

Honda, T., et al. 2002. Remote handling systems for ITER. *Fusion Engineering and Design.* s.l. : Elsevier, 2002, Vols. 63-64, pp. 507-518.

Jansson, A. and Palmberg, J. 1990. Separate Controls of Meter-In and Meter-Out Orifices in Mobile Hydraulic Systems. *International Off-Highway & Powerplant Congress & Exposition Technical Papers.* Milwaukee : SAE International, 1990, Vol. 99, 2, pp. 377-383.

Jassemi-Zargani, R., Necsulescu, D. S. and Kalaycioglu, S. 1995. Sensor fusion for impedance control of robot manipulators. *Canadian Conference on Electrical and Computer Engineering.* 1995, Vol. 1, pp. 322-325.

Jelali, Mohieddine and Kroll, Andreas. 2002. *Hydraulic Servo-systems: Modelling, Identification and Control.* London : Springer, 2002.

Khatib, O. 1987. A unified approach for motion and force control of robot manipulators: The operational space formulation. *IEEE Journal of Robotics and Automation.* 1987, Vol. 3, 1, pp. 43-53.

Khatib, O. and Bowling, A. 1996. Optimization of the inertial and acceleration characteristics of manipulators. *Proceedings of IEEE International Conference on Robotics and Automation.* 1996, Vol. 4, pp. 2883-2889.

Khosla, P. K. and Kanade, T. 1988. Experimental evaluation of nonlinear feedback and feedforward control schemes for manipulators. *The International Journal of Robotics Research.* s.l. : SAGE Publications, 1988, Vol. 7, 1, pp. 18-28.

Kircanski, M. V. 1994. Robotic isotropy and optimal robot design of planar manipulators. *Proceedings of IEEE International Conference on Robotics and Automation.* 1994, Vol. 2, pp. 1100-1105.

Klein, C. A. and Chirco, A. I. 1987. Dynamic simulation of a kinematically redundant manipulator system. *International Journal of Robotics Research.* s.l. : SAGE Publications, 1987, Vol. 4, 1, pp. 5-23.

Koeppe, R. and Yoshikawa, T. 1997. Dynamic manipulability analysis of compliant motion. *Proceedings of the IEEE/RSJ International Conference on Intelligent Robots and Systems.* 1997, Vol. 3, pp. 1472-1478.

Koskinen, K. T. and Vilenius, M. 1999. Water Hydraulic. [ed.] George E. Totten. *Handbook of Hydrualic Fluid Technology.* s.l. : Marcel Dekker Inc., 1999.

Kosuge, K., Takeo, K. and Ishida, H. 1997. Teleoperation system of power shovel for subterranean line works. *International Conference on Industrial Electronics, Control and Instrumentation.* 1997, Vol. 3, pp. 1421-1426.

Kraft TeleRobotics, Inc. 2009. *Kraft TeleRobotics Robotic Manipulator Systems and Remotely Operated Vehicles.* [Online] Kraft TeleRobotics, Inc., 04 May 2009. [Cited: 09 August 2011.] http://krafttelerobotics.com/.

Lane, J., Craiganan, C. and Akin, D. 2001. Advanced operator interface design for complex space telerobots. *Autonomous Robots.* s.l. : Springer, 2001, Vol. 11, 1, pp. 49-58.

Lawrence, D. A. 1988. Impedance control stability properties in common implementations. *Proceedings of IEEE International Conference on Robotics and Automation.* 1988, Vol. 2, pp. 1185-1190.

Liegeois, A. 1977. Automatic supervisory control of the configuration and behavior of multi-body mechanics. *IEEE Transactions on Systems, Man, and Cybernatics.* 1977, Vols. SMC-7, 12, pp. 868-871.

Linjama, M. and Virvalo, T. 2001. Robustness of some low-order controllers in an electrohydraulic position servo drive. [ed.] D. N. Johnston and K. A. Edge. *Proceedings of the 14th Symposium on Fluid Power and Motion Control, Centre of Power Transmission and Motion Control, University of Bath.* Bath : s.n., 2001.

Linjama, M. 1998. *The modelling and actuator space control of flexible hydrauli cranes.* Tampere : Tampere University of Technology, 1998.

Linjama, M., et al. 2008. Comparison of digital hydraulic and traditional servo system in demanding water hydraulic tracking control. [ed.] D. N. Johnston and A. R. Plummer. *Proceedings of the 21st Symposium on Fluid Power and Motion Control, Centre of Power Transmission and Motion Control, University of Bath.* Bath : s.n., 2008, pp. 393-403.

Linjama, M., et al. 2002a. High-speed on/off position control of a low-pressure water hydraulic cylinder drive. *Proceedings of the 49th National Conference on Fluid Power.* Las Vegas : s.n., 2002a.

Linjama, M., Koskinen, K. T. and Vilenius, M. 2002. Pseudo-Proportional Position Control of Water Hydraulic Cylinder Using On/Off Valves. *Proceedings of the 5th Japan Fluid Power Systems Society International Symposium on Fluid Power.* Nara : s.n., 2002.

Lischinsky, P., Canudas-de-Wit, C. and Morel, G. 1999. Friction compensation for an industrial hydraulic robot. *IEEE Control Systems Magazine.* 1999, Vol. 19, 1, pp. 25-32.

Liu, G. J. and Goldenberg, A. A. 1991. Robust hybrid impedance control of robot manipulators. *Proceedings of IEEE International Conference on Robotics and Automation.* 1991, Vol. 1, pp. 287-292.

Lu, W. -S. and Meng, Q. -H. 1991. Impedance control with adaptation for robotic manipulations. *IEEE Transactions on Robotics and Automation.* 1991, Vol. 7, 3, pp. 408-415 .

Maciejewski, A. A. and Klein, C. A. 1985. Obstacle avoidance for kinematically redundant manipulators in dynamically varying environments. *International Journal of Robotics Research.* s.l. : SAGE Publications, 1985, Vol. 4, 3, pp. 109-117.

Maisonnier, D., Martin, E. and Palmer, J. D. 2001. ITER R&D: Remote Handling Systems: Divertor Remote Handling Systems. *Fusion Engineering and Design.* s.l. : Elsevier, 2001, Vol. 55, 2-3, pp. 259-271.

Mäkinen, E. and Virvalo, T. 2002. Influence of position feedback signal quality on behaviour of a state controlled pneumatic position servo. *Proceedings of the 4th International Conference on Machine Automation - Human Friendly Reliable Mechatronics.* Tampere : s.n., 2002.

Mäkinen, E. 2001. *Control of a Water Hydraulic Servo System.* Tampere : Tampere University of Technology, 2001.

Mäkinen, E., Virvalo, T. and Vilenius, M. 1999. Comparison of water and oil hydraulic position servos. *Proceedings of the 4th JHPS International Symposium on Fluid power.* Tokyo : s.n., 1999.

Mamen, R. 2003. Applying space technologies for human benefit; the Canadian experience and global trends. *Proceedings of the International Conference on Recent Advances in Space Technologies.* 2003, pp. 1-8.

Martin, D. P., Baillieul, J. and Hollerbach, J. M. 1989. Resolution of kinematic redundancy using optimization techniques. *IEEE Transactions on Robotics and Automation.* 1989, Vol. 5, 4, pp. 529-533.

Matko, D., Kamnik, R. and Bajd, T. 1999. Adaptive impedance force control of an industrial manipulator. *Proceedings of the IEEE International Symposium on Industrial Electronics.* 1999, Vol. 1, pp. 129-133.

Matsueda, T., et al. 1991. JEMRMS system design and development status. *Proceedings of National Telesystems Conference.* 1991, Vol. 1, pp. 391-395.

Mattila, J., Siuko, M. and Vilenius, M. 2005. On pressure/force control of a 3 dof water hydraulic manipulator. *Proceedings of the 6th JFPS International Symposium on Fluid Power.* Tsukuba : s.n., 2005.

Mayorga, R. V., Ressa, B. and Wong, A. K. C. 1990. A dexterity measure for robot manipulators. *Proceedings of IEEE International Conference on Robotics and Automation.* 1990, Vol. 1, pp. 656-661.

Measson, Y., et al. 2003. Technology and control for hydraulic manipulators. *Fusion Engineering and Design, 22nd Symposium on Fusion Technology.* s.l. : Elsevier Science B.V., 2003, Vol. 69, 1-4, pp. 129-134.

Merritt, Herbert E. 1967. *Hydraulic Control Systems.* New York : John Wiley & Sons, Inc., 1967.

Miall, R. C. and Wolpert, D. M. 1996. Forward Models for Physiological Motor Control. *Neural Networks: Four Major Hypotheses in Neuroscience.* s.l. : Elsevier, 1996, Vol. 9, 8, pp. 1265-1279.

Mochizuki, Y., Yamashina, C. and Miyakawa, S. 1997. Servo control of a water hydraulic axial piston motor. *Proceedings of the 5th Triennial International Symposium on Fluid Control, Measurement and Vsualization.* Hayama : s.n., 1997.

Muhammad, A. and Vilenius, M. 2010. Impedance control of redundant ranipulators. [ed.] Ivantysynova Monika. *Proceedings of the 6th FPNI - PhD Symposium.* West Lafayette : s.n., 2010, Vol. 1, pp. 153-163.

Muhammad, A., et al. 2010a. Development of water hydraulic manipulator for the remote handling of heavy duty components. *Workshop proceedings of 7th International Fluid Power Conference, IFK 2010.* Achen : s.n., 2010a, Vol. 1, pp. 325-326.

Muhammad, A., et al. 2007. Development of water hydraulic remote handling system for divertor maintenance of ITER. *Proceedings of the 22nd IEEE/NPSS Symposium on Fusion Engineering - SOFE 07.* Albuquerque : s.n., 2007.

Muhammad, A., et al. 2009. Force-based and position-based impedance control of hydraulic manipulators. *Proceedings of the 11th Scandinavian International Conference on Fluid Power.* Linköping : s.n., 2009.

Muhammad, A., et al. 2006. Force-based impedance control of hydraulic manipulators and its relationship with position-based impedance control. [ed.] D. N. Johnston and K. A. Edge. *Proceedings of the 19th Symposium on Fluid Power and Motion Control, Centre of Power Transmission and Motion Control, University of Bath.* Bath : s.n., 2006, pp. 291-303.

Muhammad, A., et al. 2009b. Improved positioning accuracy for a water hydraulic manipulator with state feedback controller. [ed.] Keiichi Shirase and Seiji Aoyagi. *Service Robotics and Mechatronics : Selected papers of the International Conference on Machine Automation, ICMA2008.* Awaji : Springer, 2009b, pp. 347-352.

Muhammad, A., et al. 2008. Improvement in feedback signal quality for water hydraulic manipulator. [ed.] D. N. Johnston and A. R. Plummer. *Proceedings of the 21st Symposium on Fluid Power and Motion Control, Centre of Power Transmission and Motion Control, University of Bath.* Bath : s.n., 2008, pp. 135-148.

Muhammad, A., et al. 2009a. Modelling of a water hydraulic vane actuator. [ed.] Lu Yongxiang, et al. *Proceedings of the 7th International Conference on Fluid Power Transmission and Control.* Hangzhou : World Publishing Corporation, 2009a, pp. 480-484.

Muhammad, A., et al. 2007a. Water hydraulic teleoperation system for ITER. *Proceedings of the 10th Scandinavian International Conference on Fluid Power.* Tampere : s.n., 2007a, Vol. 3, pp. 263-276.

Nieminen, Peetu, et al. 2009. Water hydraulic manipulator for fail safe and fault tolerant remote handling operations at ITER. *Fusion Engineering and Design.* s.l. : Elsevier, 2009, Vol. 84, 7-11, pp. 1420-1424.

Palmer, J., et al. 2005. Recent developments towards ITER 2001 deivertor maintenance. *Fusion Engineering and Design.* s.l. : Elsevier, 2005, Vols. 75-79, pp. 583-587.

Palmer, J., et al. 2007. The design and development of divertor remote handling equipment for ITER. *Fusion Engineering and Design.* s.l. : Elsevier, 2007, Vol. 82, 15-24, pp. 1977-1982.

Parker, N. R., Salcudean, S. E. and Lawrence, P. D. 1993. Application of force feedback to heavy duty hydraulic machines. *Proceedings of IEEE International Conference on Robotics and Automation.* 1993, Vol. 1, pp. 375-381.

Patten, L., et al. 2002. International Space Station Robotics: A Comparative Study of ERA, JEMRMS and MSS. *7th ESA Workshop on Advance Space Technologies for Robotics and Automation.* Noordwijk : s.n., 2002.

Paul, R. P. and Stevenson, C. N. 1983. Kinematics of robot wrists. *International Journal of Robotics Research.* 1983, Vol. 2, 1, pp. 31-38.

Paul, R. P. and Zhang, H. 1986. Computationally efficient kinematics of manipulators with spherical wrists based on the homogeneous transformation representation. *International Journal of Robotics Research.* 1986, Vol. 4, 2, pp. 32-44.

Paul, R. P. 1981. *Robot manipulators: mathematics, programming and control: the computer control of robot manipulators.* s.l. : The MIT Press, 1981.

Pearce, M. 2005. Is there an alternative to fluid power? [Electrically driven linear motion technology]. *Computing and Control Engineering Journal.* 2005, Vol. 16, 2, pp. 8-11.

Pieper, D. L. 1968. *The kinematics of manipulators under computer control.* Stanford Artificial Intelligence Laboratory, Stanford University. 1968. AIM 72.

Poole, R., et al. 1998. *Implementation of communications and machine tele-operation in mine automation.* Canadian Institute of Mining. Montreal : s.n., 1998. Congress.

Raibert, M. H. and Craig, J. J. 1981. Hybrid position/force control of manipulators. *Journal of Dynamic Systmes, Measurements and Control.* s.l. : ASME, 1981, Vol. 103, pp. 126-133.

Raneda, A. 2004. *Impedance control of a water hydraulic manipulator for teleoperation applications.* Tampere : Tampere University of Technology, 2004.

Ranjbaran, F., Angeles, J. and Kecskemethy, A. 1996. On the kinematic conditioning of robotic manipulators. *Proceedings of IEEE International Conference on Robotics and Automation.* 1996, Vol. 4, pp. 3167-3172.

Richardson, Robert, et al. 2005. Impedance control for a pneumatic robot-based around pole-placement, joint space controllers. *Control Engineering Practice.* s.l. : Elsevier, 2005, Vol. 13, 3, pp. 291-303.

Riipinen, H., et al. 2003. Current understanding of pressure medium quality and quality control in water hydraulics. *Proceedings of the 8th Scandinavian International Conference on Fluid Power.* Tampere : s.n., 2003.

Riipinen, H., et al. 2002. Effects of microbial growth on filteration in water hydraulic system. *Porceedings of the National Conference on Fluid Power.* Las Vegas : s.n., 2002.

Rolfe, A. C. 2007. A prespective on fusion relevant remote handling techniques. *Fusion Engineering and Design.* s.l. : Elsevier, 2007, Vol. 82, 15-24, pp. 1917-1923.

Salcudean, S. E., et al. 1997. Impedance control of a teleoperated mini excavator. *Proceedings of th International Conference on Advanced Robotics.* 1997, pp. 19-25.

School of Computer Science at Carnegie Mellon University. 2006. Unimate Photo Album. *Robot Hall of Fame.* [Online] 25 June 2006. [Cited: 23 June 2009.] http://www.robothalloffame.org/unimate_photos.html.

Sciavicco, L. and Siciliano, B. 2001. *Modelling and control of Robot Manipulators.* 2nd Edition. s.l. : Springer, 2001.

Sepehri, N., et al. 1994. Resolved-mode teleoperated control of heavy-duty hydraulic machines. *Journal of dynamic systems, measurement, and control.* s.l. : ASME, 1994, Vol. 116, 2, pp. 232-240.

Sepehri, N., Khayyat, A. A. and Heinrichs, B. 1997. Development of a nonlinear PI controller for accurate positioning of an industrial hydraulic manipulator. *Journal of Mechatronics.* s.l. : Elsevier Science, Oxford, 1997, Vol. 7, 8, pp. 683-700.

Seraji, H. and Colbaugh, R. 1993. Adaptive force-based impedance control. *Proceedings of the IEEE/RSJ International Conference on Intelligent Robots and Systems.* 1993, Vol. 3, pp. 1537-1544.

—. 1993a. Force tracking in impedance control. *Proceedings of IEEE International Conference on Robotics and Automation.* 1993a, Vol. 2, pp. 499-506.

Shimomura, Y. 2004. The present status and future prospects of the ITER projec. *Journal of Nuclear Materials.* s.l. : Elsevier, 2004, Vols. 329-333, 1, pp. 5-11.

Singh, N., et al. 1995. Coordinated-motion control of heavy-duty industrial machines with redundancy. *Robotica.* Cambridge : Cambridge University Press, 1995, Vol. 13, 6, pp. 623-633.

Siuko, M. 1998. *Water hydraulics in fusion reactor maintenance.* Tampere : Tampere University of Technology, 1998.

Siuko, M., et al. 2003. Water hydraulic actuators for ITER maintenance devices. *Fusion Engineering and Design.* s.l. : Elsevier, 2003, Vol. 69, 1-4, pp. 141-145.

Smith, Christopher Llewellyn. 2005. The need for fusion. *Fusing Engineering and Design.* s.l. : Elsevier, 2005, Vol. 74, 1-4, pp. 3-8.

Surdilovic, Dragoljub. 2007. Robust control design of impedance control for industrial robots. *International Conference on Intelligent Robots and Systems.* 2007, pp. 3572-3579.

Tafazoli, S., de Silva, C. W. and Lawrence, P. D. 1998. Tracking control of an electrohydraulic manipulator in the presence of friction. *IEEE Transactions on Control Systems Technology.* 1998, Vol. 6, 3, pp. 401-411.

Tafazoli, S., et al. 2002. Impedance control of a teleoperated excavator. *IEEE Transactions on Control Systems Technology.* 2002, Vol. 10, 3, pp. 355-367.

Tafazoli, S., Lawrence, P. D. and Salcudean, S. E. 1999. Identification of inertial and friction parameters for excavator arms. *IEEE Transactions on Robotics and Automation.* 1999, Vol. 15, 5, pp. 966-971.

Takalo, V., et al. 2009. Validation of divertor cassette locking system with a hydraulic jack tool. *Fusion Engineering and Design.* s.l. : Elsevier, 2009, Vol. 84, 7-11, pp. 1808-1812.

Tochizawa, M. and Edge, K. A. 1999. A comparison of some control strategies for a hydraulic manipulator. *Proceedings of the American Control Conference.* San Diego, California : s.n., 1999.

Trostmann, E. 1996. *Water hydraulic control technology.* New York : Marcel Dekker Inc., 1996.

Trostmann, E., Frolund, B. and Hilbrecht, B. 2001. *Tap water as a hydraulic pressure medium.* New York : Marcel Dekker Inc., 2001.

Uebel, M., Minis, I. and Cleary, K. 1992. Improved computed torque control for industrial robots. *Proceedings of IEEE International Conference on Robotics and Automation.* 1992, Vol. 1, pp. 528-533.

Urata, E., et al. 1998. Development of a water hydraulic servovalve. *JSME International journal. Series B, fluids and thermal engineering.* Tokyo : Japan Society of Mechanical Engineers, 1998, Vol. 41, 2, pp. 286-294.

Vilenius, M., et al. 2002. Vessel/In-Vessel Technolgoy - Remote Handling and Viewing. [ed.] S. Karttunen. *FFusion 2 Yearbook 2001, Annual Report of the Finnish Fusion Research Unit.* Espoo : s.n., 2002, pp. 56-67.

Vilenius, M., Koskinen, K. T. and Lakkonen, M. 2002a. Water Hydraulics Motion Control - Possibilities and Challenges. *Proceedings of the 5th JFPS International Symposium on Fluid Power.* Nara : s.n., 2002a.

Virvalo, T. and Linjama, M. 2001. Experimental study of robustness of some controllers in a hydraulic position servo drive. *Hydraulika a Pneumatika.* Ostrava : s.n., 2001.

Virvalo, T. and Mäkinen, E. 2000. Follow-up accuracy of a foce control water hydraulic cylinder drive. *Proceedings of 6th Triennal Intenrational Symposium of Fluid Control, Measurements and Visualization.* Sherbrooke : s.n., 2000.

Virvalo, T. and Vilenius, M. 1999b. Some steps in development of modern water hydraulics. *Proceedings of the 3rd International Symposium on Fluid Power Transmission and Control.* Harbin : s.n., 1999b.

Virvalo, T. 2001. PI and PID-controllers in a hydraulic position servo system - what it is all about. *Proceedings of the 5th International Conference on Fluid Power Transmission and Control.* Hangzhou : s.n., 2001.

Virvalo, T., Mäkinen, E. and Vilenius, M. 1999. Force control of a water hydraulic cylinder drive. *Proceedings of the 6th Scaninavian international Conference on Fluid Power.* Tampere : s.n., 1999.

—. 1999a. On the damping of water hydraulic cylinder drive. [ed.] S. Yokota. *Proceedings of the Fourth JHPS International Symposium on Fluid Power.* Tokyo : s.n., 1999a.

Virvalo, Tapio and Makinen, Esa. 2000. Follow-up accuracy of a force control water hydraulic cylinder drive. [ed.] Andre Laneville. *Proceedings of the 6th Triennal International Symposium on Fluid Control, Measurement and Visualization.* Sherbrooke : Transvision Reseau Inc., 2000.

Virvalo, Tapio, Linjama, Matti and Mattila, Jouni. 1997. Comparing different controllers of an electrohydraulic position servo. *Proceedings of the 4th International Conference on Fluid Power Transmission and Control.* Hangzhou : s.n., 1997.

Volpe, R. and Khosla, P. 1993. A theoretical and experimental investigation of explicit force control strategies for manipulators. *IEEE Transactions on Automatic Control.* 1993, Vol. 38, 11, pp. 1634-1650.

—. 1995. The equivalence of second order impedance control and proportional gain explicit force control. *International Journal of Robotics Research.* 1995, Vol. 14, pp. 574-589.

Wampler, C. W. 1989. Inverse kinematic functions for redundant spherical wrists. *IEEE Transactions on Robotics and Automation.* 1989, Vol. 5, 1, pp. 106-111.

Watton, J. 1989. *Fluid Power Systems: Modeling, Simulation, Analog and Microcomputer Control.* s.l. : Prentice Hall, 1989.

Whitney, D. E. 1969. Resolved Motion Rate Control of Manipulators and Human Prostheses. *IEEE Transactions on Man Machine Systems.* 1969, Vol. 10, 2, pp. 47-53.

Whitney, D. 1985. Historical perspective and state of the art in robot force control. *Proceedings of IEEE International Conference on Robotics and Automation.* 1985, Vol. 2, pp. 262-268.

Winfield, A. F. T. 2000. Future directions in tele-operated robotics. [ed.] Tyler Schilling. *Telerobotic Applications.* s.l. : Professional Engineering Publishing Limited, 2000, pp. 147-162.

Wolovich, W. A. and Elliott, H. 1984. A computational technique for inverse kinematics. *Proceedings of the 23rd IEEE Conference on Decision and Control.* Las Vegas : s.n., 1984, Vol. 23, 1, pp. 1359-1363.

Yamashina, C., Miyakawa, S. and Urata, E. 1996. Development of water hydraulic cylinder position control system. *Proceedings of the 3rd JHPS International Symposium on Fluid Power.* Yokohama : s.n., 1996.

Yoshikawa, T. 1984. Analysis and control of robot manipulators with redundancy. [ed.] M. Brady and R. Paul. *The First International Symposium in Robotics Research.* Cambridge : MIT Press, 1984, pp. 735-747.

Yoshikawa, T. and Kiriyama, S. 1989. Four-Joint Redundant Wrist Mechanism and Its Control. *Journal of Dynamic Systems, Measurement, and Control.* 1989, Vol. 111, 2, pp. 200-204.

Yoshikawa, T. 1985. Dynamic manipulability of robot manipulators. *Proceedings of IEEE International Conference on Robotics and Automation.* 1985, Vol. 2, pp. 1033-1038.

—. 1985a. Manipulability and redundancy control of robotic mechanisms. *Proceedings of IEEE International Conference on Robotics and Automation.* 1985a, Vol. 2, pp. 1004-1009.

—. 1985b. Manipulability of Robotic Mechanisms. *International Journal of Robotics Research.* s.l. : SAGE Publications, 1985b, Vol. 4, 2, pp. 3-9.

—. 1991. Translational and rotational manipulability of robotic manipulators. *Proceedings of International Conference on Industrial Electronics, Control and Instrumentation.* 1991, Vol. 2, pp. 1170-1175.

Yuh, J. 2000. Design and Control of Autonomous Underwater Robots: A Survey. *Autonomous Robots.* s.l. : Springer, 2000, Vol. 8, 1, pp. 7-24.

Zghal, H., Dubey, R. V. and Euler, J. A. 1990. Efficient gradient projection optimization for manipulators with multiple degrees of redundancy. *Proceedings of the IEEE International Conference on Robotics and Automation.* 1990, Vol. 2, pp. 1006-1011.

APPENDIX A: KINEMATICS OF WHMAN

To obtain the direct kinematic solution of the WHMAN, Cartesian frames are attached to each link. This frame assignment is shown in Figure A.1. The relationship between two consecutive frames can be completely defined by a set of four parameters famously known as Denavit-Hartenberg kinematic parameters (or DH parameters in short).

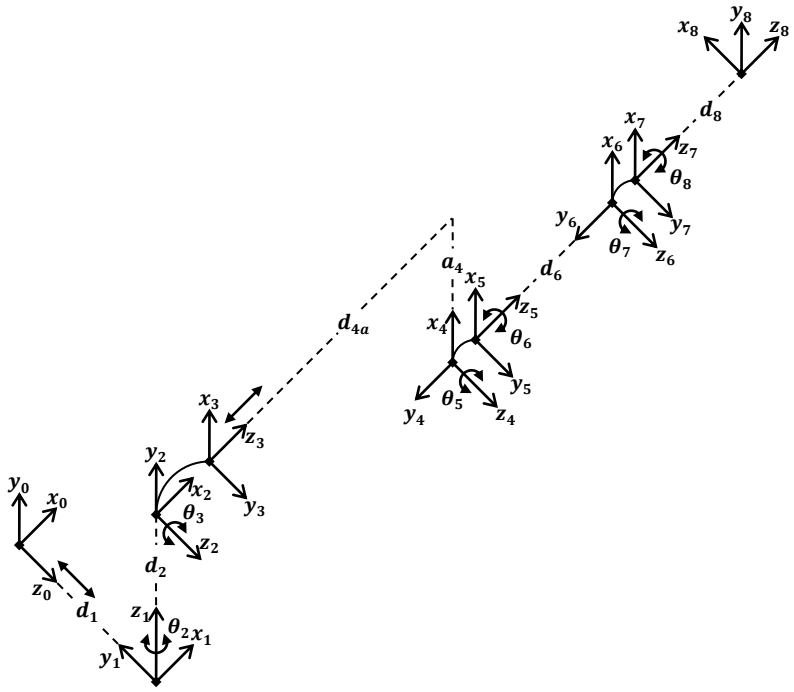

Figure A.1: Frame assignment of WHMAN

Using the set of DH parameters the homogenous transformation between two consecutive frames can be given by the matrix given in Equation A.1.

A.1
$$\boldsymbol{T_i^{i-1}}(\gamma_i) = \begin{bmatrix} c_{\theta_i} & -s_{\theta_i}c_{\alpha_i} & s_{\theta_i}s_{\alpha_i} & a_i c_{\theta_i} \\ c_{\theta_i} & c_{\theta_i}c_{\alpha_i} & -c_{\theta_i}s_{\alpha_i} & a_i s_{\theta_i} \\ 0 & s_{\alpha_i} & c_{\alpha_i} & d_i \\ 0 & 0 & 0 & 1 \end{bmatrix}$$

Here, i is the number of the link and $\boldsymbol{T}$ is the homogenous transformation matrix. γ_i is the generalized joint variable which is θ_i for a revolute joint and d_i in case of a translational joint. c_θ and s_θ are the short for $\cos(\theta)$ and $\sin(\theta)$ respectively. The list of DH parameters is given

in Table A.1 using the classical convention (Sciavicco, et al., 2001). The lengths are given in millimetres and angles are in radians.

Table A.1: Denavit-Hartenberg parameters of WHMAN

$\boldsymbol{i}$	$\boldsymbol{a_i}$	$\boldsymbol{\alpha_i}$	$\boldsymbol{d_i}$	$\boldsymbol{\theta_i}$
1	0	$-\frac{\pi}{2}$	d_1	0
2	0	$\frac{\pi}{2}$	393.5	θ_2
3	0	$\frac{\pi}{2}$	0	$\theta_3 + \frac{\pi}{2}$
4	−168.25	$-\frac{\pi}{2}$	$d_4 + 990$	0
5	0	$\frac{\pi}{2}$	0	θ_5
6	0	$-\frac{\pi}{2}$	621.3	θ_6
7	0	$\frac{\pi}{2}$	0	θ_7
8	0	0	505.1	$\theta_8 - \frac{\pi}{2}$

The direct kinematic solution of the manipulator can then be obtained in a recursive manner by multiplying the consecutive transformation matrices as shown in Equation A.2. The resulting homogenous transformation contains the WHMAN's position and orientation in the operational-space as a function of joint-space variable.

A.2 $$\boldsymbol{T_8^0} = \boldsymbol{T_1^0} \cdot \boldsymbol{T_2^1} \cdot \boldsymbol{T_3^2} \cdot \boldsymbol{T_4^3} \cdot \boldsymbol{T_5^4} \cdot \boldsymbol{T_6^5} \cdot \boldsymbol{T_7^6} \cdot \boldsymbol{T_8^7} = \begin{bmatrix} \boldsymbol{r_1} & \boldsymbol{r_2} & \boldsymbol{r_3} & \vdots & \boldsymbol{x} \\ \dots & \dots & \dots & \vdots & \dots \\ 0 & 0 & 0 & \vdots & 1 \end{bmatrix}$$

Here, $\boldsymbol{r_n} \in \mathcal{R}^{3\times1}$ represents the columns of the rotation matrix and $\boldsymbol{x} \in \mathcal{R}^{3\times1}$ is the position vector of manipulator in the operational-space. The values of these vectors are given in Equations A.3 to A.6 below.

A.3 $$\boldsymbol{r_1} = \begin{bmatrix} -c_2 s_{35}(c_6 c_7 s_8 + s_6 c_8) + s_2(s_6 c_7 s_8 - c_6 c_8) - c_2 c_{35} s_7 s_8 \\ c_{35}(c_6 c_7 s_8 + s_6 c_8) - s_{35} s_7 s_8 \\ s_2 s_{35}(c_6 c_7 s_8 + s_6 c_8) + c_2(s_6 c_7 s_8 - c_6 c_8) + s_2 c_{35} s_7 s_8 \end{bmatrix}$$

A.4 $$\boldsymbol{r_2} = \begin{bmatrix} -c_2 s_{35}(c_6 c_7 c_8 - s_6 s_8) + s_2(s_6 c_7 c_8 + c_6 s_8) - c_2 c_{35} s_7 c_8 \\ c_{35}(c_6 c_7 c_8 - s_6 s_8) - s_{35} s_7 c_8 \\ s_2 s_{35}(c_6 c_7 c_8 - s_6 s_8) + c_2(s_6 c_7 c_8 + c_6 s_8) + s_2 c_{35} s_7 c_8 \end{bmatrix}$$

A.5 $$\boldsymbol{r_3} = \begin{bmatrix} -c_2 s_{35} c_6 s_7 + s_2 s_6 s_7 + c_2 c_{35} c_7 \\ c_{35} c_6 s_7 + s_{35} c_7 \\ s_2 s_{35} c_6 s_7 + c_2 s_6 s_7 - s_2 c_{35} c_7 \end{bmatrix}$$

A.6 $$\boldsymbol{x} = \begin{bmatrix} d_8 s_7 (s_2 s_6 - c_2 s_{35} c_6) + c_2 c_{35} (d_6 + d_8 c_7) - c_2 (a_4 s_3 - (d_4 + d_{4a}) c_3) \\ d_8 c_{35} c_6 s_7 + s_{35} (d_6 + d_8 c_7) + a_4 c_3 + (d_4 + d_{4a}) s_3 + d_2 \\ \begin{pmatrix} d_8 s_7 (s_2 s_{35} c_6 + c_2 s_6) - s_2 c_{35} (d_6 + d_8 c_7) \\ + s_2 (a_4 s_3 - (d_4 + d_{4a}) c_3) + d_1 \end{pmatrix} \end{bmatrix}$$

The range of motion for each joint is given in Table A.2 below.

Table A.2: Joint ranges of WHMAN

Joint Name	**Joint Variable**	**Range**	**Units**
Linear slide	d_1	$0 \rightarrow 1200$	mm
Base	θ_2	$-\frac{3\pi}{4} \rightarrow \frac{3\pi}{4}$	rad
Shoulder	θ_3	$-\frac{\pi}{6} \rightarrow \frac{\pi}{2}$	rad
Telescopic	d_4	$0 \rightarrow 400$	mm
Elbow	θ_5	$-\pi \rightarrow \frac{\pi}{2}$	rad
Azimuth	θ_6	$-\frac{3\pi}{4} \rightarrow \frac{3\pi}{4}$	rad
Wrist	θ_7	$-\frac{3\pi}{4} \rightarrow \frac{3\pi}{4}$	rad
Tool rotation	θ_8	$-\frac{3\pi}{4} \rightarrow \frac{3\pi}{4}$	rad

The Jacobian of the manipulator can be obtained by the geometric technique. The columns of the Jacobian matrix are computed recursively using Equation A.7.

A.7 $$\begin{bmatrix} \boldsymbol{j_{x_i}} \\ \boldsymbol{j_{o_i}} \end{bmatrix} = \begin{cases} \begin{bmatrix} \boldsymbol{z_{i-1}} \\ \boldsymbol{0} \end{bmatrix} & \text{for a translational joint} \\ \begin{bmatrix} \boldsymbol{z_{i-1}} \times (\boldsymbol{x} - \boldsymbol{x_{i-1}}) \\ \boldsymbol{z_{i-1}} \end{bmatrix} & \text{for a revolute joint} \end{cases}$$

Here,

A.8 $$\boldsymbol{z_{i-1}} = \boldsymbol{R_{i-1}^0} \cdot \begin{bmatrix} 0 \\ 0 \\ 1 \end{bmatrix}$$

A.9 $$\boldsymbol{x} = \boldsymbol{T_8^0} \cdot \begin{bmatrix} 0 \\ 0 \\ 0 \\ 1 \end{bmatrix}$$

A.10 $$\boldsymbol{x_{i-1}} = \boldsymbol{T_{i-1}^0} \cdot \begin{bmatrix} 0 \\ 0 \\ 0 \\ 1 \end{bmatrix}$$

Since WHMAN has eight degrees of freedom in joint-space and six in operational space the Jacobian matrix is of the form in Equation A.11.

A.11 $$\boldsymbol{J} = [\boldsymbol{j_1} \quad \boldsymbol{j_2} \quad \boldsymbol{j_3} \quad \boldsymbol{j_4} \quad \boldsymbol{j_5} \quad \boldsymbol{j_6} \quad \boldsymbol{j_7} \quad \boldsymbol{j_8}] \in \mathcal{R}^{6\times 8}$$

where each column $\boldsymbol{j_i} \in \mathcal{R}^{6\times 1}$ of the Jacobian matrix is given in Equations A.12 to A.19 below.

A.12 $$\boldsymbol{j_1} = \begin{bmatrix} 0 \\ 0 \\ 1 \\ 0 \\ 0 \\ 0 \end{bmatrix}$$

A.13 $$\boldsymbol{j_2} = \begin{bmatrix} d_8 s_7 (s_2 s_{35} c_6 + c_2 s_6) - s_2 (d_8 c_{35} c_7 + d_6 c_{35} + (d_4 + d_{4a}) c_3 - a_4 s_3) \\ 0 \\ d_8 s_7 (c_2 s_{35} c_6 - s_2 s_6) - c_2 (d_8 c_{35} c_7 + d_6 c_{35} + (d_4 + d_{4a}) c_3 - a_4 s_3) \\ 0 \\ 1 \\ 0 \end{bmatrix}$$

A.14 $$\boldsymbol{j_3} = \begin{bmatrix} -c_2 (d_8 c_{35} c_6 s_7 + d_8 s_{35} c_7 + d_6 s_{35} + a_4 c_3 + (d_4 + d_{4a}) s_3) \\ -d_8 s_7 s_{35} c_6 + d_8 c_{35} c_7 + d_6 c_{35} + (d_4 + d_{4a}) c_3 - a_4 s_3 \\ s_2 (d_8 c_{35} c_6 s_7 + d_8 s_{35} c_7 + d_6 s_{35} + a_4 c_3 + (d_4 + d_{4a}) s_3) \\ s_2 \\ 0 \\ c_2 \end{bmatrix}$$

A.15 $$\boldsymbol{j_4} = \begin{bmatrix} c_2 c_3 \\ s_3 \\ -s_2 c_3 \\ 0 \\ 0 \\ 0 \end{bmatrix}$$

A.16 $$\boldsymbol{j_5} = \begin{bmatrix} -c_2(d_8c_{35}c_6s_7 + d_8s_{35}c_7 + d_6s_{35}) \\ -d_8s_7s_{35}c_6 + d_8c_{35}c_7 + d_6c_{35} \\ s_2(d_8c_{35}c_6s_7 + d_8s_{35}c_7 + d_6s_{35}) \\ s_2 \\ 0 \\ c_2 \end{bmatrix}$$

A.17 $$\boldsymbol{j_6} = \begin{bmatrix} d_8s_7(c_2s_{35}s_6 + s_2c_6) \\ -d_8c_{35}s_6s_7 \\ -d_8s_7(s_2s_{35}s_6 - c_2c_6) \\ c_2c_{35} \\ s_{35} \\ -s_2c_{35} \end{bmatrix}$$

A.18 $$\boldsymbol{j_7} = \begin{bmatrix} -d_8c_2(c_{35}s_7 + s_{35}c_6c_7) + d_8s_2s_6c_7 \\ -d_8(s_{35}s_7 - c_{35}c_6c_7) \\ d_8s_2(c_{35}s_7 + s_{35}c_6c_7) + d_8c_2s_6c_7 \\ c_2s_{35}s_6 + s_2c_6 \\ -c_{35}s_6 \\ -s_2s_{35}s_6 + c_2c_6 \end{bmatrix}$$

A.19 $$\boldsymbol{j_8} = \begin{bmatrix} 0 \\ 0 \\ 0 \\ -s_7(c_2s_{35}c_6 - s_2s_6) + c_2c_{35}c_7 \\ c_{35}c_6s_7 + s_{35}c_7 \\ s_7(s_2s_{35}c_6 + c_2s_6) - s_2c_{35}c_7 \end{bmatrix}$$

APPENDIX B: DYNAMICS OF WHMAN

The nonlinear equation of motion for the mechanical structure of the manipulator in joint-space can be given as Equation B.1 below.

B.1 $$\boldsymbol{\tau} = \boldsymbol{M_\theta}(\boldsymbol{\theta})\ddot{\boldsymbol{\theta}} + \boldsymbol{B_\theta}\left(\boldsymbol{\theta}, \dot{\boldsymbol{\theta}}\right)\dot{\boldsymbol{\theta}} + \boldsymbol{g_\theta}(\boldsymbol{\theta})$$

Here, $\boldsymbol{\theta} = [\theta_1, \theta_2, \dots, \theta_n]^T \in \mathcal{R}^n$ is the vector of joint variables and $\boldsymbol{\tau} = [\tau_1, \tau_2, \dots, \tau_n]^T \in \mathcal{R}^n$ is the vector of joint forces. $\boldsymbol{M_\theta}(\boldsymbol{\theta}) \in \mathcal{R}^{n\times n}$ is the inertia matrix of the manipulator which is symmetric and positive definite. Matrix $\boldsymbol{B_\theta}(\boldsymbol{\theta}, \dot{\boldsymbol{\theta}}) \in \mathcal{R}^{n\times n}$ represents the centrifugal and Coriolis forces. The $\boldsymbol{g_\theta}(\boldsymbol{\theta}) \in \mathcal{R}^n$ is the vector of gravity forces acting on the manipulator. For WHMAN with eight degrees of freedom in joint-space, $n = 8$. The elements of the inertia matrix $\boldsymbol{M_\theta}(\boldsymbol{\theta})$ of WHMAN are given below in Equations B.2 to B.37:

B.2 $$m_{11} = m_1 + m_2 + m_3 + m_4 + m_5 + m_6 + m_7 + m_8$$

B.3 $$\begin{aligned} m_{12} = m_{21} = {} & (m_4 + m_5 + m_6 + m_7 + m_8)(a_4 s_3 - (d_4 + d_{4a})c_3)c_2 \\ & - (m_6 + m_7 + m_8)(d_6 c_{35})c_2 \\ & + m_8(c_2 s_{35} c_6 s_7 - s_2 s_6 s_7 - c_2 c_{35} c_7)d_8 \end{aligned}$$

B.4 $$\begin{aligned} m_{13} = m_{31} = {} & (m_4 + m_5 + m_6 + m_7 + m_8)(a_4 c_3 + (d_4 + d_{4a})s_3)s_2 \\ & + (m_6 + m_7 + m_8)(d_6 s_{35})s_2 + m_8(c_{35} c_6 s_7 + s_{35} c_7)d_8 s_2 \end{aligned}$$

B.5 $$m_{14} = m_{41} = -(m_4 + m_5 + m_6 + m_7 + m_8)s_2 c_3$$

B.6 $$m_{15} = m_{51} = (m_6 + m_7 + m_8)d_6 s_2 s_{35} + m_8(c_{35} c_6 s_7 + s_{35} c_7)d_8 s_2$$

B.7 $$m_{16} = m_{61} = m_8(c_2 c_6 - s_2 s_{35} s_6)d_8 s_7$$

B.8 $$m_{17} = m_{71} = m_8 d_8(s_2 s_{35} c_6 c_7 + c_2 s_6 c_7 + s_2 c_{35} s_7)$$

B.9 $$m_{18} = m_{81} = 0$$

B.10 $$\begin{aligned} m_{22} = {} & (m_4 + m_5)\left((d_4 + d_{4a})c_3 - a_4 s_3\right)^2 \\ & + (m_6 + m_7)\left((d_4 + d_{4a})c_3 - a_4 s_3 + d_6 c_{35}\right)^2 \\ & + m_8\Big((d_8 c_{35} c_6 c_7)^2 + (d_6 c_{35})^2 + (d_8 c_{35} c_7)^2 \\ & - (d_8 c_{35} c_6)^2 - (d_8 c_7)^2 - (a_4 s_3)^2 + \left((d_4 + d_{4a})c_3\right)^2 \\ & + {d_8}^2 + {a_4}^2 - 2{d_8}^2 c_{35} s_{35} c_6 c_7 s_7 - 2a_4 d_6 s_3 c_{35} \\ & + 2d_8(d_6 c_{35} + a_4 s_3 + (d_4 + d_{4a})c_3)(c_{35} c_7 - s_{35} c_6 s_7) \\ & + 2(d_4 + d_{4a})c_3(d_6 c_{35} - a_4 s_3)\Big) \end{aligned}$$

B.11
$$m_{23} = m_{32} = m_8(d_8c_{35}c_6s_7 + d_8s_{35}c_7 + d_6s_{35} + a_4c_3 + (d_4 + d_{4a})s_3)d_8s_6s_7$$

B.12
$$m_{24} = m_{42} = -m_8d_8c_3s_6s_7$$

B.13
$$m_{25} = m_{52} = m_8(c_{35}c_6s_7 + s_{35}c_7 + s_{35}){d_8}^2s_6s_7$$

B.14
$$m_{26} = m_{62} = -m_8(d_8c_{35}c_6c_7 - d_8s_{35}s_7 + d_6c_{35}c_6 + (d_4 + d_{4a})c_3c_6)d_8s_7$$

B.15
$$m_{27} = m_{72} = m_8(d_8c_{35} + d_6c_{35}c_7 - a_4s_3c_7 + (d_4 + d_{4a})c_3c_7)d_8s_6$$

B.16
$$m_{28} = m_{82} = 0$$

B.17
$$m_{33} = (m_4 + m_5 + m_6 + m_7 + m_8)((d_4 + d_{4a})^2 + {a_4}^2) + (m_6 + m_7 + m_8)(d_6 + 2a_4s_5 + 2(d_4 + d_{4a})c_5)d_6 + m_8\big(2d_6c_7 + d_8{c_6}^2 + d_8{s_6}^2{c_7}^2 + 2a_4(s_5c_7 + c_5c_6s_7) + 2(d_4 + d_{4a})(c_5c_7 + s_5c_6s_7)\big)d_8$$

B.18
$$m_{34} = m_{43} = -(m_4 + m_5 + m_6 + m_7 + m_8)a_4 + (m_6 + m_7 + m_8)s_5d_6 - m_8(s_5c_7 + c_5c_6s_7)d_8$$

B.19
$$m_{35} = m_{53} = (m_6 + m_7 + m_8)(a_4s_5 + (d_4 + d_{4a})c_5 + d_6)d_6 + m_8\big(2d_6c_7 + d_8{c_6}^2 + d_8{s_6}^2{c_7}^2 + 2a_4(s_5c_7 + c_5c_6s_7) + 2(d_4 + d_{4a})(c_5c_7 + s_5c_6s_7)\big)d_8$$

B.20
$$m_{36} = m_{63} = m_8(a_4s_5 + (d_4 + d_{4a})c_5 + d_6 + d_8c_7)d_8s_6s_7$$

B.21
$$m_{37} = m_{73} = m_8\big(c_6(d_8 + d_6c_7) + a_4(c_5s_7 + s_5c_6c_7) + (d_4 + d_{4a})(s_5s_7 + c_5c_6c_7)\big)d_8$$

B.22
$$m_{38} = m_{83} = 0$$

B.23
$$m_{44} = m_4 + m_5 + m_6 + m_7 + m_8$$

B.24
$$m_{45} = m_{54} = (m_6 + m_7 + m_8)d_6s_5 - d_8m_8(s_5c_7 + c_5c_6s_7)$$

B.25
$$m_{46} = m_{64} = -m_8d_8s_5s_6s_7$$

B.26
$$m_{47} = m_{74} = -m_8(c_5s_7 + s_5c_6c_7)d_8$$

B.27
$$m_{48} = m_{84} = 0$$

B.28
$$m_{55} = (m_6 + m_7 + m_8){d_6}^2 + m_8(2d_6c_7 + d_8{c_6}^2 + d_8{s_6}^2{c_7}^2)d_8$$

B.29 $$m_{56} = m_{65} = m_8(d_8c_7 + d_6)d_8s_6s_7$$

B.30 $$m_{57} = m_{75} = m_8(d_6c_7 + d_8)d_8c_6$$

B.31 $$m_{58} = m_{85} = 0$$

B.32 $$m_{66} = m_8{d_8}^2{c_7}^2$$

B.33 $$m_{67} = m_{76} = 0$$

B.34 $$m_{68} = m_{86} = 0$$

B.35 $$m_{77} = m_8{d_8}^2$$

B.36 $$m_{78} = m_{87} = 0$$

B.37 $$m_{88} = 0$$

The elements of matrix $\boldsymbol{B_\theta}(\boldsymbol{\theta}, \dot{\boldsymbol{\theta}})$ can be computed from the elements of inertia matrix by using Equation B.38.

B.38 $$b_{ij}(\boldsymbol{\theta}, \dot{\boldsymbol{\theta}}) = \sum_{k=1}^{n} \frac{1}{2}\left(\frac{\partial m_{ij}}{\partial \theta_k} + \frac{\partial m_{ik}}{\partial \theta_j} - \frac{\partial m_{jk}}{\partial \theta_i}\right)$$

The vector $\boldsymbol{g_\theta}(\boldsymbol{\theta})$ is given in Equation B.39 below.

B.39 $$\boldsymbol{g_\theta}(\boldsymbol{\theta}) = \begin{bmatrix} 0 \\ 0 \\ \begin{pmatrix} g\big((m_4 + m_5 + m_6 + m_7 + m_8)(a_4s_3 - (d_4 + d_{4a})c_3)\big) \\ -(m_6 + m_7 + m_8)d_6c_{35} + m_8(s_{35}c_6s_7c_{35}c_7)d_8) \end{pmatrix} \\ g(m_4 + m_5 + m_6 + m_7 + m_8)s_3 \\ g\big((m_6 + m_7 + m_8)d_6c_{35} + m_8(c_{35}c_7 - s_{35}c_6s_7)d_8 \\ -gm_8d_8c_{35}s_6s_7 \\ gm_8(c_{35}c_6c_7 - s_{35}s_7)d_8 \\ 0 \end{bmatrix}$$

Here, g is the acceleration due to gravity.

The mass of each link of WHMAN is given below in Table B.1.

Table B.1: Mass of WHMAN links

Symbol	Mass	Units
m_1	27	kg
m_2	15	kg
m_3	28	kg
m_4	25	kg
m_5	39	kg
m_6	15	kg
m_7	23.5	kg
m_8	20	kg

The maximum force/torque capacity of each joint of WHMAN is given in Table B.2 below.

Table B.2: Force/torque capacity of WHMAN joints

Joint Name	Force		Units
Linear slide	3000		N
Base	2000		Nm
Shoulder	4000		Nm
Telescopic	Piston side	10000	N
	Rod side	7000	
Elbow	2000		Nm
Azimuth	600		Nm
Wrist	600		Nm
Tool rotation	600		Nm

APPENDIX C: HYDRAULICS OF WHMAN

The pump characteristics of the HPU (Hydraulic Power Unit) of WHMAN (Water Hydraulic MANipulator) are given in Table C.1.

Table C.1: Pump specifications

Characteristic	Value	Units
Manufacturer	Hytar	–
Type	Axial piston pump	–
Number of pistons	9	–
Supply pressure	210×10^5	Pa
Volume displacement	0.02×10^{-3}	m^3/rev
Maximum flow	35×10^{-5}	m^3/s
Power	12000	W

Similar servo-valves are used to control the water hydraulic vane actuators and cylinder of WHMAN. The characteristics of these servo-valves are given in Table C.2.

Table C.2: Servo-valves specifications

Characteristic	Value	Units
Manufacturer	Moog	–
Type	$030 - 417$	–
Fluid	Water	–
Supply pressure	210×10^5	Pa
Nominal pressure	70×10^5	Pa
Nominal flow	11×10^{-5}	m^3/s
Control signal	± 10	mA
Coil resistance	1000	Ω/coil
Internal leakage	3.3×10^{-6}	m^3/s
Hysteresis	< 3	%
Natural frequency	100	Hz
Damping ratio	0.5	–
Lap	Critically-lapped	–

The linear slide is driven by an electric motor via a screw shaft. The main characteristics of this motor are given in Table C.3.

Table C.3: Motor drive specifications

Characteristic	Value	Units
Manufacturer	WITTENSTEIN Cyber Motor GmbH	–
Type	Brushless MMSR 070H – 060R – 320F	–
Terminal voltage	320	V
Nominal torque	1.2	Nm
Continuous torque	2.1	Nm
Peak torque	6.6	Nm
Torque constant	$0.45 \pm 5\%$	Nm/A

The base and elbow joints are driven by similar water hydraulic vane actuators. The main characteristics of these vane actuators are given in Table C.4.

Table C.4: Base and elbow vane actuators specifications

Characteristic	Value	Units
Manufacturer	IHA/TUT	–
Specific volume	9.46×10^{-5}	m^3/rad
Dead volumes in chambers	6.66×10^{-7}	m^3
Average volume in chambers	2.23×10^{-4}	m^3
Internal leakage coefficient	3.84×10^{-13}	$m^3/s/Pa$
Effective bulk-modulus	1500×10^{6}	Pa

The main characteristics of shoulder vane actuator are given in Table C.5.

Table C.5: Shoulder vane actuator specifications

Characteristic	Value	Units
Manufacturer	IHA/TUT	–
Specific volume	18.92×10^{-5}	m^3/rad
Dead volumes in chambers	6.66×10^{-7}	m^3
Average volume in chambers	2×10^{-4}	m^3
Internal leakage coefficient	7.68×10^{-13}	$m^3/s/Pa$
Effective bulk-modulus	1500×10^{6}	Pa

A spherical wrist of WHMAN is composed of three similar vane actuators. The main characteristics of these vane actuators are given in Table C.6.

Table C.6: Wrist vane actuators specifications

Characteristic	**Value**		**Units**
Manufacturer	IHA/TUT		–
Specific volume	2.795×10^{-5}		m^3/rad
Dead volumes in chambers	Azimuth and Tool rotation	8.482×10^{-6}	m^3
	Wrist	1.414×10^{-5}	
Average volume in chambers	6.6×10^{-5}		m^3
Internal leakage coefficient	3.84×10^{-13}		$m^3/s/Pa$
Effective bulk-modulus	1500×10^{6}		Pa

A telescopic extension of WHMAN arm is driven by a water hydraulic cylinder. The main characteristics of this cylinder are given in Table C.7.

Table C.7: Telescopic extension cylinder specifications

Characteristic	**Value**		**Units**
Manufacturer	Hytar		–
Piston diameter	25×10^{-3}		m
Rod diameter	14×10^{-3}		m
Stroke	0.4		m
Dead volumes in chambers	Piston side	8.482×10^{-6}	m^3
	Rod side	1.262×10^{-5}	
Average volume in chambers	6.6×10^{-5}		m^3
Effective bulk-modulus	1500×10^{6}		Pa